Quantification of Magnetic Components in Sediments with Applications in Paleoenvironmental Studies

A DISSERTATION
SUBMITTED TO THE FACULTY OF THE GRADUATE SCHOOL
OF THE UNIVERSITY OF MINNESOTA
BY

Ioan LASCU

IN PARTIAL FULFILLMENT OF THE REQUIREMENTS
FOR THE DEGREE OF
DOCTOR OF PHILOSOPHY

Subir K. BANERJEE and Emi ITO, advisors

December 2011

Acknowledgments

First and foremost, I would like to thank the Institute for Rock Magnetism and LacCore crews for being instrumental in making this happen. My gratitude goes out to Mike Jackson, Peat Solheid, Julie Bowles, Amy Myrbo, Kristina Brady, and Anders Noren. Without your support, guidance, and friendship I would not have been able to find my way.

To my mentors, thank you for being great scientific role models. Subir Banerjee, Bruce Moskowitz, Josh Feinberg, Emi Ito, Kurt Kipfmueller, Christoph Geiss, and Kendra McLauchlan, I have learned a great deal from all our discussions and I appreciate your thoughtful comments on my various writings. Thanks must also be offered to Bryan Shuman and Carrie Jennings for serving on my early committees.

Funding for my research was generously provided by the University of Minnesota and the Geological Society of America. I have received a number of fellowships and assistantships form the Department of Geology and Geophysics and the University of Minnesota, including a Doctoral Dissertation Fellowship, for which I am grateful.

The Department of Geology and Geophysics has been a fantastic place to be a graduate student. My fellow grad peers, you've made life so much easier these past years, whether in the field, the lab, or during countless social outings. Colin Plank, Anna Henderson, and all my other contemporaries, thank you for your friendship, and for setting the bar high. Jess Till, you've been the perfect office mate. And thanks to Sharon Kressler for taking care of all my silly needs.

My parents have been a constant source of inspiration and support. They have always been in my corner, even when they did not approve of my decisions, such as foregoing a career in business and finance to become a geologist. I can undoubtedly say there aren't better parents in the world, not even in America.

Finally, Ioana, you are my rock, my foundation. I truly would not have been able to accomplish all of this without you. Thank you for being strong for both of us.

pentru Sonia

Fie să-ți urmezi calea cu înțelepciune,
Să fii cumpătată dar ageră,
Să aduni din drum tot ce e bun,
Să stai departe de ce e rău
Și să nu disprețuiești ce e urât,
Căci nu știi niciodată ce vei descoperi
sub ascunzișul unei înfățișări sărăcăcioase.

Abstract

The present dissertation is a collection of papers investigating the magnetic properties of sediments. The main aim of the work presented here is to study the magnetic characteristics of sedimentary deposits by using a methodology that efficiently quantifies the contributions of various ferrimagnetic components in sediments, and to exemplify how this model can be used to make inferences about past climatic and environmental variability. Magnetic minerals in sediments have long been used as indicators of variability in the factors controlling sediment deposition, and sediment-magnetic properties can be interpreted in terms of the processes controlling the fluxes of various magnetic components. Ferrimagnetic minerals, such as magnetite, are strong magnetically, and tend to dominate the signal from bulk measurements. Two sedimentary ferrimagnetic components that play a major role in shaping the magnetic record with time: a detrital component and a biogenic component. The detrital component of magnetic assemblages probably accounts for the greater proportion of the magnetic signal in many records, and therefore has been the focus of most environmental magnetism studies. The processes that control detrital records are mostly tied to local hydrology, climate, and vegetation cover. However, there is strong evidence that many magnetic assemblages are dominated by autochthonous magnetic particles, which in most cases are produced as a result of direct biologic control. Knowing the contribution of each of these components to the total mass of ferrimagnetic material becomes important when making inferences about past climatic or environmental conditions.

The theoretical mixing model devised here using the characteristics of detrital and biogenic end members was tested on lake sediments from Minnesota. The analysis incorporates both spatial and temporal effects on magnetic record. We have investigated the history of sediment flux to Deming Lake, Minnesota, for the past 1000 years. Our results reveal several episodes of reduced precipitation, during which less sediment is mobilized from the catchment by overland flow and runoff. The most

prominent episode occurred at the end of the Little Ice Age, indicating that this time period was not only cold but might have been drier than previously thought. The spatial control on sediment-magnetic properties was established via a survey of the magnetic properties of surface sediments from several Minnesota lakes. The magnetic properties are controlled by the competing fluxes of detrital and biogenic particles, according to location in the basin, while the position of the oxic-anoxic interface controls whether biogenic magnetite is formed in the sediment or in the water column, with implications in the preservation of intact versus collapsed bacterial chains.

The thesis concludes with an incursion into the magnetic properties of chemical sediments from caves, or speleothems. The magnetic recordings preserved in calcite speleothems hold enormous potential for paleomagnetic and paleoenvironmental reconstructions. Speleothems lock in magnetization instantly, are not affected by post-depositional effects, and can be dated with high precision. The natural remanence in speleothems is carried mainly by magnetite, and the main remanence acquisition mechanism is depositional, through physical alignment of detrital magnetic grains parallel to the Earth's magnetic field. Future speleothem magnetism studies should benefit from increasingly sensitive magnetometers, operating at high spatial resolution, that are able to resolve short-term geomagnetic variability, and characterize events such as geomagnetic excursions at an unprecedented scale.

Table of Contents

Acknowledgments i
Abstract iii
Table of Contents v
List of Figures viii
List of Tables x
Chapter 1: Introduction 1
Motivation and goals 1
Structure of the dissertation 3
Chapter 2: Quantifying the concentration of ferrimagnetic particles in sediments using rock magnetic methods 6
Synopis 7
1. Introduction 8
2. Theoretical considerations 12
2.1. Total concentration of ferrimagnetic material 12
2.1.1. Magnetic susceptibility as a ferrimagnetic concentration proxy 12
2.1.2. Saturation magnetization as a ferrimagnetic concentration proxy 14
2.1.3. Expression of total ferrimagnetic concentration 15
2.2. Concentration of remanence-carrying ferrimagnetic components 16
2.3. Concentration of superparamagnetic particles 18
3. Materials and Methods 20
3.1. Samples and non-magnetic treatments 20
3.2. Magnetic measurements 21
4. Results and discussion 23
4.1. Synthetic mixtures 23
4.2 Lake sediments 25
4.2.1. Sedimentary units and chronology 25
4.2.2. Room temperature magnetic properties 26
4.2.3. Suspended sediments 26
4.2.4. Total ferrimagnetic concentration 27
4.2.5. Concentration of remanence-carrying particles 30
4.2.6. Concentration of SP particles 32
4.2.7. Ferrimagnetic flux model 33
4.3 Discussion of modeling parameters selection 34
5. Conclusions 38
References 40
Figures 50
Tables 59
Chapter 3: Sediment-magnetic evidence for last millennium drought conditions at the prairie-forest ecotone of northern United States 61
Synopsis 62

1. Introduction 63
2. Site description 65
3. Materials and methods 66
3.1. Fieldwork, initial core studies, and sampling 66
3.2. Laboratory analyses 67
3.3. Modeling sediment magnetic parameters 69
4. Results 71
5. Discussion 73
5.1. Controls on Deming Lake sedimentary parameters 73
5.2. Evidence for last millennium drought conditions in Minnesota 75
6. Conclusions 79
References 80
Figures 86
Tables 93
Chapter 4: Magnetic properties of surface sediments from small lakes in Minnesota, USA 95
Synopsis 96
1. Introduction 97
2. Study sites 98
3. Methods 99
3.1. Surface sediment sampling 99
3.2. Magnetic measurements 99
3.3. Loss on ignition (LOI) 101
3.4. Grain size 101
3.5. Transmission electron microscopy (TEM) 101
4. Results and discussion 103
4.1. Sediment transects 103
4.2. Magnetic components 104
4.3. Controls on magnetic properties of lake sediments 106
5. Conclusions 109
References 110
Figures 115
Tables 130
Chapter 5: Speleothem magnetism 131
Synopsis 132
1. Introduction 133
2. Speleothem precipitation and the origin of detrital particles in secondary calcite deposits 135
2.1. Factors controlling calcite precipitation 136
2.2. Calcite fabrics and crystal growth 137
2.3. Annual laminations 138
2.4. Detrital sediment inputs 139
3. Magnetic particles and natural remanence acquisition in speleothems 141
4. Previous paleomagnetic studies of speleothems 146

4.1. Speleothems as geomagnetic recorders 146
4.2. Reproducibility of speleothem paleomagnetic records 148
4.3. Geomagnetic features recorded in speleothems 151
4.4. Radiometric dating issues 154
5. Future directions in speleothem magnetism research 157
5.1. Advances in magnetic instrumentation and quantitative analytical methods 157
5.2. Potential for high resolution studies of magnetic field behavior 159
5.3. Potential for studies of regional climate variability 164
6. Summary 166
References 167
Figures 180
Comprehensive bibliography 189
Appendix 213
Figures 213
Tables 234

List of Figures

Figure 2.1 Modeling synthetic mixtures of magnetic particles 52
Figure 2.2 Bulk magnetic properties of the Brownie Lake sediment core 53
Figure 2.3 Magnetic properties of filtered water samples collected from Brownie Lake 54
Figure 2.4 Low temperature magnetic properties, Mössbauer spectra, and total concnetration of ferrimagnetic material in Brownie Lake sediments 55
Figure 2.5 Modeling the remanence carrying components in Brownie Lake sediments 56
Figure 2.6 Modeling the superparamagentic component of Brownie Lake sediments 57
Figure 2.7 Model of annual flux of ferrimagnetic components in Brownie Lake..... 58
Figure 3.1 Geographical location of Deming Lake and map of the site..... 88
Figure 3.2 Deming Lake age-depth model 89
Figure 3.3 Deming Lake sedimentary and magnetic parameters 90
Figure 3.4 Comparison of Palmer Drought Severity Index (PDSI) with Deming Lake parameters..... 91
Figure 3.5 Comparison of Deming Lake parameters to other regional paleoclimatic records 92
Figure 4.1 Map of Minnesota with the locations of the eight lakes investigated in this study 117
Figure 4.2 Deming Lake transects..... 118
Figure 4.3 Mosomo Lake transects 119
Figure 4.4 Birch Lake transects..... 120
Figure 4.5 Peterson Lake transects..... 121
Figure 4.6 Sandy Lake transects..... 122
Figure 4.7 Elkhorn Lake transects..... 123
Figure 4.8 Erie Lake transects 124
Figure 4.9 Linka Lake transects 125
Figure 4.10 Magnetic grain size plots as a function of organic content..... 126
Figure 4.11 Spatial distribution of model components UNISD and ISD along the transects 127
Figure 4.12 Comparison of magnetic properties as a function of temperature for shoreline, littoral, and profundal samples..... 128
Figure 4.13 Magnetic component unmixing and TEM images of magnetic extracts. Scale bar is 1 μm for b, 0.2 μm for c, 100 nm for d, f, g, h, j, and 50 nm for e and i 129
Figure 5.1 Conceptual model of the processes affecting magnetism of speleothems 183
Figure 5.2 Flood layers and annual banding in stalagmite SVC982 from Spring Valley Caverns, Minnesota. 184
Figure 5.3 Comparison of polar wander, inclination, and declination from stalagmite VCCL, Canada with the CALS7K model curves for the region. 185

Figure 5.4 Inclination and declination records from the five Chinese stalagmites (SC01, SC02, PT02, PT03, PT04) compared to CALS7K model curves for the region. 186
Figure 5.5 Magnetic components of stalagmite specimens. 187
Figure 5.6 Low temperature properties of stalagmite specimens 188
Figure A.1 Low temperature magnetic properties of a shoreline sample from Birch 213
Figure A.2 Low temperature magnetic properties of a littoriprofundal sample from Birch 214
Figure A.3 Low temperature magnetic properties of a profundal sample from Birch215
Figure A.4 Low temperature magnetic properties of a profundal sample from Deming 216
Figure A.5 Low temperature magnetic properties of a littoriprofundal sample from Deming 217
Figure A.6 Low temperature magnetic properties of a shallow littoral sample from Deming 218
Figure A.7 Low temperature magnetic properties of a shallow-littoral sample from Elkhorn 219
Figure A.8 Low temperature magnetic properties of a profundal sample from Elkhorn 220
Figure A.9 Low temperature magnetic properties of a littoriprofundal sample from Elkhorn 221
Figure A.10 Low temperature magnetic properties of a littoriprofundal sample from Erie 222
Figure A.11 Low temperature magnetic properties of a shoreline sample from Erie 223
Figure A.12 Low temperature magnetic properties of a littoriprofundal sample from Linka 224
Figure A.13 Low temperature magnetic properties of a profundal sample from Linka 225
Figure A.14 Low temperature magnetic properties of a profundal sample from Mosomo 226
Figure A.15 Low temperature magnetic properties of a littoriprofundal sample from Mosomo 227
Figure A.16 Low temperature magnetic properties of a shallow littoral sample from Mosomo 228
Figure A.17 Low temperature magnetic properties of a profundal sample from Peterson 229
Figure A.18 Low temperature magnetic properties of a littoral sample from Peterson 230
Figure A.19 Low temperature magnetic properties of a littoral sample from Peterson 231
Figure A.20 Low temperature magnetic properties of a profundal sample from Sandy 232
Figure A.21 Low temperature magnetic properties of a profundal sample from Sandy 233

List of Tables

Table 2.1 Mean (m), standard deviation (σ[a]), and coefficient of variation (CV[b] = σ/m) values for the magnetic properties of Brownie Lake sediment units 59
Table 2.2 Magnetic hyperfine parameters at room temperature for the Brownie Lake surface sediment magnetic extract 60
Table 3.1 ^{210}Pb activity and ages 93
Table 4.1 Lake morphometric parameters 130
Table A.1 Brownie Lake magnetic parameters 234
Table A.2 Brownie Lake model components 236
Table A.3 Deming Lake freeze core sedimentary parameters 238
Table A.4 Deming Lake piston core ferrimagnetic fractions and fluxes 241
Table A.5 Birch Lake transect data 243
Table A.6 Deming Lake transect data 244
Table A.7 Elkhorn Lake transect data 246
Table A.8 Erie Lake transect data 248
Table A.9 Linka Lake transect data 249
Table A.10 Mosomo Lake transect data 251
Table A.11 Peterson Lake transect data 252
Table A.12 Sandy Lake transect data 253
Table A.13 Hysteresis ratios and component fractions for analyzed surface sediments 255

Chapter 1: Introduction

Motivation and goals

The goal of this dissertation was to investigate the magnetic properties of sedimentary deposits by using a methodology that efficiently quantifies the contributions of various ferrimagnetic components in sediments, and to exemplify how this model can be used to make inferences about past climatic and environmental variability.

Magnetic minerals in sediments have long been used as indicators of change in the external and internal factors that control sediment deposition. Sediment magnetic properties measured in the laboratory lead to information about the mineralogy, concentration, and grain size distribution of the magnetic fraction. These sedimentary characteristics, in turn, can be interpreted in terms of the processes controlling the fluxes of various magnetic components. Many attempts have been made to quantify these fluxes. The most rigorous methods necessitate that very detailed measurements be performed on each sample analyzed, to the point that time becomes a limiting variable. This is certainly not a feasible approach when dealing with a large number of samples, such as those originating from long sediment cores. Therefore, these specimens are usually subjected to a slew of conventional bulk measurements that are then presented ‘as is’, and many times left for the interpretation of the reader. However, there is much information to be mined from these bulk measurements, which may provide answers about the types and quantities of magnetic components present in the sediment.

My main motivation for tackling this problem was to find a way to use conventional bulk measurements to quantify the mass of the magnetic material that is controlling the magnetic parameters acquired in the laboratory. A secondary objective was to try to validate the use of each and every one of these conventional measurements, which are often used in concert solely from inertia. For example, parameters such as magnetic susceptibility, saturation magnetization, and various

magnetic remanences all yield some information about the concentration of the magnetic material. But is one more useful over another? The answer to this question is tied to the type of sediment measured, and/or the magnetic fraction targeted in the study.

Ferrimagnetic minerals, such as magnetite, are strong magnetically, and tend to dominate the signal from bulk measurements. This certainly is the case for the lake sediments used in this study, therefore it is the material I have focused on in this research. For lake sediments, especially in temperate climates such as in Minnesota, there are two sedimentary ferrimagnetic components that play a major role in shaping the magnetic record with time: a detrital component and a biogenic one. The relationship between these two components is a direct outcome of the natural processes affecting the depositional environment.

The detrital component of magnetic assemblages probably accounts for the greater proportion of the magnetic signal in many records, and therefore has been the focus of most environmental magnetism studies. The processes that control detrital records are mostly tied to local hydrology, climate, and vegetation cover. However, there is strong evidence that many magnetic assemblages are dominated by autochthonous magnetic particles, which in most cases are produced as a result of direct biologic control. These particles are known as ‘magnetosomes’, and are produced intra-cellularly by magnetotactic bacteria. Due to a precise control on their formation, magnetosomes have very characteristic shapes, and narrow grain size distributions, making them ideally suited for a number of magnetic measurements.

Knowing the contribution of each of these components to the total mass of ferrimagnetic material becomes important when making inferences about past climatic or limnologic conditions. But even if these fluxes are precisely determined, it may still take non-magnetic sedimentary parameters to aid these environmental interpretations.

The outcome of my exercise is a ferrimagnetic flux model that distills bulk magnetic measurements into a palpable quantity (i.e., the mass of ferrimagnetic material). As one of our referees pointed out, this is the first model that comprehensively makes use of magnetic parameters in such way, and that “this could

be a very important work changing how people use rock magnetic parameters to quantify in an absolute sense, the concentration of ferrimagnetic minerals in a sediment". All I can hope for is that this method will gain some traction in the rock magnetic and environmental magnetic research community, and that it may be expanded to incorporate other magnetic materials (e.g., antiferromagnetic), and extended to additional geological settings.

Structure of the dissertation

The present dissertation is structured into four chapters, all prepared as manuscripts for publication in specialty journals. All papers benefited from the contributions of co-authors. However, the main interpretations, writing, and all mistakes are mine.

The first paper, "Quantifying the concentration of ferrimagnetic particles in sediments using rock magnetic methods", presents the basis of my methodology (Chapter 2). The quantification method is based mainly on bulk room-temperature measurements, with some low temperature measurements used for calibration purposes. Saturation magnetization (M_s) is used for determining the total ferrimagnetic concentration. Anhysteretic and saturation isothermal remanences (ARM and M_{rs}) are used to model the concentrations of the remanence-carrying ferrimagnetic fractions. This is done using a three-component mixing model that is tested on mixtures of magnetite end members of know concentrations. The remanence ratio (M_{rs}/M_s) is used as true grain-size indicator, while the ARM ratio is used as a proxy for inter-particle magnetostatic interactions. The ferrimagnetic susceptibility is used in the quantification of the ultrafine superparamagnetic particles. We use sediment composition, density, and sedimentation rates to calculate the annual fluxes of each of the components considered in our model. This method eliminates dilution effects on magnetic properties by weakly magnetic substances in high concentrations, and allows the calculation of ferrimagnetic particle fluxes for dated sedimentary sequences. The paper was published in Geochemistry, Geophysics, Geosystems (2010, doi:10.1029/2010GC003182) with co-authors Subir K. Banerjee and Thelma Berquó.

Berquó performed the Mössbauer analysis and interpreted the results. Banerjee met with me weekly for half a year to discuss the method developments, and has provided guidance and encouragement throughout the process. Both co-authors revised several manuscript drafts prior to submission.

The second paper, “Sediment-magnetic evidence for last millennium drought conditions at the prairie-forest ecotone of northern United States” (Chapter 3), is a direct application of the method developed in Chapter 2. We investigated the magnetic properties of sediments from Deming Lake, a meromictic lake close to Minnesota’s prairie-forest boundary, from which we inferred a history of sediment flux into the lake basin for the past 1000 years. Our results reveal several episodes of elevated ARM ratios, with the most prominent one at the end of the Little Ice Age, between the years 1700 and 1900. Based on the comparison of the ARM ratio with instrumental records of climate change for the 20th century, we find that high ARM ratios correspond with periods of drought, in which less sediment is mobilized from the catchment by overland flow and runoff, due to a decrease in the amount of precipitation. This magnetic record of reduced precipitation matches other regional records of drought. This paper was co-authored with Kendra K. McLauchlan, Amy Myrbo, and Subir K. Banerjee and is in revision for Palaeogeography, Palaeoclimatology, Palaeoecology. All co-authors helped with the interpretation of the proxies, and revised the manuscript prior to submission. Myrbo produced the age model using the program ‘Bacon’.

The third paper, “Magnetic properties of surface sediments from small lakes in Minnesota, USA” (Chapter 4), is a survey of the magnetic properties of surface sediments from eight Minnesota lakes. The surface samples used in this study were taken along two intersecting, shore-to-shore transects in each of the investigated lakes. The main goal was to characterize the spatial variation of the magnetic properties, and their variability across sedimentary facies. We have found that the magnetic properties are controlled by the competing fluxes of detrital and biogenic particles, according to location in the basin. The position of the oxic-anoxic interface controls whether biogenic magnetite is formed in the sediment or in the water column, with

implications in the preservation of intact versus collapsed bacterial chains. The latter have a higher proportion in the profundal facies of strongly stratified lakes, due to the clumping of particles during settlement to the bottom. The paper is co-authored with Colin Plank, who collected the sediment samples, performed the particle size analysis, and determined sediment composition via loss on ignition.

The fourth paper, “Speleothem magnetism” (Chapter 5), is an incursion into the magnetic properties of speleothems. The paper is co-authored with Joshua Feinberg, and has been published in Quaternary Science Reviews (2011, doi:10.1016/j.quascirev.2011.08.004). We are revisiting a topic that has been virtually abandoned in the mid 1990s due to issues related to instrument sensitivity, resolution, and age control of the specimens. The paper contains an ample review of the work previously done in the field, followed by our preliminary analysis of the rock magnetism of speleothem specimens. We have performed the first low temperature remanence measurements on speleothems, which reveal the presence of magnetite and goethite as magnetization carriers. We have also performed the first coercivity deconvolution analysis on speleothems, which indicate that two low coercivity (<100 mT) ferrimagnetic components are present in all samples, one representative of detrital/pedogenic magnetite, and one representative of eolian maghemite. We have proposed the hypothesis that magnetite found in speleothems from fossil cave passages (i.e., not being flooded since the formation of the speleothem) is pedogenic, and not authigenic (i.e., precipitated *in situ*) as previously suggested. The paper concludes with a discussion of future directions in speleothem magnetism research, which promises new and exciting avenues to be explored in coming years.

Chapter 2: Quantifying the concentration of ferrimagnetic particles in sediments using rock magnetic methods[*]

Ioan Lascu[§], Subir K. Banerjee, Thelma S. Berquó

Institute for Rock Magnetism, Department of Geology & Geophysics, University of Minnesota, 310 Pillsbury Drive SE, Minneapolis MN, 55455, USA

[§]*Corresponding author (Lascu003@umn.edu)*

Reprinted from Geochemistry, Geophysics, Geosystems, Volume 11, Number 8, Q08Z19, doi:10.1029/2010GC003182, Copyright 2010, by permission of American Geophysical Union

[*] We thank the National Lacustrine Core Repository (LacCore) at the University of Minnesota for access to the Brownie Lake core and initial description data, Amy Chen for help with water sampling and filtering, Bruce Moskowitz and Brian "The Dude" Carter for access to the synthetic mixtures. Mike Jackson's comments and suggestions significantly improved the development of our methodology; he also provided a constructive review of this manuscript. Constructive reviews by Leonardo Sagnotti and an anonymous referee have helped improve this manuscript. IL benefited from the support of a University of Minnesota Doctoral Dissertation Fellowship. The Institute for Rock Magnetism is funded by the National Science Foundation, the Keck Foundation, and the University Of Minnesota. This is IRM contribution 1003.

Synopis

We have developed a quantification method that uses mainly room temperature rock-magnetic measurements to calculate concentrations of ferrimagnetic particles in sediments. Our method uses saturation magnetization (M_s) as a total ferrimagnetic concentration proxy, the saturation remanence ratio (M_{rs}/M_s) as a magnetic grain-size proxy, the anhysteretic remanence ratio (χ_a/M_{rs}) to estimate inter-particle magnetostatic interactions, and the normalized susceptibility of the ferrimagnetic fraction (χ_f/M_s) to calculate the proportion of ultrafine, superparamagnetic particles. This approach eliminates the effect of dilution of the magnetic properties by weakly magnetic matter, and allows the calculation of direct concentrations (or fluxes for dated sedimentary profiles) of constituent ferrimagnetic components. We test our method on a short sediment core from an urban Minnesota lake, for which we calculate ferrimagnetic fluxes of four magnetic components, and compare their pre and post-European settlement values. Our quantification technique can be applied for reconstructing past environmental changes in a range of sedimentary environments, and is particularly useful for large sets of samples, where detailed magnetic unmixing methods are unfeasible due to time or instrument constraints.

Keywords: quantification; rock magnetism; sediments; magnetic unmixing; magnetostatic interactions.

1. Introduction

Iron-bearing minerals with characteristic magnetic properties are ubiquitous in sedimentary environments, and are used in environmental magnetism studies as indicators of past climatic conditions (e.g., Geiss and Banerjee, 1997, 1999; Dearing, 1999a; Paasche et al., 2004; Zillén and Snowball, 2009; Haltia-Hovi et al., 2010), soil and vegetation development (e.g., Oldfield et al., 2003; Geiss et al., 2003, 2008), erosion (e.g., Rosenbaum et al., 1996; van der Post et al., 1997; Reynolds et al., 2004; Rosenbaum and Reynolds, 2004a, 2004b), water and sediment (bio)geochemistry (e.g., Snowball, 1994; Snowball et al., 2002; Kim et al., 2005), and diagenetic conditions (e.g., Peck and King, 1996; Dearing et al., 1998; Gibbs-Eggar et al., 1999; Snowball et al., 1999; Demory et al., 2005; Ortega et al., 2006; Larrasoaña et al., 2007). Natural samples contain mixtures of magnetic phases of different origins, mineralogical compositions, and grain sizes. The most important magnetic carriers are ferrimagnetic minerals, such as magnetite (Fe_3O_4), maghemite (γ-Fe_2O_3), and greigite (Fe_3S_4). Antiferromagnetic minerals like hematite (α-Fe_2O_3) and goethite (α-FeOOH) have weak ferromagnetism, and contribute significantly to the total magnetization of sediments only if the total antiferromagnetic material represents at least 90% (by mass) of the ordered magnetic phases (Frank and Nowaczyk, 2008). Bulk magnetic properties such as mass susceptibility (χ), isothermal remanent magnetization (IRM), anhysteretic remanent magnetization (ARM), saturation magnetization (M_s), saturation remanence (M_{rs}), coercivity (H_c), remanent coercivity (H_{cr}), and a number of their interparametric ratios are used to characterize magnetic mineral assemblages in terms of concentration, mineralogy, and grain size. Magnetic mineral assemblage characteristics are used in turn to make inferences about the processes that lead to the accumulation of these minerals in the depositional environment (Evans and Heller, 2003).

Magnetic components, i.e., the ensemble of particles with common origin, biogeochemical history, and a characteristic array of magnetic properties (Egli, 2004), have been successfully modeled using magnetization spectrum methods, which exploit

the subtleties of entire magnetization curves, reducing the non-uniqueness of a bulk parameter approach (e.g., Robertson and France, 1994; Roberts et al., 2000; Carter-Stiglitz et al., 2001; Kruiver et al., 2001; Heslop et al., 2002; Egli 2003, 2004, 2006a; Egli et al., 2010). However, the relatively involved methodology inherent to spectral techniques poses the disadvantage of only being able to process a limited number of samples in a given time span. On the other hand, bulk magnetic measurements are fast, inexpensive, non-destructive, and extremely sensitive to very small quantities of magnetic material, but they sometimes lack the ability to distinguish between different sedimentary magnetic components. For the analysis of large numbers of samples, such as typically encountered in long core studies, a technique that makes use of a limited number of spectral analyses on selected samples to calibrate numerous bulk measurements is particularly desirable.

Several attempts have been made to quantify the concentration of various magnetic components using bulk parameters like χ, ARM, or IRM. Lees (1997) has quantified the concentration of magnetic components in synthetic mixtures of up to six sedimentary sources by using linear modeling techniques, and has found χ to be the most reliable concentration-dependent parameter in case of complex mixtures. Large errors were encountered in the deconvolution of mixtures with a large number of components, implying that linearity does not apply for complex source mixing due to the extreme heterogeneity of considered samples, in addition to effects of magnetic viscosity of materials, interactions between particles, and inter-instrument calibration issues. In an attempt to unmix bulk χ measurements, von Dobenek (1998) introduced the concept of partial susceptibilities, which states that the bulk susceptibility of a sample is the sum of the susceptibilities of its constituent components. The method was subsequently developed in studies by Frederichs et al. (1999), S. Xie et al. (1999), Bleil and von Dobenek (2003), Funk et al (2003), and Q. Xie et al. (2009). The contribution of individual components to the bulk susceptibility is calculated via multiple regression, whereby each partial susceptibility term is related by a proportionality factor to the value of a magnetic parameter that is diagnostic for that particular component (e.g., ARM for ferrimagnetic SD particles). The partial

susceptibility method assumes linear proportionality between the susceptibility of the individual component and the magnetic parameter used as diagnostic, an assumption that does not always hold true. The method offers the advantage of reducing everything to susceptibilities, and the potential to eliminate the diagnostic parameter measurements if an empirical proportionality factor is universally found for every component considered in the model.

The property of linear additivity of individual components that contribute towards a remanence parameter was used by Dunlop (2002) in developing theoretical mixing curves of simple two-component numerical mixtures, based on hysteresis properties. Linear additivity of remanence was applied by Geiss and Zanner (2006) to understand pedogenic enhancement in loessic soils in North American Great Plains. Bulk ARM and IRM measurements were used to quantify magnetite formed as a result of biogeochemical processes occurring in the topsoil. The pedogenic fraction obtained via this binary mixing model was found to underestimate calculations based on hysteresis parameter modeling, and coercivity spectra deconvolution. One reason for this discrepancy is their ARM-IRM model ignores the effects of magnetostatic interactions between particles in the sediment matrix, which tend to lower ARM values even for low ferrimagnetic concentrations (Egli, 2006b). The decrease of ARM values as a result of inter-particle interactions was investigated by Yamazaki (2008), who uses first-order reversal curve (FORC) diagrams in addition to bulk ARM and IRM measurements, and coercivity analysis of IRM acquisition curves to unmix sedimentary components in North Pacific sediment cores. The FORC analysis reveals the presence of a fine-grained non-interacting component, a fine-grained interacting component, and a coarse-grained background component. The concentration of the interacting particles is inversely related to the ARM ratio (ARM normalized by saturation IRM), indicating that interactions between particles are an important ARM-controlling factor. This is highly significant because the ARM ratio is widely used as a grain-size indicator in enviromagnetic studies. Since ARM is sensitive to magnetostatic interactions between proximal particles, the ratio can be artificially lowered if small particles occur in clumps, as is the case of collapsed bacterial

magnetite chains, or clusters of pedogenic magnetite washed into a basin. Therefore, small-scale variations in the ARM ratio could point to interactions between particles rather than grain size changes, potentially offering information about the packing and arrangement of magnetic particles in the sediment matrix (Egli et al., 2006b; Kopp et al., 2006; Yamazaki 2008).

In this paper we present a quantification method that uses bulk rock-magnetic measurements to calculate mass fractions, mass per volume concentrations, and fluxes of ferrimagnetic particles in sediments. Detailed rock-magnetic and non-magnetic measurements are performed on representative samples to calibrate the modeling parameters. The quantification method consists of three parts: 1) Calculation of total ferrimagnetic concentration from in-field magnetization parameters, 2) Modeling the remanence-carrying fractions using remanent magnetizations to gain information about magnetic grain size and inter-particle interactions; this is tested on a selection of synthetic mixtures of stable single domain (SD), pseudo single domain (PSD), and multi domain (MD) magnetite (Carter-Stiglitz et al., 2001; Dunlop and Carter-Stiglitz, 2006), and 3) Calculation of the superparamagnetic (SP) fraction from ferrimagnetic susceptibility and SP grain size distribution data. The quantification method is applied to a short sediment core from a Minnesota urban lake, but is applicable to a range of environments, including marine sediments, loess deposits, and soils.

2. Theoretical considerations

2.1. Total concentration of ferrimagnetic material

Magnetic susceptibility, remanent magnetizations (ARM and IRM), and saturation magnetization are generally used to qualitatively assess the amount of magnetic material present in sediments. Saturation magnetization is an intrinsic property of magnetic materials, so should theoretically offer the most reliable concentration estimates. Susceptibility-based concentration estimates are widespread due to low cost and ease of measurement, but require information about magnetic mineralogy, grain size, and grain shape. Remanence measurements are accurate as concentration proxies only when magnetic composition is uniform (with respect to mineralogy and grain size) over the sedimentary interval investigated, because of the varying degree of remanence acquisition efficiency for different categories of magnetic particles. In this section we focus on χ and M_s, and discuss their use as ferrimagnetic concentration proxies.

2.1.1. Magnetic susceptibility as a ferrimagnetic concentration proxy

Low-field magnetic susceptibility (χ_{lf}) is the most common magnetic property measured on sediments, popularized by the use of multi-sensor core loggers equipped with loop or point susceptibility meters (Nowaczyk, 2001). Large-scale drilling expeditions employ the use of core loggers to measure unsplit sections of core immediately after retrieval for initial characterization of the sediments. At this stage χ_{lf} is mainly used to stratigraphically correlate between parallel cores from the same basin, and to roughly estimate the concentration of magnetic minerals in the core sections. χ_{lf} is strongly controlled by the presence of ferrimagnetic minerals, but this signature can be diluted by contributions of diamagnetic, paramagnetic, and antiferromagnetic materials (e.g., Dearing, 1999b). Bulk χ_{lf} can be expressed as the sum of the magnetic contributions of all components to the total susceptibility signal:

$$\chi_{lf} = \sum_{i=1}^{n} \chi_i f_i \quad (1),$$

where χ_i is the susceptibility of component i, and f_i is the mass fraction of component i ($\Sigma f_i = 1$). This expression equates to the partial susceptibilities concept of von Dobenek (1998), but expressed in terms of fractions of pure substance susceptibilities. Since the ferrimagnetic component exerts the major control on χ_{lf}, its fraction (f_{ferri}) is of interest for calculating mass or volume based concentration parameters. In order to determine f_{ferri}, the contribution of diluting sedimentary matrix must be subtracted from the bulk value. Diamagnetic and paramagnetic substances have weak susceptibilities, but can amount to significant portions of bulk χ_{lf} if they are present in abundance, as in the case of water-laden, organic, carbonate-rich, or siliciclastic sediments (Rochette, 1987). Susceptibility values for these substances are known from experimental work (see compilations by Hunt et al. (1995a) and Dearing (1999b)), and have average values of ~ $-9 \cdot 10^{-9}$ m^3/kg for water and organic matter, ~ $-8 \cdot 10^{-9}$ m^3/kg for calcite, ~ $-6 \cdot 10^{-9}$ m^3/kg for feldspar and quartz, 0.1-$7 \cdot 10^{-6}$ m^3/kg for paramagnetic and imperfect antiferromagnetic minerals. By comparison, ferrimagnetic mineral susceptibilities are on the order of 10^{-4}-10^{-3} m^3/kg. Mass fractions f_i can be obtained from geochemical or mineralogical methods (e.g., loss on ignition (LOI), X-ray diffraction, etc.). After all non-ferrimagnetic contributions are determined and subtracted from χ_{lf}, equation (1) is reduced to:

$$\chi_f = f_{ferri} \chi_{ferri} \quad (2),$$

where χ_f is the susceptibility corrected for non-ferrimagnetic contributions, and χ_{ferri} is the susceptibility of the ferrimagnetic component. Average χ_{ferri} values are 0.2-$1.2 \cdot 10^{-3}$ m^3/kg for magnetite, 0.025-$0.29 \cdot 10^{-3}$ m^3/kg for titanomagnetite, 0.3-$0.5 \cdot 10^{-3}$ m^3/kg for maghemite, and 0.026-$0.194 \cdot 10^{-3}$ m^3/kg for greigite (Hunt et al., 1995a; Dearing, 1999b;Peters and Dekkers, 2003). For SP grains these values are expected to be one order of magnitude higher (Dunlop and Özdemir, 1997), because they have very high intrinsic susceptibilities, and are thermally unstable, thus being easily and efficiently magnetized even in small magnetic fields. They will dominate the χ_{ferri}

signal even when in low concentrations. The main challenge posed by the exercise of determining f_{ferri} from χ_f is finding an appropriate value for χ_{ferri}, which implies some a priori knowledge about the ferrimagnetic mineralogy, grain size, and grain shape. Alternatively, if f_{ferri} can be determined from measurements of saturation magnetization, χ_{ferri} can be calculated from equation (2). This scenario is discussed below.

2.1.2. Saturation magnetization as a ferrimagnetic concentration proxy

Saturation magnetization M_s is an intrinsic property of a magnetic mineral, and provides a more straightforward measure of f_{ferri} than magnetic susceptibility. The only a priori information necessary for f_{ferri} calculation is knowledge of the ferrimagnetic mineralogy. Ferrimagnetic mass fraction is calculated as:

$$f_{ferri} = \frac{M_s}{\mu_{ferri}} \quad (3),$$

where bulk M_s is obtained from hysteresis measurements after correcting for high field non-ferrimagnetic contributions, and μ_{ferri} is the ferrimagnetic saturation magnetization, which can be written as a linear combination of the saturation magnetizations of the ferrimagnetic constituents:

$$\mu_{ferri} = \sum_{j=1}^{m} p_j \mu_j \quad (4),$$

where p_j is the fraction of total ferrimagnetic mass represented by component j ($\Sigma p_j = 1$) and μ_j is its intrinsic mass-normalized saturation magnetization. Ferrimagnetic mineral composition can be determined either from magnetic or non-magnetic methods. Magnetic methods are based mainly on thermal order-disorder transitions (Curie or Néel points) or spin reorientations and are semi-quantitative, while non-magnetic methods, such as Mössbauer spectroscopy and X-ray diffraction on magnetic extracts, permit a direct calculation of the ferrimagnetic mineral fractions. The main ferrimagnetic minerals found in lake and marine sediments are magnetite

(μ_{Mt} = 92 Am^2/kg), maghemite (μ_{Mh} = ~74.3 Am^2/kg) (Dunlop and Özdemir, 1997), and greigite (μ_{Gr} = ~59 Am^2/kg) (Chang et al., 2008). Magnetite and maghemite are by far the most common, so in the absence of reliable methods of ferrimagnetic mineral determination, calculating concentrations both as magnetite and maghemite will set the concentration interval boundaries, assuring accuracy of results, although at the expense of reduced precision.

The slope correction applied to raw hysteresis loop measurements also offers an alternative way to determine the contribution of non-ferrimagnetic components to χ_{lf}, bypassing the need for sediment composition information. The high field susceptibility χ_{hf} is calculated from the slope of a loop at magnetic fields larger than the saturating field, which is typically a few hundred mT for important ferrimagnets, and is equivalent to the sum of partial susceptibilities of all non-ferrimagnetic components contributing of χ_{lf}. The ferrimagnetic contribution to χ_{lf} can thus be expressed as:

$$\chi_f = \chi_{lf} - \chi_{hf} \quad (5).$$

Having calculated f_{ferri} and χ_f (from equations 3-5), χ_{ferri} can now be obtained from equation (2). This is done in order to calculate the SP particle fraction contributing to the total ferrimagnetic concentration (see section 2.3).

2.1.3. Expression of total ferrimagnetic concentration

The fraction of ferrimagnetic material is in effect a mass concentration, i.e., the mass ferrimagnetic component of total sediment mass. Since ferrimagnetic concentrations are on the order of thousandths of the total sediment mass, it is more convenient to express f_{ferri} as a part per thousand (ppt, mg/g, g/kg, etc.) concentration:

$$c_{ferri} = 10^3 f_{ferri} \quad (6).$$

The concentration of ferrimagnetic minerals can also be expressed as mass ferrimagnetic material per unit volume sediment:

$$C_{ferri} = f_{ferri} \rho_{wet} f_{sed} \quad (7),$$

where C_{ferri} is the total ferrimagnetic concentration as mass per volume unit, ρ_{wet} is the wet sediment density, and f_{sed} is the mass fraction sediment (i.e., the ratio of dry mass to wet mass). Wet sediment density is a standard parameter measured during initial core logging, but can also be calculated on samples of known volume by dividing the wet mass of a sample by its volume. If sample volume is unknown, ρ_{wet} can be obtained from compositional analysis (e.g., LOI) as a sum of pure substance densities (e.g., 1000 kg/m^3 for water) weighed by their respective mass fractions. C_{ferri} is of interest for calculating ferrimagnetic particle fluxes in sediment cores with established chronologies. The flux of ferrimagnetic material ϕ_{ferri} to the sediment column is obtained from multiplying C_{ferri} by the sediment accumulation rate R_{sed} (expressed in length units per time):

$$\phi_{ferri} = C_{ferri} R_{sed} \quad (8).$$

In order to separate the fluxes of various ferrimagnetic components, an unmixing method is necessary.

2.2. Concentration of remanence-carrying ferrimagnetic components

In this section we present a three-component mixing model that makes use of bulk remanence measurements to quantify the remanence-carrying fractions of f_{ferri}. Unmixing models using either hysteresis or bulk remanence parameters have been used to analyze synthetic, natural, and numerical mixtures of two components, and are based on the linear additivity of remanence properties when the mixture is monomineralic (Dunlop, 2002; Dunlop and Carter-Stiglitz, 2006; Geiss and Zanner, 2006). The mixing model presented here combines the remanence aspect of the hysteresis approach of Dunlop (2002) and Dunlop and Carter-Stiglitz (2006) with the ARM-IRM modeling of Geiss and Zanner (2006). However, we use the ARM ratio primarily to evaluate particle interactions rather than grain size, essentially extending two-component models to mixtures of three end members, here MD (including PSD), uniaxial non-interacting SD (UNISD (Egli et al., 2010)), and interacting SD (ISD).

Our model accounts for all the remanence-carrying contributors to f_{ferri}, i.e., the non-SP ferrimagnetic fraction.

Bulk ARM and saturation IRM (or M_{rs}) values can be written as linear combinations of the ARM and M_{rs} values of the mixture end members. Since the absolute remanence values of end-member components are not invariant, they are normalized by M_s (μ_{ferri} is constant across the mixture) in order to obtain comparable ratios. The resulting system of equations for the three-component (MD, UNISD, and ISD) mixing model is:

$$\begin{cases} \left(\frac{M_{rs}}{M_s}\right)_{bulk} = \sum_{i=1}^{3} g_i \left(\frac{M_{rs}}{M_s}\right)_i \\ \left(\frac{\chi_a}{M_s}\right)_{bulk} = \sum_{i=1}^{3} g_i \left(\frac{\chi_a}{M_s}\right)_i \\ \sum_{i=1}^{3} g_i = 1 \end{cases} \quad (9),$$

where χ_a is the ARM susceptibility (ARM normalized by acquisition bias field), $(M_{rs}/M_s)_{bulk}$ and $(\chi_a/M_s)_{bulk}$ are ratios obtained from measured parameters, $(M_{rs}/M_s)_i$ and $(\chi_a/M_s)_i$ are the respective ratios of end member i, and g_i is the fraction of component i. The system is solved for g_i. Since χ_a/M_s is not a commonly used ratio, the second equation in (9) can be divided by the first in order to obtain the expression for the ARM ratio (χ_a/M_{rs}). The system then becomes:

$$\begin{cases} \left(\frac{M_{rs}}{M_s}\right)_{bulk} = \sum_{i=1}^{3} g_i \left(\frac{M_{rs}}{M_s}\right)_i \\ \left(\frac{\chi_a}{M_{rs}}\right)_{bulk} = \frac{\sum_{i=1}^{3} g_i \left(\frac{\chi_a}{M_s}\right)_i}{\sum_{i=1}^{3} g_i \left(\frac{M_{rs}}{M_s}\right)_i} \\ \sum_{i=1}^{3} g_i = 1 \end{cases} \quad (10).$$

Note that ARM and M_{rs} combine in a non-linear fashion. Theoretical values for M_{rs}/M_s and χ_a/M_{rs} can be predicted by varying the end member fractions g_i over the interval (0,1) with the third condition of the system always satisfied. The model ratio values can be plotted in M_{rs}/M_s versus χ_a/M_{rs} scatter diagrams at regular g_i intervals (e.g., 0.1) as "mixing grids", and overlain with the experimental values for comparison. The mixing grids are equivalent to ternary diagrams in g_i coordinates. The choice of end-member ratios will be discussed in section 4.

2.3. Concentration of superparamagnetic particles

In order to calculate the absolute concentrations of the remanence-carrying components, the SP concentration must be first subtracted from the total ferrimagnetic concentration. Rearranging equation (2) to solve for χ_{ferri}, and substituting f_{ferri} with M_s/μ_{ferri} (equation 3), we find that χ_{ferri} is nothing but a multiple of χ_f/M_s, where the multiplier is the ferrimagnetic saturation μ_{ferri}. The ratio χ_f/M_s has been used in a quantitative way to express fluctuations in high susceptibility SP grains relative to a non-SP baseline for Chinese loess plateau deposits (Hunt et al., 1995b). SP concentrations obtained this way were found to be in good agreement with concentrations calculated via the more reliable thermal demagnetization of low temperature remanence method (Hunt and Banerjee, 1992), and are much easier to perform. The non-SP susceptibility (χ_{nonSP}), carried by SD and MD grains, has values an order of magnitude lower compared to the typical susceptibility of SP particles (χ_{SP}). χ_{ferri} can be written as the linear combination of χ_{SP} and χ_{nonSP}, an expression which can be rearranged to solve for the SP fraction (f_{SP}):

$$f_{SP} = \frac{\chi_{ferri} - \chi_{nonSP}}{\chi_{SP} - \chi_{nonSP}} \qquad (11).$$

χ_{nonSP} is typically characterized by a narrow range of values ($0.4\text{-}0.8\cdot10^{-3}$ m^3/kg for magnetite (Dunlop and Özdemir, 1997)), while χ_{SP} can be determined using information about the SP grain size distribution. For very small particles (<10 nm) the relationship between χ_{SP} and particle volume is linear at room temperature, according

to Néel (1949) theory of thermally activated magnetization. Larger SP particles (10-20 nm) exhibit frequency dependence of susceptibility at room temperature, because their magnetization relaxation times are comparable to the observation times of the experiment. Worm (1998) has investigated the nature of the SP-SD transition and the behavior of the magnetic susceptibility across this boundary. The relationship between χ_{SP} and particle volume is no longer linear, and the transition to SD susceptibilities is gradual, especially if the particles are characterized by a distribution of coercivities (see Figure 2 of Worm (1998)). In Worm's (1998) approach, frequency-dependent susceptibility measurements across a range of temperatures are necessary to estimate the SP particle size distribution, and thus χ_{SP} (which for magnetite is found to have values of up to $8 \cdot 10^{-3}$ m^3/kg). The choice of χ_{SP} depends from case to case and will be discussed in context in Section 4.

3. Materials and Methods

3.1. Samples and non-magnetic treatments

The synthetic mixtures used for testing our remanence model (Section 2.2) have been prepared by Carter-Stiglitz et al. (2001) by combining an SD end member with PSD and MD end members in incremental mass fractions. The SD particles are freeze-dried cells of vibroid magnetotactic bacterium MV1, which produces prismatic magnetite magnetosomes with mean volumes of $0.65 \cdot 10^{-22}$ m^3 and aspect ratios of 1.5, aligned in linear chains (samples from the same batches have also been used by Moskowitz et al. (1993)). The PSD and MD phases are Wright Company magnetites 3006 and 041183 with grain sizes of 1.06 ± 0.71 μm and 18.3 ± 12 μm respectively (Yu et al., 2002). The non-SD component was first dispersed in CaF_2 using a blender; the MV1 freeze-dried cells were then added in the desired mixing proportions, and gently mixed together using a mortar and pestle (Carter-Stiglitz et al., 2001).

The natural samples used in this study are lacustrine sediments from Brownie Lake, a small urban water body in Minneapolis, Minnesota. Brownie Lake has a surface area of $\sim 5 \cdot 10^4$ m^2 and a maximum depth of 14.1 m (5.6% relative depth). The lake has been meromictic (permanently stratified) since the lake level was artificially lowered by ~3 m in 1917 (Swain, 1984; Tracey at al., 1996). A 139 cm core was retrieved in 2007 from 13 m water depth, using a drive-rod surface corer. The core was logged and described at the University of Minnesota Limnological Research Center, and sampled at a resolution of 1 cm. Aliquots of ~1 cm^3 were used for LOI analysis, according to the procedure described by Dean (1974) and Heiri et al. (2001). Separate subsamples were freeze dried, weighed, and packed in plastic boxes for magnetic analyses. On 15 September 2009 a water column profile of dissolved oxygen (DO) was recorded using a Hydrolab multi-sensor probe. Water samples were collected using a Van Dorn sampler at a resolution of 0.5-1 m across the oxic-anoxic interface (OAI) and 1-1.5 m below the OAI. Between 150 and 200 ml of each sample were filtered in the laboratory using 0.1 μm filters, which were then frozen and packed

in plastic straws. A surface sediment (top 10-15 cm of the sediment column) sample was collected on the same date from a water depth of 13.5 m using an Ekman dredge. A subsample was disaggregated with sodium hexametaphosphate (0.5 g to 100 ml sediment slurry) and circulated through an in-house magnetic separator. The magnetic fraction was extracted using a high-gradient permanent magnet, collected on a daily basis for a two-week period, and stored in isopropanol at 4°C. The extract was then dried at 25°C for 24 hours, and used for room-temperature ^{57}Fe Mössbauer spectroscopy. Mössbauer analysis was performed with a conventional constant-acceleration spectrometer in transmission geometry with a source of ^{57}Co in an Rh matrix. Hyperfine parameters such as magnetic hyperfine field (B_{HF}), isomer shift (IS) and quadrupole shift (QS) have been determined by NORMOS program (Brand, 1987), and α-Fe at room temperature was used to calibrate isomer shifts and velocity scale.

3.2. Magnetic measurements

All magnetic measurements were performed at the University of Minnesota Institute for Rock Magnetism. Magnetic susceptibility was measured on a Kappabridge KLY-2 susceptometer operating at a frequency of 920 Hz. A D-Tech 2000 demagnetizer was used for ARM acquisition, which was imparted in a 0.1 mT steady field superimposed on an AF field decaying from a peak value of 200 mT, with a rate of 5 μT per half cycle. Stepwise alternating frequency (AF) demagnetization of the ARM was performed on the filtered water samples using an automated 2G Enterprises superconducting quantum interference device (SQUID) magnetometer, with peak fields increasing from 0.5 to 170 mT. The demagnetization procedure contains one hundred measurement steps spaced on a logarithmic scale. IRM was imparted on the same samples by pulsing the samples in a 200 mT field using a 2G core pulse magnetizer. This was done two times in order to remove any viscous effects. The IRM was demagnetized following the same procedure as for the ARM. For coercivity component analysis, first derivatives of the demagnetization curves were fitted with skewed generalized Gaussian distributions using MAG-MIX (Egli,

2003). Hysteresis loops were measured on a Princeton Measurements vibrating sample magnetometer using a maximum applied field of 1 T. The loop slopes at high fields (>0.7 T) were used to correct raw M_s values, and to calculate the contribution of non-ferrimagnetic minerals to low field susceptibility. A Quantum Design magnetic properties measurement system (MPMS-2) was used to perform low temperature demagnetization experiments on representative lake sediment samples. Thermal demagnetization of saturation IRM (SIRM) acquired at 10 K in a 2.5 T field after cooling the sample in zero magnetic field (the so-called ZFC treatment) was measured from 10 K to room temperature at 5 K intervals. Room temperature SIRM imparted in a 2.5 T field was partially decayed by cooling the sample to 10 K and rewarming it back to 300 K. Measurements were performed in zero field at 5 K intervals. The MPMS was also used to measure susceptibility as a function of temperature and frequency on the selected lake samples. AC susceptibility was measured in 10 K steps from 10 to 300 K at frequencies of 1, 10, and 100 Hz.

4. Results and discussion

4.1. Synthetic mixtures

We use the synthetic samples of known end-member proportions to test the validity of our mixing model defined by system (9). The M_{rs}/M_s and χ_a/M_{rs} values of the SD-MD and SD-PSD mixtures are plotted in Figure 1a, together with theoretical values for mixture bulk ratios determined from varying g_i in (10). The measured values fall on the PSD-SD and MD-SD mixing lines (i.e., two-component mixtures; g_3=0), where the SD end member ratio values are $M_{rs}/M_s = 0.498$, and $\chi_a/M_{rs} = 1.6 \cdot 10^{-3}$ m/A. For comparison, Moskowitz et al. (1993) measured ARM ratios on freeze-dried MV1 cells and obtained values of $1.8\text{-}2.1 \cdot 10^{-3}$ m/A, while Kopp et al. (2006) report ARM ratios of $1.59\text{-}1.79 \cdot 10^{-3}$ m/A for intact and treated (with sodium dodecyl sulfate and/or ultrasonication followed by dilution in sucrose) freeze-dried MV1 cells. Moskowitz et al. (1993) have also performed ARM acquisition experiments on wet MV1 cell suspensions fixed with 1% glutaraldehyde, and obtained ARM ratio values of $3.1\text{-}3.5 \cdot 10^{-3}$ m/A. Fragile bacterial cell membranes must be partially ruptured or destroyed in the process of freeze drying, which involves freezing the sample and extracting the water fraction by sublimation in vacuum. The partial destruction of the cell membranes results in magnetosome chain clumping, which explains the lower ARM ratios of freeze-dried samples as the effect of interactions between the disturbed magnetosomes. Transmission electron microscope (TEM) analysis of the untreated, freeze-dried MV1 samples of Kopp et al. (2006) reveals that only about 10% of the magnetosomes are isolated from other crystals and chains, while the bulk of the chains are either in side-to-side arrangements, or collapsed into loop configurations (Figure 2a of Kopp et al. (2006)). Given the ARM ratio value of $1.6 \cdot 10^{-3}$ m/A for the SD end-member component in our mixtures, we conclude that the SD end-member physically added to the mixtures is in fact a combination of non-interacting and interacting particles and chains, which means the synthetic samples can be modeled as mixtures of three components.

We first assign values to the remanence ratio (M_{rs}/M_s) and ARM ratio of the non-interacting SD end member. For magnetite, M_{rs}/M_s has a value of 0.5 by definition of randomly oriented UNISD particles (Stoner and Wohlfarth, 1948). The determination of the value for the ARM ratio is not as clear cut. Egli and Lowrie (2002) have developed an analytical solution for the ARM of assemblages of UNISD particles, and have found that the ARM ratio of UNISD grains characterized by uniform rotation depends chiefly on grain size and grain shape, and only weakly on microcoercivity. They calculate a maximum χ_a/M_{rs} value of $3.7 \cdot 10^{-3}$ m/A for prismatic crystals with volumes of $1.25\text{-}2.2 \cdot 10^{-22}$ m^3, and aspect (length to width) ratios of 1.43-2.5 (see Figure 11c of Egli and Lowrie (2002)). Mean volumes of $0.65 \cdot 10^{-22}$ m^3 and aspect ratios of 1.5 (as is the case with our MV1 samples) yield ARM ratios of $\sim 2 \cdot 10^{-3}$ m/A according to the Egli and Lowrie (2002) model, and yet χ_a/M_{rs} values obtained from wet suspensions of the same batches of particles used in this study (Moskowitz et al., 1993) are close to the maximum values predicted by theory. This discrepancy can be explained by the fact that Egli and Lowrie (2002) model randomly oriented non-interacting isolated particles, and not magnetosome chains. The arrangement of particles in linear chains should have the same effect as particle elongation, namely to increase dipole moment and coercivity. The increase in chain magnetic moment would lead to a higher chain ARM ratio than that of its isolated magnetosomes. Therefore having a UNISD end-member with a χ_a/M_{rs} value of $3.7 \cdot 10^{-3}$ m/A is not an unreasonable assumption.

The ISD end member ratios ($M_{rs}/M_s = 0.497$ and $\chi_a/M_{rs} = 0.47 \cdot 10^{-3}$ m/A) were determined so that a) M_{rs}/M_s of the 100% SD mixture would fall on the ISD-UNISD mixing line; b) the correlation between the (non) SD fraction added to the mixture and the inverted (non) SD fraction obtained from the solution to system (9) approaches a 1:1 relationship (i.e., the slope of a linear fit to the data is close to 1); and c) Pearson's correlation coefficient R of the fits for each mixture is maximized (R=0.999, Figure 1c). The ARM ratio of the ISD end member is close to the value of $0.41 \cdot 10^{-3}$ m/A measured by Kopp et al. (2006) on ultrasonicated MV1 cells diluted at 1 ppt in sucrose (their sample V2a). The ultrasonic treatment destroys the bacterial cell membrane but

keeps the magnetosome organelles intact, while the dilution prevents the particles from clumping. TEM images of V2a show collapsed chains throughout, but there are no major magnetosome clumps, and some of the particles remain isolated (Figure 2b of Kopp et al. (2006)). According to the calculations of Egli (2006b) this corresponds to an average spacing of three particle diameters. The SD component of our mixtures is therefore a combination of intact chains and isolated magnetosomes (the UNISD end member), and collapsed chains of particles that still preserve their magnetosome membranes (the ISD end member). The mixing grids between the three end members are calculated using system (10), but we plot only the outer contours of these grids (continuous lines Figure 1a) in order not to unnecessarily clutter the diagram. For reference, a similar mixing grid, calculated at fraction increments of 0.1, is plotted in Figure 5a. We find that the ISD component in our synthetic samples comprises 60-75% of the total SD grains in the mixtures (shaded area in Figure 1b), compared to the 90% visual estimate of Kopp et al. (2006) from TEM analysis of samples with equivalent ARM ratios.

4.2 Lake sediments

4.2.1. Sedimentary units and chronology

European settlement in the Brownie Lake area began shortly after 1850. In the core it is expressed as a change in sedimentary characteristics at a depth of 65 cm, marking the boundary between the post-settlement sedimentary succession (Unit 1) and the pre-settlement sediments (Unit 2). Unit 1 (0-65 cm; ca. 1850-present) is a laminated clayey silt with authigenic calcite and diatoms. The laminae are discontinuous, and of variable thickness of up to 0.5 cm. Organic matter (mostly sapropel) and carbonate contents each average between 10-20% of the dry sedimentary matter. A tan sandy layer that occurs at 50 cm marks an artificial lowering of the water level in 1917, the year a canal connecting Brownie Lake with Cedar Lake to the south was completed. Unit 2 (65-140 cm; <1850) is a dark brown, massive, partly humic peat composed of terrestrial mosses and aquatic plants. Organic

matter fluctuates between 30-60%, while carbonate content is constant at ~5%. The chronology of the Lake Brownie core is based on the correlation with the ^{210}Pb dated core of Swain (1984). The correlation is drawn from organic matter concentration variations, and is aided by the recognition of marker horizons such as the 1917 sand lens.

4.2.2. Room temperature magnetic properties

Sediment-magnetic properties of the Brownie Lake core are presented in Figure 2, and the mean (m) and standard deviation (σ) of each parameter are listed for both sedimentary units in Table 1. The standard deviation was calculated for the detrended magnetic parameters, in order to remove variability introduced by long-term shifts in mean. In Table 1 is also computed the coefficient of variation (CV = σ/m) for each magnetic parameter within a sedimentary unit. The concentration-dependent parameters χ_{lf}, χ_a, M_{rs}, and M_s show higher variability in Unit 1 compared to Unit 2 (higher CVs), and a general increase in values with the decrease in depth in core over the past 150 years. In Unit 2 the concentration-dependent parameters exhibit a larger shift in mean to lower values, but the detrended variance is lower, indicating a steady decrease in concentration with time, up to the European settlement horizon. The concentration-independent magnetic parameters M_{rs}/M_s, χ_a/M_{rs}, and χ_f/M_s have weak increasing trends with decreasing depth in Unit 1. In Unit 2 M_{rs}/M_s and χ_a/M_{rs} have weak decreasing trends and lower variability than in Unit 1 (lower CV values), while χ_f/M_s has a weak increasing trend and slightly higher variability.

4.2.3. Suspended sediments

ARM and IRM profiles of the water filtrates are shown in Figure 3a, along with the DO profile. Oxygen concentrations are close to saturation values in the epilimnion (7.6-8 mg/l), but then decrease to 0.2 mg/l at 4m, with a maximum gradient between 2.5 and 3 m. At the depth of 3 m DO = 1.3 mg/l, and both ARM and IRM values are lowest in the profile. DO drops to 0.75 mg/l between 3 and 3.5 m, with a

simultaneous increase in ARM and IRM, which reach maximum values at 4m, immediately below the OAI. Below 4 m oxygen levels remain low, with a slight increase from 0.2 to 0.35 mg/l in the bottom waters. ARM and IRM are still elevated at 5 m, but decrease significantly below 5 m. The ARM ratio peaks (2.6-2.7·10^{-3} m/A) at the OAI (3.5-4 m), is lowest (<1·10^{-3} m/A) between 7-9 m, and has values of 1-1.5·10^{-3} m/A for the rest of the filtrates.

The biogenic contribution to both ARM and IRM was separated by coercivity component analysis from first derivatives of ARM and IRM demagnetization curves, using the fitting model proposed by Egli (2003, 2004). Figure 3b shows three coercivity components present below the OAI, each defined by two distribution parameters: median coercivity and dispersion. According to the definitions of Egli (2004) the low coercivity component comprises large detrital grains, and fine extracellular particles mediated by dissimilatory microorganisms (D); the intermediate coercivity component is identified as biogenic "soft" (BS), and the high coercivity component as biogenic "hard" (BH). The ARM ratio of each component is plotted in Figure 3c. The two biogenic components have maximum ARM ratios at the OAI (3.4·10^{-3} m/A for BS; 3.82·10^{-3} m/A for BH). Below the OAI BS decreases to <1·10^{-3} m/A at 8 m (where BH peaks at 3.2·10^{-3} m/A), and increases again towards the bottom (where BH <1·10^{-3} m/A). Integrating BS and BH remanences over the entire water column profile, we obtain average ARM ratios of 2.44·10^{-3} m/A for component BS, and for 2.13·10^{-3} m/A for component BH. The ARM and IRM values of the two biogenic components were respectively added for each sample in order to calculate an average biogenic ARM ratio (BS + BH in Figure 3c). At the OAI the ARM ratio of BS + BH is 3.47·10^{-3} m/A , while its integrated value over the water column is 2.36·10^{-3} m/A.

4.2.4. Total ferrimagnetic concentration

To calculate the total mass concentration of ferrimagnetic particles in a particular sample using equation (3), the nature of the ferrimagnetic carrier must first be identified. The low temperature magnetization experiments reveal the presence of

partially oxidized magnetite in both sedimentary units, with more pronounced maghemitization in Unit 2. Zero field cooled (ZFC) 10 K SIRM warming curves of typical samples for each sedimentary unit are shown in Figure 4a. The Unit 1 sample demagnetization rate is highest between 10 and 50 K, where ~30% of the SIRM is lost, decreases between 50 and 100 K (10% loss), increases again (20% loss) between 100 and 130 K through the Verwey transition (T_V), and is lowest between 130 and 300 K, interval in which only 10% more is lost. The remanence retained at room temperature is a little over 30%. By comparison, the Unit 2 sample memory is almost double. The initial remanence loss of this sample is steep but the magnitude of loss (~20%) is less than in Unit 1. This is followed by a decrease in demagnetization rate with a broad (%10 loss over 30K) but still distinct T_V, shifted to lower temperatures (80-110 K). Above T_V the demagnetization rate remains constant at ~7% per 100 K. The depressed and broadened T_V, shifted to lower temperature is a trait of non-stoichiometric magnetite, while remanence loss below and above T_V have also been attributed to magnetite oxidation in well characterized starting material (Özdemir et al., 1993). The degree of oxidation also dictates the magnitude of the demagnetization rate below and above T_V. The initial remanence loss is thus highest for surface oxidized magnetite particles, while severely maghemitized particles demagnetize at a higher rate above T_V (Özdemir and Dunlop, 2010). However, this remanence loss can also occur due to unblocking of magnetite SP particles during sample warming. To avoid the effect of superposition of the two phenomena, we examine the behavior of room temperature remanence during low temperature cycling (Figure 4b). Typical Unit 1 curves show a 1% increase in remanence with cooling from 300 to 250 K, followed by a loss of ~25% to T_V, and only a slight increase in remanence at temperatures lower than 70 K. The cooling curve is reversible from 10 to 60 K, temperature above which the remanence recovery is incomplete. Above T_V, the warming curve peaks around 170 K, followed by a steady decrease to room temperature. The total remanence recovery is above 75%. The Unit 2 cooling curve shows the same magnitude increase in remanence between 300 and 250 K, but is followed by a gradual decrease to 110 K corresponding to a remanence loss < 2%.

Below T_V there is a ~2% increase in remanence, which is reversible upon warming from 10 to 100 K. Above 100 K it steadily decreases to room temperature, first gradually to ~ 250 K and then more steeply from 250 to 300 K. Compared to the Unit 1 sample, only 5% of the room temperature SIRM is lost in the low temperature cycling process. According to Özdemir and Dunlop (2010) the hump-shaped cooling and warming curves above T_V, together with the high degree of room temperature remanence memory are diagnostic for magnetite in the advanced stages of maghemitization. Özdemir and Dunlop (2010) have also proposed a semi-quantitative method for estimating the oxidation parameter z (O'Reilly and Banerjee, 1967; Readman and O'Reilly, 1971), by comparing the room temperature memory loss (ΔM_c) with the difference in magnetization between 20 K and T_V (ΔM_m). Although this method has not been extensively tested on a range of particle size fractions (or mixtures thereof), it can be useful as a first-pass estimate of the degree of maghemitization (Özdemir and Dunlop, 2010). In our case, Unit 2 ΔM_c and ΔM_m values fall in the range of PSD magnetite characterized by z values of 0.8-0.9, whereas in Unit 1 the small ΔM_m value, determined by the predominance of a low coercivity MD component (Muxworthy et al., 2003), does not allow a comparison.

The room temperature Mössbauer spectrum of the surface sediment magnetic extract (Figure 4c) gives us a quantitative measure of maghemite concentration for Unit 1 in this case. The fitted parameters correspond to the sextets of hematite, maghemite, site A (tetrahedral) and site B (octahedral) of magnetite, and doublets of Fe^{2+} and Fe^{3+} (Figure 4c, Table 2). The B_{HF} of site A and B of magnetite, maghemite and hematite are in agreement with values from the literature and suggest iron phases without presence of foreign elements (e.g., Ti or Al substitutions) in their structure (Murad and Cashion, 2004). However, the magnetite site A/site B concentration ratio (Table 2) is higher than 0.5, showings some deviation from a stoichiometric form. The non-stoichiometry is interpreted as the combined effect of a stoichiometric magnetite core, a non-stoichiometric magnetite transition zone (characterized by a distribution of z), and an outer maghemite shell. The Fe^{2+} doublet is associated with paramagnetic minerals (e.g., iron phyllosilicates), and the Fe^{3+} doublets correspond to paramagnetic

iron minerals (wide Fe^{3+} doublet), as well as to superparamagnetic iron oxides (narrow Fe^{3+} doublet). If we consider only the magnetically ordered ferrimagnetic particles, then 91% of the iron is in contained in non-stoichiometric magnetite, and 9% is in maghemite. If we assume the SP fraction is entirely ferrimagnetic (i.e., no ferrihydrite) and fully oxidized, then only 81% of the iron is in contained in non-stoichiometric magnetite, and 19% is in maghemite. Since ΔM_c of Unit 1 samples is ~0.25, the average remanence ratio is 0.16 ± 0.02 (characteristic of generic PSD behavior), and room temperature SIRM memory is partially due to SD grains, an upper limit for z can be set at 0.5 for Unit 1, based on the model of Özdemir and Dunlop (2010). The Mössbauer-based calculation helps lower this upper limit to 0.3. The oxidation parameter is necessary for determining μ_{ferri} values for Units 1 and 2 from equation (4), where the two components considered are magnetite (μ_{Mt} = 92 Am^2/kg) and maghemite (μ_{Mh} = 74.3 Am^2/kg), and the weighing factor is none other than z, according to the quasi-linear relationship between z and either end-member fractions of the magnetite-maghemite oxidation series (Readman and O'Reilly, 1972). For Unit 1 we find an average ferrimagnetic component with μ_{ferri} = 88 Am^2/kg (corresponding to z = 0.3), while for Unit 2 the average μ_{ferri} = 78 Am^2/kg (z = 0.8). The total mass concentration of ferrimagnetic material (c_{ferri}) is obtained by normalizing bulk M_s measurements by the respective μ_{ferri} value (equation 3). Figure 4d shows c_{ferri} delimited by total ferrimagnetic mass concentration calculated as magnetite (lower limit) and maghemite (upper limit).

4.2.5. Concentration of remanence-carrying particles

The sedimentary MD, UNISD, and ISD components are modeled using system (9), which has been successfully tested on the synthetic mixtures. The choice for end-member component ratios is driven by the characteristics of the end-member components in the depositional environment examined.

The UNISD component comprises all SD particles or chains of particles that are isolated from other magnetic grains in the sediment matrix. These particles can

have various sources, but in lake sediments they are overwhelmingly biogenic (Egli et al., 2010). Lakes generally have diverse magnetotactic bacteria communities that live in specific geochemical conditions (Moskowitz et al., 2008), so it is expected that populations of magnetosomes originating in different environmental stress zones have characteristic magnetic properties, specifically the ratios used in this model. The magnetosomes present in our samples have been identified as non-stoichiometric magnetite, based on the Mössbauer analysis and the presence of Verwey transition in the low-temperature experiments. The remanence ratio of the UNISD component is therefore set to 0.5 (Stoner and Wohlfarth, 1948). The ARM ratio should reflect the average value of non-interacting magnetosomes and chains from all bacterial strains. Since it is difficult to identify all the species that produce magnetosomes in natural samples, and there is little data for wild strain magnetic properties, the choice of UNISD ARM ratio should be based on measurements of samples collected from the horizons inhabited by magnetotactic bacteria. The Brownie Lake water column ARM ratio of the integrated biogenic coercivity component peaks at the OAI (BS+BH in Figure 3c). The decrease of the ARM ratio with depth is partially due to the incipient breakdown during settling of some of the chains produced at the OAI, and partially due to possibly lower intrinsic ARM ratios of magnetosome chains produced by some of the strains in the low-oxygen layers (Egli, 2004). It is also plausible that some of low coercivity particles are non-interacting pedogenic particles that also have lower intrinsic ARM ratios (Geiss et al., 2008). Coercivity spectra deconvolution does not discriminate between interacting and non-interacting particles, but isolating the biogenic component in its immediate environment is the most important step in the process of choosing a representative ARM ratio for the UNISD. Based on the BS+BH ARM ratio value at the OAI, the habitat of magnetotactic bacteria, we use $(\chi_a/M_{rs})_{UNISD} = 3.5 \cdot 10^{-3}$ m/A in our model. The ISD end-member ratios were chosen to represent strongly interacting SD particles ($M_{rs}/M_s = 0.41$; $\chi_a/M_{rs} = 0.12 \cdot 10^{-3}$ m/A (Moskowitz et al., 1988)), e.g., clumps of collapsed magnetosomes from bacterial cells with totally degraded organic membranes, or washed-in pedogenic particle aggregates. The MD component end-member ratios ($M_{rs}/M_s = 0.05$; $\chi_a/M_{rs} = 0.1 \cdot 10^{-3}$ m/A)

represent average values for MD grains sensu lato (i.e., account for the presence PSD particles).

Figure 5 illustrates the modeling results. Bulk M_{rs}/M_s and χ_a/M_{rs} are compared to theoretical values in Figure 5a. A mixing grid is formed by the lines connecting the three end-member components (defined above), which are calculated using system (10). The fractions of the end members in each sample are plotted in a ternary diagram (Figure 5b), which is equivalent to the mixing grid, but in g_i coordinates. On average, Unit 1 samples contain 60-80% MD, 20-30% ISD, and <10% UNISD particles. Comparatively, pre-settlement samples contain only 30-50% MD grains, while ISD and UNISD end-members are well represented with 20-40% of the total ferrimagnetic mass each. In Figure 5c we plot results from eight model runs that used all possible combinations of the following end-member ratio pairs (M_{rs}/M_s, χ_a/M_{rs}), which represent boundaries defined for each component: (0.5, $3\cdot10^{-3}$ m/A) and (0.5, $4\cdot10^{-3}$ m/A) for UNISD, (0.41, $0.1\cdot10^{-3}$ m/A) and (0.45, $0.15\cdot10^{-3}$ m/A) for ISD, (0.01, $0.05\cdot10^{-3}$ m/A) and (0.05, $0.1\cdot10^{-3}$ m/A) for MD. The curves are mean g_i values of the model runs, and the length of the error bars is two standard deviations.

4.2.6. Concentration of SP particles

A broad distribution of particle sizes was inferred for the SP grains based on frequency dependence of susceptibility across the whole spectrum of measurement temperatures (Figure 6a). This implies that the χ_{SP} value to be used in equation (11) for the calculation of f_{SP} must be the average of SP susceptibilities over the entire range of SP volumes. We calculate χ_{SP} following Worm (1998), which assumes even coercivity distributions between 40 and 60 mT for of each grain size fraction. For a measurement frequency of 100 Hz, average χ_{SP} across the frequency-dependence interval is $4\cdot10^{-3}$ m^3/kg. χ_{nonSP} was calculated using an SD value of $0.4\cdot10^{-3}$ m^3/kg, and an MD value of $0.6\cdot10^{-3}$ m^3/kg (average values for nonstoichiometric magnetite; Dunlop and Özdemir (1997)), weighed by their respective fractions as obtained from system (9). SP fraction f_{SP} is plotted in Figure 6b (continuous line); Unit 1 SP fractions

are between 0.05 and 0.1, while Unit 2 values are in the interval 0.1-0.2. For comparison, dashed lines are f_{SP} curves calculated using χ_{SP} values of $3 \cdot 10^{-3}$ m^3/kg (higher values), and $5 \cdot 10^{-3}$ m^3/kg (lower values). Figure 6c illustrates the contributions of the SP and non-SP fractions to χ_{ferri}. The SP particles account for as much as 50% of χ_{ferri} in some intervals, even though their concentration is only ~10%.The non-SP baseline in Unit 1 has slightly higher values than in Unit 2 because of the prevalence of MD particles, but the average baseline value is equivalent to the one used by Hunt et al. (1995b). Support for our method is provided by the Mössbauer analysis of the magnetic extract. The SP concentration given by the narrow Fe^{3+} doublet in Figure 4c (representing paramagnetic and SP iron oxides) is 12% of the ferrimagnetic material (9% of total Fe). Given that not only ferrimagnetic SP material contributes to this doublet, this value should be taken as a maximum SP concentration. By comparison, our ferrimagnetic SP fraction calculation for the top 10-15 cm of the core (equivalent to the surface sample from which the extract was prepared) yields an average concentration of 8%.

4.2.7. Ferrimagnetic flux model

In the previous sections we have calculated the mass of ferrimagnetic material relative to the total dry sediment mass (Figure 4d), and the partition between its constituent components: UNISD, ISD, MD (Figure 5c), and SP (Figure 6b). Knowing the pre- and post-settlement sedimentation rates from the Brownie Lake age model (Swain, 1984), sediment density from core logging, and composition from LOI, the calculated mass fractions of the ferrimagnetic components can be expressed as sediment loads or fluxes (Figure 7) according to equations (7) and (8). The full interpretation of the temporal fluctuations of the ferrimagnetic components in terms of regional environmental and anthropogenic forcing factors will be discussed in detail elsewhere (Lascu et al., manuscript in preparation); however, a synopsis follows. The annual sedimentary ferrimagnetic flux before European settlement is fairly constant at 0.01-0.02 mg/cm^2, and is dominated by the SD and SP fractions (~70%). After 1850 the total flux steadily increases and by 1950 is an order of magnitude higher than in

pre-settlement times. This tenfold increase is observed in the MD, ISD, and SP components. The 1917 lake level lowering is marked by short-lived abrupt increase in sediment delivery from the surrounding catchment, marked in Figure 7 by peaks in the MD and ISD components. The annual UNISD flux is on the order of 2-6 $\mu g/cm^2$ before, and 4-12 $\mu g/cm^2$ after settlement, with the lowest values (<2 $\mu g/cm^2$) occurring in the eighteenth and nineteenth centuries. By comparison to the other components, whose fluxes are controlled by increased erosion rates, UNISD post-settlement values are only two times higher than in pre-settlement times, and are tied to an increase in nutrient delivery brought by anthropogenically-driven eutrophication of the lake in the twentieth century (Swain, 1984). The low UNISD values that predate the 1917 lake level lowering are interpreted as a sign of the reductive dissolution front migrating downwards into the sediment column after the establishment of meromictic conditions.

4.3 Discussion of modeling parameters selection

We here focus on the significance of the choice of modeling parameters in understanding ferrimagnetic components in their sedimentary context. The total ferrimagnetic mass calculation is based on M_s, an intrinsic property of ferromagnetic materials (Dunlop and Özdemir, 1997). The error associated with f_{ferri} (or c_{ferri}) is strictly related to the determination of ferrimagnetic mineralogy, and has a maximum value of 19% in the general case of non-stoichiometric magnetite (i.e., unknown oxidation parameter z). To decrease this error, low temperature magnetization curves and Mössbauer ^{57}Fe spectroscopy have been employed to narrow down possible z values for each of sedimentary unit. The low temperature magnetic behavior of Unit 1 samples and the Mössbauer analysis of the surface sample indicate that the magnetite is only oxidized at the particle surface. Brownie Lake has been meromicitic since the 1920s, having anoxic and reducing bottom waters that are rich in dissolved Fe^{2+} and Mn^{2+} (Swain, 1984; Tracey et al., 1996), an unfavorable environment for oxidation of magnetite particles. On the contrary, reductive dissolution can potentially remove SP nanoparticles and reduce the size of SD grains to SP (Anderson and Rippey, 1988;

Tarduno, 1995; Geiss et al., 2004). The magnetite particles must either have been already oxidized before deposition and have survived without being completely reduced, or underwent oxidation during the laboratory storage period of the core and samples, between collection and measurement. Before settlement, the lake water was only seasonally anoxic, complete mixing of epilimnetic and hypolimnetic waters occurring at spring and fall turnover events. Evidence for this can be inferred from the lake's reduced relative depth, the absence of annually-laminated sediments, higher sedimentary Fe/Mn ratio, and the presence of a diatom flora in a higher-trophic status (Swain, 1984; Tracey et al., 1996). Because of the more oxic conditions, and of the one order of magnitude lower sedimentation rate (Swain, 1984), Unit 2 ferrimagnetic particles are in a more advanced oxidation state. The average magnetic grain size is also lower than in Unit 1, which means an increased surface-to-volume ratio, making the grains more susceptible to oxidation. The choice of μ_{ferri} for each unit was therefore determined by a combination of sediment-magnetic characteristics and evidence of limnological conditions at the time of deposition.

The remanence-carrying components have been modeled by way of a three-component mixing model, using specific end-member values for remanence and ARM ratios. According to our model, bulk M_{rs}/M_s and χ_a/M_{rs} of a sample can be translated into mass fractions for each component considered, here UNISD, ISD and MD. The basis for defining these particular components is the ability of the two ratios to discriminate between grain-size categories (M_{rs}/M_s) and inter-particle interactions (χ_a/M_{rs}). A judicious choice of end-member ratios will result in lower model errors. The components for Brownie Lake were defined with the knowledge that lake sediments in temperate-climate areas are characterized by a mixture of detrital and endogenic magnetic particles (Snowball et al., 2002; Geiss et al., 2003; Egli, 2004), and that nonstoichiometric magnetite is the ferrimagnetic carrier in our sediments. The detrital fraction is generally dominated by MD particles, but can also contain finer SD and SP grains (e.g., of pedogenic origin). The MD component sensu stricto (no PSD grains) has low remanence and ARM ratio values ($M_{rs}/M_s < 0.05$, $\chi_a/M_{rs} \sim 0.1 \cdot 10^{-3}$

m/A). A PSD end member would have a higher remanence ratio (e.g., 0.2 for 1 μm grains), but a similar ARM ratio. We use the cutoff M_{rs}/M_s value of 0.05 (Day et al., 1977; Dunlop, 2002) as an average in our model, in order to incorporate the effects of both true MD and PSD grains. This value corresponds to an average grain size of ~20 μm (Yu et al., 2002). The 0.01 M_{rs}/M_s value used in the error estimation for the MD component (g_3 in Figure 5c) corresponds to much larger particles (~100-200 μm) (Day et al., 1977; Dunlop, 2002), and would be a limit case. The detrital SD grains can be transported into a depositional basin either independently through sorting, or in most cases as part of clay/organic matter aggregates that also contain larger ferrimagnetic particles. In both situations the SD particles are disturbed to a certain extent from their original configuration (e.g., dispersion in a soil matrix). It is then reasonable to assume that they contribute to both ISD and UNISD end members. The ISD component is characterized by SD-like remanence ratios, and MD-like ARM ratios, and was defined to represent the extreme case of strong interactions between SD particles clumped in aggregates (Moskowitz et al., 1993; Kopp et al., 2006). Both detrital (e.g., pedogenic) and endogenic (biogenic and inorganic) SD particles that occur in such closely-packed configurations are expected to contribute to ISD. The UNISD component is designed to include only isolated grains or undisturbed linear chains of bacterial magnetosomes (Yamazaki, 2008; Egli et al., 2010). The remanence ratio for magnetite UNISD particles is 0.5 by definition (Stoner and Wohlfarth, 1948). For greigite magnetosomes the remanence ratio usually exceeds 0.5, approaching a theoretical value of 0.83 as H_{cr}/H_c approaches unity, due to a (100) easy axis of magnetization and the prevalence of magnetocrystalline anisotropy over shape anisotropy (e.g., Roberts, 1995; Sagnotti and Winkler, 1999; Chang et al., 2009). The ARM ratio of UNISD can be determined with the help of coercivity deconvolution of samples harvested from the OAI, by calculating the ARM ratio of the biogenic coercivity-spectrum component ($3.5 \cdot 10^{-3}$ m/A in our model). The biogenic component defined by its coercivity is likely to include interacting particles from magnetosome clusters and bundled or collapsed chains (Egli et al., 2010), which can artificially lower $(\chi_a/M_{rs})_{UNISD}$. On the other hand, the detrital coercivity-spectrum component may include non-interacting particles with

lower initial ARM ratios (e.g., $1\text{-}3\cdot10^{-3}$ m/A for pedogenic particles (Egli, 2004; Geiss et al., 2008)), which should truly lower $(\chi_a/M_{rs})_{UNISD}$. Our error estimation for the UNISD end member (g_1 in Figure 5c) was based on ARM ratios in the interval $3\text{-}4\cdot10^{-3}$ m/A. The error is higher for Unit 2 samples, indicating that the choice of ARM ratio for the UNISD component is more critical for finer grained magnetic assemblages.

The SP component fraction is modeled using the ferrimagnetic susceptibility χ_{ferri} (derived from χ_f/M_s) by subtracting the non-SP baseline susceptibility (Hunt et al., 1995b). The critical parameter in the calculation of f_{SP} is the susceptibility of the SP ferrimagnetic grains, which can vary over an order of magnitude with SP grain size (Worm, 1998). Frequency-dependent susceptibility measurements across a range of temperatures are therefore necessary to characterize the SP particle size distribution, as a preliminary step for calculating a representative χ_{SP}. Sediments usually comprise magnetic particles characterized by a wide grain-size distribution in the SP realm (Dearing et al., 1996), so an average χ_{SP} value calculated over the SP size spectrum is a reasonable assumption in most cases. This approach is preferred to the traditional room-temperature susceptibility measurements at two frequencies (χ_{fd} parameter), which captures only a narrow interval of the grain-size distribution curve.

5. Conclusions

We provide a quantitative model for calculating the concentrations of ferrimagnetic sedimentary components using rock magnetic properties. The quantification method is based mainly on bulk room-temperature measurements, and translates raw magnetic parameters into ferrimagnetic mass concentrations. This method eliminates dilution effects on magnetic properties by weakly magnetic substances in high concentrations, such as water, organic matter, carbonates, clay minerals, etc., and allows the calculation of ferrimagnetic particle fluxes for dated sedimentary sequences. It can be applied for reconstructing past environmental changes in a range of sedimentary environments, and is particularly useful for large sets of samples, where detailed magnetic unmixing methods (especially low-temperature techniques) are unfeasible due to time or instrument constraints.

Total ferrimagnetic concentration is most accurately determined from in-field magnetization measurements. Saturation magnetization corrected for non-ferrimagnetic contributions (M_s) is the most reliable parameter, only ferrimagnetic mineralogy being needed for concentration calculations. Susceptibility-based concentrations are less reliable because they require a priori knowledge about ferrimagnetic grain size and shape in addition to magnetic mineralogy. Remanence measurements are useful as concentration proxies only when magnetic composition is uniform with respect to mineralogy and grain size, due to the varying degree of remanence acquisition efficiency for different categories of magnetic particles.

Anhysteretic and saturation isothermal remanences are used here to model the concentrations of the remanence-carrying ferrimagnetic fractions via a three-component mixing model, which is tested on mixtures of SD and non-SD magnetite grains of know concentrations. The use of the ARM ratio (χ_a/M_{rs}) as a proxy for inter-particle magnetostatic interactions allows the separation of SD particles into two separate components (UNISD and ISD), which may have independent origins. The remanence ratio (M_{rs}/M_s) is a true grain-size indicator, whereas χ_a/M_{rs} should be used in that capacity only when the proportion of interacting particles is constant.

For a robust quantification of the superparamagnetic fraction, we propose a technique that corroborates ferrimagnetic susceptibility calculations with information about the SP particle size distribution obtained from the frequency and temperature dependence of magnetic susceptibility. This approach is recommended, when possible, in lieu of frequency-dependent susceptibility measurements at room temperature only.

References

Anderson, N. J., and B. Rippey (1988), Diagenesis of magnetic minerals in the recent sediments of a eutrophic lake, Limnol. Oceanogr., 33, 1476-1492.

Bleil, U., and T. von Dobeneck (2004), Late Quaternary terrigenous sedimentation in the western Equatorial Atlantic: South American versus African provenance discriminated by magnetic mineral analysis, in The South Atlantic in the late Quaternary: reconstruction of material budgets and current systems, edited by G. Wefer, S. Mulitza and V. Ratmeyer, pp. 213-236, Springer-Verlag, Berlin, Germany.

Brand, R.A., 1987. Improving the validity of hyperfine field distributions from metallic alloys. Part I: unpolarized source. Nucl. Instr. Meth. B, 28, 398-405.

Carter-Stiglitz, B., B. Moskowitz, and M. Jackson (2001), Unmixing magnetic assemblages and the magnetic behavior of bimodal mixtures, J. Geophy. Res., 106(B11), 26,397-26,411, doi: 10.1029/2001JB000417.

Chang, L., A. P. Roberts, Y. Tang, B. D. Rainford, A. R. Muxworthy, and Q. W. Chen (2008), Fundamental magnetic parameters from pure synthetic greigite (Fe_3S_4), J. Geophy. Res., 113, B06104, doi: 10.1029/2007JB005502.

Chang, L., A. P. Roberts, C. J. Rowan, Y. Tang, P. Pruner, Q. Chen, and C. Horng (2009), Low-temperature magnetic properties of greigite (Fe_3S_4), Geochem. Geophys. Geosyst., 10, Q01Y04, doi: 10.1029/2008GC002276.

Day, R., M. Fuller, and V. A. Schmidt (1977), Hysteresis properties of titanomagnetites: grain-size and compositional dependence, Phys. Earth Planet. Inter., 13, 260-267.

Dean, W. E. (1974), Determination of carbonate and organic matter in calcareous sediments and sedimentary rocks by loss on ignition; comparison with other methods, J. Sediment. Petrol., 44, 242-248, doi: 10.1306/74D729D2-2B21-11D7-8648000102C1865D.

Dearing, J. A. (1999a), Holocene environmental change from magnetic proxies in lake sediments, in Quaternary climates, environments and magnetism, edited by B.

A. Maher and R. Thompson, pp 231-278, Cambridge University Press, Cambridge, UK.

Dearing, J. A. (1999b), Magnetic susceptibility, in Environmental Magnetism: a practical guide, edited by J. Walden, F. Oldfield and J. P. Smith, pp. 35-53, Quaternary Research Association, London, UK.

Dearing, J. A., R. J. L. Dann, K. Hay, J. A. Lees, P. J. Loveland, B. A. Maher, and K. O'Grady (1996), Frequency-dependent susceptibility measurements of environmental materials, Geophysical Journal International, 124, 228-240.

Dearing, J. A., J. F. Boyle, P. G. Appleby, A. W. Mackay, and R. J. Flower (1998), Magnetic properties of recent sediments in Lake Baikal, Siberia; Lake Baikal paleolimnology, J. Paleolimnol., 20, 163-173.

Demory, F., H. Oberhaensli, N. R. Nowaczyk, M. Gottschalk, R. Wirth, and R. Naumann (2005), Detrital input and early diagenesis in sediments from Lake Baikal revealed by rock magnetism, Global Planet. Change, 46, 145-166, doi: 10.1016/j.gloplacha.2004.11.010.

Dunlop, D. J. (2002), Theory and application of the Day plot (M_{rs}/M_s versus H_{cr}/H_c): 1. Theoretical curves and tests using titanomagnetite data, J. Geophy. Res., 107(B3), 22, doi: 10.1029/2001JB000486.

Dunlop, D. J., and B. Carter-Stiglitz (2006), Day plots of mixtures of superparamagnetic, single-domain, pseudosingle-domain, and multidomain magnetites, J. Geophy. Res., 111(B12), doi: 10.1029/2006JB004499.

Dunlop, D. J., and Ö. Özdemir (1997), Rock magnetism: fundamentals and frontiers, 573 pp., Cambridge University Press, Cambridge, UK.

Egli, R. (2003), Analysis of the field dependence of remanent magnetization curves, J. Geophy. Res., 108(B2), 25, doi: 10.1029/2002JB002023.

Egli, R. (2004), Characterization of individual rock magnetic components by analysis of remanence curves: 1. Unmixing natural sediments, Stud. Geophys. Geod., 48, 391-446.

Egli, R. (2006a), Theoretical aspects of dipolar interactions and their appearance in first-order reversal curves of thermally activated single-domain particles, J. Geophy. Res., 111(B12), doi: 10.1029/2006JB004567.

Egli, R. (2006b), Theoretical considerations on the anhysteretic remanent magnetization of interacting particles with uniaxial anisotropy, J. Geophy. Res., 111(B12), doi: 10.1029/2006JB004577.

Egli, R., and W. Lowrie (2002), Anhysteretic remanent magnetization of fine magnetic particles, J. Geophy. Res., 107(B10), 21, doi: 10.1029/2001JB000671.

Egli, R., A. P. Chen, M. Winklhofer, K. P. Kodama, and C.-S. Horng (2010), Detection of noninteracting single domain particles using first-order reversal curve diagrams, Geochem. Geophys. Geosyst., 11, Q01Z11, doi: 10.1029/2009GC002916.

Evans, M. E., and F. Heller (2003), Environmental magnetism: principles and applications of enviromagnetics, 299 pp., Academic Press, San Diego, USA.

Frank, U., and N. R. Nowaczyk (2008), Mineral magnetic properties of artificial samples systematically mixed from haematite and magnetite, Geophys. J. Int., 175, 449-461, doi: 10.1111/j.1365-246X.2008.03821.x.

Frederichs, T., U. Bleil, K. Daeumler, T. von Dobeneck, and A. M. Schmidt (1999), The magnetic view on the marine paleoenvironment; parameters, techniques and potentials of rock magnetic studies as a key to paleoclimatic and paleoceanographic changes, in Use of proxies in paleoceanography; examples from the South Atlantic, edited by G. Fischer and G. Wefer, pp. 575-599, Springer, Berlin, Germany.

Funk, J. A., T. von Dobeneck, T. Wagner, and S. Kasten (2004), Late Quaternary sedimentation and early diagenesis in the Equatorial Atlantic Ocean; patterns, trends and processes deduced from rock magnetic and geochemical records, in The South Atlantic in the late Quaternary; reconstruction of material budgets and current systems, edited by G. Wefer, S. Mulitza and V. Ratmeyer, pp. 461-497, Springer-Verlag, Berlin, Germany.

Geiss, C. E., and S. K. Banerjee (1997), A multi-parameter rock magnetic record of the last glacial-interglacial paleoclimate from south-central Illinois, USA, Earth Planet. Sci. Lett., 152, 203-216.

Geiss, C. E., and S. K. Banerjee (1999), Comparison of two interglacial records from the midwestern U.S.A: Rock magnetism, palaeomagnetism and environmental magnetism, Phys. Chem. Earth A, 24, 793-798.

Geiss, C. E., and C. W. Zanner (2006), How abundant is pedogenic magnetite? Abundance and grain size estimates for loessic soils based on rock magnetic analyses, J. Geophy. Res., 111(B12), doi: 10.1029/2006JB004564.

Geiss, C. E., R. Egli, and C. W. Zanner (2008), Direct estimates of pedogenic magnetite as a tool to reconstruct past climates from buried soils, Journal of Geophysical Research, 113, B11102, doi: 10.1029/2008JB005669.

Geiss, C. E., C. E. Umbanhowar, P. Camill, and S. K. Banerjee (2003), Sediment magnetic properties reveal Holocene climate change along the Minnesota prairie-forest ecotone; Lake basins as archives of continental tectonics and paleoclimate, J. Paleolimnol., 30, 151-166.

Geiss, C. E., S. K. Banerjee, P. Camill, and C. E. Umbanhowar (2004), Sediment-magnetic signature of land-use and drought as recorded in lake sediment from south-central Minnesota, USA, Quat. Res., 62, 117-125, doi: 10.1016/j.yqres.2004.06.009.

Gibbs-Eggar, Z., B. Jude, J. Dominik, J. Loizeau, and F. Oldfield (1999), Possible evidence for dissimilatory bacterial magnetite dominating the magnetic properties of Recent lake sediments, Earth Planet. Sci. Lett., 168, 1-6.

Haltia-Hovi, E., N. Nowaczyk, T. Saarinen, and B. Plessen (2010), Magnetic properties and environmental changes recorded in Lake Lehmilampi (Finland) during the Holocene, J. Paleolimnol., 43, 1-13, doi: 10.1007/s10933-009-9309-8.

Heiri, O., A. F. Lotter, and G. Lemcke (2001), Loss on ignition as a method for estimating organic and carbonate content in sediments; reproducibility and comparability of results, J. Paleolimnol., 25, 101-110.

Heslop, D., M. J. Dekkers, P. P. Kruiver, and I. H. M. van Oorschot (2002), Analysis of isothermal remanent magnetization acquisition curves using the expectation-maximization algorithm, Geophys. J. Int., 148, 58-64.

Hunt, C. P., and S. K. Banerjee (1992), Thermal demagnetization of low-temperature SIRM: a new method for magnetic granulometry, EOS Trans. Am. Geophys. Union, 73, 138.

Hunt, C. P., B. M. Moskowitz, and S. K. Banerjee (1995a), Magnetic properties of rocks and minerals, in Rock Physics and Phase Relations: a Handbook of Physical Constants, edited by Ahrens, T. J., pp. 189-204, AGU, Washington DC, USA.

Hunt, C. P., S. K. Banerjee, J. Han, P. A. Solheid, E. Oches, W. Sun, and T. Liu (1995b), Rock-magnetic proxies of climate change in the loess-Palaeosol sequences of the western Loess Plateau of China, Geophys. J. Int., 123, 232-244.

Kim, B. Y., K. P. Kodama, and R. E. Moeller (2005), Bacterial magnetite produced in water column dominates lake sediment mineral magnetism: Lake Ely, USA, Geophys. J. Int., 163, 26-37, doi: 10.1111/j.1365-246X.2005.02735.x.

Kopp, R. E., C. Z. Nash, A. Kobayashi, B. P. Weiss, D. A. Bazylinski, and J. L. Kirschvink (2006), Ferromagnetic resonance spectroscopy for assessment of magnetic anisotropy and magnetostatic interactions; a case study of mutant magnetotactic bacteria, J. Geophy. Res., 111(B12), doi: 10.1029/2006JB004529.

Kruiver, P. P., M. J. Dekkers, and D. Heslop (2001), Quantification of magnetic coercivity components by the analysis of acquisition curves of isothermal remanent magnetisation, Earth Planet. Sci. Lett., 189, 269-276.

Larrasoaña, J. C., A. P. Roberts, R. J. Musgrave, E. Gracia, E. Pinero, M. Vega, and F. Martinez-Ruiz (2007), Diagenetic formation of greigite and pyrrhotite in gas hydrate marine sedimentary systems, Earth Planet. Sci. Lett., 261, 350-366, doi: 10.1016/j.epsl.2007.06.032.

Lees, J. A. (1997), Mineral magnetic properties of mixtures of environmental and synthetic materials; linear additivity and interaction effects, Geophys. J. Int., 131, 335-346.

Moskowitz, B. M., R. B. Frankel, and D. A. Bazylinski (1993), Rock magnetic criteria for the detection of biogenic magnetite, Earth Planet. Sci. Lett., 120, 283-300.

Moskowitz, B. M., D. A. Bazylinski, R. Egli, R. B. Frankel, and K. J. Edwards (2008), Magnetic properties of marine magnetotactic bacteria in a seasonally stratified coastal pond (Salt Pond, MA, USA), Geophys. J. Int., 174, 75-92, doi: 10.1111/j.1365-246X.2008.03789.x.

Murad, E. and J. Cashion (2004), Mössbauer spectroscopy of environmental materials and their industrial utilization. Kluwer, Boston, USA

Muxworthy, A. R., D. J. Dunlop, and Ö. Özdemir (2003), Low-temperature cycling of isothermal and anhysteretic remanence; microcoercivity and magnetic memory, Earth Planet. Sci. Lett., 205, 173-184.

Néel, L. (1949), Théorie du traînage magnétique des ferromagnétiques en grains fins avec applications aux terres cuites, Ann. Geophys., 5, 99-136.

Nowaczyk, N. R. (2001), Logging of magnetic susceptibility, in Tracking environmental change using lake sediments; Volume 1, Basin analysis, coring, and chronological techniques, edited by W. M. Last and J. P. Smol, pp. 155-170, Kluwer, Dordrecht, Netherlands.

Oldfield, F., R. Wake, J. Boyle, R. Jones, S. Nolan, Z. Gibbs, P. Appleby, E. Fisher, and G. Wolff (2003), The late-Holocene history of Gormire Lake (NE England) and its catchment: a multiproxy reconstruction of past human impact, The Holocene, 13, 677-690, doi: 10.1191/0959683603hl64rp.

O'Reilly, W., and S. K. Banerjee (1967), The mechanism of oxidation in titanomagnetites: a magnetic study, Mineralogical Magazine, 36, 29-37.

Ortega, B., M. Caballero, S. Lozano, G. Vilaclara, and A. Rodriguez (2006), Rock magnetic and geochemical proxies for iron mineral diagenesis in a tropical lake; Lago Verde, Los Tuxtlas, east-central Mexico, Earth Planet. Sci. Lett., 250, 444-458, doi: 10.1016/j.epsl.2006.08.020.

Özdemir, Ö., and D. J. Dunlop (2010), Hallmarks of maghemitization in low-temperature remanence cycling of partially oxidized magnetite nanoparticles, J. Geophys. Res., 115, B02101, doi: 10.1029/2009JB006756.

Özdemir, Ö., D. J. Dunlop, and B. M. Moskowitz (1993), The effect of oxidation on the Verwey transition in magnetite, Geophys. Res. Lett., 20, 1671-1674, doi: 10.1029/93GL01483.

Paasche, O., R. Lovlie, S. O. Dahl, J. Bakke, and A. Nesje (2004), Bacterial magnetite in lake sediments: late glacial to Holocene climate and sedimentary changes in Northern Norway, Earth Planet. Sci. Lett., 223, 319-333, doi: 10.1016/j.epsl.2004.05.001.

Peck, J. A., and J. W. King (1996), Magnetofossils in the sediment of Lake Baikal, Siberia, Earth Planet. Sci. Lett., 140, 159-172.

Peters, C., and M. J. Dekkers (2003), Selected room temperature magnetic parameters as a function of mineralogy, concentration and grain size, Phys. Chem. Earth, 28, 659-667, doi: 10.1016/S1474-7065(03)00120-7

Readman, P. W., and W. O'Reilly (1971), Oxidation Processes in Titanomagnetites, Z. Geophys., 37, 329-338.

Readman, P. W., and W. O'Reilly (1972), Magnetic Properties of Oxidized (Cation-Deficient) Titanomagnetites $(Fe,Ti)_3O_4$, J. Geomagn. and Geoel., 24, 69-90.

Reynolds, R. L., J. G. Rosenbaum, J. Rapp, M. W. Kerwin, P. J. Bradbury, S. Colman, and D. Adam (2004), Record of Late Pleistocene Glaciation and Deglaciation in the Southern Cascade Range. I. Petrological Evidence from Lacustrine Sediment in Upper Klamath Lake, Southern Oregon, J. Paleolimnol., 31, 217-233, doi: 10.1023/B:JOPL.0000019230.42575.03.

Roberts, A. P. (1995), Magnetic properties of sedimentary greigite (Fe_3S_4), Earth Planet. Sci. Lett., 134, 227-236.

Roberts, A. P., C. R. Pike, and K. L. Verosub (2000), First-order reversal curve diagrams; a new tool for characterizing the magnetic properties of natural samples, J. Geophy. Res., 105(B12), 28,461-28,475, doi: 10.1029/2000JB900326.

Robertson, D. J., and D. E. France (1994), Discrimination of remanence-carrying minerals in mixtures, using isothermal remanent magnetisation acquisition curves, Phys. Earth Planet. Inter., 82, 223-234.

Rochette, P. (1987), Magnetic susceptibility of the rock matrix related to magnetic fabric studies, J. Struct. Geol., 9, 1015-1020.

Rosenbaum, J. G., and R. L. Reynolds (2004a), Record of Late Pleistocene Glaciation and Deglaciation in the Southern Cascade Range. II. Flux of Glacial Flour in a Sediment Core from Upper Klamath Lake, Oregon, J. Paleolimnol., 31, 235-252, doi: 10.1023/B:JOPL.0000019229.75336.7a.

Rosenbaum, J. G., and R. L. Reynolds (2004b), Basis for Paleoenvironmental Interpretation of Magnetic Properties of Sediment from Upper Klamath Lake (Oregon): Effects of Weathering and Mineralogical Sorting, J. Paleolimnol., 31, 253-265, doi: 10.1023/B:JOPL.0000019228.46421.f4.

Rosenbaum, J. G., R. L. Reynolds, D. P. Adam, J. Drexler, A. M. Sarna-Wojcicki, and G. C. Whitney (1996), Record of middle Pleistocene climate change from Buck Lake, Cascade Range, southern Oregon; evidence from sediment magnetism, trace-element geochemistry, and pollen, Geol. Soc. Am. Bull., 108, 1328-1341, doi: 10.1130/0016-7606(1996)108<1328:ROMPCC>2.3.CO;2.

Sagnotti, L., and A. Winkler (1999), Rock magnetism and palaeomagnetism of greigite-bearing mudstones in the Italian peninsula, Earth Planet. Sci. Lett., 165, 67-80.

Snowball, I. F. (1994), Bacterial magnetite and the magnetic properties of sediments in a Swedish lake, Earth Planet. Sci. Lett., 126, 129-142.

Snowball, I., P. Sandgren, and G. Petterson (1999), The mineral magnetic properties of an annually laminated Holocene lake-sediment sequence in northern Sweden, Holocene, 9, 353-362, doi: 10.1191/095968399670520633.

Snowball, I., L. Zillen, and P. Sandgren (2002), Bacterial magnetite in Swedish varved lake-sediments; a potential bio-marker of environmental change, Quat. Int., 88, 13-19.

Stoner, E. C., and E. P. Wohlfarth (1948), A Mechanism of Magnetic Hysteresis in Heterogeneous Alloys, Phil. Trans. R. Soc. Lond. A, 240, 599-642, doi: 10.1098/rsta.1948.0007.

Swain, E. B. (1984), The paucity of blue-green algae in meromictic Brownie Lake; iron limitation or heavy metal toxicity? Ph.D. thesis, University of Minnesota, Twin Cities, MN, USA.

Tarduno, J. A. (1995), Superparamagnetism and reduction diagenesis in pelagic sediments: enhancement or depletion? Geophys. Res. Lett., 22, 1337-1340, doi: 10.1029/95GL00888.

Tracey, B., N. Lee, V. Card, and L. C. K. Shane (1996), Sediment indicators of meromixis; comparison of laminations, diatoms, and sediment chemistry in Brownie Lake, Minneapolis, USA, J. Paleolimnol., 15, 129-132.

van der Post, K. D., F. Oldfield, E. Y. Haworth, P. R. J. Crooks, and P. G. Appleby (1997), A record of accelerated erosion in the Recent sediments of Blelham Tarn in the English Lake District, J. Paleolimnol., 18, 103-120.

von Dobeneck, T. (1998), The concept of partial susceptibilities, Geol. Carpath., 49, 228-229.

Worm, H. (1998), On the superparamagnetic-stable single domain transition for magnetite, and frequency dependence of susceptibility, Geophys. J. Int., 133, 201-206.

Xie, Q., T. Chen, H. Xu, J. Chen, J. Ji, H. Lu, and X. Wang (2009), Quantification of the contribution of pedogenic magnetic minerals to magnetic susceptibility of loess and paleosols on Chinese Loess Plateau: Paleoclimatic implications, J. Geophys. Res., 114, B09101, doi:10.1029/2008JB005968.

Xie, S., J. A. Dearing, and J. Bloemendal (1999), A partial susceptibility approach to analysing the magnetic properties of environmental materials: a case study, Geophys. J. Int., 138, 851-856.

Yamazaki, T. (2008), Magnetostatic interactions in deep-sea sediments inferred from first-order reversal curve diagrams: implications for relative paleointensity

normalization, Geochem. Geophys. Geosyst., 9, Q02005, doi: 10.1029/2007GC001797.

Yu, Y., D. J. Dunlop, and Ö. Özdemir (2002), Partial anhysteretic remanent magnetization in magnetic: 1. Additivity, J. Geophy. Res., 107(B10), doi: 10.1029/2001JB001249.

Zillen, L., and I. Snowball (2009), Complexity of the 8 ka climate event in Sweden recorded by varved lake sediments, Boreas, 38, 493-503, doi: 10.1111/j.1502-3885.2009.00086.x.

Figures

Figure 1. a) Cross plot of M_{rs}/M_s versus χ_a/M_{rs} for MD-SD (diamonds) and PSD-SD (circles) mixtures. Number next to each symbol represents fraction SD component added to mixture. Mixing lines (dashed) for theoretical mixtures of two end members were calculated using a nil fraction for the third component in system (10). The symbols on the mixing lines represent theoretical values of M_{rs}/M_s and χ_a/M_{rs} calculated at fraction increments of 0.1. The continuous lines are outer contours of mixing grids calculated for three end members, where the SD component was subdivided into UNISD and ISD (see text for discussion of end-member ratios); b) Ternary diagram of calculated fractions for each component (UNISD, ISD, and MD or PSD) of the synthetic mixtures, according to the three end-member mixing model (g_i are solutions to the system of equations). Shaded area is the interval 60-75% interacting component in a ISD-UNISD mixture; c) Inverted fractions of end members UNISD, ISD, and MD (left) or PSD (right) versus fractions SD (top) and MD (bottom) added to each mixture.

Figure 2. Bulk magnetic properties of the Brownie Lake sediment core: ARM susceptibility χ_a, low-field susceptibility χ_{lf}, saturation remanence M_{rs}, saturation magnetization M_s, ARM ratio χ_a/M_{rs}, remanence ratio M_{rs}/M_s, and χ_f/M_s. The magnetic parameters define two sediment-magnetic units (separated by dashed line): Unit 1 (1850-present) and Unit 2 (<1850).

Figure 3. Magnetic properties of filtered water samples collected from Brownie Lake. a) Profiles of dissolved oxygen, ARM, IRM, and ARM ratio; b) Component analysis of ARM (diamonds) and IRM (squares) demagnetization curves showing three components defined by median coercivity and distribution width: D (detrital + dissimilatory), BS (biogenic “soft”), and BH (biogenic “hard”); c) ARM ratio of the bulk filtrates, individual components, and total biogenic contribution (BS+BH).

Figure 4. a) Thermal demagnetization of SIRM applied at 10 K after ZFC treatment of representative samples from the two sedimentary units; b) behavior of room-temperature SIRM with cooling to 10 K and warming back 300 K for the same

samples; c) ^{57}Fe Mössbauer spectrum of magnetic extract from the surface sediment; d) Time series of total ferrimagnetic concentration by mass (c_{ferri}) on a water-free basis: thick line represents solution of equation (10) with μ_{ferri} = 88 Am^2/kg for Unit 1 and 78 Am^2/kg for Unit 2, thin lines are solutions calculated for magnetite (lower bound) and maghemite (upper bound) and delimit a solution space for c_{ferri} considering the entire range of z (0,1).

Figure 5. a) Cross plot of M_{rs}/M_s versus χ_a/M_{rs} for Brownie Lake Units 1 (triangles) and 2 (dots). Theoretical values for bulk ratios were calculated from system (10) at 0.1 fraction increments of end-member components (see text for end-member ratio values); b) Ternary diagram of calculated fractions for each component (UNISD, ISD, and MD or PSD) in Brownie Lake sediments, according to the three end-member mixing model (g_i are solutions to system 9); c) Time series of end-member component fractions for model runs with eight different end-member combinations. Lines represent mean values, and uncertainty bars are two standard deviations in length (see text for error calculation method).

Figure 6. a) Frequency and temperature dependence of susceptibility for representative samples of each sedimentary unit. Both samples are frequency dependent in the interval 30-300 K, indicating a broad SP grain size distribution; b) SP fraction calculated for $\chi_{SP} = 4 \cdot 10^{-3}$ m^3/kg (thick line), bracketed by calculations for χ_{SP} values of $5 \cdot 10^{-3}$ m^3/kg (left), and $3 \cdot 10^{-3}$ m^3/kg (right); c) SP and non-SP contributions to χ_{ferri}.

Figure 7. Model of annual ferrimagnetic flux of UNISD, ISD, MD, and SP particles in Brownie Lake (note that Units 1 and 2 are plotted on separate axes).

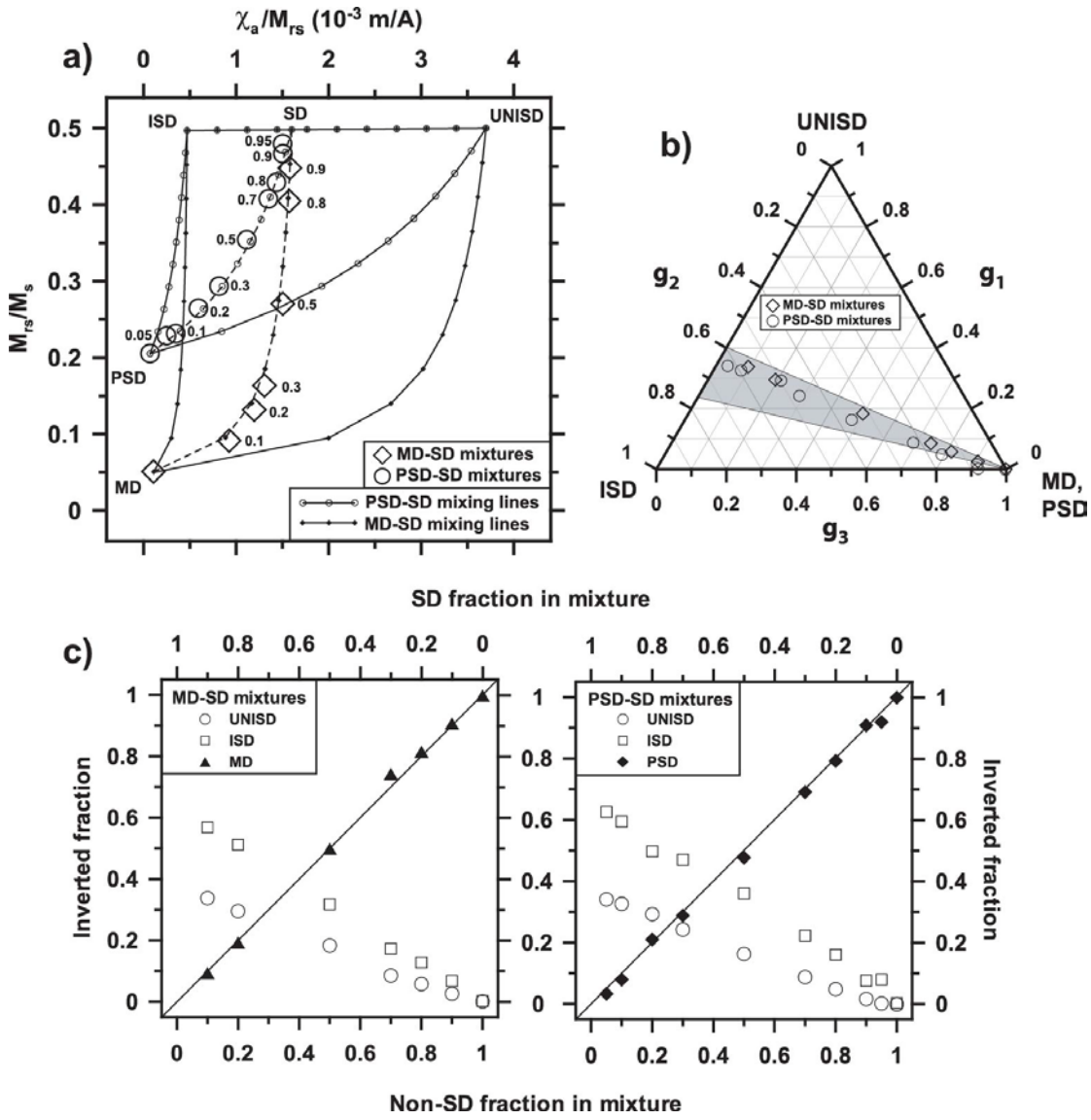

Figure 2.1 Modeling synthetic mixtures of magnetic particles

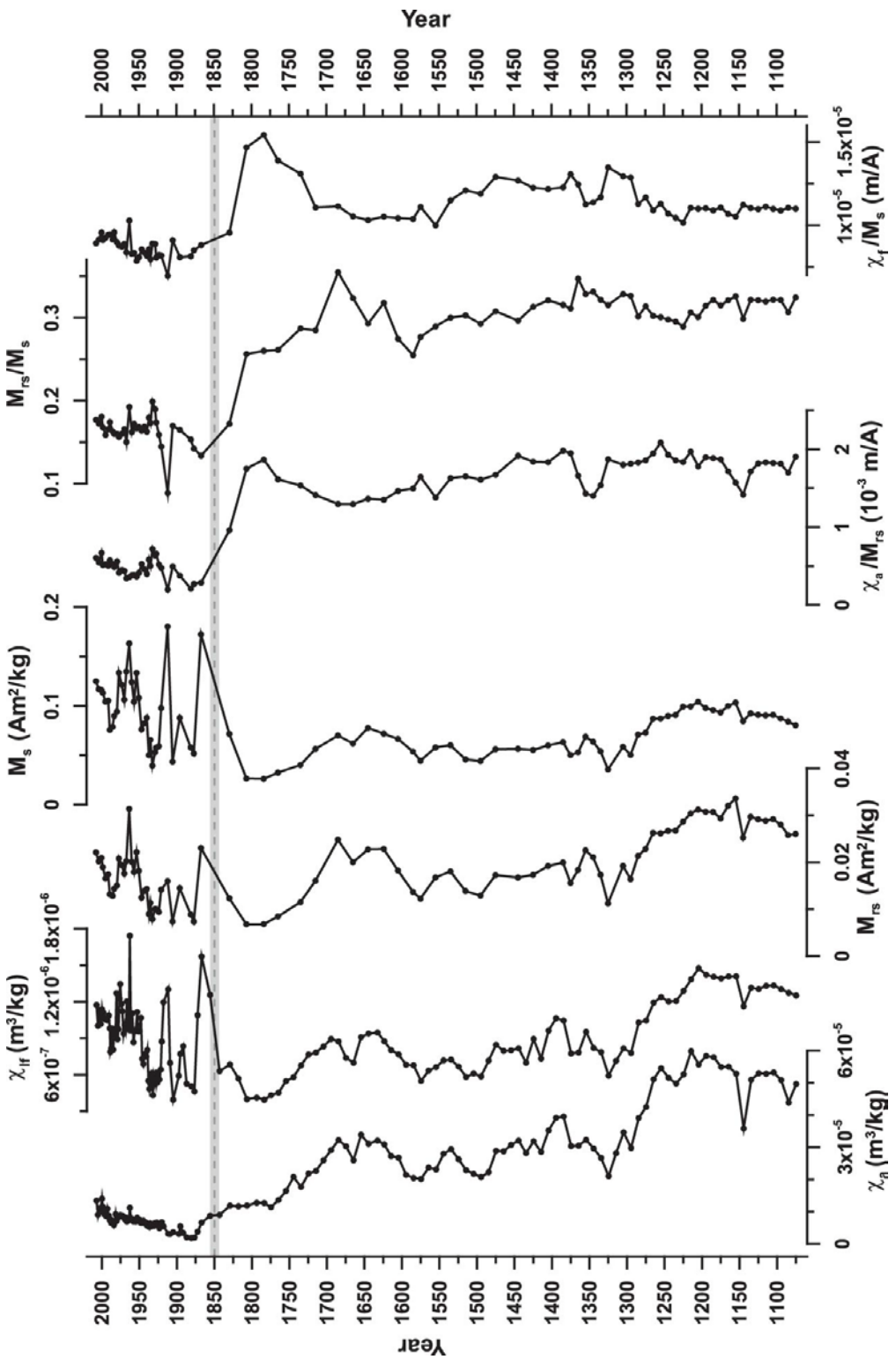

Figure 2.2 Bulk magnetic properties of the Brownie Lake sediment core

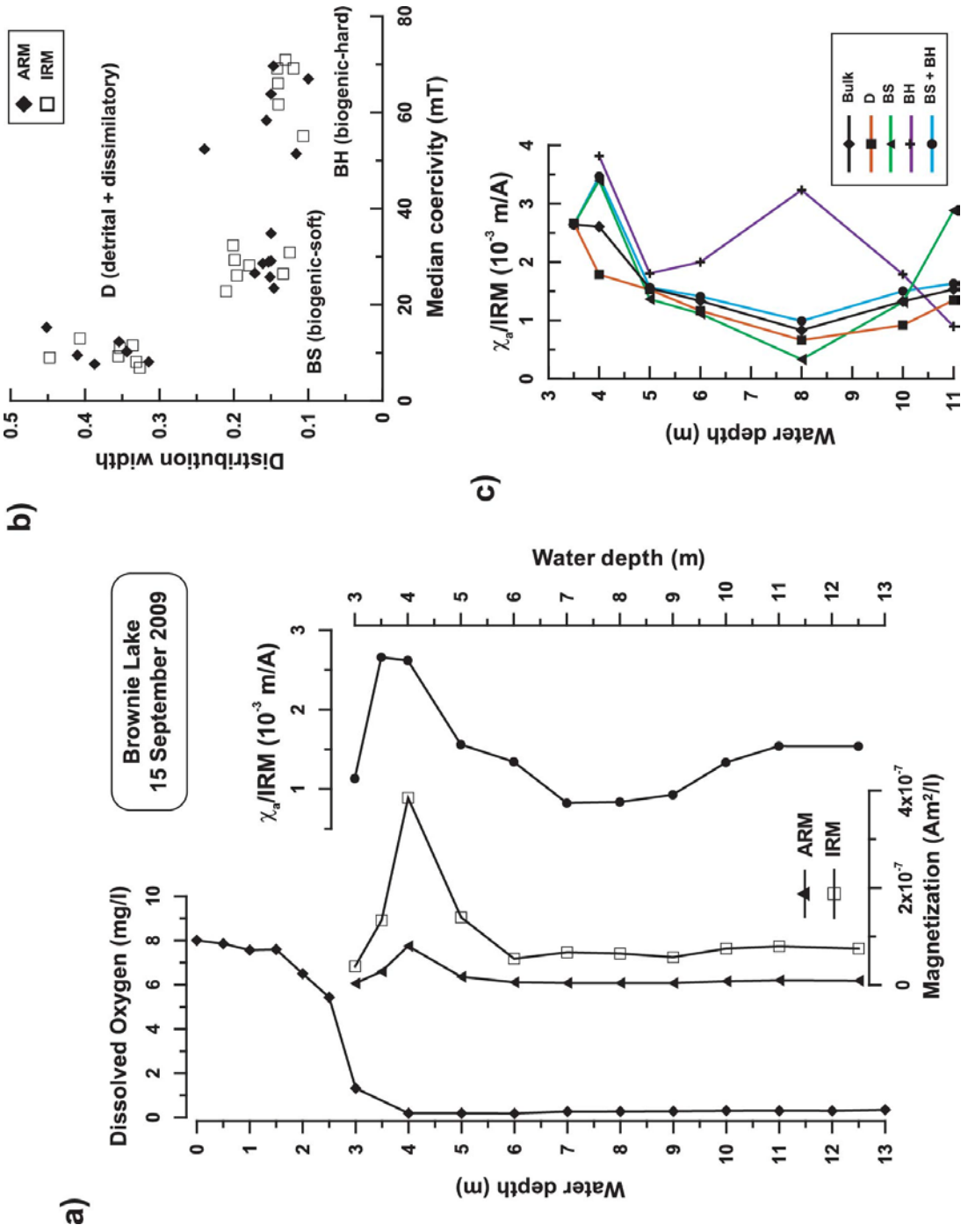

Figure 2.3 Magnetic properties of filtered water samples collected from Brownie Lake

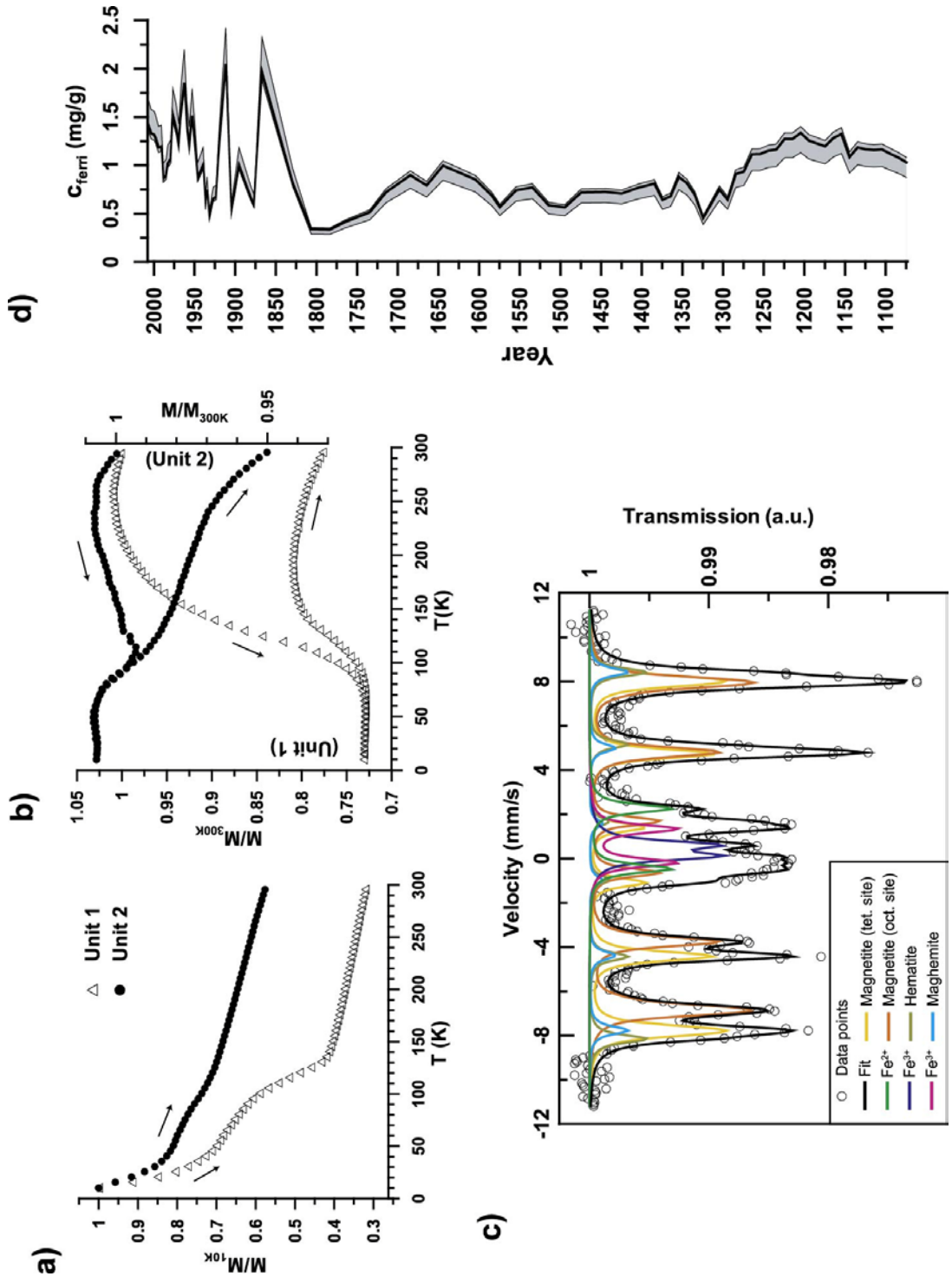

Figure 2.4 Low temperature magnetic properties, Mössbauer spectra, and total concnetration of ferrimagnetic material in Brownie Lake sediments

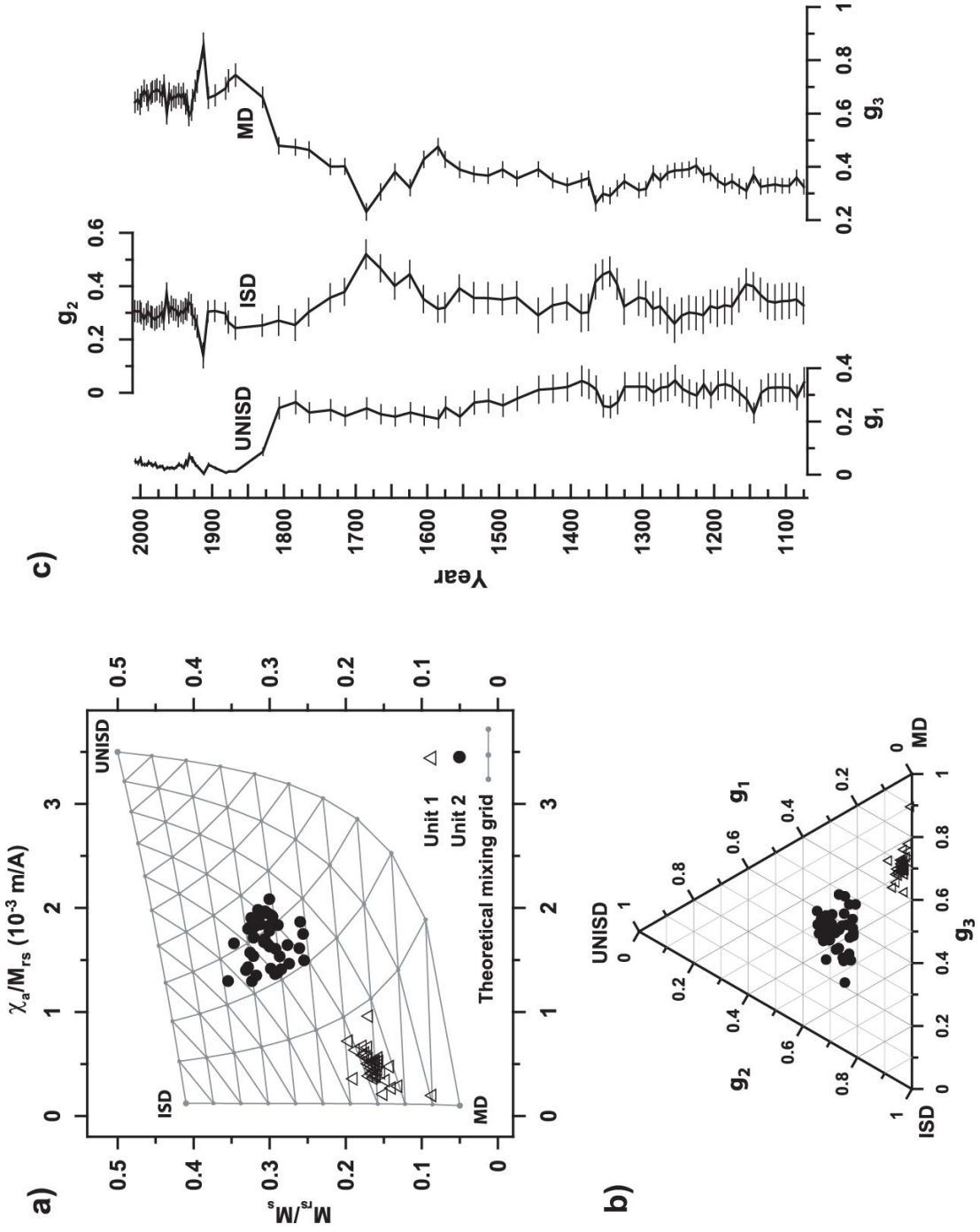

Figure 2.5 Modeling the remanence carrying components in Brownie Lake sediments

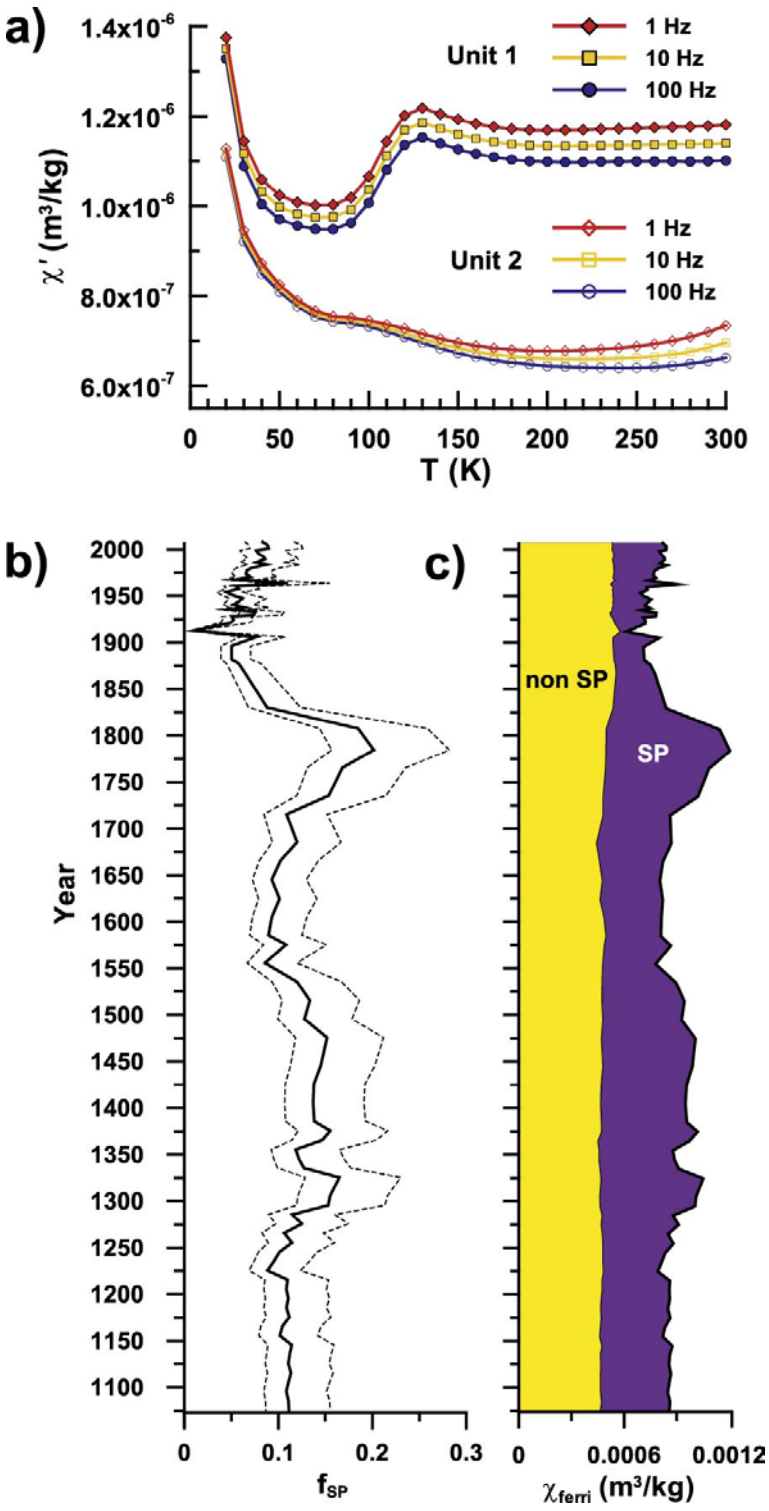

Figure 2.6 Modeling the superparamagentic component of Brownie Lake sediments

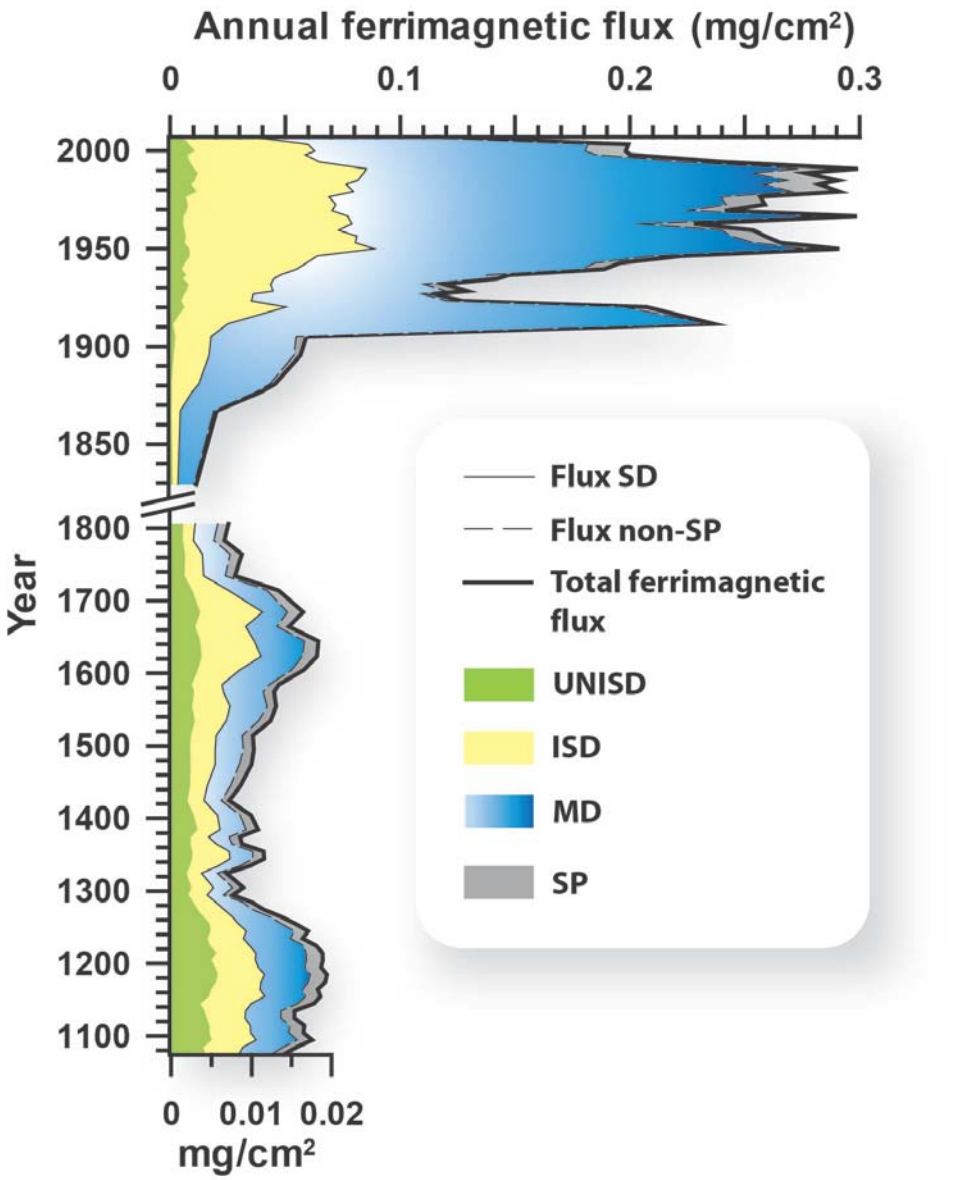

Figure 2.7 Model of annual flux of ferrimagnetic components in Brownie Lake

Tables

Table 2.1 Mean (m), standard deviation (σ[a]), and coefficient of variation (CV[b] = σ/m) values for the magnetic properties of Brownie Lake sediment units

Magnetic parameter	Unit 1			Unit 2		
	m	σ	CV	m	σ	CV
χ_{lf} (10^{-7} m^3/kg)	8.95	2.52	0.28	8.96	1.67	0.19
χ_a (10^{-5} m^3/kg)	0.71	0.2	0.28	3.32	0.7	0.21
M_{rs} (10^{-3} Am^2/kg)	15.6	4.8	0.31	21.5	4.4	0.2
M_s (10^{-3} Am^2/kg)	96.7	34.4	0.36	69.7	13.9	0.2
χ_a/M_{rs} (10^{-3} m/A)	0.48	0.15	0.31	1.71	0.18	0.1
M_{rs}/M_s	0.16	0.02	0.1	0.31	0.02	0.06
χ_f/M_s (10^{-5} m/A)	0.87	0.06	0.07	1.16	0.11	0.09

[a]standard deviations are calculated after subtracting the effect of any long-term trends on the magnetic parameters

[b]CV is a unitless measure

Table 2.2 Magnetic hyperfine parameters at room temperature for the Brownie Lake surface sediment magnetic extract

Iron phase	B_{HF}[a] (T)	QS[b] (mm/s)	IS[c] (mm/s)	%Fe[d]
Magnetite (site A-tetrahedral)	49.0(2)[e]	-0.04(2)	0.26(2)	28
Magnetite (site B-octahedral)	45.8(4)	0.02(2)	0.67(1)	34
Hematite	51.3(3)	-0.22(1)	0.38(2)	9
Maghemite	50.2(5)	0.03(2)	0.43(5)	6
Fe^{3+} narrow doublet	-	0.51(1)	0.49(1)	9
Fe^{3+} wide doublet	-	1.53(3)	0.70(2)	7
Fe^{2+}	-	2.72(3)	1.03(1)	7

[a]magnetic hyperfine field

[b]quadrupole splitting

[c]isomer shift

[d]relative concentration

[e]errors quoted in parentheses refer to the last decimal

Chapter 3: Sediment-magnetic evidence for last millennium drought conditions at the prairie-forest ecotone of northern United States*

Ioan Lascu[1,2,§], Kendra K. McLauchlan[3], Amy Myrbo[2], Subir K. Banerjee[1]

[1]*Institute for Rock Magnetism, N. H. Winchell School of Earth Sciences, University of Minnesota, 310 Pillsbury Drive SE, Minneapolis, Minnesota, U.S.A. 55455*

[2]*Limnological Research Center, N. H. Winchell School of Earth Sciences, University of Minnesota, 310 Pillsbury Drive SE, Minneapolis, Minnesota, U.S.A. 55455*

[3]*Department of Geography, 118 Seaton Hall, Kansas State University, Manhattan, Kansas, U.S.A. 66506*

[§]*Corresponding author: Lascu003@umn.edu*

Submitted for publication to Palaeogeography, Palaeoclimatology, Palaeoecology

* We thank Kristina Brady and Colin Plank for help with fieldwork, Rachel Murray for preparing the piston core samples and performing some of the measurements, Vania Stefanova for palynological assistance with selecting the samples for radiocarbon dating, and Dan Engstrom for analytical assistance with ^{210}Pb dating. Peter Leavitt and Bjoern Wissel conducted the carbon analyses. IL benefited from the support of a University of Minnesota Doctoral Dissertation Fellowship. KKM was supported by NSF # BCS-0955225. The Institute for Rock Magnetism and LacCore are National Science Foundation funded facilities. This is IRM contribution 1104.

Synopsis

Droughts are recurrent features in sedimentary records at the prairie-forest ecotone of northern U.S.A. It is therefore important to understand the duration of such events, as well as their severity and consequences beyond the century-scale instrumental record. The existing drought records can be complemented with additional proxies that clearly document the interactions between external factors and the depositional environment. Here we attempt to reconstruct the last millennium drought history of Deming Lake, a small lake at Minnesota's prairie-forest ecotone, using sediment magnetism. This approach allows us to explore the interactions between lake and catchment, and to investigate a less intuitive consequence of drought. Based on the correlation with instrumental records, we demonstrate that moisture deficit at Deming Lake translates to a decrease in detrital sediment transport from the catchment to the lake, as a consequence of reduced hydrologic flow and erosional pathways. Concordantly, during dry episodes we find that the mass fractions of in-lake produced organic matter and biogenic magnetic particles increase relative to allochthonous component fractions. We identify several episodes of reduced precipitation at Deming Lake that match the existing regional drought reconstructions. The most prominent dry event occurred at the end of the Little Ice Age, suggesting that the second half of this cold interval was drier in the region than previously thought.

Key words: sediment magnetism; biogenic magnetite; drought; prairie-forest ecotone; Minnesota; Little Ice Age.

1. Introduction

Droughts are climatic events of prolonged deficiency in precipitation and runoff, which can significantly affect natural ecosystems, water supplies, agricultural practices, and functioning of society (Cook et al., 2007). Multidecadal to multimillennial-scale records of drought frequency and severity are essential to understanding the causes and consequences of droughts. Instrumental records of climate change, along with historical accounts, show that moderate to severe droughts recur with subcentennial periodicities (Wilhite, 2007). However, proxy records demonstrate that extremely severe droughts, whose magnitude and duration dwarf recorded nineteenth and twentieth century droughts, have occurred repeatedly during the past thousand years, especially in the western U. S. (e.g., Woodhouse and Overpeck, 1998).

Boundaries between prairie and forest ecosystems are considered especially sensitive to moisture variability because their position follows the zero moisture balance line, where precipitation is equal to evapotranspiration (P=ET). One well-studied prairie-forest ecotone is located in northern Minnesota at the junction of three air masses: the cold and dry arctic airstream to the north, the dry Pacific airstream to the west, and the humid, warm airstream from the Gulf of Mexico (Bryson, 1966). Thus, this region is likely to have responded to past climate fluctuations. Indeed, a variety of sedimentary proxy records indicate widespread and/or persistent drought conditions during the last millennium in Minnesota: pollen (St. Jacques et al., 2008), charcoal (Clark, 1990; Umbanhowar et al., 2004), clastic material (Dean, 1997; Shuman et al., 2009, Dasgupta et al., 2010), testate amoeba (Booth et al., 2006), and oxygen isotopes (Tian et al., 2006). These proxy records, which document drought conditions, would be complemented by additional measurements that clearly document interactions between external factors and the depositional environment, such as the relationship between catchment and limnologic processes in a lacustrine depositional setting.

Sediment-magnetic parameters can provide environmental and climatic reconstructions from sedimentary records based on the flux of magnetic material from the terrestrial landscape as well as from within the aquatic system (e.g., Thompson and Oldfield, 1986; Evans and Heller, 2003). This can be achieved because it generally takes only a limited number of bulk magnetic parameters to compute estimates of magnetic mineral concentration, mineralogy, and grain size, and the partition between basic magnetic components (Lascu et al., 2010). Here we investigate the timing, severity, and consequences of regional drought episodes by examining the magnetic record contained in the sediments of Deming Lake, a meromictic (i.e., permanently stratified) lake situated in the coniferous forest ecosystem in the vicinity of Minnesota's prairie-forest boundary.

Our first goal is to reconstruct the drought history of this site for the past millennium. The second goal is to explore a less intuitive consequence of drought. It is well documented that drought can destabilize the landscape and cause increased flux of materials to a lake from its catchment. However, in certain ecological settings, dry conditions may affect the stability of the landscape only minimally, thereby causing reduced hydrologic flow and erosional pathways, such that fluxes of materials from the catchment to the lake are decreased. We investigate this consequence by interpreting the variations in biologically-produced magnetic particles in Deming Lake in a non-traditional manner. Based on the correlation with instrumental records, we show that high relative concentrations of magnetite produced by magnetotactic bacteria are indicative of periods with low influx of catchment-derived magnetic particles, corresponding to episodes of reduced precipitation. We can therefore use this proxy to reconstruct drought conditions during the past 1000 years.

2. Site description

Deming Lake is located close to the headwaters of the Mississippi River in north-central Minnesota (Fig. 1), within the boundaries of Itasca State Park, in the Itasca Moraine till. The lake is situated in a conifer forest dominated by *Pinus strobus* and *P. resinosa*, mixed with deciduous hardwood species such as *Acer saccharum*, *Tilia americana*, *Populus tremuloides*, and *Betula papyrifera*. The surface of the lake is 5.4 ha, occupying 14% of its catchment (Clark, 1990). The maximum water depth is 16.7 m, with a relative depth of 6.4%. Due to its small size, large relative depth, and wind protection by 30-40 m tall tree stands on abrupt slopes, lake water circulation is restricted, and mixing during fall and spring turnovers is incomplete, resulting in a permanently stratified, oxygen-depleted layer (monimolimnion) at the bottom of the water column. These conditions produce annual laminations in the sediments. The monimolimnion is separated from the mixolimnion (seasonally stratified surface layer in which mixing occurs at fall and spring turnover) by a chemocline situated at ~13 m depth. The oxycline at Deming Lake moves vertically in the mixolimnion, according to seasonal oxygen demand and temperature stratification.

Deming Lake has no inlet or outlet streams, and is mostly supplied by groundwater. Terrestrial input of clastic sediments is achieved mainly from overland flow, with the main source being the sandy glacial till of the Itasca moraine, and only subordinately from eolian transport. There has been no recorded Euro-American land use such as logging or agriculture in the watershed, although an access road was constructed in the vicinity of the lake in the 1920s, and later paved in the 1970s, to facilitate access to Itasca State Park from the south. Deming Lake is situated a few km from Elk Lake, a site of extensive interdisciplinary paleolimnological work (Bradbury and Dean, 1993).

3. Materials and methods

3.1. Fieldwork, initial core studies, and sampling

Two surface cores were retrieved from the deepest part of the lake in October 2007. A piston core was collected using a polycarbonate barrel connected to a coring head, transported to National Lacustrine Core Repository (LacCore) at the University of Minnesota, and stored at 4 °C. A freeze core was collected using a wedged-shape box filled with a mixture of dry ice and isopropanol. The frozen slabs of sediment were packed in dry ice and transported to LacCore, where they were stored at -20 °C.

The piston core was processed using the standard LacCore protocol for initial core studies. Convoluted volume-normalized magnetic susceptibility (using a loop sensor) and sediment density (by gamma-ray attenuation) were logged at 1 cm resolution on the whole core barrel using a standard Geotek multi sensor core logger (MSCL). The core was then split lengthwise into working and archive halves, and the exposed core surfaces were cleaned by scraping the surface parallel to bedding with a glass microscope slide. The archive half was imaged using a digital line scanner at a resolution of 10 pixels/mm. Volume-normalized magnetic susceptibility was measured on the archive half at 0.5 cm resolution using a point sensor attached to a multi-section Geotek MSCL. The sediment structure was described macroscopically on the working half. Smear slides were prepared from select horizons for initial microscopic compositional characterization . The section was then sampled continuously at 2 cm intervals for loss on ignition (LOI) and magnetic measurements.

The freeze core slabs were prepared for imaging and sampling by polishing the surfaces, first with a power planer and then with a razor blade. After imaging (see above), the slabs were sampled at 0.5 cm resolution using a stainless steel microtome. The slabs were kept in frozen state throughout the process by having been surrounded with dry ice pellets on a cardboard tray with raised edges. The samples were weighed, freeze dried, and then weighed again, and the water content for each sample calculated as the difference between the wet and dry sediment masses. The dried samples were used for ^{210}Pb dating, magnetic measurements, and carbon (C) geochemistry.

3.2. Laboratory analyses

Mass-normalized magnetic susceptibility (χ) was measured on a Kappabridge KLY-2 susceptometer operating at a frequency of 920 Hz. Remanence measurements were performed using a 2G superconducting quantum interference device rock magnetometer. A D-Tech 2000 demagnetizer was used for anhysteretic remanent magnetization (ARM) acquisition, which was imparted in a 0.1 mT direct field superimposed on an AF field decaying from a peak value of 200 mT at a rate of 5 μT per half cycle. ARM susceptibility (χ_{ARM}) was calculated by normalizing the ARM to the direct field. Isothermal remanent magnetization (IRM) was imparted using an ASC Scientific IM-10-30 impulse magnetizer. Each sample was pulsed twice using a 200 mT direct field. The so-called 'ARM ratio' (χ_{ARM}/IRM) was computed by normalizing the ARM susceptibility to the IRM. Hysteresis loops were measured on the piston core samples with a Princeton Measurements vibrating sample magnetometer using a maximum applied field of 1 T. The loop slopes at high fields were used to correct raw saturation magnetization (M_s) and saturation remanent magnetization (M_{rs}) values, and to calculate the contribution of non-ferrimagnetic minerals to the low field susceptibility.

Elemental and isotopic analyses for C were conducted at the Stable Isotope Lab at the University of Regina, by using standard combustion methods on a Finnigan-MAT Thermoquest Delta Plus mass spectrometer interfaced with a Carlo Erba NC2500 elemental analyzer. Analytical error was better than 0.1% for $\delta^{13}C$. Elemental carbon is reported as total carbon (TC). Samples were not acidified because inorganic carbon concentrations throughout the core were negligible as measured by carbon coulometry (McLauchlan et al., 2011).

After collecting the magnetic data, the piston core samples were used for LOI compositional analysis, according to the procedure described by Dean (1974) and Heiri et al. (2001). The water content was determined by weighing the sample wet, drying overnight at 105°C, and reweighing the dry matter. The organic matter (OM) content was determined by weighing the sample after combusting the sediment for 4

hours at 550°C, temperature at which OM is thermally decomposed, and evolved as CO_2. The 2:1 relationship that emerges from the cross correlation of the OM and TC percentages (not shown) is additional evidence that no carbonate carbon is present in the Deming Lake sediments.

The chronology of sediment deposition was determined using eighteen ^{210}Pb dates from the freeze core and one ^{14}C age from the piston core (Fig. 2). Sediment samples from the top 30 cm of the freeze core were analyzed for excess ^{210}Pb activity at the Saint Croix Watershed Research Station of the Science Museum of Minnesota (Table 1). ^{210}Pb was measured through its grand-daughter product ^{210}Po, with ^{209}Po added as an internal yield tracer. The polonium isotopes were distilled from dry sediment at 550 °C following pretreatment with concentrated HCl and plated directly onto silver planchets from a 0.5 N HCl solution (modified from Eakins and Morrison, 1976). Activity was measured for $1\text{-}6\cdot10^5$ s with ion-implanted surface barrier detectors and an Ortec alpha spectroscopy system. Unsupported ^{210}Pb was calculated by subtracting supported activity from the total activity measured at each level; supported ^{210}Pb was estimated from the asymptotic activity at depth, as the mean of the lowermost analyzed samples. Dates and sedimentation rates were determined according to the constant rate of supply (CRS) model, with confidence intervals calculated by first-order error analysis of counting uncertainty (Appleby, 2001). The CRS model assumes that the flux of unsupported ^{210}Pb to the sediment surface is constant, while the initial concentration of ^{210}Pb varies with changes in total sedimentation rate. The CRS model provides a reliable basis for interpreting ^{210}Pb profiles in lakes where the watershed contribution of ^{210}Pb is small and depositional hiatuses are absent (Appleby, 2001).

An accelerator mass spectrometry ^{14}C age of 970 ± 35 years from a pollen concentrate collected near the base of the piston core was obtained at Lawrence Livermore National Laboratory (lab number CAMS 144042). A Bayesian age model was constructed using the software package BACON (Blaauw and Christen, 2011), which also calibrated the ^{14}C age using the Intcal09 dataset (Reimer et al., 2009) with a resulting calendar age in the interval 993-1183 of the common era (CE; all ages are

reported as CE years henceforth). Age model errors increase significantly prior to 1800, as the age control is only constrained by one point beyond the ^{210}Pb-dated portion (Fig. 2). The extrapolation beyond the ^{14}C-dated sample is based on the age model constructed for the Deming Lake Holocene sedimentary sequence (McLauchlan et al., 2011).

3.3. Modeling sediment magnetic parameters

Sediment magnetic parameters are dominated by the ferrimagnetic fraction (most commonly magnetite and/or maghemite) present in the sample, which is usually a mixture of detrital (allochthonous) and endogenic (autochthonous) particles. The detrital particles can be transported into the depositional system by water or wind. The endogenic particles can be precipitated purely chemically, or formed via biological mediation. A common endogenic ferrimagnetic mineral from lake and marine sediments is biogenic magnetite, a product of controlled intracellular biomineralization by magnetotactic bacteria (Blakemore, 1975), often found in the form of linear chains of crystals (Egli et al., 2010). The magnetite crystals grow in individual organelles called magnetosomes, which control the extent of crystal growth. Bacterial magnetite is single domain (SD—consisting of only one uniformly magnetized magnetic domain), with uniaxial magnetic anisotropy controlled by particle shape. Depending on bacterial strain, average magnetite particle size is on the order of 30-100 nm, with aspect (length to width) ratios between 1 and 2.

ARM acquisition is very efficient for assemblages of uniaxial non-interacting SD (UNISD) particles (Egli and Lowrie, 2002; Egli, 2006) and linear chains of particles, and less efficient for larger, multi-domain (MD) grains. As a consequence, the ARM ratio can be used as a magnetic grain-size proxy, with larger values indicating a predominance of smaller grains. However, ARM acquisition can be hindered by magnetostatic interactions between SD particles in close proximity to one another (Egli, 2006), commonly clusters of small pedogenic grains, but also collapsed bacterial chains (Moskowitz et al., 1993; Egli et al., 2010). The ARM ratio will thus be lower for an assemblage of interacting magnetic grains, compared to an assemblage

of identically sized particles that are non-interacting. The ARM ratio is unable to discriminate between strongly interacting SD (ISD) particles and coarse MD particles (Moskowitz et al., 1993). However, using the ARM ratio in conjunction with the saturation remanence ratio (M_{rs}/M_s) has allowed us to discriminate between these three components (Lascu et al., 2010).

The magnetic measurements obtained from the piston core samples were converted to mass concentrations of ferrimagnetic components using the quantifying method developed previously (Lascu et al., 2010). Due to small sample size, the freeze core aliquots were too weak for reliable hysteresis measurements. Since Deming Lake is meromictic, with anoxic bottom waters, we have modeled the ferrimagnetic components as magnetite (M_s = 92 Am^2/kg). However, we cannot discount the possibility that some oxidation might have occurred before deposition, or after collection, during core handling and storage. If we were to assume complete oxidation to maghemite (M_s = 74.3 Am^2/kg), ferrimagnetic concentrations would increase by 19%. The ultrafine, superparamagnetic (SP) component was calculated using a susceptibility value of 0.04 m^3/kg (Dunlop and Özdemir, 1997). The non-SP component was modeled as a mixture of UNISD, ISD, and MD grains, characterized by the following end-member saturation remanence and ARM ratios, respectively: 0.5 and 3.5 mm/A for UNISD, 0.41 and 0.12 mm/A for ISD, and 0.05 and 0.1 mm/A for MD. The rationale for choosing these end-member modeling parameters for lake sediments has been discussed by Lascu et al. (2010). The flux for each component was calculated as the product of its mass fraction, sediment accumulation rate (from the age model), sediment density (from Geotek gamma attenuation measurements), and sediment mass fraction (from LOI).

4. Results

The sedimentary sequence is composed of light to dark brown faintly to distinctly laminated sapropel. The laminations are annual (Clark, 1990), with darker brown winter layers and light to reddish brown spring-summer layers, where distinct. The reddish brown laminations are rich in poorly crystallized iron oxy-hydroxides. The organic matter (40-60% by mass) is fine-grained, with no visible macroscopic remains, consisting of algal and bacterial remains of autochthonous origin. The ARM ratio, relative carbon concentration, carbon isotopes, and sediment flux vary over time during the last millennium, determined from the high-resolution sampling of the freeze core (Fig. 3a). The sedimentary ferrimagnetic fraction can be broken down into components, as determined from modeling of the magnetic parameters measured on the piston core samples (Fig. 3b). Annual mass fluxes and relative proportions of the ferrimagnetic components are shown for comparison. Because of the very good correlation between the ARM ratio and %TC, and between the MD flux and the non-OM sediment flux (Fig. 3), we interpret the LOI residue as minerogenic fraction.

The highest pre-European settlement mass input of sediment in Deming Lake occurred in the period 1000-1200 (Fig. 3). Peak influx was recorded at ca. 1150, when sedimentation was dominated by clay and silt deposition (spike in sediment flux curve, and near-zero values for %TC). This maximum is bracketed by two episodes of increased mineral flux coupled with high organic flux. Sedimentary $\delta^{13}C$ values were variable, with values between -32‰ and -30‰. The ARM ratio was the lowest for the whole sequence, with mean values <1.5 mm/A. Ferrimagnetic flux was relatively high, dominated by MD grains (>50% by mass). During this period there was at least one short episode (~1050) of decreased magnetic flux, marked by peaks in the relative proportion of the UNISD, ISD, and SP components, and local maxima in the ARM ratio and %TC curves (Fig. 3).

The next significant minimum in ferrimagnetic flux occured around 1300, coupled with peaks in the ARM ratio and the relative concentration of UNISD and SP components (Fig. 3b). The sediment flux decreased after 1250 and remained relatively

constant until 1700. The proportion between organic and mineral matter was fairly constant as well during this interval, as seen from the %TC values. Sedimentary $\delta^{13}C$ was more positive, with values between -29‰ and -28‰ in the interval 1260-1440, and between -30‰ and -29‰ in the interval 1480-1540. The ferrimagnetic flux decreased around 1500, once again coupled with an increase in the relative proportion of UNISD and SP particles (Fig. 3b). Between 1540 and ca. 1700 ferrimagnetic flux increased, while $\delta^{13}C$ mean values are lower than -30‰.

Between 1700 and 1900 mineral flux decreased, while OM flux remained relatively constant, resulting in a higher relative concentration of organic carbon during this period. The highest ARM ratio values were also recorded in this period, as were the relative concentrations of the UNISD and SP components. The total ferrimagnetic flux was concomitantly low during this period. After a brief excursion to more positive values before 1700, $\delta^{13}C$ attained the most negative values in the sequence during this time period.

At the end of the nineteenth century all sedimentary fluxes increased as a result of Euro-American settlement. The settlers did not establish communities or exploit timber in the immediate vicinity of Deming Lake, but the effects of regional settlement and logging can be readily observed in the increase of mineral, organic, and ferrimagnetic matter of up to one order of magnitude higher than in pre-settlement times. Mass sediment flux steadily increased from settlement onward, with a larger increase of minerogenic material relative to OM. During the twentieth century the ferrimagnetic flux was controlled mainly by the MD component, present in proportion of 50-70%. The UNISD component decreased initially, but recovered in the most recent decades. Sedimentary $\delta^{13}C$ exhibits the most positive values in the sequence, with a maximum value of -27‰ around 1945.

5. Discussion

5.1. Controls on Deming Lake sedimentary parameters

There are two possibilities for how sediment flux to a lake basin can change with moisture availability. In areas with reduced forest cover, drought conditions can destabilize the landscape by hindering the growth of the soil-stabilizing plants, leading to increased sediment transport to the lake from its catchment. However, in forested areas decreased moisture availability does not lead to landscape destabilization, but decreases hydrologic and erosional flux from the catchment to the lake, leading to reduced fluxes of allochthonous sediment to the lake.

The tight coupling between the ARM ratio and %TC in Deming Lake is due to the similar response of these proxies to their main controlling factor, detrital sediment input.

In general, relative OM concentrations will increase if any of the following scenarios occur: a) OM flux increases while mineral flux either decreases, remains constant, or increases at a lower rate; b) OM flux stays constant and mineral flux decreases; or c) OM flux decreases while mineral flux decreases at a higher rate. In the case of Deming Lake, the initial changes in %TC are determined by the faster decrease in OM flux compared to mineral flux prior to 1250. Between 1250 and 1700 both organic and mineral fluxes are relatively constant, causing no change in %TC. The high TC values (~35%) in the period 1700-1850 are the result of the OM flux remaining constant, while the influx of clastic material from the catchment decreases. The post-settlement decrease in %TC is caused by the larger increase in mineral flux compared to OM flux increase.

The Deming Lake ARM ratio closely follows the organic carbon relative concentration, with maximum values between 1700 and 1900 (Fig. 3a). The ARM ratio is determined by the relative concentration of the UNISD component, which in turn is controlled by the relationship between the fluxes of the ferrimagnetic components, in similar fashion as discussed above for organic matter. Comparatively

higher fluxes of detrital components (i.e., MD and ISD) will dilute the fraction of UNISD particles, and thus lower ARM ratio values.

Sediment input thus plays a critical role in controlling the proportion of in-lake produced matter, whether organic or mineral. Since Deming Lake does not have an inlet, the main sediment transport mechanism to the lake is through catchment runoff associated with precipitation events. Detrital input is therefore controlled by moisture availability. In support of this premise, we have found a strong relationship during the twentieth century between the Palmer Drought Severity Index (PDSI; Palmer, 1965) and three freeze core parameters: ARM ratio, %TC, and annual mineral flux (Fig. 4). In general, ARM ratio and %TC local maxima, and mineral flux local minima occur during dry periods (negative PDSI), and vice versa.

These patterns provide support for the hypothesis regarding moisture availability and sediment flux from the catchment to the lake, namely that detrital input is significant only during rainy periods, when sediment is being mobilized through catchment runoff. During dry periods detrital input is reduced, so the proportions of biogenic magnetic particles and organic matter increase. In particular, some of the highest ARM ratios for the twentieth century in Deming Lake occur at the time of the most severe historic droughts in Minnesota, the 1930s Dust Bowl and the late 1980s drought (Trenberth et al., 1988). The same response to twentieth century drought was observed at Sharkey Lake, a small lake situated at the prairie-forest ecotone of SE Minnesota, where elevated ARM ratios and high relative organic matter concentrations, coupled with low sediment accumulation rates, characterize the Dust Bowl and the late 1980s drought (Geiss et al., 2004).

The carbon isotopic composition of bulk organic matter may be controlled by a variety of factors, such as external loading, primary productivity, composition of source material, as well as concentration and isotopic composition of dissolved inorganic carbon (e.g., Hollander and Smith, 2001; Teranes and Bernasconi, 2005; Gu et al., 2006; Myrbo and Shapley, 2006). For Deming Lake, a basic interpretation of the $\delta^{13}C$ values is that they reflect changing proportions of algal versus microbial biomass, the main two sources of sedimentary organic matter. A greater proportion of ^{13}C-

depleted microbial biomass from the anaerobic monimolimnion will shift the isotopic signature to more negative values (Hollander and Smith, 2001). At Deming Lake we hypothesize this happens during times of decreased flux of organic matter of algal origin from the epilimnion. Epilimnetic productivity is expected to be lower in cold years with short growing seasons and late ice-out than in warm years with longer growing seasons and early ice-out. Therefore, we associate the more negative sedimentary organic matter isotopic signature with cold episodes. This effect can be readily seen during the Little Ice Age (LIA; ca. 1550-1900), when $\delta^{13}C$ values were lower relative to those characterizing the "medieval warm period" (ca. 1100-1550) (Fig. 3).

5.2. Evidence for last millennium drought conditions in Minnesota

We can achieve our objective of reconstructing drought conditions at Deming Lake through the application of the process-based understanding of the magnitude of the ARM ratio, organic matter relative concentration, and detrital sediment fluxes during the twentieth century. There were at least three episodes in the last millennium (around 1300, 1500, and 1700-1900), and perhaps a fourth (~1050), during which the ARM ratio, %TC, and fraction UNISD were elevated, while detrital ferrimagnetic flux was low (Fig. 3). The highest ARM ratios and %TC values, as well as some of the lowest detrital fluxes occured between 1700 and 1900, during the second half of the LIA. We interpret these intervals as being moisture deficient.

Additional studies from the site and region support this interpretation. During the second half of the LIA (1700-1900), forest fires at Deming Lake occurred in distinct intervals of frequent fires with abundant charcoal deposition, separated by intervals with less charcoal (Clark, 1988, 1990). This marked a change from a regime with frequent fires and fairly continuous charcoal deposition between 1300 and 1700. Peak charcoal deposition at Deming Lake occurred in the intervals 1700-1740, 1770-1820, and 1860-1900 (Fig. 5). For approximately the same period (1680-1900), diatom assemblages at Elk Lake reflect the combined effects of climate and fire, and are characterized by intervals with an abundant presence of *Stephanodiscus minutulus,* a

planktonic species that thrives in periods with low Si/P ratios. (Bradbury and Dieterich-Rurup, 1993). These conditions can be generated if ice-out is followed by prolonged cool weather, which allows for extended deep circulation that brings nutrient rich waters, including phosphorus, into the epilimnion (Nuhfer et al., 1993). Low silicon influx due to reduced winter and spring precipitation would also decrease the Si/P ratio (Bradbury and Dietrich-Rurup, 1993). *Stephanodiscus minutulus* is dominant in the periods 1690-1730, 1750-1795, and 1820-1870 (Fig. 5), corresponding to the times of increased charcoal flux in Deming Lake (Clark, 1990).

There is additional corroborating evidence for drought conditions in the region during the past millennium from Elk Lake. Episodes of increased fluxes of quartz and feldspar occurred at Elk around 1300 and 1700, and are attributed to deposition by wind, which intensified in drier periods (Dean, 1997, 2002). Although a runoff transport mechanism for these minerals cannot be overlooked, it seems plausible that eolian transport is more important at Elk Lake compared to Deming Lake, due to less sheltering from wind of the much larger Elk Lake. The presence of the diatom *Aulacoseira ambigua* around 1300 supports the inference of increased windiness, as this species requires more turbulent waters to keep the colonies suspended in the photic zone (Kilham et al., 1986). *Pinus strobus*, a fire sensitive conifer species, which is also rather intolerant of dry conditions (Jacobson, 1979), especially in the summer (cf. Bryson and Wendland, 1967), experienced a decline in relative abundance at Elk Lake after 1200 (Whitlock et al., 1993), being replaced by the more fire-adapted species *P. banksiana*, and *P. resinosa*. This trend is also seen at Deming Lake, where minimum percentages of *P. strobus* pollen are recorded in the period 1700-1900 (Clark, 1993).

Lake Mina, another lake situated at the prairie-forest ecotone of Minnesota, provides a quantitative, pollen-based record of temperature and effective moisture for the last 900 years (St. Jacques et al., 2008). Long-term changes in the temperature reconstruction at Mina correspond to the broad variation of $\delta^{13}C$ at Deming Lake (Fig. 5), reinforcing the idea of temperature control on the carbon isotopic values in our record. The effective moisture reconstruction indicates that two notable dry periods

occurred around 1300-1400 and 1650-1800, roughly coinciding with our magnetism-derived drought signal at Deming Lake.

Drought conditions are also reflected by the paleohydrology of Hole Bog, a raised peat bog located approximately 70 km ENE of Deming. Reconstruction of water table fluctuations based on taxonomic analysis of testate amoeba shows severe droughts centered at 1000 and 1300, followed by a hiatus in peat deposition until ~1850 (Booth et al., 2006). The very low water table levels support the idea of persistent drought conditions after 1300, even in the forest ecosystem of northern Minnesota. The Steel Lake (40 km SE of Deming Lake) authigenic carbonate $\delta^{18}O$ record is also punctuated by a series of episodes of enriched isotopic values during the last millennium, interpreted as effects of a negative moisture balance (Tian et al., 2006). These drought events are dated at ~1130, 1170, 1300, 1550, 1650, and 1800, and are correlated with the Pacific decadal oscillation-type periodicities, and episodes of maximum solar activity (Tian et al., 2006).

Shuman et al. (2009) have demonstrated, through a combination of lake-level reconstructions, sediment composition, and pollen, that forest expansion in the Big Woods area of central Minnesota's prairie-forest ecotone occurred during prolonged drought conditions after 1300. Succession from woodland to forest was facilitated by the decline in natural fire severity as a consequence of reduced moisture availability, which led to a decline in the biomass of grasses, the principal fuel for woodland fires (Umbanhowar, 2004; Shuman, et al., 2009). Umbanhowar (2004) found declining grass charcoal fluxes and grass pollen since 1150 in seventeen Big Woods lakes, and based on the positive relationship between moisture and grass productivity (Briggs and Knapp, 1995), proposed that this decline occurred during dry, not wet, conditions (e.g., Grimm, 1983). Interestingly, Umbanhowar (2004) documented increasing trends in the organic fraction and ARM ratios for at least ten of the sites, all with peak values in the interval 1700-1900, but did not make connections between these proxies and regional drought conditions. Banerjee et al. (1981) have also documented an increase in the proportion of fine-grained magnetic particles of Long Lake in the Big Woods area during this period, but have tentatively interpreted it as an indication of topsoil

erosion during wetter conditions, following Grimm (1981). It is very likely however that biogenic (rather than pedogenic) magnetite is responsible for the high ARM and coercivity values observed in the Long Lake sedimentary record, reflecting the same processes described above.

Finally, SE of the Big Woods area, Dasgupta et al. (2010) have reconstructed the frequency of flooding events in SE Minnesota by investigating flood band occurrence in two stalagmites from Spring Valley Caverns. The deposition of detrital material on the speleothem surfaces occurred during complete flooding of the cave passage during extreme rainfall events. They found that the period between 1300 and 1860 was characterized by less than three extreme rainfall events per decade, which is the lowest frequency for the last millennium. Between 1700 and 1860 only four floods are recorded, with 1730-1830 being the longest time period since 1300 with no decadal-scale floods, making it the driest interval in the last 700 years.

6. Conclusions

We have reconstructed the last millennium drought history of Deming Lake, a small, sheltered, meromictic lake situated close to the prairie-forest ecotone of northern U.S.A., based on the magnetic properties of its sediments. Using sediment magnetism has allowed us to explore the interactions between the lake and its catchment during these periods of reduced precipitation. In addition, it has allowed us to demonstrate that droughts are expressed in less intuitive ways in sedimentary records of stable environments, such as forest ecosystems. Lack of precipitation is translated at Deming Lake as a decrease in detrital sediment transport from the catchment to the lake as a consequence of reduced hydrologic flow and erosional pathways. During moisture deficient episodes the concentration of biogenic magnetic particles increases relative to allochthonous components. Magnetic parameters will be important to measure in lacustrine sediments at other sites to determine if those systems responded similarly to drought or if alternative mechanisms may have been functioning. Our results indicate several moisture deficient episodes during the last 1000 years, which match other regional drought reconstructions. The most prominent dry event occurred at the end of the LIA. Detrital fluxes were extremely low during this period, resulting in high values for the relative concentrations of in-lake-produced organic matter and biogenic magnetic particles. This finding suggests that the second half of the LIA was not only very cold but also drier than previously thought.

References

Appleby, P.G., 2001. Chronostratigraphic techniques in recent sediments, in Last, W.M., Smol, J.P. (Eds.), Tracking Environmental Change using Lake Sediments, Vol. 1, Basin Analysis, Coring, and Chronological Techniques. Kluwer Academic Publishers, Dordrecht, Netherlands, pp. 171-204.

Blaauw, M., Christen, J.A., 2011. Flexible Paleoclimate Age-Depth Models Using an Autoregressive Gamma Process. Bayesian Analysis 6, 457-474.

Blakemore, R., 1975. Magnetotactic bacteria. Science 190, 377.

Booth, R.K., Notaro, M., Jackson, S.T., Kutzbach, J.E., 2006. Widespread drought episodes in the western Great Lakes region during the past 2000 years: geographic extent and potential mechanisms. Earth and Planetary Science Letters 242, 415-427.

Bradbury, J.P., Dean, W.E., 1993. Elk Lake, Minnesota: evidence for rapid climate change in the north-central United States. Geological Society of America Special Paper 276, 336 pp.

Bradbury, J.P., Dieterich-Rurup, K.V., 1993. Holocene diatom paleolimnology of Elk Lake, Minnesota, in Bradbury, J.P., Dean, W.E. (Eds.), Elk Lake, Minnesota: Evidence for Rapid Climate Change in the North-Central United States. Geological Society of America Special Paper 276, pp. 215-237.

Briggs, J.M., Knapp, A.K., 1995. Interannual variability in primary production in tallgrass prairie: climate, soil moisture, topographic position, and fire as determinants of aboveground biomass. American Journal of Botany 82, 1024-1030.

Bryson, R.A., Wendland, W.M., 1967. Tentative climatic patterns for some late glacial and post-glacial episodes in central North America. Life, land, and water: Proceedings of the 1966 conference on environmental studies of the Glacial Lake Agassiz region , 271-298.

Clark, J.S., 1993. Fire, climate change, and forest processes during the past 2000 years, in Bradbury, J.P., Dean, W.E. (Eds.), Elk Lake, Minnesota: Evidence for Rapid Climate Change in the North-Central United States. Geological Society of America Special Paper 276, pp. 295-308.

Clark, J.S., 1990. Fire and climate change during the last 750 yr in northwestern Minnesota. Ecological Monographs 60, 133-159.

Clark, J.S., 1988. Effect of climate change on fire regimes in northwestern Minnesota. Nature 334, 233-235.

Cook, E.R., Woodhouse, C.A., Eakin, C.M., Meko, D.M., Stahle, D.W., 2004. Long-term aridity changes in the western United States. Science 306, 1015-1018.

Cook, E.R., Seager, R., Cane, M.A., Stahle, D.W., 2007. North American drought: reconstructions, causes, and consequences. Earth-Science Reviews 81, 93-134.

Dasgupta, S., Saar, M.O., Edwards, R.L., Shen, C., Cheng, H., Alexander, E.C., 2010. Three thousand years of extreme rainfall events recorded in stalagmites from Spring Valley Caverns, Minnesota. Earth and Planetary Science Letters 300, 46-54.

Dean, W.E., 2002. A 1500-year record of climatic and environmental change in Elk Lake, Clearwater County, Minnesota: II, Geochemistry, mineralogy, and stable isotopes. Journal of Paleolimnology 27, 301-319.

Dean, W.E., 1997. Rates, timing, and cyclicity of Holocene eolian activity in north-central United States: evidence from varved lake sediments. Geology 25, 331-334.

Dean, W.E.,Jr, 1974. Determination of carbonate and organic matter in calcareous sediments and sedimentary rocks by loss on ignition: comparison with other methods. Journal of Sedimentary Petrology 44, 242-248.

Dunlop, D.J., Özdemir, Ö., 1997. Rock Magnetism: Fundamentals and Frontiers. Cambridge University Press, Cambridge, United Kingdom.

Eakins, J.D., Morrison, R.T., 1978. New Procedure for Determination of ^{210}Pb in Lake and Marine Sediments. International Journal of Applied Radiation and Isotopes 29, 531-536.

Egli, R., Chen, A.P., Winklhofer, M., Kodama, K.P., Horng, C.-S., 2010. Detection of noninteracting single domain particles using first-order reversal curve diagrams. Geochemistry, Geophysics, Geosystems 11, doi: 10.1029/2009GC002916.

Egli, R., Lowrie, W., 2002. Anhysteretic remanent magnetization of fine magnetic particles. Journal of Geophysical Research 107, doi: 10.1029/2001JB000671.

Egli, R., 2006. Theoretical considerations on the anhysteretic remanent magnetization of interacting particles with uniaxial anisotropy. Journal of Geophysical Research 111, doi: 10.1029/2006JB004577.

Evans, M.E., Heller, F., 2003. Environmental Magnetism: Principles and Applications of Enviromagnetics. Academic Press, San Diego, United States.

Geiss, C.E., Banerjee, S.K., Camill, P., Umbanhowar, C.E., 2004. Sediment-magnetic signature of land-use and drought as recorded in lake sediment from south-central Minnesota, USA. Quaternary Research 62, 117-125.

Grimm, E.C., 1983. Chronology and Dynamics of Vegetation Change in the Prairie-Woodland Region of Southern Minnesota, USA. New Phytologist 93, 311-350.

Grimm, E.C., 1981. An ecological and paleoecological study of the vegetation in the Big Woods region of Minnesota. , PhD Dissertation, University of Minnesota, Minneapolis, USA.

Gu, B., Chapman, A.D., Schelske, C.L., 2006. Factors controlling seasonal variations in stable isotope composition of particulate organic matter in a soft water eutrophic lake. Limnology and Oceanography 51, 2837-2848.

Heiri, O., Lotter, A.F., Lemcke, G., 2001. Loss on ignition as a method for estimating organic and carbonate content in sediments: reproducibility and comparability of results. Journal of Paleolimnology 25, 101-110.

Hollander, D.J., Smith, M.A., 2001. Microbially mediated carbon cycling as a control on the $\delta^{13}C$ of sedimentary carbon in eutrophic Lake Mendota (USA): New models for interpreting isotopic excursions in the sedimentary record. Geochimica et Cosmochimica Acta 65, 4321-4337.

Jacobson, G.L., 1979. Paleoecology of White Pine (Pinus strobus) in Minnesota. Journal of Ecology 67, 697-726.

Kilham, P., Kilham, S.S., Hecky, R.E., 1986. Hypothesized Resource Relationships among African Planktonic Diatoms. Limnology and Oceanography 31, 1169-1181.

Lascu, I., Banerjee, S.K., Berquo, T.S., 2010. Quantifying the concentration of ferrimagnetic particles in sediments using rock magnetic methods. Geochemistry, Geophysics, Geosystems 11, doi: 10.1029/2010GC003182.

McLauchlan, K.K., Lascu, I., Myrbo, A., Leavitt, P.R., 2011, Variable ecosystem response to climate change during the Holocene in northern Minnesota, USA. Ecology, submitted.

Moskowitz, B.M., Frankel, R.B., Bazylinski, D.A., 1993. Rock magnetic criteria for the detection of biogenic magnetite. Earth and Planetary Science Letters 120, 283-300.

Myrbo, A., Shapley, M.D., 2006. Seasonal water-column dynamics of dissolved inorganic carbon stable isotopic compositions ($\delta^{13}C_{DIC}$) in small hardwater lakes in Minnesota and Montana. Geochimica et Cosmochimica Acta 70, 2699-2714.

Nuhfer, E.B., Anderson, R.Y., Bradbury, J.P., Dean, W.E., 1993. Modern sedimentation in Elk Lake, Clearwater County, Minnesota, in Bradbury, J.P.,

Dean, W.E. (Eds.), Elk Lake, Minnesota: Evidence for Rapid Climate Change in the North-Central United States. Geological Society of America Special Paper 276, pp. 75-96.

Palmer, W.C., 1965. Meteorological Drought. Weather Bureau Research Paper No. 45, U.S. Dept. of Commerce, Washington D.C.

Reimer, P.J., Baillie, M.G.L., Bard, E., Bayliss, A., Beck, J.W., Blackwell, P.G., Ramsey, C.B., Buck, C.E., Burr, G.S., Edwards, R.L., Friedrich, M., Grootes, P.M., Guilderson, T.P., Hajdas, I., Heaton, T.J., Hogg, A.G., Hughen, K.A., Kaiser, K.F., Kromer, B., McCormac, F.G., Manning, S.W., Reimer, R.W., Richards, D.A., Southon, J.R., Talamo, S., Turney, C.S.M., van der Plicht, J., Weyhenmeye, C.E., 2009. Intcal09 and Marine09 Radiocarbon Age Calibration Curves, 0-50,000 Years Cal BP. Radiocarbon 51, 1111-1150.

Shuman, B., Henderson, A.K., Plank, C., Stefanova, I., Ziegler, S.S., 2009. Woodland-to-forest transition during prolonged drought in Minnesota after ca. AD 1300. Ecology 90, 2792-2807.

St. Jacques, J., Cumming, B.F., Smol, J.P., 2008. A 900-year pollen-inferred temperature and effective moisture record from varved Lake Mina, west-central Minnesota, USA. Quaternary Science Reviews 27, 781-796.

Teranes, J.L., Bernasconi, S.M., 2005. Factors controlling $\delta^{13}C$ values of sedimentary carbon in hypertrophic Baldeggersee, Switzerland, and implications for interpreting isotope excursions in lake sedimentary records. Limnology and Oceanography 50, 914-922.

Thompson, R., Oldfield, F., 1986. Environmental Magnetism. Allen and Unwin, London, UK.

Tian, J., Nelson, D.M., Hu, F.S., 2006. Possible linkages of late-Holocene drought in the North American midcontinent to Pacific Decadal Oscillation and solar activity. Geophysical Research Letters 33, doi: 10.1029/2006GL028169.

Trenberth, K.E., Branstator, G.W., Arkin, P.A., 1988. Origins of the 1988 North-American Drought. Science 242, 1640-1645.

Umbanhowar, C.E., 2004. Interaction of fire, climate and vegetation change at a large landscape scale in the Big Woods of Minnesota, USA. The Holocene 14, 661-676.

Whitlock, C., Bartlein, P.J., Watts, W.A., 1993. Vegetation history of Elk Lake, in Bradbury, J.P., Dean, W.E. (Eds.), Elk Lake, Minnesota: Evidence for Rapid Climate Change in the North-Central United States. Geological Society of America Special Paper 276, pp. 251-274.

Wilhite, D.A., 2007. Drought, in Stoltman, J.P., Lidstone, J., Dechano, L.M. (Eds.), International Perspectives on Natural Disasters: Occurrence, Mitigation, and Consequences. Springer Netherlands, pp. 147-162.

Woodhouse, C.A., Overpeck, J.T., 1998. 2000 years of drought variability in the central United States. Bulletin of the American Meteorological Society 79, 2693-2714.

Figures

Figure 1. Map of Deming Lake (DL, square) in relation to the other sites (dots) mentioned throughout the paper: Elk Lake (EL), Steel Lake (SL), Hole Bog (HB), Lake Mina (LM), and Spring Valley Caverns (SVC). The Big Woods area is denoted by BW.

Figure 2. Deming Lake last millennium age-depth model with 2σ errors (hatched area). The circle represents calibrated ^{14}C age.

Figure 3. a) Sedimentary parameters measured on the freeze core: annual sediment (organic and mineral) flux, carbon isotopes, total carbon relative concentration (%TC), and ARM ratio (χ_{ARM}/IRM). b) Absolute and relative mass concentrations of model ferrimagnetic components: uniaxial non-interacting single domain (UNISD), interacting single domain (ISD), multi domain (MD), and superparamagnetic (SP). Gray horizontal bands mark periods of reduced detrital ferrimagnetic flux and increased relative concentrations of biogenic magnetite, highlighting episodes of inferred dry conditions at Deming Lake.

Figure 4. Comparison of Palmer Drought Severity Index (PDSI) (a), with detrended standard scores (DSS) for the ARM ratio (b), %TC (c), and mineral flux (d) during the twentieth century. The smoothed PDSI was obtained by applying a 10 year filter. DSS plots incorporate ^{210}Pb age uncertainty from Table 1 (shades of gray). PDSI values are from Cook et al. (2004), grid point 188 (N 47.5, W 95), located 40 km NNE of Deming Lake. Standard scores (Z-scores) were calculated as departure from trend, normalized by population standard deviation. Last century trends were found to be linear for %TC and ARM ratio, and exponential for mineral flux, which reflects modern settlement effects on sedimentation.

Figure 5. a) Comparison of long-term trends of $\delta^{13}C$ at Deming Lake (this study) and February temperature at Lake Mina (St. Jacques et al., 2008); b) Comparison of Deming Lake ARM ratio (χ_{ARM}/IRM, this study) with Deming Lake charcoal index (Clark, 1990), and Elk Lake *Stephanodiscus minutulus* relative

concentration (Bradbury and Dieterich-Rurup, 1993). All records are plotted on their respective time scales.

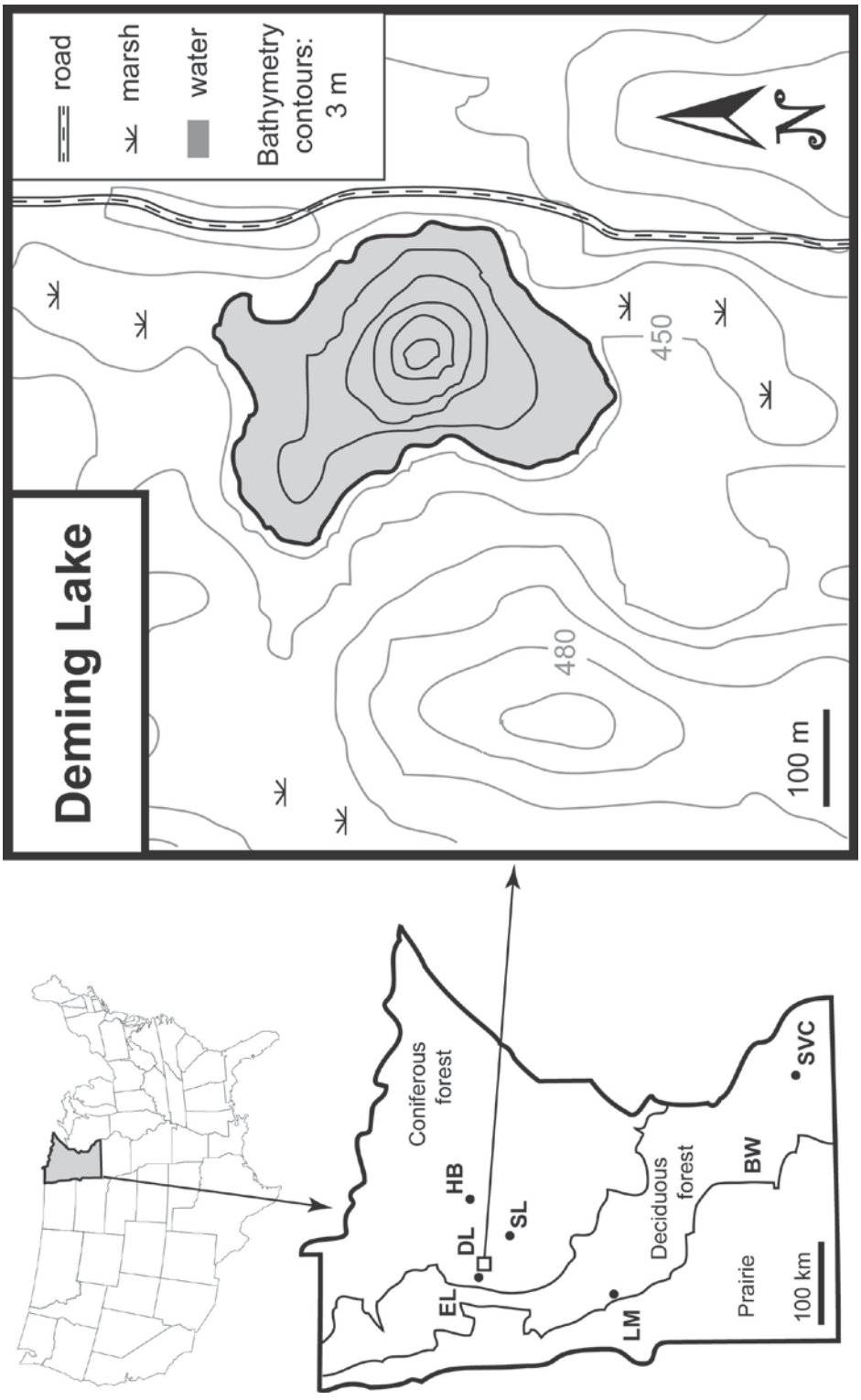

Figure 3.1 Geographical location of Deming Lake and map of the site

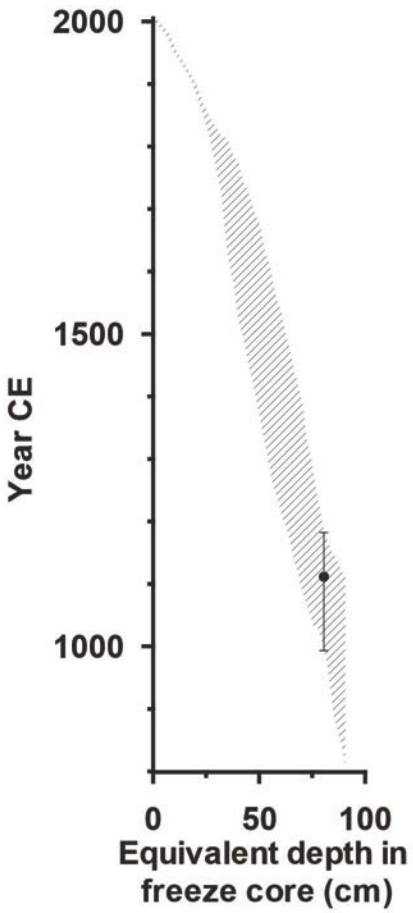

Figure 3.2 Deming Lake age-depth model

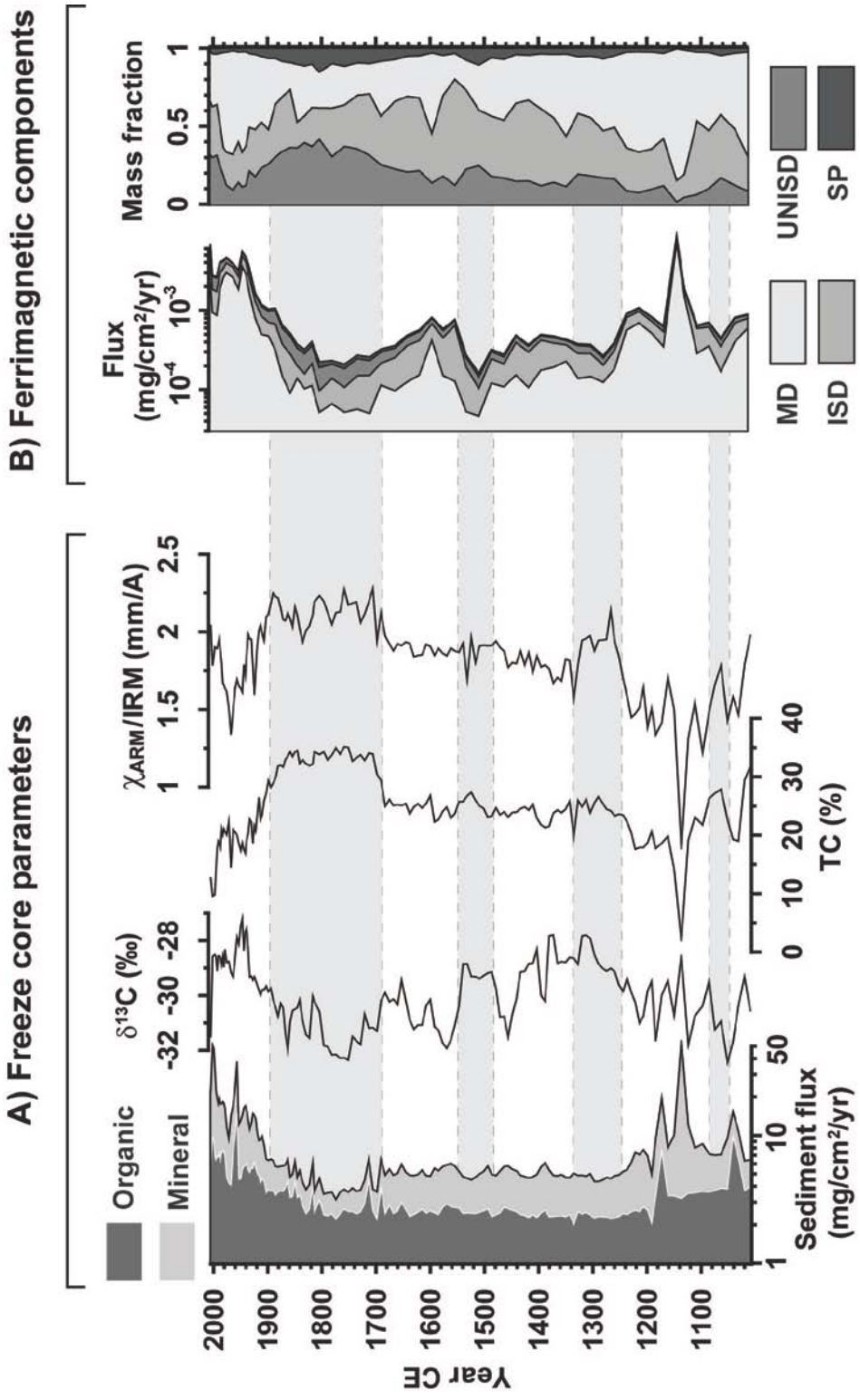

Figure 3.3 Deming Lake sedimentary and magnetic parameters

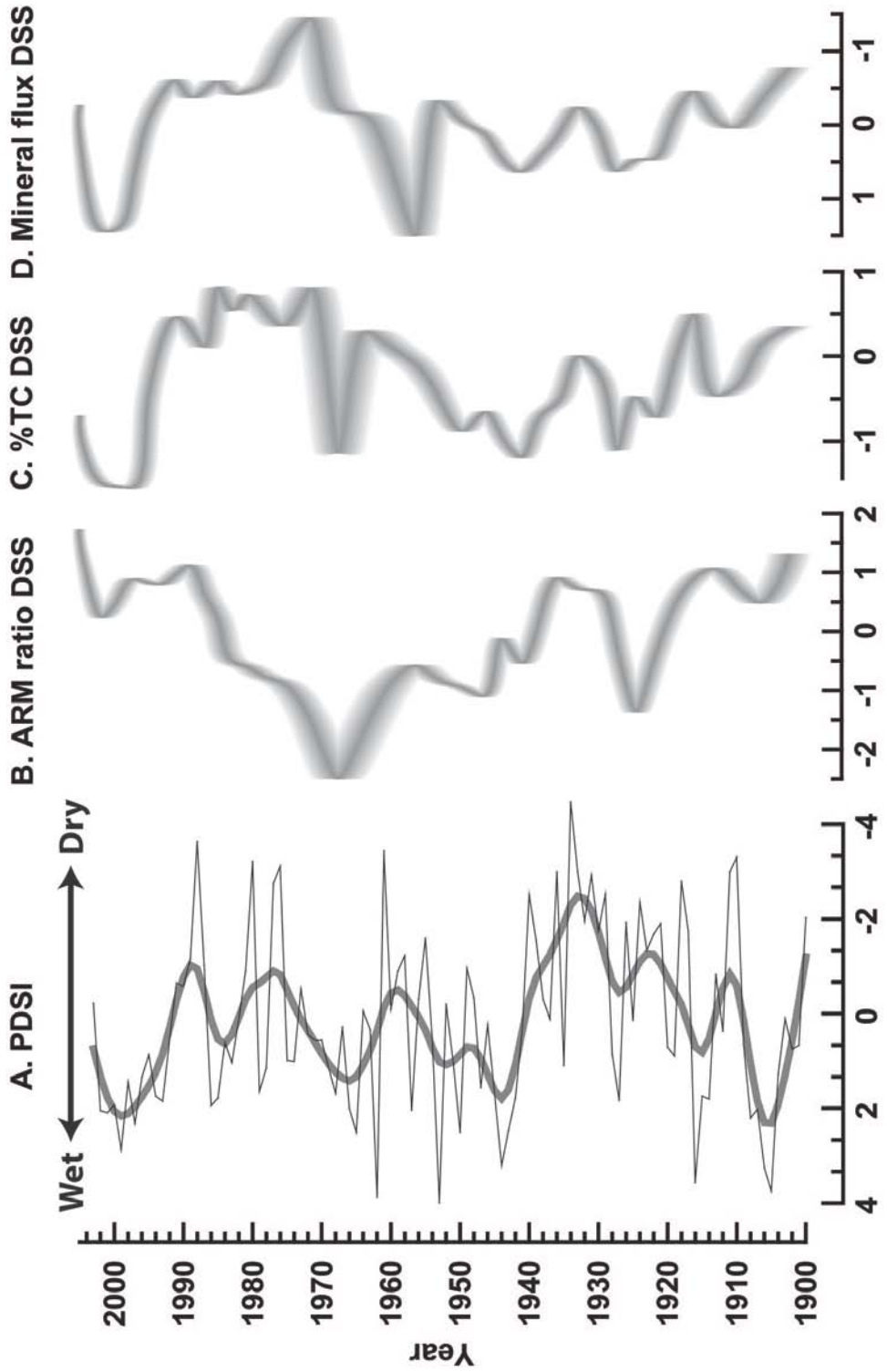

Figure 3.4 Comparison of Palmer Drought Severity Index (PDSI) with Deming Lake parameters

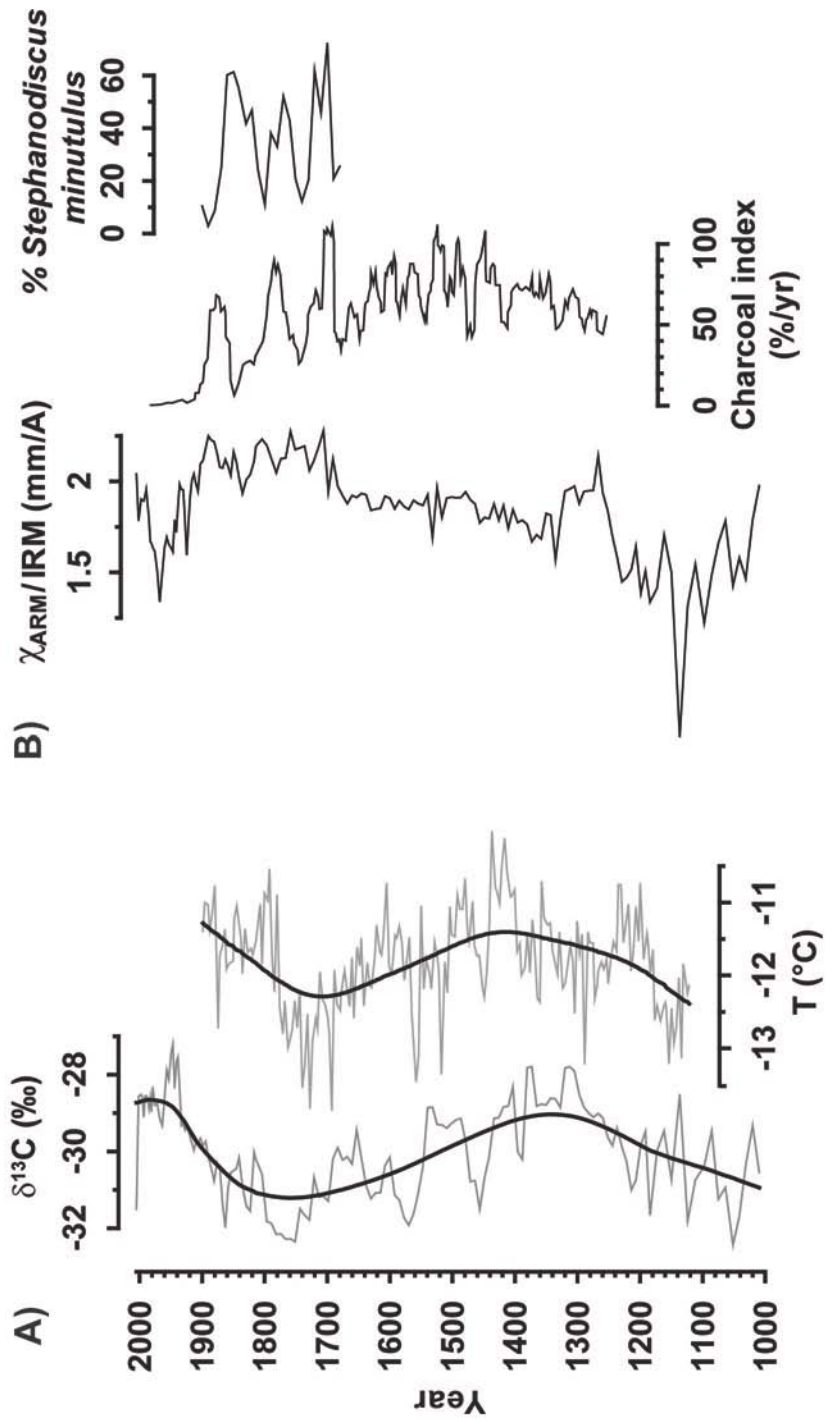

Figure 3.5 Comparison of Deming Lake parameters to other regional paleoclimatic records

Tables

Table 3.1 ^{210}Pb activity and ages

Top of interval (cm)	Base of interval (cm)	Cumulative dry mass (g/cm^2)	Unsupported activity (pCi/g)	Error of unsupported activity (± st.dev.)	Cumulative activity below interval (pCi/cm^2)
0	0.6	0.0904	24.2460	1.0049	17.5817
0.6	1.6	0.2452	10.1979	0.4347	16.0031
1.6	2.1	0.3196	10.4096	0.4608	15.2286
2.6	3.1	0.4301	20.1272	0.7065	13.3492
3.6	4.1	0.5115	20.1810	0.7205	11.7071
4.6	5.1	0.5853	18.4738	0.7043	10.3135
6.6	7.1	0.7282	15.6648	0.5153	7.9300
8.6	9.1	0.9563	12.5527	0.5557	4.8346
10.6	11.1	1.1771	5.3297	0.2507	3.1424
12.6	13.1	1.3522	4.8877	0.1617	2.2576
14.6	15.1	1.5222	3.4681	0.1223	1.5837
15.6	16.1	1.5953	3.0549	0.1140	1.3527
17.6	18.1	1.7228	3.5253	0.1187	0.9267
19.6	20.1	1.8359	3.1163	0.1190	0.5571
21.6	22.1	1.9445	1.8183	0.1014	0.3113
23.6	24.1	2.0376	1.1562	0.0715	0.1812
25.6	26.1	2.1284	0.6792	0.0739	0.1045
27.6	28.1	2.2605	0.2964	0.0540	0.0484

Supported ^{210}Pb: 1.3602 ± 0.0291 pCi/g (3 supported samples); cumulative unsupported ^{210}Pb: 19.7726 pCi/cm^2; unsupported ^{210}Pb flux: 0.6503 pCi/cm^2/yr.

Table 3.1 - continued

Top of interval (cm)	Base of interval (cm)	Age at base of interval (yr)	Error of age (± st.dev.)	Date CE
0	0.6	3.77	1.76	2004.0
0.6	1.6	6.79	1.85	2001.0
1.6	2.1	8.39	1.91	1999.4
2.6	3.1	12.62	1.96	1995.1
3.6	4.1	16.83	2.14	1990.9
4.6	5.1	20.90	2.34	1986.8
6.6	7.1	29.34	2.81	1978.4
8.6	9.1	45.23	4.00	1962.5
10.6	11.1	59.07	1.71	1948.7
12.6	13.1	69.69	2.02	1938.1
14.6	15.1	81.07	1.89	1926.7
15.6	16.1	86.13	2.09	1921.6
17.6	18.1	98.28	2.64	1909.5
19.6	20.1	114.62	3.96	1893.1
21.6	22.1	133.31	4.20	1874.4
23.6	24.1	150.69	5.60	1857.1
25.6	26.1	168.36	8.11	1839.4
27.6	28.1	193.08	12.46	1814.7

Chapter 4: Magnetic properties of surface sediments from small lakes in Minnesota, USA[*]

Ioan Lascu[1,2], Colin Plank[2]

[1]*Institute for Rock Magnetism, N. H. Winchell School of Earth Sciences, University of Minnesota, 310 Pillsbury Drive SE, Minneapolis, Minnesota, U.S.A. 55455*

[2]*Limnological Research Center, N. H. Winchell School of Earth Sciences, University of Minnesota, 310 Pillsbury Drive SE, Minneapolis, Minnesota, U.S.A. 55455*

[*] We thank NSF-REU interns Marcia Ferrera and Rachel Murray for help in the field and for performing some of the laboratory analyses, and Bob Hafner for help with TEM-related issues. TEM analysis was carried out in the University of Minnesota Characterization Facility, which receives partial support from NSF through the MRSEC program. IL benefited from a Geological Society of America Student Research Grant and a University of Minnesota Doctoral Dissertation Fellowship. CP benefited from an NSF Doctoral Dissertation Research Improvement Grant and a University of Minnesota Doctoral Dissertation Fellowship. This is IRM contribution 1105.

Synopsis

We have investigated the variability of the magnetic properties of surface sediments across eight Minnesota lake basins. The measured magnetic properties are controlled by the competing fluxes of detrital and biogenic particles, and differ according to location in the basin. Shoreline sediments are dominated by the detrital fraction, whereas littoral and profundal sediments are characterized by a combination of biogenic and detrital particles. The biogenic fraction and the relative concentration of organic matter are both controlled by detrital inputs. The position of the oxic-anoxic transition in lakes controls the site of biogenic magnetite formation, and determines the degree of preservation of biogenic particles as chains. The likelihood of preservation of undisturbed chains is higher for bacterial magnetite formed at the top of the sediment column in the littoral area, which may coincide with the oxic-anoxic interface, than for biogenic magnetite originating in the water column in the profundal area. Bacterial magnetite in the profundal facies will contain a higher proportion of chains collapsed during settlement to the bottom of the lake. This process increases the fraction of interacting biogenic grains, and artificially lowers the ARM ratio, which ceases to be a reliable grain size indicator in the profundal environment. A thorough understanding of factors such as basin morphology and limnologic conditions is therefore crucial for a more confident interpretation of the sedimentary record in terms of environmental conditions at the time of sediment deposition.

Keywords: surface sediments; magnetic properties; small lakes; Minnesota.

1. Introduction

The temporal variations of the magnetic properties of sediments have long been used in paleoenvironmental reconstructions, with a significant proportion of these studies based on lake sediments (Evans and Heller, 2003). Magnetic measurements have been used to reconstruct environmental change either via multi-parameter environmental magnetic studies (e.g., Snowball, 1994; Rosenbaum et al., 1996; Geiss and Banerjee, 1997, 1999; Snowball et al., 1999, 2002; Geiss et al., 2003, 2004; Egli, 2004; Kim et al., 2005; Zillén and Snowball, 2009), or in conjunction with other paleoclimatic proxies (e.g., Williamson et al., 1999; Oldfield et al., 2003; Ortega et al., 2006; Garcin et al., 2006). In general, paleoenvironmental reconstructions from lakes are based on single cores taken from the deepest part of the basin. However, some studies have relied on the collection of multiple cores along transects for a better characterization of the basin-wide changes in response to environmental forcings (e.g., Digerfeldt, 1986; Dearing, 1997; Li et al., 2006; Wohlfarth et al., 2008). Knowledge about the spatial distribution of magnetic properties and components (as well as non-magnetic sedimentologic parameters) in lakes would be very useful because it could potentially help researchers make informed decisions regarding the selection of coring locations for multi-core studies. Sediment-magnetic characteristics of modern sediments have been measured in fluvial and marine settings, and have mostly been employed in fingerprinting sediment sources (e.g., Ellwood et al., 2006; Hatfield and Maher, 2009; Liu et al., 2010). However, heterogeneities in the spatial distribution of magnetic properties exist even for simple, self-contained systems such as the types of lakes often used in paleoenvironmental reconstructions, but a survey of the magnetic properties of surface sediments has not been conducted for lake basins. Here we investigate the magnetic properties of surface sediments collected along shore-to-shore transects in eight Minnesota lakes with the aim of providing a more detailed view of the distribution of sediment-magnetic properties across lake basins.

2. Study sites

Eight lakes (Deming, Mosomo, Birch, Sandy, Peterson, Erie, Elkhorn, Linka) were chosen to span a range of climatic settings, from the more humid, forest-dominated landscapes in the east to the dry prairie in the west (Fig. 1). The substrate is composed of glacial outwash in the case of Mosomo and Sandy, and glacial till in the case of Deming (situated in the Itasca moraine), Elkhorn, Linka (both in the Alexandria moraine), Erie (Altamount moraine), Peterson (Pine City moraine), and Birch (Altamount moraine and Pine City moraine). All lakes have simple morphologies, are groundwater fed, and exhibit seasonal thermal and chemical stratification. Morphometric parameters for each lake are listed in Table 1.

3. Methods

3.1. Surface sediment sampling

Surface sediments were collected along two transects in each lake, with a sample being retrieved at every meter of bathymetric change. The transects were selected based on an initial survey of lake bathymetry using a global positioning system (GPS) receiver with sonar. For each lake, one transect was chosen to coincide with the prevailing wind direction (NW-SE), with the other transect approximately perpendicular to the first. A total of 349 samples were collected using either a Hongve mini-gravity corer or an Ekman dredge, which resulted in the retrieval of the top 10-15 cm of the sediment column. The position of each sample was recorded using the GPS receiver, while the depth was recorded either using the sonar, or manually for shallow samples in the macrophyte-abundant areas. The samples were sealed inside polyethylene bags, transported to the Limnological Research Center at the University of Minnesota, where they were stored at 4º C. Before subsampling, each sample was homogenized by stirring with a glass rod.

3.2. Magnetic measurements

Magnetic susceptibility (χ), anhysteretic remanent magnetization (ARM), and isothermal remanent magnetization (IRM) were measured on all samples Wet sediment was weighed and packed into plastic boxes with an internal volume of 5.28 cm^3. Susceptibility was measured at a frequency of 920 Hz on an Geofyzika KLY-2 Kappabridge Susceptibility Meter. Remanence measurements were performed with a 2G superconducting quantum interference device rock magnetometer. ARM was imparted using a D-Tech 2000 alternating frequency (AF) demagnetizer. A bias field of 0.1 mT was superimposed on an AF field decaying from a peak value of 200 mT, at a rate of 10 μT per half cycle. ARM susceptibility (χ_{ARM}) was calculated by normalizing the ARM to the direct field. Stepwise alternating AF demagnetization of the ARM was performed on selected samples, using peak fields progressively

increasing from 0.5 to 200 mT, for a total of 100 measurement steps spaced on a logarithmic scale. IRM was imparted in a 200 mT direct field, using an ASC Scientific IM-10-30 impulse magnetizer. The ARM ratio was computed by normalizing the ARM susceptibility by the IRM (χ_{ARM}/IRM). The IRM was demagnetized following the same procedure as for the ARM on the selected samples. IRM stepwise acquisition experiments were performed using a Princeton Measurements vibrating sample magnetometer (VSM) using fields of up to 200 mT. Coercivity components were obtained using the software package MAG-MIX (Egli, 2003) from the ARM and IRM curves, by fitting skewed generalized Gaussian distributions to the first derivatives of the curves. Finally, all the samples were then dried and reweighed, and the measurements renormalized to the dry sediment mass.

Hysteresis measurements were conducted on a third of the total number of samples, and were chosen to be representative for the shoreline, littoral, and profundal depositional settings. Hysteresis loops were measured on dry samples with the VSM, using a maximum applied field of 1 T. The following parameters were obtained from the hysteresis loops: saturation magnetization (M_s), saturation remanence (M_{rs}), coercivity (H_c) and remanent coercivity (H_{cr}). The loop slopes at high fields were used to correct raw saturation magnetization values, and to calculate the contribution of non-ferrimagnetic minerals to the low field susceptibility.

A subset of the samples that underwent hysteresis analysis was selected for low temperature experiments using a Quantum Design magnetic properties measurement system (MPMS), for a more robust determination of the mineralogy and grain size of the magnetic carriers. The sediment was physically homogenized to randomize the magnetic moment acquired during hysteresis measurements, and packed tightly into gelatin capsules with an internal volume of 0.1 cm^3. Frequency dependence of susceptibility was measured as a function of temperature at 1, 10, and 100 Hz, from 10 to 300 K at 10 K intervals. Low temperature saturation IRM (SIRM) was acquired in a 2.5 T field at 10 K following two separate treatments: field cooling (FC) in a 2.5 T field and zero-field cooling (ZFC), from 300 to 10 K. The remanence behavior was then recorded on warming to room temperature at 5 K intervals. Finally,

a room temperature SIRM imparted in a 2.5 T field was partially decayed by cooling the sample to 10 K and then rewarming it to 300 K. Measurements were performed in zero field at 5 K intervals.

ARM ratios and remanence ratios (M_s/M_{rs}) were used to calculate the contributions of fine-grained (30-100 nm) single domain (SD), and large (>10 μm) multi domain (MD) ferrimagnetic particles to the total magnetization of the sediments, as described in Lascu et al. (2010).

3.3. Loss on ignition (LOI)

LOI was employed as a rapid and inexpensive method for determining the organic matter (OM), carbonate, and silicic content of the sediments (Dean, 1974; Heiri et al., 2001). The organic matter and carbonate mineral contents are calculated as percent mass loss after combusting the sediment at 550 and 1000º C respectively, relative to the dry mass of the sample. The ignition residue consists of siliciclastic material and amorphous silica.

3.4. Grain size

Grain size analysis was performed using a Horiba laser diffractometer. Organic matter was digested using a 30% hydrogen peroxide solution at 85° C for 30 minutes, followed by treatment with 11 M nitric acid solution for 10 minutes. Biogenic silica was digested using 1M sodium hydroxide solution at 85° C for 15 minutes. The samples were centrifuged and rinsed after each digestion step. The remaining sedimentary fraction was dispersed with sodium hexametaphosphate solution mixed at 5 g/l, and shaken overnight. The sand-rich samples were mixed manually in the particle size analyzer in order to assure representative sampling of the grain size fractions.

3.5. Transmission electron microscopy (TEM)

The magnetic fraction was extracted from selected samples for TEM analysis. Sediment subsamples were disaggregated using sodium hexametaphosphate (0.5 g to

100 ml sediment slurry) and circulated through an in-house built magnetic separator. The magnetic fraction was extracted using a high-gradient permanent magnet, collected on a daily basis for a two-week period, and stored in isopropanol at 4°C. TEM copper grids were briefly immersed in the medium containing the extract, and then air-dried at room temperature for 24 hours in a fume hood. TEM images were obtained at the University of Minnesota Characterization Facility using a FEI Tecnai T-12 transmission electron microscope operating at 120 kV.

4. Results and discussion

4.1. Sediment transects

We have grouped the eight lakes, according to their geographic location, into a northern group (Deming and Mosomo), an eastern group (Peterson, Sandy, Birch), and a western group (Erie, Elkhorn, Linka). Sediment transect data for all eight lakes are presented in figs. 2-9. Each transect contains information on bathymetry (a), grain size (b), composition (c), ARM ratio (d), and ferrimagnetic concentration reflected by ARM and IRM (e).

Following the classification of Wetzel (2001), for each lake we can distinguish: 1) a shoreline facies; 2) a littoral facies, above wave base, comprising the zone of macrophyte growth extending from shoreline down to the aphotic zone; and 3) a profundal facies, below wave base, with vegetation-free sediment due to the lack of light. The littoral-profundal transition area of the littoral facies (referred to as the littoral slope or littoriprofundal facies) is characterized by a steepening of the basin slope, and by the presence of non-macrophyte plants in the photic zone (Moeller and Wetzel, 1988). The shoreline and littoriprofundal facies are thus higher energy facies, with particle entrainment due to the action of waves, and gravitational movement on a steeper slope respectively (Cyr, 1998; Smyth and Hay, 2002). The shoreline and littoral facies are areas of erosion and transport, while the profundal facies is an area of accumulation (Håkanson, 1977). Compositionally, the shoreline facies is dominated by siliciclastic material (>90%). The littoral and profundal samples are mixtures of siliciclastic material (20-100%), and non-siliciclastic material (<80%), dominated by organic matter in the northern and eastern lakes, and carbonates in the western lakes (Figs. 2-9, panel c). The clastic material in the shoreline facies is predominantly sand-sized. The littoral facies contains a mixture of sand, silt (50-90%), and clay (<50%), with coarser particles in the littoriprofundal zone. A mixture of silt (60-85%) and clay (<40%) characterizes the profundal facies (Figs. 2-9, panel b).

The magnetic concentration-dependent parameters IRM, ARM, and χ (Tables A.5-A.12) indicate variable mass concentrations of ferrimagnetic material across the lake basins (Figs. 2-9, panel e). The littoriprofundal and profundal sediments are characterized by higher concentrations of magnetic particles than the shoreline and shallow littoral sediments in most of the lakes. The one exception is Elkhorn Lake, where the NW and SW shorelines are developed as residential areas. The ARM ratio (Figs. 2-9, panel d) reflects the proportion of grains which can efficiently acquire ARM, i.e., SD magnetic particles. ARM ratio values higher than 1 mm/A are a good indication for the presence of these fine-grained particles (Moskowitz et al., 1993), and are commonly encountered in littoral and profundal settings. Values higher than 3 mm/A are indicative for SD particles that do not interact magnetostatically, which can be either isolated or aligned in linear chains. We refer to this sediment-magnetic fraction as the uniaxial non-interacting SD (UNISD) component, which is usually the magnetic expression of intact single chains of magnetite produced by magnetotactic bacteria. ARM ratios exceed 3 mm/A in the littoral facies of the northern lakes, Deming and Mosomo. The profundal samples have slightly lower values than the littoral ones, indicating a higher relative concentration of particles that do not efficiently acquire ARM, i.e., MD grains, or clumps of magnetostatically interacting SD particles (ISD). Samples from the shoreline and some littoral slope settings (e.g., Sandy, Erie and Linka) are lower than 1 mm/A, suggesting a more abundant relative proportion of MD or ISD grains.

4.2. Magnetic components

In spite of the large scatter, the ARM ratio correlates positively with %OM (Fig. 10a), indicating both parameters are in general controlled by input of terrigenous sediment containing siliciclastic material and large MD ferrimagnetic particles. Remanence and coercivity ratios (respectively M_{rs}/M_s and H_{cr}/H_c) obtained from hysteresis measurements show that organic-poor samples have abundant MD grains (Fig. 10b), while samples containing larger fractions of SD grains are organic rich. This suggests that low ARM ratios are broadly controlled by the presence of MD,

rather than ISD particles. The exceptions are the organic-rich northern lakes which have reduced detrital input. Figure 11 shows the distribution of the UNISD and ISD components along the transects. For the transects where the UNISD and ISD curves are positively correlated, it is the MD component (not shown) that controls the ARM ratio. In such cases the ARM ratio can be used as a grain size indicator. If the curves are not correlated, then the ISD component will partially control the ARM ratio. This occurs in the organic-rich northern lakes, Deming and Mosomo, which have reduced detrital input, and have stronger seasonal stratification.

The low temperature (LT) experiments (Figs. 12, A1-A21) confirm that shoreline samples are dominated by the presence of MD magnetite, while the littoral and profundal are finer grained and may contain magnetic mineral phases such as maghemite and goethite. A diagnostic feature of magnetite is a sharp change in magnetization intensity at ~120 K (Verwey transition, T_v). MD particles show no frequency dependence of susceptibility (panel a), higher values for the ZFC LT remanence below T_v (panel c), and little to no recovery of room temperature (RT) remanence that has been cooled to 10 K before rewarming (panel d). Littoral and profundal samples show frequency dependence of susceptibility, FC LT remanence values equal or higher than after ZFC treatment, and partial recovery of the RT remanence on warming. The frequency dependence is attributed to the presence of nm-sized superparamagnetic (SP) grains, while higher FC than ZFC remanence values and RT remanence recovery are indicative of an SD-like component. The increasing trend observed in the cooling of the RT remanence is due to the presence of ferric oxy-hydroxides such as maghemite and/or goethite (Dekkers et al., 1989; Özdemir and Dunlop, 2010).

The coercivity analysis (Fig. 13) indicate that the magnetic fraction of the sediment consist of three magnetite components: a low coercivity (20 mT) detrital component, and two biogenic components, one with a median coercivity of ~40 mT (biogenic soft), and one with a median coercivity of 70 mT (biogenic hard) (Egli, 2004). Two shoreline samples also contain a detrital component with higher median coercivity, attributed to more oxidized phases (Egli, 2004). The detrital components

have a larger dispersion parameter, signifying a wide grain size range. The biogenic components have narrower grain size distributions as reflected by lower dispersion parameters. The biogenic hard component is attributed to more grains with higher shape anisotropy, while the biogenic soft component is generally thought to arise from more equidimensional grains. The TEM images show that the two main types of biogenic magnetite grains are indeed equidimensional (cubo-octahedral), and elongated (prismatic and bullet-shaped magneto-fossils (Fig. 13). The cubo-octahedral particles have aspect ratios of ~1, while the prismatic and bullet shaped particle aspect ratios can attain values of up to 3.

4.3. Controls on magnetic properties of lake sediments

The magnetic properties of modern sediments in the eight lakes considered for this study are controlled by input of detrital versus biogenic particle fluxes, and this is dependent on the lacustrine facies. Where palustrine vegetation is absent, shoreline sediments are devoid of organic matter (Shuman, 2004), and are coarser, due to the high-energy environment created by wave motion (Smyth and Hay, 2002). The absence of organic matter means there is no oxygen depletion from decomposition processes. Therefore, the high-energy, oxic environment is not favorable for magnetotactic bacteria subsistence, so the magnetic properties of shoreline sediments are controlled exclusively by external sediment fluxes, via overland flow or eolian transport pathways. Magnetic properties are dominated by the MD component, possibly with a minor SD contribution from catchment soils.

The littoral facies is situated above wave base, in the erosion and transport zone (Håkanson, 1977), but is a much quieter sedimentary environment than the shoreline due to the presence of macrophytes. Relative organic concentrations peak in the littoral facies in all lakes because of macrophyte biomass. In the western lakes the observed relative carbonate concentration increase in the littoral facies is attributed to enhanced calcite incrustation due higher pH conditions inside the vegetation (Koschel et al., 1983; van Donk and van de Bund, 2002). The lower energy, coupled with lower oxygen levels in the sediment due to organic matter decomposition, leads to an

increase in biogenic magnetic particles relative to detrital magnetic grains, due to a more favorable for magnetotactic bacteria survival. Furthermore, the oxic-anoxic transition zone, where magnetotactic bacteria reside, is at, or immediately below, the sediment water interface, which leads to a rapid and rather undisturbed incorporation of bacterial magnetite in the sediment, explaining the high ARM ratios encountered in the shallow littoral facies. The littoral slope is a slightly higher energy environment due to the increased mobilization of grains on a steeper slope (Lam Lau and Engel, 1999). Concordantly we observe an increase in the proportion of sand-sized grains, which in some cases is accompanied by a parallel shift to a larger magnetic grain size, accompanied by a lowering of the ARM ratio (e.g., at Linka, Sandy).

The profundal facies is an area of deposition (Håkanson, 1977) and is dominated by fine-grained clastics (clay and silt) and organics (mostly of lacustrine origin) in the northern and eastern lakes. The organic material is replaced by carbonates in the western lakes, which are situated in a slightly drier climate, and have higher concentrations of $CaCO_3$, Ba and Sr supplied from shale and carbonate-bearing tills (Dean and Gorham, 1976; Dean et al., 1993). While magnetic concentration increases due to sediment focusing, the ARM ratio tends to have similar values as in the littoral zone, indicating that the proportion between MD and SD grains remains relatively constant. However, for at least half of the transects, the ARM ratio is slightly lower for profundal sediments. This may be an effect of sediment focusing, whereby the deepest part of the lake, as the ultimate locus of sediment deposition, receives a more significant supply of MD particles than the littoral zone (Davis and Ford, 1982). This can certainly be argued for lakes like Elkhorn and Sandy, for which the UNISD and ISD components correlate positively (Fig. 11). However, for lakes like Deming and Mosomo, where the UNISD and ISD components are almost anticorrelated, the explanation for the lowering of ARM values must be different. We propose two mechanisms that might account for this phenomenon. First, Deming and Mosomo have stronger water column stratification, with Deming being meromictic (permanently stratified). This means that the oxic-anoxic transition is high in the water column, and therefore so are the living magnetotactic bacterial communities. When the

bacteria die, there is more chance for the disruption of the chain structures as the particles sink to the bottom. Collapsed chains have been observed in suspended particulate matter filtered from water samples collected in Brownie Lake, Minnesota (Lascu et al., 2010; Lascu, unpublished data), so the process must commence shortly after the bacterium dies. The collapse of the chain structure translates to the classification of those grains as part of the ISD component, whereas they would have remained under the UNISD category if there had been no vertical transport, as is the case for the shallow littoral facies. Second, magnetotactic bacteria strains that produce elongated particles may not have a firm requirement for slightly oxygenated waters (Yamazaki and Kawahata, 1998), so more abundant elongated particles in anoxic environments may be directly responsible for low ARM ratio values, because they are more prone to collapse due to their shape (Egli et al., 2010; Li et al., 2010). In addition, elongated magnetic particles may originatte from bacterial strains that produce multiple chains that are parallel or bundled (Hanzlik et al., 1996, 2002), so the bacterial strain itself contributes in this case to the lowering of the ARM ratio values.

5. Conclusions

The magnetic properties of surface sediments in eight Minnesota lakes are controlled by the competing fluxes of detrital and biogenic magnetite. Shoreline samples are dominated by the detrital fraction, whereas littoral and profundal samples are a mixture of biogenic and detrital particles. The biogenic fraction is correlated with the relative concentration of organic matter, indicating that detrital input is a common controlling factor to both parameters. The position of the oxic-anoxic transition in lakes controls the locus of biogenic magnetite formation, and determines the way in which biogenic particles are preserved. The chance of preservation of undisturbed chains is higher for bacterial magnetite formed at the top of the sediment column in the littoral area, than for biogenic magnetite originating in the water column in the profundal area. Bacterial magnetite in the profundal facies will contain a higher proportion of chains collapsed during settlement to the bottom of the lake. This process increases the fraction of interacting SD grains, and artificially lowers the ARM ratio, which ceases to be a reliable grain size indicator in the profundal environment. The findings presented here should have implications for the interpretation of the variability of magnetic properties observed in sediment cores, at least in temperate-climate regions. That is, a thorough understanding of factors such as basin morphology and limnologic conditions is crucial for a more confident interpretation of the sedimentary record in terms of environmental conditions at the time of sediment deposition.

References

Cyr, H., 1998. Effects of wave disturbance and substrate slope on sediment characteristics in the littoral zone of small lakes. Canadian Journal of Fisheries and Aquatic Sciences 55, 967-976.

Davis, M.B., Ford, M.S., 1982. Sediment focusing in Mirror Lake, New Hampshire. Limnology and Oceanography 27, 137-150.

Dean, W.E., Gorham, E., 1976. Major chemical and mineral components of profundal surface sediments in Minnesota lakes. Limnology and Oceanography 21, 259-284.

Dean, W.E., Gorham, E., Swaine, D.J., 1993. Geochemistry of surface sediments of Minnesota lakes, in Bradbury, J.P., Dean, W.E. (Eds.), Elk Lake, Minnesota: Evidence for Rapid Climate Change in the North-Central United States. Geological Society of America Special Paper 276, pp. 115-133.

Dearing, J.A., 1997. Sedimentary indicators of lake-level changes in the humid temperate zone: a critical review. Journal of Paleolimnology 18, 1-14.

Dekkers, M.J., 1989. Magnetic Properties of Natural Goethite-II. TRM Behaviour During Thermal and Alternating Field Demagnetization and Low-Temperature Treatment. Geophysical Journal International 97, 341-355.

Digerfeldt, G., 1986. Studies on past lake-level fluctuations, in Berglund, B.E. (Ed.), Handbook of Holocene Palaeoecology and Palaeohydrology. John Wiley & Sons, Chichester, United Kingdom, pp. 127-144.

Egli, R., Chen, A.P., Winklhofer, M., Kodama, K.P., Horng, C.-S., 2010. Detection of noninteracting single domain particles using first-order reversal curve diagrams. Geochemistry, Geophysics, Geosystems 11, doi: 10.1029/2009GC002916.

Egli, R., 2004. Characterization of individual rock magnetic components by analysis of remanence curves: 1. Unmixing natural sediments. Studia Geophysica et Geodetica 48, 391-446.

Egli, R., 2003. Analysis of the field dependence of remanent magnetization curves. Journal of Geophysical Research 108, 10.1029/2002JB002023.

Ellwood, B.B., Balsam, W.L., Roberts, H.H., 2006. Gulf of Mexico sediment sources and sediment transport trends from magnetic susceptibility measurements of surface samples. Marine Geology 230, 237-248.

Evans, M.E., Heller, F., 2003. Environmental Magnetism: Principles and Applications of Enviromagnetics. Academic Press, San Diego United States.

Garcin, Y., Williamson, D., Taieb, M., Vincens, A., Mathe, P., Majule, A., 2006. Centennial to millennial changes in maar-lake deposition during the last 45,000 years in tropical Southern Africa. Palaeogeography, Palaeoclimatology, Palaeoecology 239, 334-354.

Geiss, C.E., Banerjee, S.K., 1999. Comparison of two interglacial records from the midwestern U.S.A; Rock magnetism, palaeomagnetism and environmental magnetism. Physics and Chemistry of the Earth.Part A: Solid Earth and Geodesy 24, 793-798.

Geiss, C.E., Banerjee, S.K., 1997. A multi-parameter rock magnetic record of the last glacial-interglacial paleoclimate from south-central Illinois, USA. Earth Planet. Sci. Lett. 152, 203-216.

Geiss, C.E., Banerjee, S.K., Camill, P., Umbanhowar, C.E., 2004. Sediment-magnetic signature of land-use and drought as recorded in lake sediment from south-central Minnesota, USA. Quaternary Research 62, 117-125.

Geiss, C.E., Umbanhowar, C.E., Camill, P., Banerjee, S.K., 2003. Sediment magnetic properties reveal Holocene climate change along the Minnesota prairie-forest ecotone; Lake basins as archives of continental tectonics and paleoclimate. J. Paleolimnol. 30, 151-166.

Håkanson, L., 1977. The influence of wind, fetch, and water depth on the distribution of sediments in Lake Vanern, Sweden. Canadian Journal of Earth Sciences 14, 397-412.

Hanzlik, M., Petersen, N., Keller, R., Schmidbauer, E., 1996. Electron microscopy and ^{57}Fe Moessbauer spectra of 10-nm particles, intermediate in composition

between Fe_3O_4 and γ-Fe_2O_3, produced by bacteria. Geophysical Research Letters 23, 479-482.

Hanzlik, M., Winklhofer, M., Petersen, N., 1996. Spatial arrangement of chains of magnetosomes in magnetotactic bacteria. Earth and Planetary Science Letters 145, 125-134.

Hatfield, R.G., Maher, B.A., 2009. Fingerprinting upland sediment sources; particle size-specific magnetic linkages between soils, lake sediments and suspended sediments. Earth Surface Processes and Landforms 34, 1359-1373.

Heiri, O., Lotter, A.F., Lemcke, G., 2001. Loss on ignition as a method for estimating organic and carbonate content in sediments; reproducibility and comparability of results. Journal of Paleolimnology 25, 101-110.

Hutchinson, G.E., 1957. A Treatise on Limnology, Volume 1. Geography, Physics and Chemistry, Wiley, New York.

Kim, B., Kodama, K.P., Moeller, R.E., 2005. Bacterial magnetite produced in water column dominates lake sediment mineral magnetism: Lake Ely, USA. Geophysical Journal International 163, 26-37.

Koschel, R., Benndorf, J., Proft, G., Recknagel, F., 1983. Calcite precipitation as a natural control mechanism of eutrophication. Archiv Für Hydrobiologie 98, 380-408.

Lascu, I., Banerjee, S.K., Berquo, T.S., 2010. Quantifying the concentration of ferrimagnetic particles in sediments using rock magnetic methods. Geochemistry, Geophysics, Geosystems 11, doi: 10.1029/2010GC003182.

Lau Lam, Y., Engel, P., 1999. Inception of sediment transport on steep slopes. Journal of Hydraulic Engineering 125, 544-547.

Li, Y., Yu, Z., Kodama, K.P., Moeller, R.E., 2006. A 14,000-year environmental change history revealed by mineral magnetic data from White Lake, New Jersey, USA. Earth and Planetary Science Letters 246, 27-40.

Liu, J., Chen, Z., Chen, M., Yan, W., Xiang, R., Tang, X., 2010. Magnetic susceptibility variations and provenance of surface sediments in the South China Sea. Sedimentary Geology 230, 77-85.

Moeller, R.E., Wetzel, R.G., 1988. Littoral vs. profundal components of sediment accumulation: contrasting roles as phosphorous sinks. Verh. Internat. Verein. Limnol. 23, 386-393.

Moskowitz, B.M., Frankel, R.B., Bazylinski, D.A., 1993. Rock magnetic criteria for the detection of biogenic magnetite. Earth and Planetary Science Letters 120, 283-300.

Oldfield, F., Wake, R., Boyle, J., Jones, R., Nolan, S., Gibbs, Z., Appleby, P., Fisher, E., Wolff, G., 2003. The late-Holocene history of Gormire Lake (NE England) and its catchment: a multiproxy reconstruction of past human impact. The Holocene 13, 677-690.

Ortega, B., Caballero, M., Lozano, S., Vilaclara, G., Rodriguez, A., 2006. Rock magnetic and geochemical proxies for iron mineral diagenesis in a tropical lake: Lago Verde, Los Tuxtlas, east-central Mexico. Earth and Planetary Science Letters 250, 444-458.

Özdemir, Ö., Dunlop, D.J., 2010. Hallmarks of maghemitization in low-temperature remanence cycling of partially oxidized magnetite nanoparticles. J. Geophys. Res. 115, B02101.

Rosenbaum, J.G., Reynolds, R.L., Adam, D.P., Drexler, J., Sarna-Wojcicki, A.M., Whitney, G.C., 1996. Record of middle Pleistocene climate change from Buck Lake, Cascade Range, southern Oregon; evidence from sediment magnetism, trace-element geochemistry, and pollen. Geological Society of America Bulletin 108, 1328-1341.

Shuman, B., 2003. Controls on loss-on-ignition variation in cores from two shallow lakes in the northeastern United States. Journal of Paleolimnology 30, 371-385.

Smyth, C., Hay, A.E., 2002. Wave friction factors in nearshore sands. Journal of Physical Oceanography 32, 3490-3498.

Snowball, I.F., 1994. Bacterial magnetite and the magnetic properties of sediments in a Swedish lake. Earth Planet. Sci. Lett. 126, 129-142.

Snowball, I., Sandgren, P., Petterson, G., 1999. The mineral magnetic properties of an annually laminated Holocene lake-sediment sequence in northern Sweden. Holocene 9, 353-362.

Snowball, I., Zillen, L., Sandgren, P., 2002. Bacterial magnetite in Swedish varved lake-sediments; a potential bio-marker of environmental change. Quaternary International 88, 13-19.

van Donk, E., van de Bund, W.J., 2002. Impact of submerged macrophytes including charophytes on phyto- and zooplankton communities: Allelopathy versus other mechanisms. Aquatic Botany 72, 261-274.

Wetzel, R.G., 2001. Limnology: Lake and River Ecosystems, 3rd ed. Academic Press, San Diego, California, United States.

Wetzel, R.G., Likens, G.E., 1991. Limnological Analyses. Springer-Verlag, New York, New York, United States.

Williamson, D., Jackson, M.J., Banerjee, S.K., Marvin, J., Merdaci, O., Thouveny, N., Decobert, M., Gibert-Massault, E., Massault, M., Mazaudier, D., Taieb, M., 1999. Magnetic signatures of hydrological changes in a tropical Maar-Lake (Lake Massoko, Tanzania): preliminary results. Physics and Chemistry of the Earth 24, 799-803.

Wohlfarth, B., Veres, D., Ampel, L., Lacourse, T., Blaauw, M., Preusser, F., Andrieu-Ponel, V., Keravis, D., Lallier-Verges, E., Bjorck, S., Davies, S.M., de Beaulieu, J., Risberg, J., Hormes, A., Kasper, H.U., Possnert, G., Reille, M., Thouveny, N., Zander, A., 2008. Rapid ecosystem response to abrupt climate changes during the last glacial period in Western Europe, 40-16 ka. Geology 36, 407-410.

Yamazaki, T., Kawahata, H., 1998. Organic carbon flux controls the morphology of magnetofossils in marine sediments. Geology 26, 1064-1066.

Zillen, L., Snowball, I., 2009. Complexity of the 8 ka climate event in Sweden recorded by varved lake sediments. Boreas 38, 493-503.

Figures

Figure 1. Map of Minnesota with the locations of the eight lakes investigated in this study.

Figure 2. Deming Lake transects: a) bathymetric profile; b) percent sand, silt and clay; c) relative concentrations of organic matter, carbonate and silicic material as determined from LOI; d) ARM ratio; e) ARM and IRM.

Figure 3. Mosomo Lake transects. See Fig. 2 for explanation of plots.

Figure 4. Birch Lake transects. See Fig. 2 for explanation of plots.

Figure 5. Peterson Lake transects. See Fig. 2 for explanation of plots.

Figure 6. Sandy Lake transects. See Fig. 2 for explanation of plots.

Figure 7. Elkhorn Lake transects. See Fig. 2 for explanation of plots.

Figure 8. Erie Lake transects. See Fig. 2 for explanation of plots.

Figure 9. Linka Lake transects. See Fig. 2 for explanation of plots.

Figure 10. a) ARM ratio versus percent organic matter for all lakes. Note the positive relationship between the two parameters; b) Day plot (M_{rs}/M_s versus H_{cr}/H_c) by percent organic matter. Organic-rich samples tend towards the upper left corner and correspond to finer particle sizes. Organic-poor samples are found in the lower right corner, and correspond to MD grains.

Figure 11. Spatial distribution of model components UNISD and ISD along the transects.

Figure 12. Comparison of magnetic properties as a function of temperature for shoreline, littoral, and profundal samples. a) Magnetic susceptibility as a function of temperature and frequency; b) Imaginary component of magnetic susceptibility as a function of temperature and frequency. The increase of χ" with increasing temperature represents the tail end of a distribution of grain sizes, and corresponds to increased frequency dependence of the real susceptibility component in a; c) Low temperature (LT) isothermal remanence behavior on warming to room temperature (RT) after pretreating the sample by cooling in a 2.5 T field (FC) and in zero field (ZFC); d) RT isothermal remanence behavior on cooling to 10 K and rewarming to 300 K.

Fig. 13. a) Plot of dispersion parameter versus median coercivity for the coercivity components obtained from the deconvolution of (de)magnetization curves. The diamonds and squares are detrital (lithogenic and pedogenic) components, the circles represent the low coercivity (soft) biogenic component, and the triangles represent the high coercivity (hard) biogenic component. b-j) TEM images of magnetic extracts from littoral and profundal samples of Birch (c, d, g, i, j), Erie (b, e, f), and Mosomo (h). Lithogenic octahedra of MD (titano)magnetite can be seen in b and c. The rest of the images contain bacterial magnetite, mostly as aggregates of particles resulting from the disruption of the chain structure during the extraction procedure. Intact chains can be observed in d and f. Cubo-octahedral magnetite crystals are featured in images c-g, while elongated (mostly bullet-shaped) particles appear are featured in images h-j.

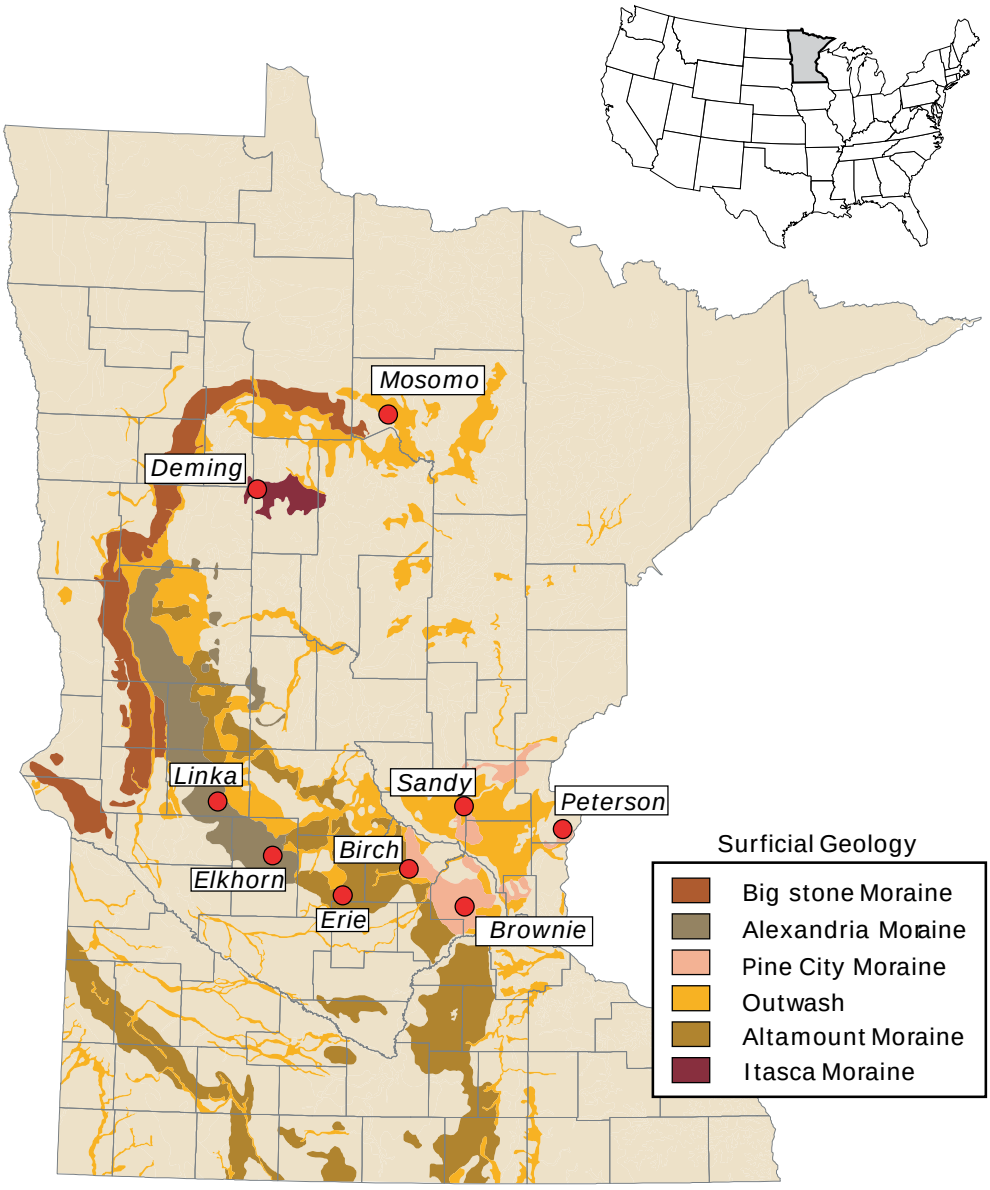

Figure 4.1 Map of Minnesota with the locations of the eight lakes investigated in this study

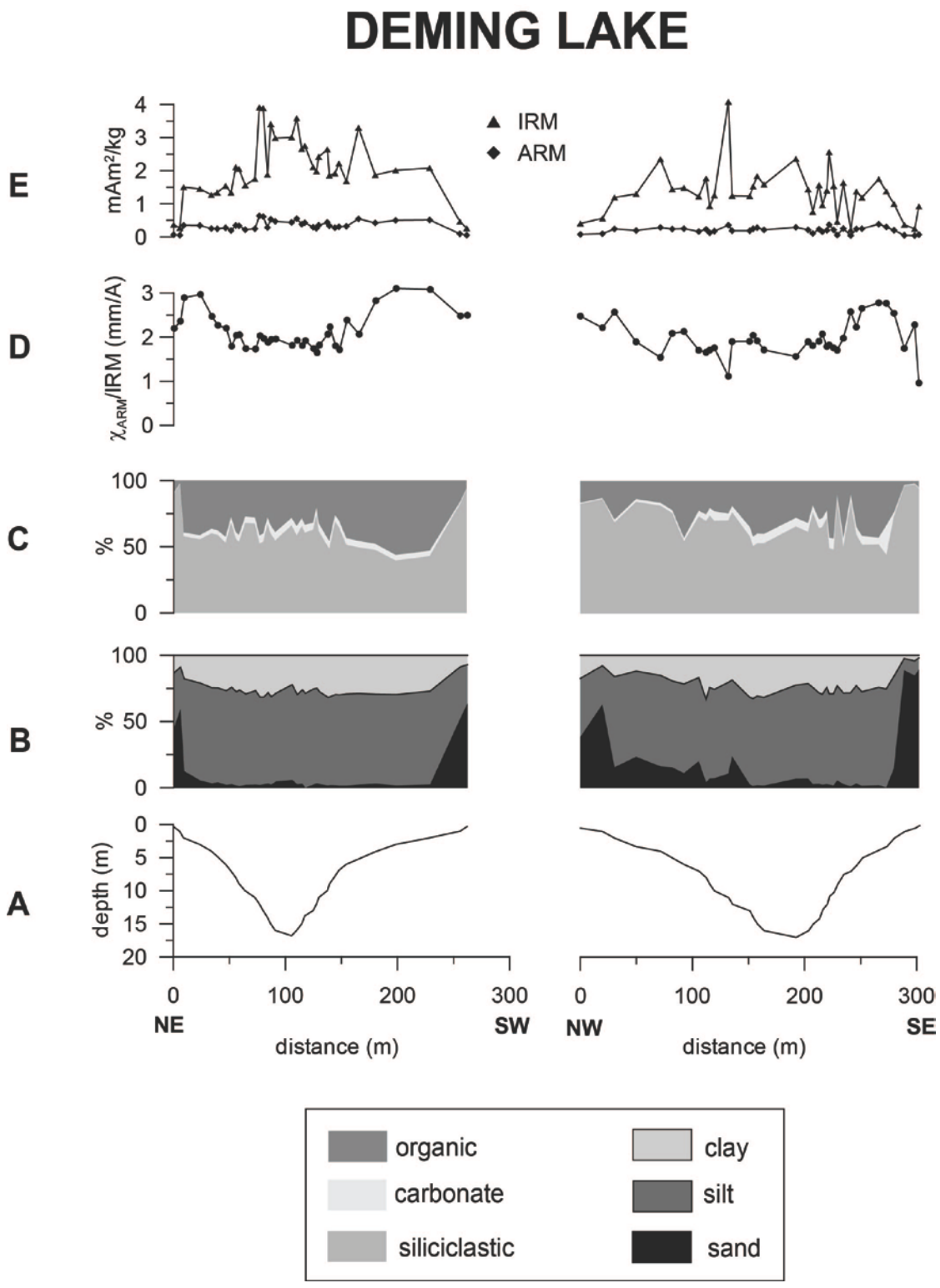

Figure 4.2 Deming Lake transects

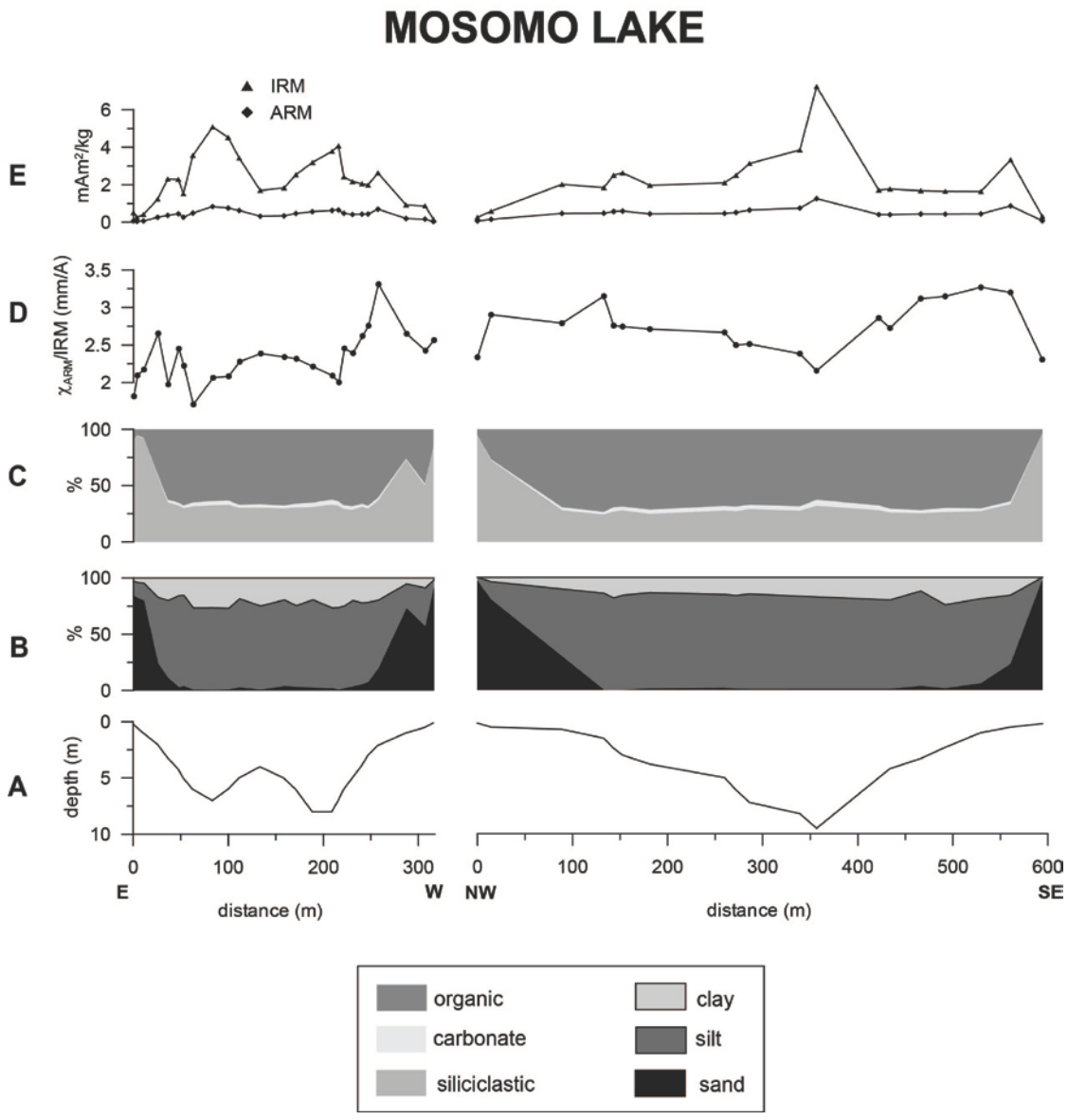

Figure 4.3 Mosomo Lake transects

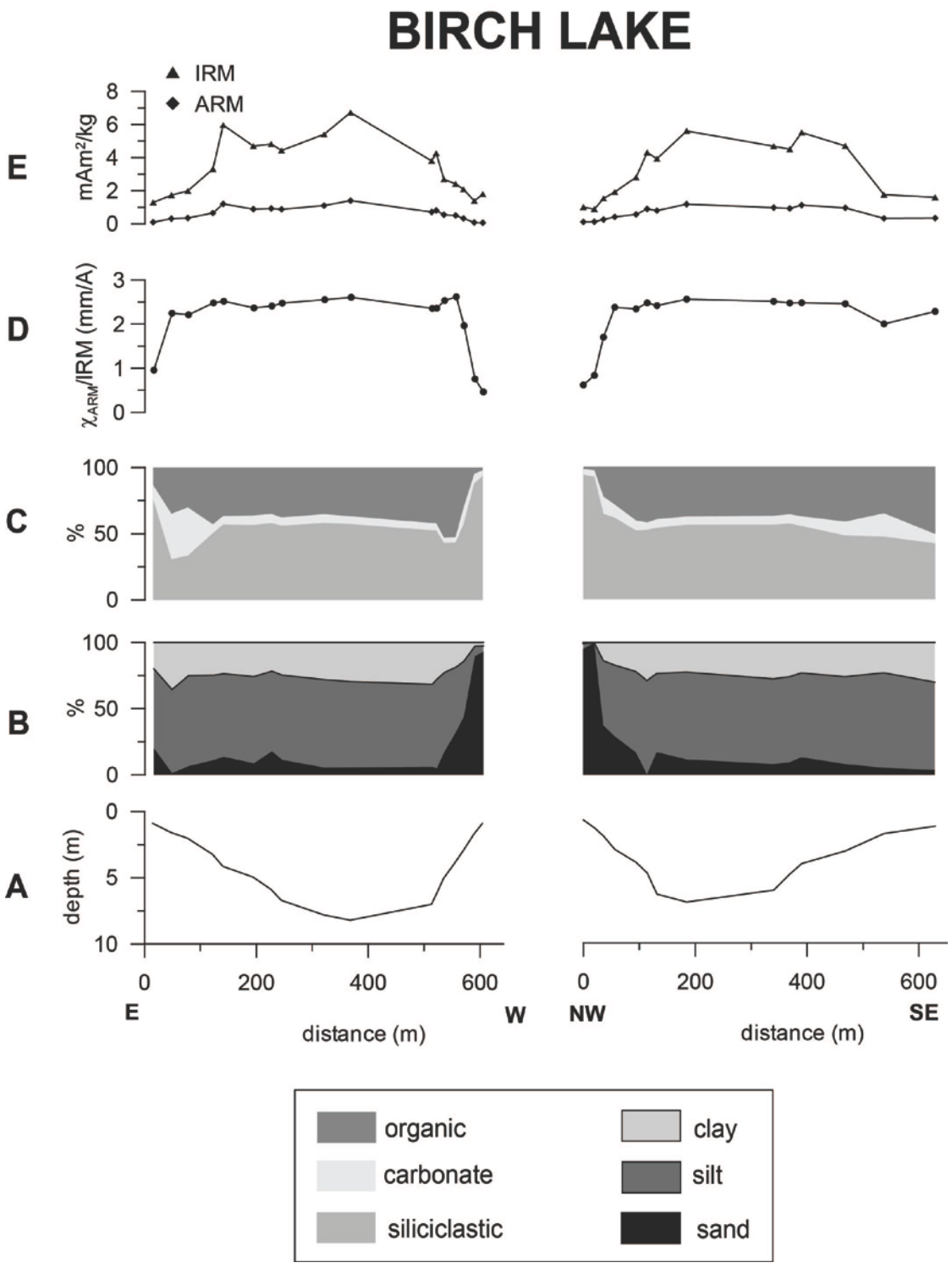

Figure 4.4 Birch Lake transects

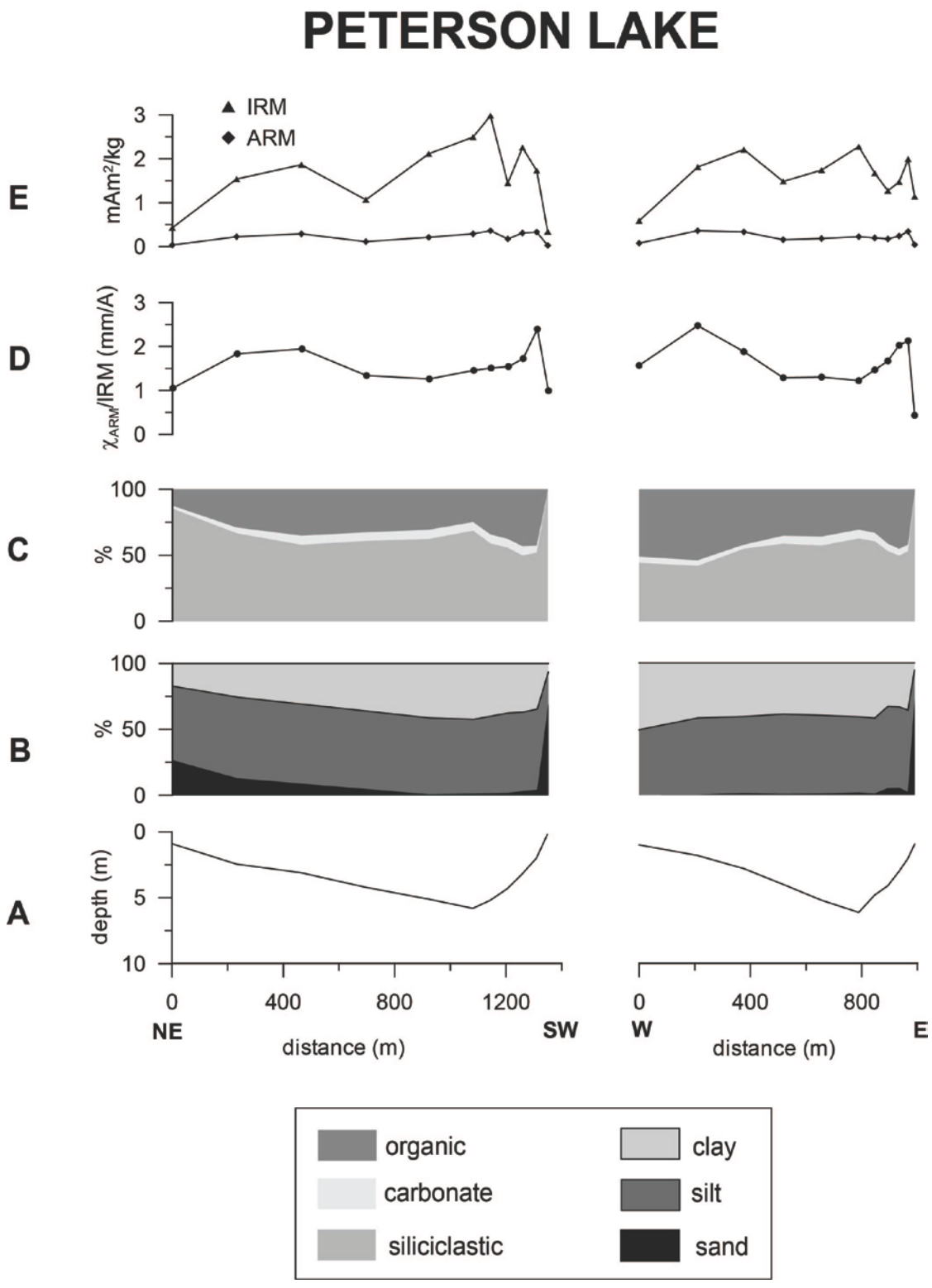

Figure 4.5 Peterson Lake transects

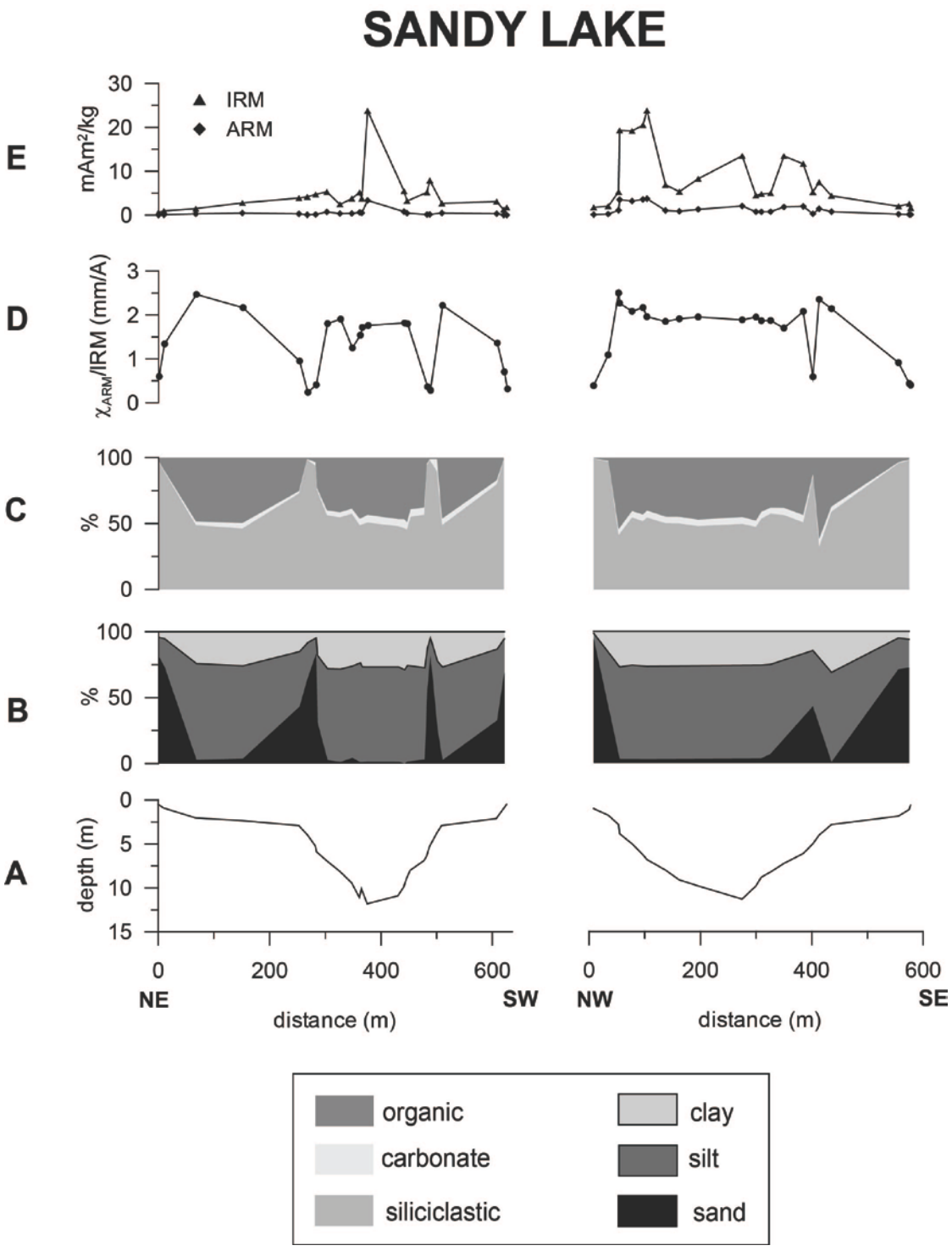

Figure 4.6 Sandy Lake transects

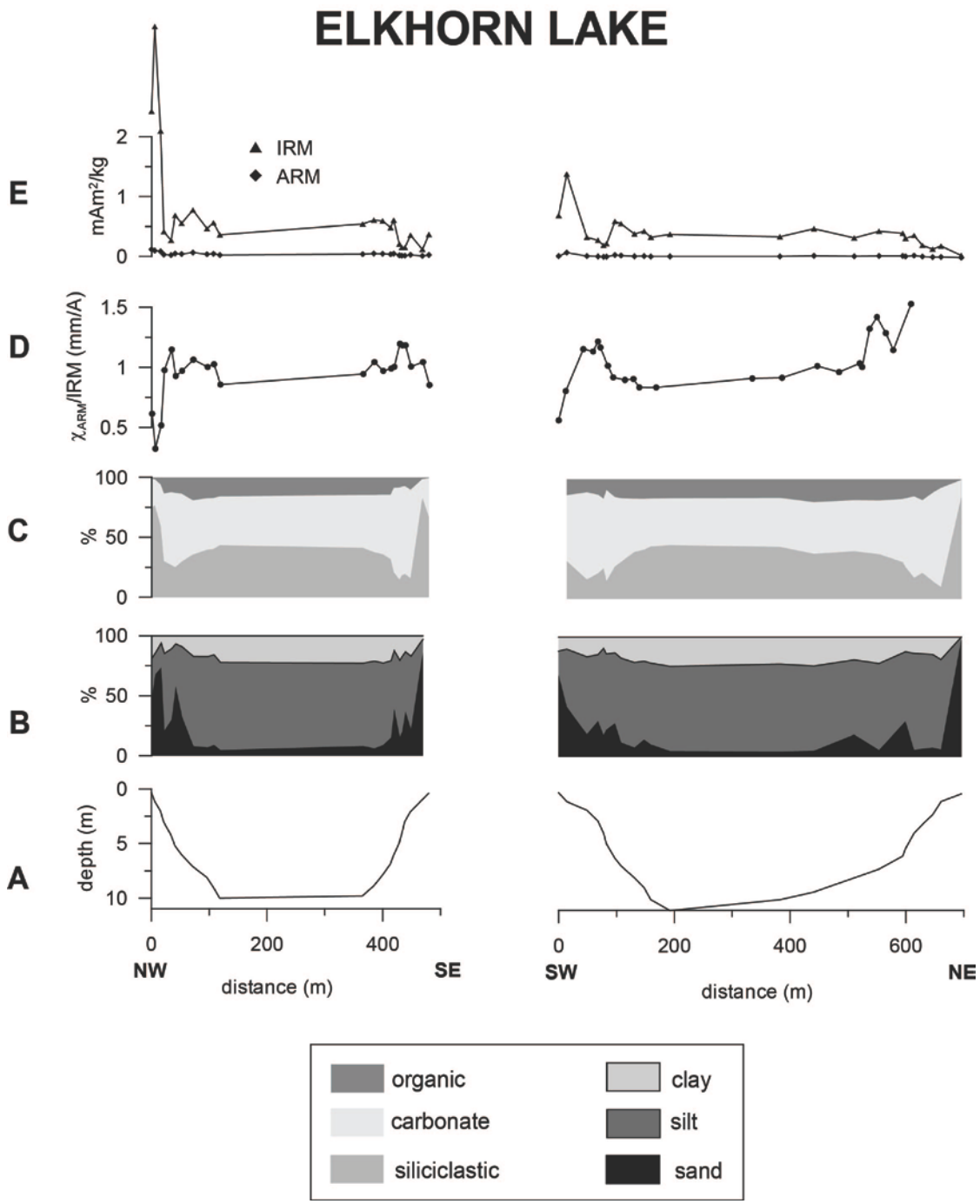

Figure 4.7 Elkhorn Lake transects

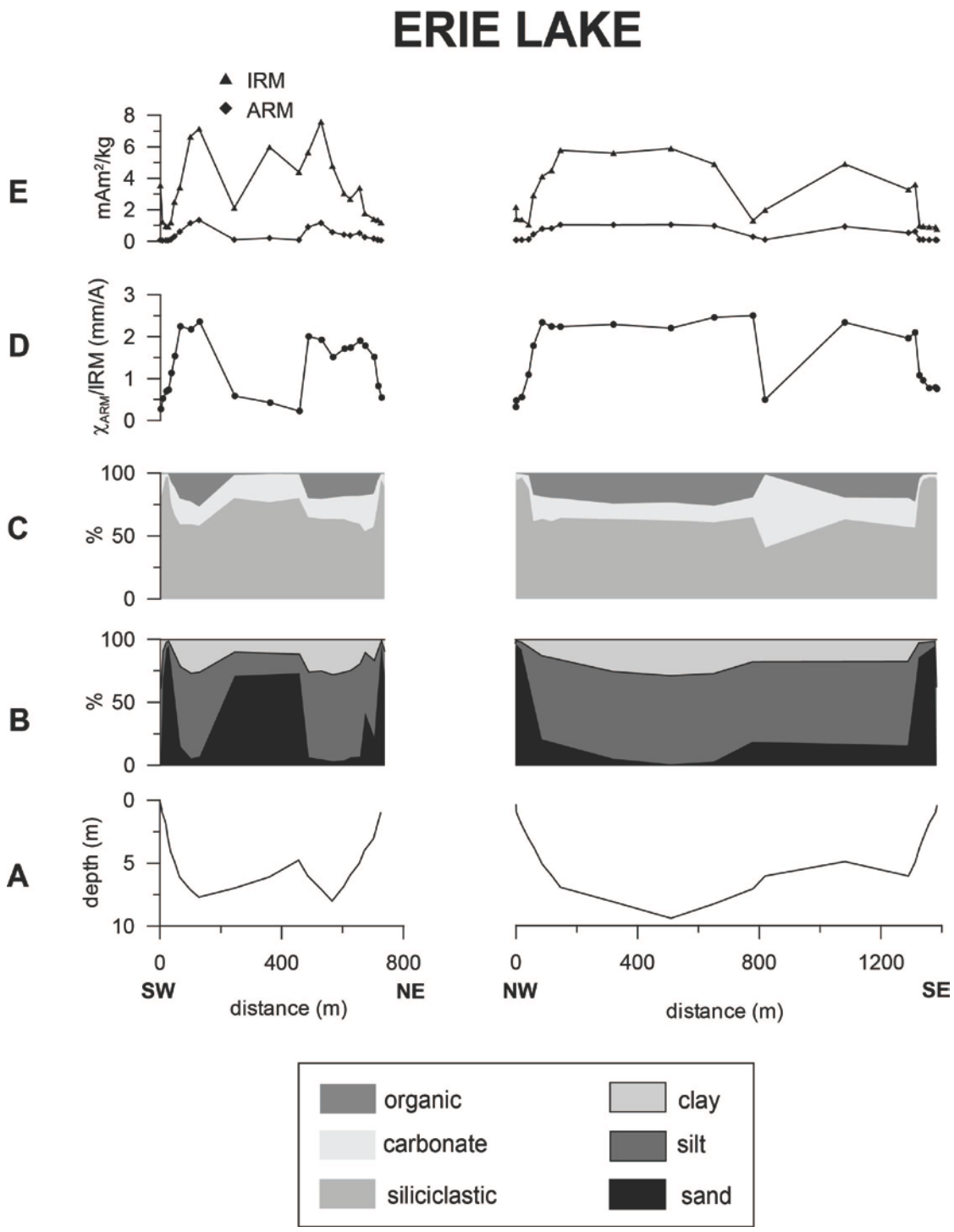

Figure 4.8 Erie Lake transects

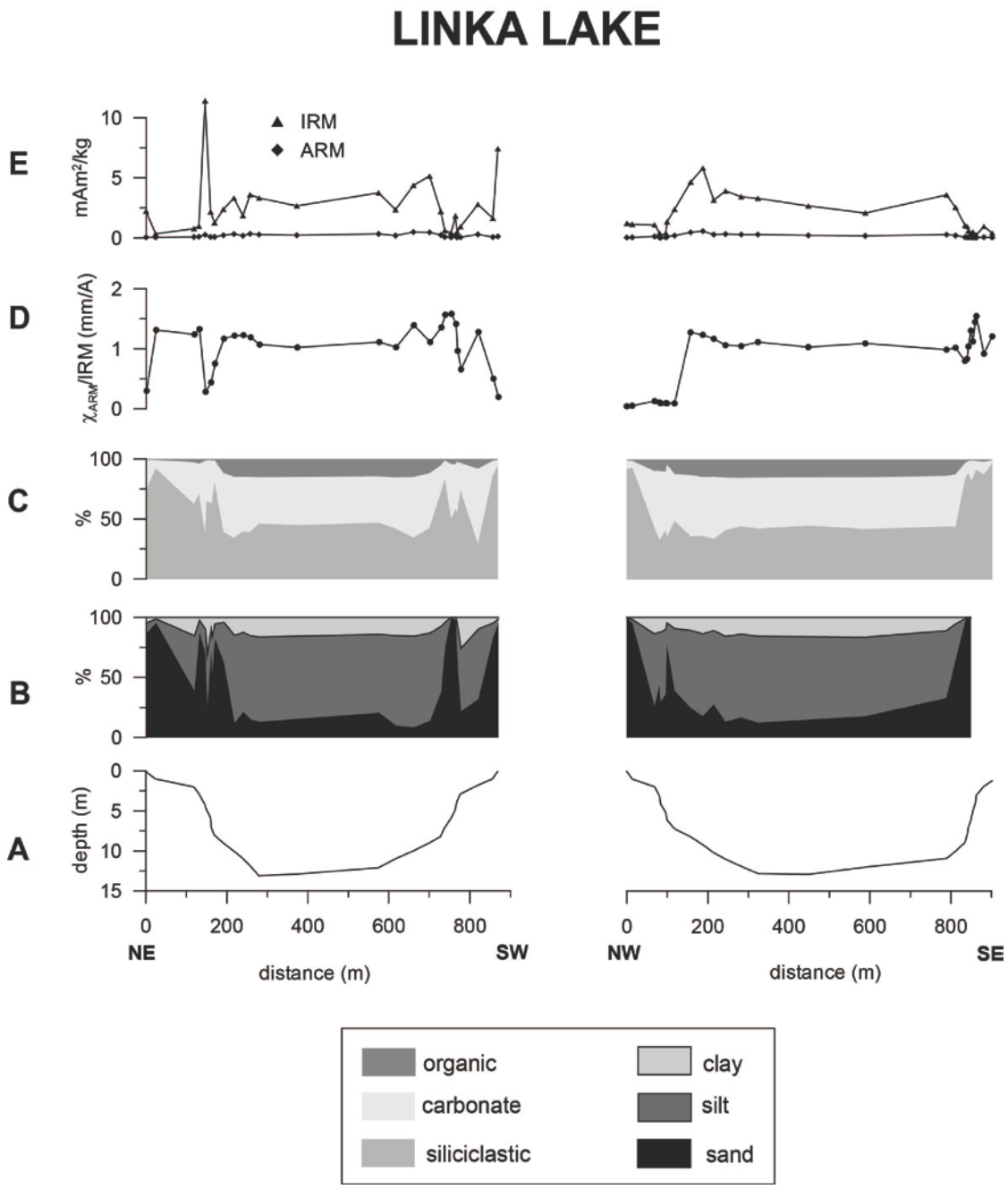

Figure 4.9 Linka Lake transects

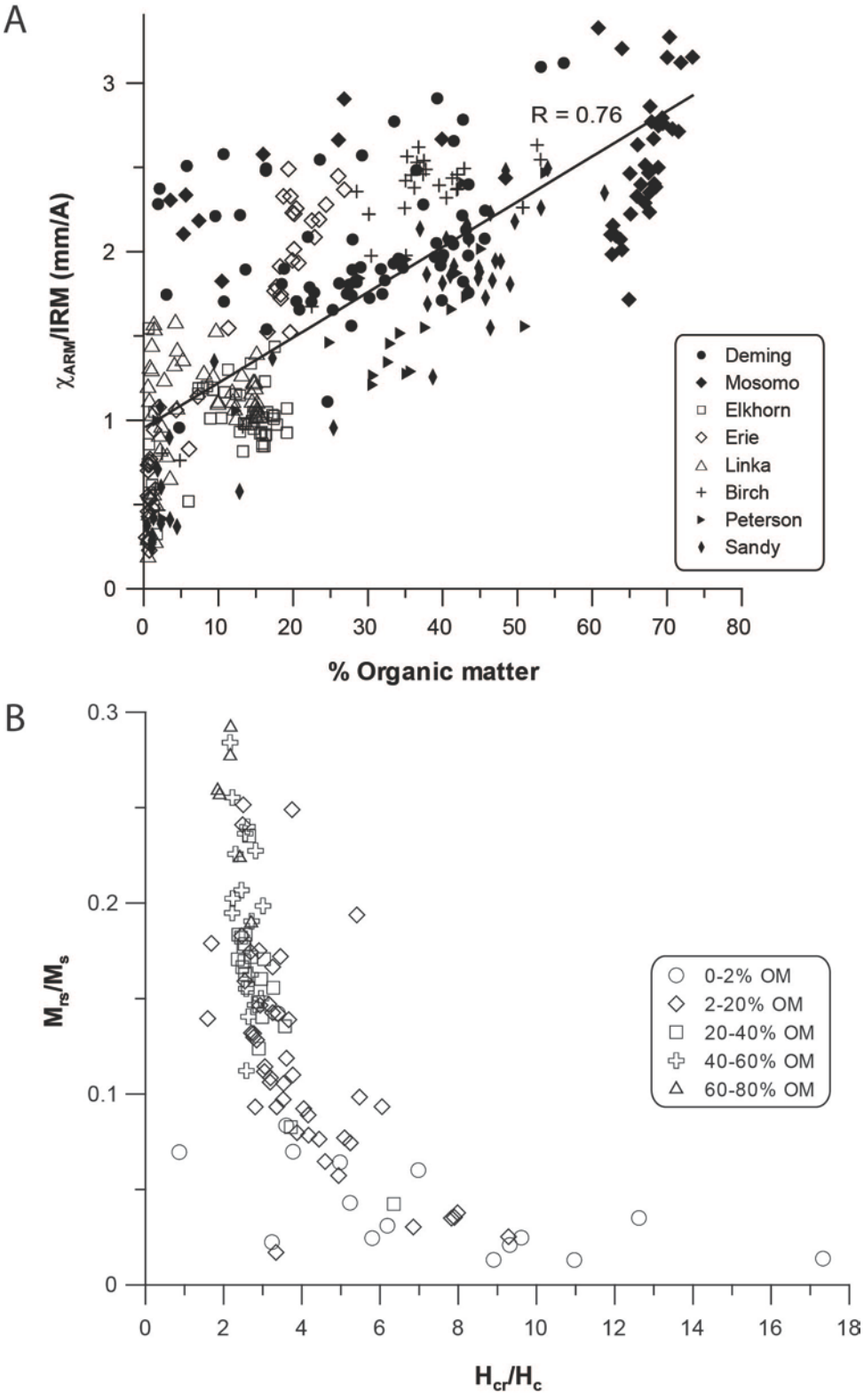

Figure 4.10 Magnetic grain size plots as a function of organic content

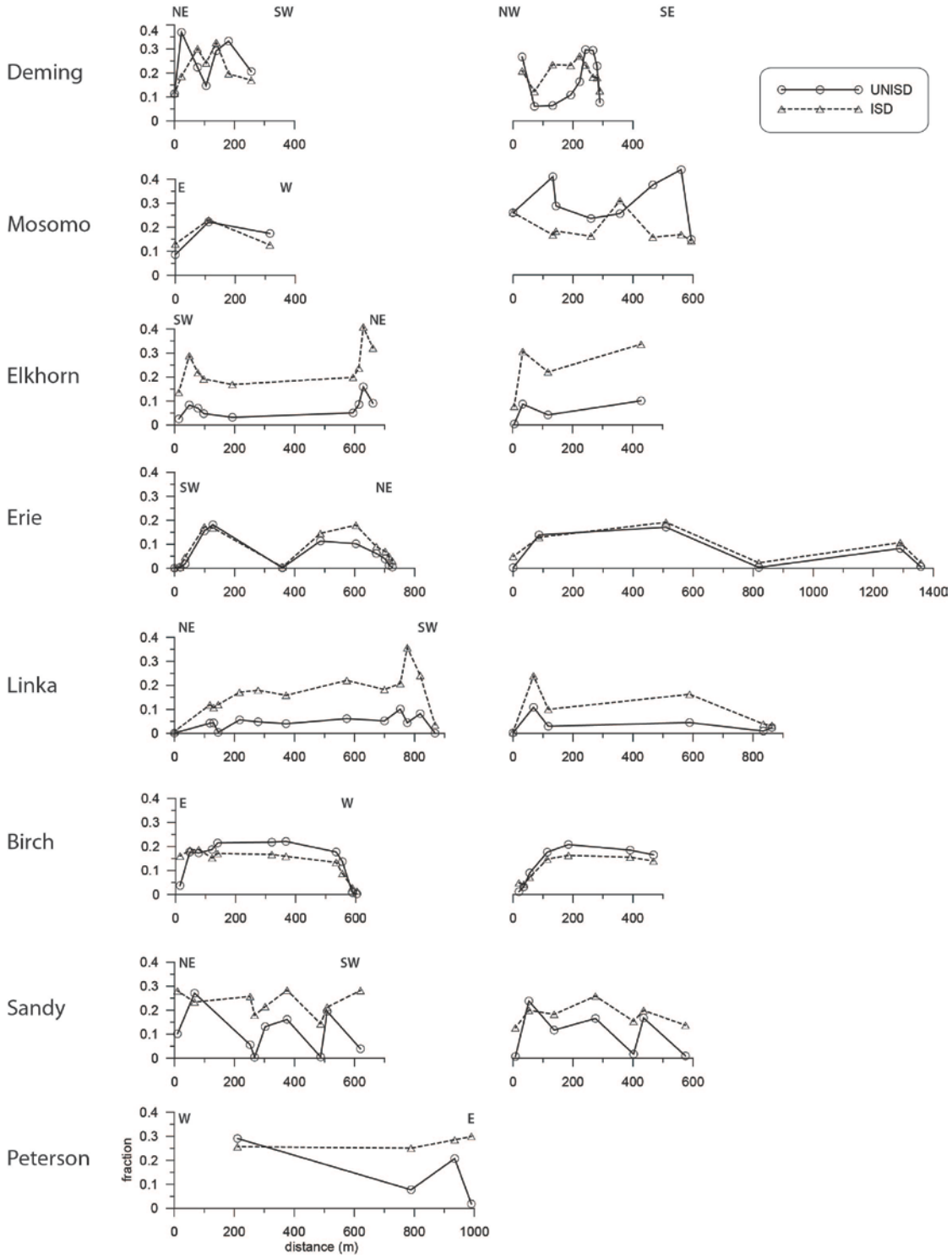

Figure 4.11 Spatial distribution of model components UNISD and ISD along the transects

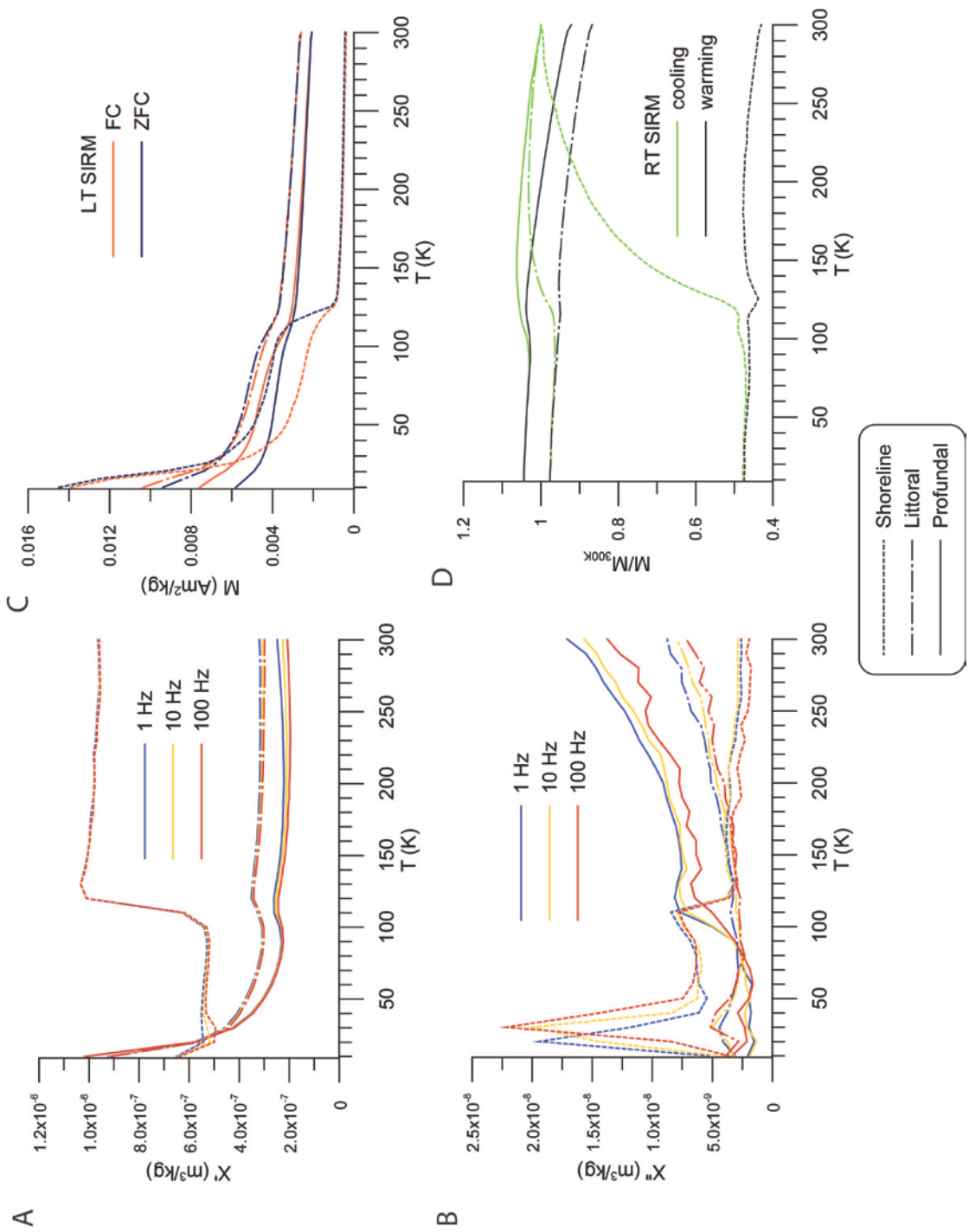

Figure 4.12 Comparison of magnetic properties as a function of temperature for shoreline, littoral, and profundal samples

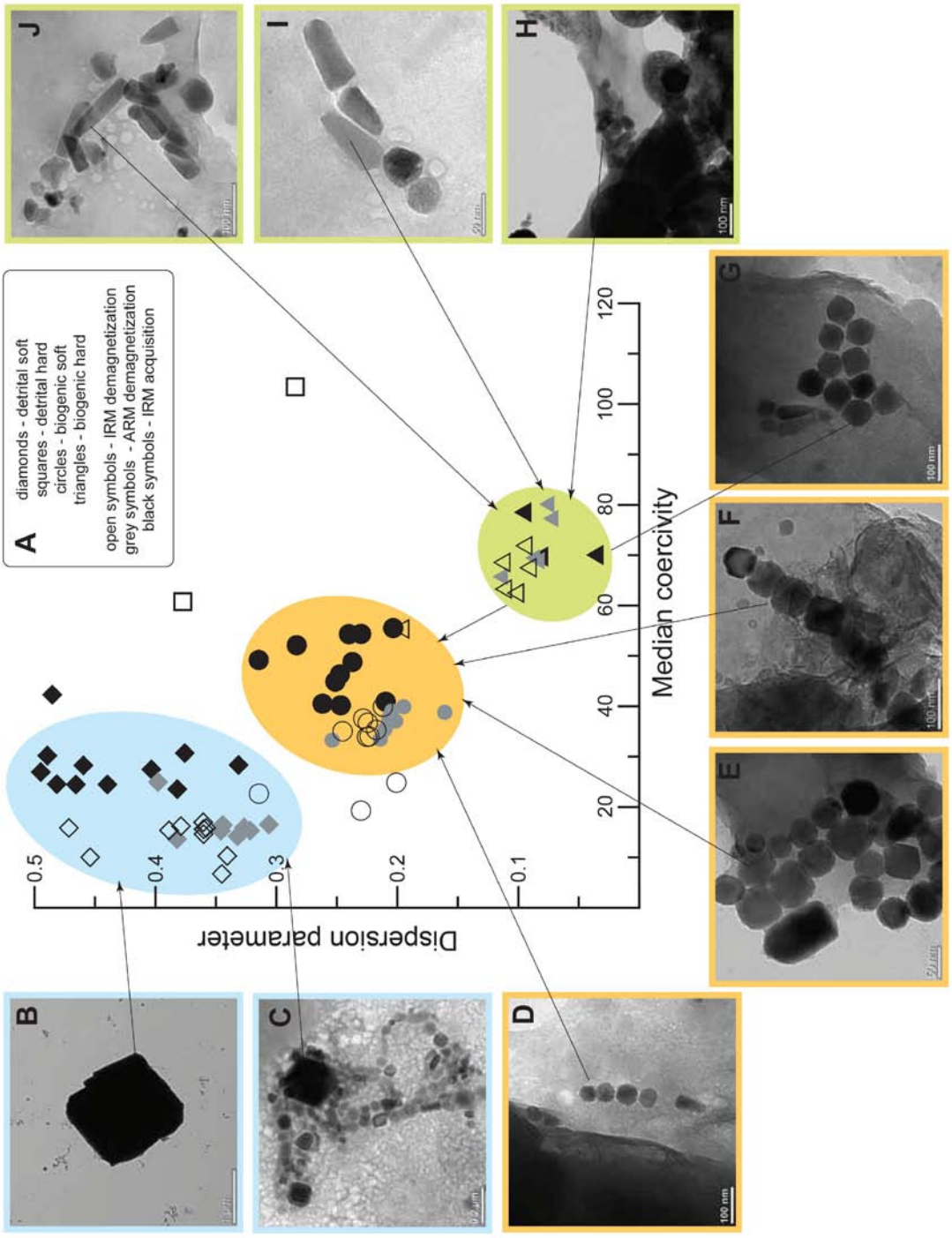

Figure 4.13 Magnetic component unmixing and TEM images of magnetic extracts. Scale bar is 1 μm for b, 0.2 μm for c, 100 nm for d, f, g, h, j, and 50 nm for e and i

Tables

Table 4.1 Lake morphometric parameters

Lake	Lake area (km^2)	Catchment area (km^2)	Lake: catchment ratio	Shoreline length (km)	Shoreline development[a]
Birch	0.41	1.84	0.22	2.67	1.17
Deming	0.06	0.41	0.14	1.10	1.30
Elkhorn	0.30	0.91	0.32	2.59	1.35
Erie	0.79	2.60	0.30	3.99	1.27
Linka	0.72	1.90	0.38	3.23	1.07
Mosomo	0.20	1.20	0.16	1.80	1.15
Peterson	0.07	2.21	0.03	1.22	1.32
Sandy	0.25	0.88	0.29	2.02	1.14

Lake	Maximum depth (m)	Mean depth (m)[b]	Relative depth (%)[c]	Volume development[d]	Lake volume (m^3)
Birch	9.44	4.19	1.30	1.33	1732614
Deming	17.60	8.15	6.55	1.39	462744
Elkhorn	12.20	7.68	1.99	1.89	2267623
Erie	9.40	5.43	0.94	1.73	4287463
Linka	13.56	8.73	1.42	1.93	6287707
Mosomo	10.00	3.80	2.00	1.14	745914
Peterson	7.39	2.50	2.50	1.02	171256
Sandy	12.54	6.16	2.21	1.47	1557396

[a]Ratio of shoreline length to the circumference of a circle of area equal to that of the lake; reflects the potential for development of littoral communities (Hutchinson, 1957).

[b]Ratio of lake volume to lake area (Wetzel & Likens, 1991).

[c]Ratio of maximum depth to the diameter of a circle of area equal to that of the lake; reflects potential for water column stratification, typically expressed as percentage (Hutchinson, 1957; Wetzel & Likens, 1991).

[d]Ratio of mean depth to a third of the maximum depth; reflects the departure of the shape of the lake basin from that of a cone (Hutchinson, 1957).

Chapter 5: Speleothem magnetism*

Ioan Lascu§ and Joshua M. Feinberg

Institute for Rock Magnetism, N. H. Winchell School of Earth Sciences, University of Minnesota, 310 Pillsbury Drive SE, Minneapolis MN, 55455, USA

§*Corresponding author (Lascu003@umn.edu)*

Reprinted from Quaternary Science Reviews, Volume 30, Issues 23-24, Pages 3306-3320, doi:10.1016/j.quascirev.2011.08.004, Copyright 2011, with permission from Elsevier

* We thank Larry Edwards and Calvin Alexander for constructive discussions and for facilitating our access to samples, and Hai Cheng, Yongjin Wang, and Sushmita Dasgupta for providing the specimens and some of the data associated with our pilot study. Comments from Eric Font and an anonymous referee helped improve the quality of this manuscript. The preliminary research presented here was generously supported through a University of Minnesota Grants-In-Aid award to JMF. This is IRM contribution 1103.

Synopsis

The magnetic recordings preserved in calcite speleothems and the nature of their constituent magnetic minerals hold enormous potential for paleomagnetic and paleoenvironmental reconstructions. Speleothems lock in magnetization instantly, are not affected by post-depositional effects, and can be dated with high precision. The natural remanence in speleothems is carried mainly by magnetite, and the main remanence acquisition mechanism is depositional, through physical alignment of detrital magnetic grains parallel to the Earth's magnetic field. Detrital particles are deposited on speleothem surfaces either from receding flood waters, or directly from drip water percolating through overlying rock and soil. Chemical remanence, acquired *in situ* by particles growing through a critical volume, is of secondary importance. Previous studies of speleothem magnetism have shown that geomagnetic features are successfully recorded by speleothems, and can be reproduced at a local and regional scale. Future studies that benefit from increasingly sensitive magnetometers, operating at high spatial resolution, should be able to resolve short-term geomagnetic variability, and characterize events such as geomagnetic excursions at an unprecedented scale. The environmental magnetism of speleothems is still an untapped reservoir, but holds the promise of bridging the gap between mineral-magnetic records from other sedimentary archives and established speleothem environmental proxies (e.g., oxygen and carbon isotopes).

Keywords: speleothem; magnetic minerals; remanence acquisition; paleomagnetism; environmental magnetism.

1. Introduction

Speleothems were first introduced as potential archives for investigating Earth's magnetic field by Latham et al. (1979), who presented paleomagnetic data obtained from calcite stalagmites and flowstones, and made a case for their utility in complementing existing paleomagnetic records from sediments, lava flows, and archaeological artifacts. Over the following two decades a number researchers (e.g., Latham et al., 1982, 1986, 1987, 1989; Morinaga et al., 1986, 1989, 1992; Martin, 1990; Perkins and Maher, 1993; Lean et al., 1995; Openshaw et al., 1997) took on the challenge of testing and expanding the ideas put forth in the pioneering work of Latham et al. (1979). Almost twenty years later Openshaw et al. (1997, p. 485) wrote that "[c]urrently the main aims in speleothem paleomagnetic research are to *acquire and compare speleothem records from similar locations in order to ensure repeatability and to expand the global coverage and time-span of such sets of records.*" Unfortunately, very little speleomagnetic research designed to pursue these goals has been carried out since, even though tremendous advances have been made in instrument sensitivity and in both the fields of geomagnetism and isotope geochemistry.

However, other applications of speleothem magnetism have been explored, of which magnetostratigraphic dating of mixed siliciclastic-calcitic cave deposits containing flowstone older than the limit of ^{230}Th dating is the most notable (e.g., Partridge et al., 1999, 2000; Berger et al., 2002; Bosak et al., 2002; Lacruz et al., 2002; Thackeray et al., 2002; Herries et al., 2006a,b; Adams et al., 2007; Dirks et al., 2010; Pruner et al., 2010; Herries and Shaw, 2011). Rock magnetic properties of speleothems have been used, although to a lesser extent, to aid paleoclimatic reconstructions based on oxygen and carbon isotopic records (Brook et al., 2006). Additionally, paleomagnetic directions have been employed in fold tests on dome-shaped speleothems to determine whether the apparent tilt of such structures is primary (Pruner et al., 2010).

The goal of this review is to synthesize the existing body of work in speleothem magnetism, in order to create a foundation for future research, in light of recent progress in magnetic instrumentation and dating techniques. Further, we aim to describe the specific scientific questions that will drive speleothem magnetism research in the immediate future, and the challenges that will need to be overcome to address these questions.

2. Speleothem precipitation and the origin of detrital particles in secondary calcite deposits

Calcite speleothems are secondary deposits formed by the chemical precipitation of calcium carbonate ($CaCO_3$) in caves. Water infiltrating through the overlying soil and bedrock is enriched in carbon dioxide (CO_2) from decaying organic matter and bicarbonate (HCO_3^-) from carbonate rock dissolution. Once it reaches the cave environment, the percolating water loses CO_2 through degassing in its attempt to equilibrate with the partial pressure of CO_2 (pCO_2) of the cave atmosphere, resulting in speleothem formation by precipitation of $CaCO_3$ out of solution. In addition to abiotic precipitation, the formation of calcite may be mediated by a wide range of microorganisms. For a detailed treatment of caves and cave deposits the reader is directed to the comprehensive works of White (1988) and Ford and Williams (2007), as well as to excellent recent reviews of speleothem processes by McDermott (2004), Fairchild et al. (2006, 2007), Lachniet (2009), and Jones (2010), who cover topics as diverse as speleothem crystallography and fabric, microbial processes, stable isotope composition, filtering of environmental signals, and climatic reconstructions from geochemical elements found in speleothems.

Of interest to speleothem magnetism are the processes that lead to the incorporation of magnetic minerals in the calcite matrix. Speleothems may contain sedimentary material transported into the cave by drip water, or stream water during episodic flooding of cave passages (Latham and Ford, 1993; Perkins and Maher, 1993; Dasgupta et al., 2010). Some speleothems may collect particles borne by air currents, if cave morphology and airflow patterns allow it (White, 1988). The detrital material, which typically contains iron-bearing minerals with characteristic magnetic properties, is deposited on the speleothem surface and immediately encapsulated by the precipitation of new layers of calcite from the water film draping the speleothem. In addition to detrital particles, there is evidence for *in situ* precipitation of iron oxy-hydroxides (Perkins, 1996; Rusanov et al., 2000). The time between particle deposition (or oxy-hydroxide formation) and immobilization is sufficiently long to

allow the magnetic moments to align with the Earth's magnetic field, while rapid enough to allow the accurate recording of the geomagnetic field behavior at exceptionally high temporal resolution (e.g., Latham et al., 1986; Morinaga et al., 1986). Figure 1 illustrates the various processes influencing speleothem magnetism discussed in sections 2 and 3.

2.1. Factors controlling calcite precipitation

Speleothem calcite precipitates from water moving gravitationally through the carbonate host rock. The typical drip water feeding a speleothem is a mixture of slow flowing water from matrix storage and faster flowing water along planar aquifer discontinuities (fractures, fissures, cracks, fault planes, joints, bedding planes, etc.). Drip water flow paths, from land surface to speleothem surface, have a crucial role in speleothem formation. Matrix storage is paramount in the formation of stalagmites, while fracture flow is of increased importance in the formation of flowstone (Fairchild et al., 2007).

The amount and composition of drip water is determined by climate (i.e., by the frequency and intensity of rain events in relation to evapotranspiration), vegetation and soil types, surface topography, and aquifer architecture. For example, warm climates with positive moisture balance are associated with well developed, organic-rich soils with high pCO_2. In such settings, percolating water will have a higher dissolution potential after equilibrating with soil pCO_2. The longer the travel time through the bedrock, the higher the dissolved carbonate content, leading to the precipitation of more calcite once the drip water enters the cave environment. Well aerated cave passages tend to have atmospheres with lower pCO_2, creating a larger partial pressure difference between drip water and cave atmosphere CO_2, which promotes more degassing and thus higher rates of calcite precipitation.

Speleothem growth rates are a function of drip rate, calcium concentration, thickness of the water film draping the speleothem, and cave temperature, and are typically <100 μm/year for temperate regions, and can reach 800 μm/year in warm and humid climates (White, 2004; Fairchild et al., 2007; and references therein).

Faster flowpath settings may result in lower dissolved carbonate and lower calcite precipitation rates, but have the potential for transporting suspended load, including magnetic minerals.

2.2. Calcite fabrics and crystal growth

It is unclear whether calcite fabric, growth rate, and crystal habit influence the final orientation of magnetic carriers in speleothems. Stalagmites are composed of composite calcite crystals, with crystallographic c-axes generally oriented perpendicular to the growth substrate, formed by individual crystallites with separate terminations on the growth horizon (Fairchild et al., 2007). The geometrical arrangement of the terminations on the stalagmite surface determines if the spaces between the individual crystallites are eliminated by crystallite coalescence during growth, or if they are preserved as fluid inclusions (Kendall and Broughton, 1978). If pedogenic particles are transported to the spelean environment through bedrock fractures, some grains will presumably occupy a portion of these spaces, while others will rest on flat crystallite terminations. The competition for space at the speleothem growth surface increases during cave flooding events, when particles of various compositions introduced by flood waters create the potential for competitive growth fabrics to occur (Dickson, 1993). The thickness of the solution film (<100 μm) limits the size of the crystals that compete in this way. A large number of detrital particles deposited during one flood pulse would likely generate more exposed surface for additional growth reactions (Fairchild et al., 2007). In some cases microbes may play an active role in trapping and binding detrital particles to speleothem surfaces (Jones, 2010, and references therein).

2.3. Annual laminations

Annual laminations in speleothems are generated via two processes that result in two main types of laminations: seasonal couplets reflecting changes in mineralogy and/or fabric, and impurity pulse laminae (Fairchild et al., 2007). Couplets of alternating mineralogy and/or fabric are a result of seasonal variability in drip water composition and/or flow rate. This type of lamination may be detected under ultraviolet (UV) light if associated with variable input of soil-derived humic and fulvic acids (Perrette et al., 2005). Discrete pulses of impurities from overlying soils are related to enhanced infiltration events, and the intrinsic hydrological characteristics of the aquifer. Aquifer filling beyond a critical level at certain times of the year (e.g., spring snowmelt) may result in flushing of solid matter through previously air-filled spaces (Fairchild et al., 2007). Impurity laminations exhibit fluorescence under UV light (see Figure 2 for an example) indicating enhanced input of organic matter from the overlying soil (Shopov et al., 1994). If such pedogenic material in speleothems contains magnetic particles, then this would be visible as peaks in magnetic concentration-dependent parameters, but the resolution at which magnetic analyses have been conducted in previous speleomagnetic studies makes it virtually impossible to detect such subannual pulses. In this light, the application of recently developed magnetic instrumentation capable of rapidly measuring magnetic properties at millimeter and micrometer length-scales is a promising line of future research and will be discussed in more detail below.

2.4. Detrital sediment inputs

The processes that transport clastic sediment into cave environments are important to consider when trying to ascertain the origin and composition of magnetic minerals incorporated into speleothems. A short synopsis of these processes and their related depositional facies in caves follows, but the reader is encouraged to view Bosch and White (2004) for a more detailed overview.

The bulk of detrital sedimentary particles are transported into cave systems by streams and sinkhole runoff. Only a small proportion is delivered through fissures in the host rock, but this fraction is an important source of fine-grained particles incorporated in speleothem calcite. Sedimentation in caves has an episodic character, with most material being transported and deposited as a result of storms that may cause partial or total flooding of a cave passage. This can be readily observed in the case of cave floods by streams, but is not as evident in the case of diffuse sedimentation through fissures and cracks.

Detrital sediments introduced into caves by streams and sinkhole runoff are wide ranging in terms of provenance, composition, grain size, and modes of sedimentation. A sinking stream can transport sediments from a large area in its drainage basin, while sinkhole runoff has a more local character. Particles sizes in streams range from very coarse cobbles and boulders to fine silts and clay, and show evidence of varying degrees of transport (e.g., rounding, abrading). Sediments entering the aquifer through sinkholes are either injected through the open throat of the sinkhole, or are released as a result of piping failures after accumulating at the bottom of the sinkhole for a period of time. Sediments flushed in sinkholes range in size from coarse boulders and blocks to fine clays and soil material, and may eventually reach underground streams and become part of the stream load. The particles that are typically deposited on speleothem surfaces are part of the suspended load, and settle during quiescent periods following floods, when conduits are partially or totally submerged. The sedimentary grains can be part of the load carried in the normal flow direction, or may originate from the suspended load of stream water backflooding cave

passages, resulting in the equivalent of bank storage from flow reversals (Bosch and White, 2004).

Fine-grained material can also make its way to the cave environment by diffuse infiltration through the network of fractures and bedding planes of the karst aquifer (Bull, 1981; Bosch and White, 2004). Episodic sediment pulses in this case are controlled by a translatory flow mechanism, where inputs to ground water from storms create a push-through effect that displaces water and sediment stored in the aquifer, leading to sediment deposition in cave passages below. This model, proposed by Bull (1981) as a mechanism that explains the deposition of finely laminated clays and silts in flooded cave passages, may also apply for dry passages, whereby the sediment is carried by drip water and deposited on speleothem surfaces. The detrital material deposited as a result of diffuse sedimentation processes is mostly a steady flux of soil and regolith infiltrated from the surface, but may also contain insoluble residue from the dissolution of the carbonate bedrock by CO_2-rich percolating water (Bosch and White, 2004). This chemical weathering residue may mix with the infiltration material moving gravitationally from the surface, or may be transported via separate pathways to drip points feeding speleothems.

3. Magnetic particles and natural remanence acquisition in speleothems

Magnetic minerals have been identified in speleothems mostly by means of magnetic methods, but non-magnetic techniques, such as transmission electron microscopy (TEM), have also been employed by some researchers (e.g., Perkins, 1996; Rusanov et al., 2000).

The main remanence carrier in speleothems is magnetite (Fe_3O_4), identified from Curie temperature estimates (Latham et al., 1986; Morinaga et al., 1986, Lean et al., 1995; Herries et al., 2006a,b; Adams et al., 2007; Herries and Shaw, 2011), and isothermal remanence acquisition curves that saturate by 300 mT (Latham et al., 1979, 1986, 1987, 1989; Morinaga et al., 1986; Lean et al., 1995; Herries et al., 2006b). Maghemite (γ-Fe_2O_3), formed by the progressive oxidation of magnetite, is often associated with the latter (Brook et al., 2006; Adams et al., 2007; Herries et al., 2006a,b; Herries and Shaw, 2011).

For the low coercivity components in the magnetite-maghemite solid solution series, remanence-to-saturation ratios determined from hysteresis loops (e.g., Latham et al., 1989; Latham and Ford, 1993) have values characteristic of mixtures of stable single domain (SSD) grains and either multi domain (MD) or superparamagnetic (SP) grains (Dunlop, 2002). Herries et al. (2006a, b), Adams et al. (2007), Dirks et al. (2010), and Herries and Shaw (2011) argue for the presence of SSD grains based on hysteresis data and dependence of susceptibility on temperature and frequency, and Lowrie-Fuller tests that showed harder anhysteretic remanent magnetization (ARM) demagnetization behavior compared to that of an isothermal remanent magnetization (IRM). Lean et al. (1995) also argue for the presence of SSD grains based on the Lowrie-Fuller test corroborated with bulk coercivities of 35-50 mT for mixtures of magnetite and maghemite.

Titanomagnetite has been identified in the detrital fraction of a handful of Mexican stalagmites (Latham et al., 1986, 1989). Hematite (α-Fe_2O_3) and goethite (α-FeO[OH]) have been identified in flowstone by unmixing coercivity spectra obtained from IRM acquisition curves Pruner et al. (2010). Median coercivities of ~275 mT and

1260 mT were attributed to the two minerals respectively. Brook et al. (2006) noted pale tan to orange-red thin bands that appeared in their specimens after cutting and subsampling. They interpret them as fine-grained hematite or maghemite resulting from the oxidation of siderite, but no evidence is offered for either of the three minerals. However, rapid oxidation of dissolved iron usually leads to formation of poorly crystalline phases such as ferrihydrite or nanogoethite (e.g., Guyodo et al., 2003; Burleson and Penn, 2006).

Iron oxy-hydroxides have also been described using non-magnetic techniques. The presence of hematite and goethite was determined by Rusanov et al. (2000) using Mössbauer spectroscopy, while magnetite and goethite were identified via TEM by Perkins (1996). The latter work is the sole TEM study of magnetic minerals in speleothems to date, and describes three distinct morphological categories of magnetic particles: (1) Irregularly shaped, abraded grains, ranging in size from submicron to a few tens of micrometers, inferred to be (titano)magnetite and/or hematite grains that have undergone transport; (2) Cubic, unabraded magnetite grains smaller than 0.1 μm, which have an affinity with inorganically precipitated and/or bacterially mediated pedogenic magnetite. The minimal wear of these grains indicates limited transport; and (3) Acicular particles inferred to be goethite crystals precipitated from iron-rich groundwater. The fragility of these needles does not allow them to be transported without suffering damage, and all indications are that they were precipitated *in situ* (see insets in Figure 1).

The inferred origins of these magnetic minerals are still speculative, and different models have been proposed to explain how they acquire natural remanent magnetization (NRM). The primary magnetizing mechanism in most models is the physical alignment of magnetic grains parallel to the Earth's magnetic field during accumulation of detritus on the speleothem surface. The NRM is therefore a depositional remanent magnetization (DRM). Abraded and pedogenic grains indicate this may be done either by periodic floods or through flow along bedrock fissures (Latham et al., 1989; Latham and Ford, 1993; Perkins and Maher, 1993; Perkins, 1996). In the case of stalagmites, the drip water that splashes regularly on the top

surface will remobilize and concentrate most of the detrital particles off to the sides of the speleothem (Latham and Ford, 1993; Dasgupta et al., 2010). Irrespective of where the magnetic detritus is incorporated in the speleothem structure, it has been shown that paleomagnetic directions recorded by speleothems are comparable in central and lateral samples that were collected along the same growth layer (Latham et al., 1979, 1986; Morinaga et al., 1989; Perkins and Maher, 1993; Lean et al., 1995; Openshaw et al., 1997), suggesting no change in the amplitude of paleomagnetic secular variation (PSV) due to depositional effects. With the exception of calcite recrystallization, which can be identified in polished and/or thin sections, there are no known mechanisms for post-depositional remanent magnetization (PDRM) acquisition in speleothems.

A second magnetization mechanism involves the chemical precipitation of magnetic minerals directly from groundwater rich in dissolved iron. Magnetic minerals formed by this mechanism lock in a recording of the Earth's magnetic field as they grow through a critical volume. Their *in situ* precipitation would lead to the acquisition of a chemical remanent magnetization (CRM). The evidence for this mechanism, particularly for magnetite, is only circumstantial (Latham and Ford, 1993; Lean et al., 1995). In speleothems with no measurable NRM, IRM experiments revealed the presence of fine-grained ferrimagnetic particles (Latham et al., 1982, 1989; Latham and Ford, 1993). Moreover, the magnetic particles seem to be concentrated in darker, organic-rich bands (Elmore et al., 1987; Latham and Ford, 1993). In this model, the presence of organic matter in the drip water is postulated to be necessary for the chemical precipitation of magnetic grains, as it contributes to the decrease of a solution's redox potential (Eh) by oxygen consumption during remineralization of organic carbon (Latham and Ford, 1993; Lean et al. 1995). The resulting reducing conditions would cause chelated iron to enter the solution in ferrous state (Fe^{2+}), and subsequently precipitate as magnetite.

Cave atmospheres are usually oxygenated, so precipitation of magnetite is not thermodynamically favored (Huber, 1958). Instead, the cave environment most likely creates the conditions for the oxidation of ferrous iron and its precipitation as a ferric

(Fe^{3+}) iron oxy-hydroxide. This is evidenced by the goethite needles observed in TEM images (Perkins, 1996), which are too fragile to survive extensive transport, and thus are most likely formed *in situ*. However, magnetite precipitation is known to occur in soils (e.g., Özdemir and Banerjee, 1982; Maher, 1998; Geiss et al., 2004; Liu et al., 2007), so it is reasonable to assume that a portion of the fine grained magnetite found in speleothems is actually pedogenic rather than inorganically precipitated at speleothem surfaces. In this scenario, magnetite precipitated either in the overlying soils, or en route to the cave in oxygen-deficient conditions, is deposited via diffuse sedimentation after short-distance transport through overlying carbonate rock fractures, joints, and bedding planes.

The most accommodating model for NRM acquisition in "clean" speleothems (those with a negligible detrital component) must therefore rely on a combination of physical and chemical processes, where (bio)chemically-precipitated magnetic grains are physically deposited on the speleothem surface after limited vertical transport. True CRM may be achieved only in minerals unambiguously precipitated in situ, such as goethite. In addition to Eh conditions, chemical remanence acquisition would also be a function of the thickness and residence time of the water film at the surface of the speleothem (Perkins and Maher, 1993).

In summary, natural remanence acquired in speleothems is predominantly a DRM, possibly combined with a CRM, and is contemporaneous with the calcite matrix (Latham et al., 1989). The absence of depositional direction errors means there is sufficient time for detrital grains to align with the geomagnetic field in the film of water from which calcite precipitation is completed. If some form of CRM is associated with authigenic magnetic grains, then their moments are aligned during precipitation. Since redox conditions at speleothem surfaces do not favor *in situ* magnetite precipitation, CRM is likely associated with weakly magnetic minerals such as goethite, and is negligible unless it is the only form of NRM. Barring speleothem recrystallization, PDRM is not a factor in speleothem remanence acquisition. Any viscous magnetic overprints acquired after speleothem formation can be removed in the laboratory by magnetic cleaning involving partial alternating field (AF)

demagnetization using peak fields from 5-10 mT (Latham et al., 1979, 1982, 1986, 1987; Morinaga et al., 1986, 1989) up to 30 mT (Openshaw et al., 1997), or thermal demagnetization using temperatures in the range of 100-210 °C (Latham et al., 1982). Higher temperatures may produce mineral alteration and calcite expansion, so a hybrid AF-thermal demagnetization is recommended by Herries et al. (2006b) in order to isolate the primary remanence.

4. Previous paleomagnetic studies of speleothems

4.1. Speleothems as geomagnetic recorders

Before assessing the scientific potential of magnetic records preserved in speleothems, it is important to briefly summarize the advantages and limitations of other geologic materials used in paleomagnetic studies. The majority of past geomagnetic field reconstructions are based on the study of NRM preserved in volcanic rocks, archaeological artifacts, and sediments. Volcanic rocks and archaeological materials (e.g., baked clay, copper slag) are usually discontinuous records, but provide quantitative constraints of the full vector behavior of the Earth's magnetic field due to the thermoremanent magnetization (TRM) that is acquired during original cooling. Sediments, on the other hand, have the potential of providing long, continuous records of PSV, but are flawed by a number of issues. Marine and lacustrine sediments have uncertainties associated with the timing of ambient geomagnetic field "lock-in". Freshly deposited sediments are unconsolidated and water-rich, which allows magnetic mineral grains to rotate freely until these sediments are compacted by overlying, accumulating sediments (Verosub, 1977; Roberts and Winklhofer, 2004). The time lag between sedimentation and consolidation is in most cases significant enough to introduce errors in pinpointing the actual time of magnetization acquisition, and creates a smoothed paleomagnetic record. Compaction, slumping, turbidity currents, bioturbation, and dewatering can also bias the direction (e.g., via inclination shallowing/flattening) and intensity recorded by the magnetic minerals (Perkins and Maher, 1993; Tauxe and Kent, 2004). In addition, dissolution of existent magnetic minerals, and precipitation of secondary minerals that may record the ambient magnetic field at the time of their formation can occur during diagenesis (e.g., Tarduno, 1995; Roberts et al., 2011). Other problems associated with unconsolidated materials include sediment disturbance during collection, transport, and sampling in the laboratory (Nilsson et al., 2010). Most archived marine cores are unoriented, and their core tops are either missing or are severely disturbed. Finally, sediment age models are not robust outside the range of radiocarbon, which is limited

to a maximum of 60 ka before present (BP) and comes with uncertainties associated with the origin of carbon contained within the datable material (Wagner, 1998).

Speleothems hold certain key advantages over sediments for PSV studies. They are solid mineral deposits, which allows researchers to sidestep the complications associated with remanence in soft sediments. While post-depositional processes, such as calcite recrystallization or dissolution, can potentially mobilize magnetic grains and perturb the original geomagnetic record, these effects can be easily recognized in thin sections or polished surfaces, thereby allowing workers to avoid measurement of these altered areas. Compared to sediment cores, stalagmites can be easily oriented when sampling (Perkins and Maher, 1993; Openshaw et al., 1997). One of the most important paleomagnetic advantages to using speleothems is the minimal time lag between the deposition of magnetic particles and their immobilization by subsequent calcite precipitation. This is demonstrated by fact that the tops of actively-growing stalagmites preserve the same magnetic direction as the ambient magnetic field at the time of collection (e.g., Latham et al., 1979; Morinaga et al., 1989). Speleothems can grow continuously, provided there is a constant source of moisture and a fixed drip source, and can be dated with very high precision using ^{230}Th dating, a technique that can be reliably used on specimens <600 ka in age (Edwards et al., 2003; Dorale et al., 2004). However, recent developments could potentially extend the current age limit to >700 ka (Larry Edwards, pers. comm.), approaching the lower boundary of the Brunhes magnetic polarity chron.

Until recently, the primary limitation of using speleothems for paleomagnetic studies has been their low magnetic mineral concentration, which gives rise to samples whose magnetic moments are near the limit of sensitivity for many cryogenic rock magnetometers. For this reason, many of the earlier speleomagnetic studies focused on speleothems that grew in the presence of a sustained supply of detrital particles. However, the downside of using samples with a high concentration of allochthonous material incorporated into the speleothem calcite is that fine-grained impurities, such as clays, contain elevated levels of detrital thorium (i.e., not a product of decay from the uranium initially encapsulated in the calcite matrix), which will adversely affect

the ^{230}Th count used for age calculations. Such contamination by detrital thorium can be corrected in certain limited cases (Latham et al., 1982), but the issue of "excess thorium" should be avoided if possible.

Magnetometer sensitivity forced many of the earlier studies of speleothem magnetism to rely on large sample volumes (>8 cm^3), which tended to smooth out PSV paths by averaging over large periods of calcite growth, thereby downgrading the utility of the results. Such limitations are now readily overcome due to the development of increasingly sensitive cryogenic rock magnetometers, capable of collecting continuous data at high resolution (e.g., Roberts, 2006; Weiss et al., 2007). Some techniques (discussed in more detail below) are capable of measuring magnetization at submillimeter accuracy, which is important when considering that speleothem growth rates are usually lower than sediment accumulation rates in lakes and in some marine settings. Another limitation of speleothems is that continuous records from individual stalagmites are often shorter than those encapsulated by sediment cores. However, cave sites in areas with long-term moisture availability have the potential of yielding composite speleothem records that span several hundreds of thousands of years (e.g., Wang et al., 2001; Wang et al., 2008).

4.2. Reproducibility of speleothem paleomagnetic records

Previous speleothem magnetism studies that have focused on PSV reconstructions have demonstrated a consistency in the remanent magnetization between samples and locations, which can be correlated with established local or regional paleomagnetic curves (e.g., Latham et al. 1982, 1986, 1987, 1989; Openshaw et al. 1997).

Earlier workers examined the effect of the orientation of speleothem growth layers (i.e., horizontal versus inclined) on the remanence properties of individual paleomagnetic samples. Detrital material deposited during floods is initially distributed uniformly on speleothem surfaces, which typically appear draped in a thin clayey or silty veneer after flood waters recede. When normal conditions resume, the drip water that splashes regularly on a stalagmite will entrain the material deposited on

the top surface and redeposit some of the grains to the sides of the speleothem in a randomly distributed fashion (Latham and Ford, 1993; Dasgupta et al., 2010). Paleomagnetic measurements of central and lateral stalagmite samples collected along the same growth horizon show consistent directions, suggesting no change in either PSV amplitude or direction due to surface roughness, dip, water flow, or crystal growth habit (Latham et al., 1979, 1986; Morinaga et al., 1986, 1989; Perkins and Maher, 1993; Lean et al., 1995; Openshaw et al., 1997). Samples taken from the same growth layer of flowstones, both parallel and perpendicular to the dip, also show no directional bias (Latham et al., 1982).

The most common sampling technique employed for testing the consistency of paleomagnetic recording in laterally equivalent samples involved cutting the speleothems into cubes with 2-2.5 cm sides, and comparing subsamples that include coeval growth layers (e.g., Latham et al., 1979, 1986; Lean et al., 1995; Openshaw et al. 1997). This method not only averages over a longer time period, but the sampling has the potential of including different horizons in the subsamples containing lateral growth layers, many of which may be curved. Morinaga et al. (1986, 1989, 1992) used an alternative sampling technique, by which multiple cores from the same stalagmite were drilled perpendicular to the growth layers, both from the top and the sides of the speleothem. Each core was sectioned into thin (~1.5 mm) subsamples, assuring minimal time averaging and more or less parallel growth layers. For both subsampling methods equivalent samples show good reproducibility, and can be averaged with respect to their stable directions, obtained after accounting for viscous overprints, which are eliminated after a “magnetic cleaning” treatment is applied. Fisher statistics on the averaged clean values obtained from both horizontal and inclined equivalent surfaces agree within error (α_{95} <3-7°) (Latham et al., 1979, 1986; Morinaga et al., 1986, 1989, 1992; Lean et al., 1995; Openshaw et al. 1997), indicating that speleothems are accurate recorders of the Earth’s magnetic field, with no significant forms of remanence anisotropy.

Earlier workers also assessed the reproducibility of records between samples collected from the same cave or geographical area. Perkins and Maher (1993)

collected a stalagmite from a cave in the United Kingdom with an existing speleothem paleomagentic record published by Latham et al. (1979), and presented a tentative correlation between the inclination and declination features of the two records. Unfortunately Perkins and Maher (1993) did not have an absolute chronology for their record, and were forced to assume that their speleothem was contemporaneous with that of Latham et al. (1979) based on comparison of the paleomagnetic vector recorded by the top of the stalagmite with the modern field at the time of collection. Morinaga et al. (1989) used the same approach for several stalagmites from a cave in Japan, but their records also suffer from lack of absolute dating. In this instance, age determinations were made based on inferred speleothem growth rates, and the fact that the stalagmites were actively growing at the time of collection, and had inclination and declination values corresponding to local geomagnetic field values at the time of collection. The paleomagnetic features from all the speleothems analyzed by Morinaga et al. (1989) were reproducible, and inclination and declination features were compared to "coeval" features from a Japanese archaeomagnetic master curve, but the lack of absolute age control on all samples renders the correlation tentative. An interesting aspect of the methodology of Morinaga et al. (1989) is that they applied severe quality control criteria for selecting the samples used in their analysis, which resulted in almost half of the measurements being discarded. This strict interpretation of the data was rooted in the belief that there should not be any dramatic change in paleomagnetic direction between two adjacent specimens. By discarding what they considered to be spurious measurements, the authors essentially discounted the possibility of high-frequency variations of the geomagnetic field, which would have been an important find at the time. Recent work by Gallet et al. (2003, 2009), Ben-Yosef et al. (2009), Bogue and Glen (2010) and Shaar et al. (2010, 2011) demonstrates that paleomagnetic directions and intensities can vary dramatically on decadal timescales, several orders of magnitude faster than typical of secular variation.

4.3. Geomagnetic features recorded in speleothems

Most of the published speleothem paleomagnetic records capture some aspect of the behavior of the non-dipole component of the geomagnetic field. Speleothem samples from Canada, Mexico, and China all reveal a clockwise looping of the virtual geomagnetic pole (VGP), which has been interpreted as a result of the westward drift of a non-dipole field component through time (Latham et al., 1982, 1986; Lean et al., 1995; Openshaw et al., 1997). Geomagentic polarity reversals recorded by flowstone are reported from South African infilled paleocaves containing hominin fossils (Partridge et al., 1999, 2000; Berger et al., 2002; Lacruz et al., 2002; Thackeray et al., 2002; Herries et al., 2006a,b; Adams et al., 2007; Dirks et al., 2010; Herries and Shaw, 2011), and from Slovenian karst (Bosak et al., 2002; Pruner et al., 2010).

A Holocene stalagmite from Vancouver Island, Canada contains a record of two and a half clockwise loops of the VGP in the period 5.4-2.1 ka BP (cyclicity of 1.1 ka), thought to be due to the westward drift of a localized non-dipole field feature. The field for the average VGP has far sided and left-handed bias, and the periodicity of the looping is almost 1 ka shorter than that observed in other records at the same latitude (Latham et al., 1982). The same clockwise looping pattern can be identified in the CALS7K model (Korte and Constable, 2005) VGP curve for this location, but has roughly half the amplitude exhibited in the stalagmite record (Figure 3a). The dampened amplitude can also be seen in the inclination and declination curves, which show that peaks in the stalagmite record can be correlated to peaks in the model, within age error (Figure 3b). The discrepancies between the speleothem record and the CALS7K model are likely due to a combination of factors. The speleothem record is highly localized and is based on a relatively coarse sampling method, while the CALS7K model is meant to capture more regional/global features and is based on a spherical harmonics technique that filters out and dampens local high frequency variations in field behavior. Despite these differences, it is worth emphasizing that both the speleothem record and the CALS7K model capture the same general

geomagnetic field phenomena. In this way, paleomagnetic studies of speleothems may eventually contribute to improved models of geomagnetic field behavior through time.

A complementary speleothem record from the same cave provides a window into the magnetic field behavior at the end of the Last Glacial Maximum (Latham et al., 1987). A notable feature of this record is a shallow inclination swing with an easterly bias, in which the vector returns along its outward path, rather than looping. The PSV pathway is inferred to be a result of either a pulsating or oscillating non-dipole source to the west of the site (the absence of clockwise looping argues against westward drifting sources). Another explanation is that there might be anticlockwise precession of the main dipole away from the site, followed by reversal of the precession (Latham et al., 1987). Lean et al. (1995) analyzed an additional Vancouver Island stalagmite, which grew between 16.9 and 13.3 ka BP. The earlier part of their record contains a linear VGP wander path (part of a great circle) thought to have arisen from the growth and decay of a standing, oscillating, inward-pointing source of secular variation located to the northwest of the site. The later part of the record provides evidence of clockwise looping that may indicate westward drift of a non-dipole component of the magnetic field. Other explanations for this feature include out-of-phase intensity variations of stationary features, and precession of the main dipole (Lean et al., 1995). However, as with many other paleomagnetic studies of speleothems, their chronology contains large errors (of up to 8 ka), and any dating should be regarded as tentative.

Latham et al. (1989) described paleomagnetic records from nine Mexican speleothems, only one of which was dated using radioisotopic methods and yielded a coherent paleomagnetic record (Latham et al., 1986). A prominent feature at the base of the stalagmite is a 20 degree swing in declination towards the west, which was interpreted as the drift of the Guinea negative magnetic anomaly westward across Mexico one thousand years ago. The shallow inclinations compared to the geocentric axial dipole (GAD) can be accounted for by the tilting of the main dipole away from the site, but the inclination waveform of the anomaly is not recorded. The authors suggest the wobbling of the main dipole may have an effect on both the looping and

the shallow bias in the field direction. The mean directions show a clear serial correlation and VGPs compare well with archaeomagnetic data from North America's southwest and with lake sediment data from the northwestern United States (Bohnel and Molina-Garza, 2002).

Openshaw et al. (1997) analyzed five speleothems from two caves in China that show consistent paleomagnetic records for the last 8.9 ka. Mean declinations were found to have westward biases relative to the GAD. They concluded that the magnetizations demonstrated routine secular variation recorded by the speleothems, and that the observed angular deviations are not a sign of remanence anisotropy. Secular variation averages out to the GAD field when viewed over times scales greater than 10 ka, but because each of their subsamples captured less than 500 years, they are interpreted to provide a window into the short-term behavior of the geomagnetic field. A comparison with CALS7K inclination and declination for this location shows fairly good reproducibility when taking into account dating errors, and the varying temporal resolutions of the stalagmites analyzed (Figure 4). The majority of the record shows clockwise looping of the VGP, indicating a predominance of westward drifting non-dipole sources. The authors argue that the later part of the record provides evidence of interaction between a drifting non-dipole component and a stationary non-dipole anomaly of oscillating intensity. The speleothem records can be compared to regional paleointensity curves from China and Japan, but the dating of the samples contains relatively large errors due to detrital thorium contamination (Openshaw et al., 1997).

For samples older samples than the ^{230}Th dating limit, magnetostratigraphy can be applied if the record contains a sufficient number of polarity reversals that it can be uniquely tied to the geomagnetic polarity time scale (GPTS), and if the depositional rate is fairly uniform throughout the sequence and there are no hiatuses or immeasurable units, so that polarity zones are not distorted or omitted (Herries et al. 2006a). Otherwise, other geochronological methods (relative and absolute) must be used in combination with the magnetic polarity record to constrain ages. This approach was used by several workers in South African caves (e.g., Partridge et al., 1999, 2000; Berger et al., 2002; Lacruz et al., 2002; Thackeray et al., 2002; Herries et

al., 2006a,b; Adams et al., 2007; Dirks et al., 2010; Herries and Shaw, 2011) in order to date sequences containing Pleistocene faunal assemblages. Lithostratigraphy, vertebrate biostratigraphy, and magnetostratigraphy have been used in combination with absolute dating techniques (e.g., U-Pb, cosmogenic nuclides, or electron spin resonance) to constrain the ages of hominin-bearing sequences at several sites of archeological interest. At most of the locations flowstone alternates with siliciclastic deposits, and only a small number of speleothem samples were retrieved for analysis at low temporal resolution. However, at Sterkfontein Cave, South Africa, an important *Australopithecus* site, Herries and Shaw (2011) sampled only speleothem units in order to avoid problems associated with clastic sediments, breccias, and contaminated flowstone. Their results constrain *Australopithecus* ages to a narrow interval approximately 2 Ma ago, which is more than 1 Ma younger than initially determined by Partridge et al. (1999, 2000), and later revised by Berger et al. (2002). In Slovenia, magnetostratigraphic studies have been conducted on flowstone sequences containing normal and reverse polarity magnetizations (Bosak et al., 2002; Pruner et al; 2010). Bosak et al. (2002) have found seven zones of normal polarity separated by zones of reverse polarity in flowstone sequence from an alpine cave in northeastern Slovenia. They suggest ages older than 1.8 Ma for the sequence, but the correlation to the GPTS is very tentative. In a study conducted on a sequence of alternating clay and flowstone layers in a cave from the classical karst area of SW Slovenia, Pruner et al. (2010) have combined magnetostratigraphy with vertebrate biostratigraphy to constrain the age of their sequence. The succession of the polarity zones was tentatively correlated to the GPTS from present to ~3.5 Ma, but the correlation is not without problems owing to the presence of numerous hiatuses.

4.4. Radiometric dating issues

As alluded to above, one of the pitfalls of using speleothems as geomagnetic recorders has been the uncertainty carried by age models from ^{230}Th dating due to (1) contamination by detrital thorium, (2) far from robust age-depth models, and (3) the

dating method available at the time being less sensitive to thorium concentrations, compared to newer generation dating techniques.

Although detrital material is the principal source of magnetic signal in speleothems, it is also a contaminating agent for the calcite used for radiometric dating. Fine-grained clastic material incorporated into speleothems is a source of external ^{230}Th, which creates the undesirable situation of having a radioisotopically open system. Contamination by detrital ^{230}Th can be traced from the presence of the accompanying ^{232}Th, and in some cases a correction can be applied. For example, Latham et al. (1982) used a ^{230}Th/^{232}Th = 1.5 correction factor for their ^{230}Th dates, but still ended with rather large uncertainties in their age model.

Another source of error in these earlier studies comes from the fact that all the chronologies were based on linear age-depth models, which do not necessarily reflect true speleothem growth patterns. In some cases multiple linear fits to the data were considered (e.g., Lean et al., 1995) but without providing substantial chronology improvements. Some examples of calculated growth rates are 140 μm/year (Latham et al., 1982), 200 μm/year (Latham et al., 1979), 20-200 μm/year (Openshaw et al., 1997), 234 μm/year (Latham et al., 1987), 600 μm/year (Latham et al., 1986), or 15 μm/year with no absolute chronology (Morinaga et al., 1986). The large growth rates found for temperate-climate speleothems (>100 μm/year) are likely due to a combination of dating errors, and using inadequate linear fits to the data.

Finally, earlier studies were limited by the fact that dating was carried out using alpha spectrometry, a technique that requires a large amount of material (tens of grams), which adds to the dating error due to the need for lower resolution sampling. The ^{230}Th dating limit for alpha spectrometry is ~350 ka, therefore a number of speleothems outside that range were inferred to be either of Brunhes or Matuyama in age based solely on polarity (e.g., Latham et al., 1979, 1982; Lauritzen et al., 1990). The temporal limitation of the ^{230}Th dating method using modern techniques (e.g., inductively coupled plasma mass spectrometry) is almost twice that of alpha spectrometry, so speleothem paleomagnetic data could potentially extend the

usefulness of speleothems in paleoclimate research beyond the current limit of ^{230}Th dating by providing a new dating means. However, assigning absolute ages by calibrating to the GPTS through wiggle matching of inclination and declination records would only be possible under a particularly narrow set of conditions, which includes the necessity of having a continuous record that intersects the ^{230}Th dating limit, in the absence of floating chronologies based on annual layer counting.

5. Future directions in speleothem magnetism research

5.1. Advances in magnetic instrumentation and quantitative analytical methods

The major limitations previous speleothem magnetism researchers have faced are tied to their inability to (1) detect very low concentrations of magnetic particles due to sensitivity limitations associated with older generations of cryogenic magnetometers, (2) measure magnetic properties continuously over a section of speleothem, thus introducing errors related to cutting (e.g., material loss, positioning), and (3) achieve a resolution on the order of the annual growth rates of speleothems.

Superconducting quantum interference device (SQuID) moment magnetometers are now capable of measuring samples with volume magnetizations as low as 10^{-6} A/m (i.e., for a 1 cm^3 sample this corresponds to a moment of 10^{-12} Am^2), which is an order of magnitude more sensitive than what instruments available two decades ago could achieve. In addition, the emergence of u-channel magnetometers in the 1980s has allowed researchers to measure a variety of magnetic properties on continuous sections (e.g., Weeks et al., 1993; Roberts, 2006), with a maximum resolution of 5 mm after data deconvolution (Jackson et al., 2010). Speleothem cores containing horizontal layers, analyzed at this kind of spatial resolution, would allow the assembly of geomagnetic records with a temporal resolution of centuries or better.

The Scanning SQuID Microscope (SSM) is another type of magnetometer that has been used successfully for fine-scale paleomagnetic analysis in the last decade (Weiss et al., 2002, 2007; Gattacceca et al., 2006; Oda et al., 2011). SSMs are capable of detecting magnetic fields generated by dipoles with moments as weak as 10^{-15} Am^2, with an optimal resolution better than 0.1 mm (Weiss et al., 2007). SSMs are ideal for small samples and thin sections with thicknesses of up to 0.1 mm. The advantage of such scans is that they can isolate small magnetized regions and even dipolar point sources contained in larger samples. The problem with mapping the magnetic field above a sample is that there are multiple configurations of dipole moments that can

generate such a field. Recently, Weiss et al. (2007) addressed this problem of non-uniqueness by developing a constrained least squares inversion technique that allows the retrieval of full vector spatial magnetization from magnetic field data. SSM measurements are ideal for speleothems because the intensity of magnetization of thin sections prepared from speleothem calcite is within the sensitivity range of the SSM, and the scanning resolution is comparable to speleothem annual growth rates.

In addition to instrumental advances, major progress has been made in magnetic unmixing methods over the past two decades. These unmixing techniques aim to quantify the contributions of different populations of magnetic grains to the overall magnetization observed in a sample. Such magnetic components have been successfully isolated from induced and remanent magnetization curves (e.g., Robertson and France, 1994; Roberts et al., 2000; Kruiver et al., 2001; Heslop et al., 2002; Egli 2003, 2004; Egli et al., 2010), as well as from bulk magnetic parameters (e.g., Lees, 1997; Frederichs et al., 1999; Xie et al., 1999; Bleil and von Dobenek, 2004; Xie et al., 2009; Lascu et al., 2010). When compared with TEM-based particle analysis of extracted magnetic grains from rocks and sediments, magnetic unmixing is clearly a much faster, albeit indirect method of magnetic component quantification. In Figure 5 we illustrate preliminary magnetic unmixing results from four speleothems, based on the deconvolution of ARM and IRM demagnetization curves (Egli, 2004). The specimens analyzed consistently contain two low coercivity (<100 mT, “soft”) components and one high coercivity (>200 mT, “hard”) component. Median coercivities and distribution widths for the magnetically soft components overlap with those of the non-biogenic magnetite and maghemite components defined by Egli (2004). They may also reflect the contributions of the abraded and unabraded categories of grains observed via TEM by Perkins (1996). The larger, abraded, detrital grains may correspond to the lower coercivity soft component, whereas the unabraded grains, if partially or fully maghemitized, could potentially be a match for the higher coercivity soft component. The magnetically hard component corresponds to component H of Egli (2004), representing contributions from hematite and/or goethite to the total magnetization. The needle-shaped goethite particles identified by Perkins

(1996) are direct proof for the existence the hard component defined using magnetic methods. We have also conducted a pilot investigation of the magnetic mineralogy of two speleothems using low-temperature SQuID magnetometry, and have confirmed the presence of partially-oxidized magnetite in both samples and of goethite in one of them (Figure 6). The goethite was identified using a rock magnetic test designed specifically to target this mineral. Our approach is similar to that employed by Guyodo et al. (2006), who have isolated the goethite in their soil samples by demagnetizing the low coercivity minerals. Due to the weak magnetization of our speleothem aliquots, instead of demagnetizing the stronger, low coercivity component, we have thermally demagnetized the goethite, and the difference between the total magnetization and the remainder (i.e., the low coercivity component) was taken to represent the concentration of goethite (Fig. 6, a and b) These rock magnetic results are important because they allow researchers to directly quantify the fluxes of different magnetic minerals throughout a speleothem. Similar to speleothem stable isotopic records, these fluxes act as proxies for environmental change occurring above the cave system, and can be used to reconstruct local and regional climate variations.

5.2. Potential for high resolution studies of magnetic field behavior

One of the key challenges in paleomagnetism and geomagnetism research is recovering high fidelity records of past geomagnetic field behavior. Continuous paleomagnetic records provide uninterrupted time series reflecting geodynamo processes, therefore high quality paleomagnetic data can better inform theoretical and numerical geodynamo models. The body of paleomagnetic observations amassed in the past few decades has lead to robust reconstructions of geomagnetic field variability, and has allowed coherent geodynamo model testing for Earth's recent history (cf. Gubbins, 2010; Hulot et al., 2010). However, due to limitations in temporal and spatial resolution, traditional paleomagnetic archives have only provided information about large scale dynamo processes (e.g., convection flows at the scale of the entire outer core, which produce the dipolar configuration of the geomagnetic field). The combination of paleomagnetic and chronological errors of such records

constrains geomagnetic field modeling to the reconstruction of its dominant, dipolar component, while higher-order, non-dipolar components are at best comparable in magnitude to the total error (Hulot et al., 2010). Nevertheless, time-dependent, deterministic global field models based on spherical harmonic functions have been assembled for the last seven millennia (e.g., Korte and Constable, 2003, 2005, 2011; Donadini et al., 2009; Korte et al., 2009). These models are good representations of the Earth's magnetic field for spherical harmonics of low degree, but they only resolve large scale core field processes. Understanding the nature of geomagnetic events on subdecadal to centennial scales is important because they offer clues about core dynamics on short time scales (Mandea et al., 2010; Finlay et al., 2010), and can better inform global field models. This can only be achieved, however, through a combination of high resolution records with tightly constrained age models. The problem with most sedimentary archives is that they tend to smooth out such very short-lived geomagnetic features, unless the record is of exceptionally high quality in terms of resolution and magnetization lock-in mechanism.

Continuous, high-resolution NRM records from speleothems could help answer some of the lingering questions related to the fine-scale temporal behavior of the geomagnetic field. Precisely dated paleomagnetic records obtained from speleothems could be important for constraining submillennial events such as geomagnetic jerks, geomagnetic intensity spikes, archeomagnetic jerks, or geomagnetic excursions farther back in time compared to the historical and archeological records.

Geomagnetic jerks are subannual reorganizations of the large-scale secular variation, and are manifestations of sudden changes in the acceleration of outer core flows (Hulot et al., 1993, Mandea et al., 2010). They are particularly related to flows associated with torsional oscillations (Bloxham et al., 2002), which are decadal-scale azimuthal fluid motions that propagate as waves along the cylindrically radial component of the magnetic field perpendicular to Earth's rotation axis (Dumberry, 2008). Torsional oscillations are very important for core dynamics because they are the most robust small scale dynamic features observed in the outer core, providing a

link between magnetic field observations and dynamo theory (Mandea and Olsen, 2009). Geomagnetic jerks often occur worldwide, and have been mainly observed from observatory and satellite data during the twentieth century, and historical recordings prior to 1900 (Bloxham et al., 2002; Hulot et al., 2002). The quality of the data however decreases with increasing time, with a sharp drop off prior to the twentieth century. High resolution, well dated records from speleothems could provide the unique opportunity to study these phenomena beyond the era of modern observations, and offer a more complete picture of geodynamo processes further back in time.

High frequency geomagnetic features described in recent years from archeological proxies indicate that abrupt changes in the intensity and direction of Earth's magnetic field can occur on the timescale of decades (Gallet et al., 2003, 2009; Ben-Yosef et al., 2009; Shaar et al., 2010, 2011). These features are termed archeomagnetic jerks if they are characterized by abrupt changes in direction and intensity, and geomagnetic spikes if they are characterized by unusually high intensities spanning a short time period.

Archeomagnetic jerks have temporal characteristics intermediate between geomagnetic jerks and excursions. They are multi-decadal features characterized by sharp cusps in field direction coincident with maxima in field strength, and separate 500-1000 year periods of smooth secular variation (Genevey and Gallet, 2002; Gallet et al., 2003). Archeomagnetic jerks with the clearest angular signature appear at times when the dipole component of the geomagnetic field is weakened relative to the non-dipole component, and when the apparent dipole center displays a strong eccentricity, being shifted from the Earth's center. They occur at times when the field produced by the dynamo is most asymmetric, with the field being more intense on average in a specific hemisphere (Gallet et al., 2009). The occurrence of archeomagnetic jerks was linked to changes in the hemispherical asymmetry in the distribution of magnetic flux patches at the core surface (Dumberry and Bloxham, 2006; Gallet et al., 2009). Dynamics at the core surface are likely responsible for azimuthal drift of field structures involving both eastward and westward motion at mid to high latitudes in the

Northern Hemisphere, corresponding to the displacement and distortion of the two present quasi-stationary high-latitude magnetic flux patches (Dumberry and Finlay, 2007). The eccentric dipole interpretation is based on data originating mainly from Western Europe and the Middle East archeological records that are younger than 3000 years. High-resolution speleothem data from different time periods and geographic areas could provide additional information about the local or global nature of archeomagnetic jerks, and could aid in further testing of the dipole eccentricity hypothesis.

Geomagnetic spikes are large changes in field strength which occur on time scales of a few decades. The local field strength may reach values that are almost double the current intensity, with a rate of change several times higher than seen in direct measurements of the magnetic field during the past 50 years, or in high resolution models for the past four centuries (Jackson et al., 2000). Shaar et al. (2011) have recently published a new absolute paleointensity curve for the Levant based on the study of the magnetization of ancient copper smelting waste material. The curve includes two geomagnetic spikes, documented at two locations in the Middle East that occurred during the Iron Age (Ben-Yosef et al., 2009; Shaar et al., 2010). The field virtual axial dipole moment (VADM) during these events attained intensities in excess of 200 ZAm^2, and experienced an increase of more than 70 ZAm^2 in a matter of three decades. The maximum VADM values are 30% higher than values reported from global and local stacks of paleointensity data, as well as from models based on spherical harmonics (e.g., CALS7K, Korte and Constable, 2005). The Levant case is a fortunate instance in which a combination of high quality, high resolution data, which benefited from a robust age model, captured two high intensity events with durations of a few decades. However, such instances are largely serendipitous. In most sedimentary environments these high frequency events would have been smoothed out, while volcanic eruptions are by nature too infrequent to capture such events. By contrast, speleothems are globally distributed, have a wide temporal span, can be continuously deposited over thousands of years with potentially annual resolution, and

therefore may prove to be suitable recorders of such decadal-scale geomagnetic features, and could help constrain their spatial and temporal extent.

Another frontier of paleomagnetic research focuses on the understanding of the Earth's magnetic field behavior during centennial to millennial events known as geomagnetic excursions. During excursions the virtual geomagnetic dipole deviates from the normal range of secular variation, often by more than 45° from the geographic pole (Merrill and McFadden, 1994); these directional changes are positively correlated with lows in paleointensity (Laj and Channell, 2007). It is not clear if excursions are aborted reversals or just anomalous secular variation, and interpretations of their anatomies range from simple dipole-dominated structures to more complex configurations controlled by a large non-dipole component (Roberts, 2008). Most of the problems with documenting excursions are related to the unreliability of sedimentary records with regards to their ability to provide high quality geomagnetic data, coupled with robust chronologies. Lava flows are more reliable paleomagnetic recorders and can be dated with greater precision, but long, continuous volcanic sequences that are highly resolved are extremely rare (Singer et al., 2009). High resolution, well dated speleothem records spanning well known excursions could help test whether excursions are (1) global, with consistent virtual geomagnetic pole (VGP) pathways resulting from a significant departure of the dipole field from the rotation axis, (2) global, with variable VGP pathways resulting from a large non-dipole to dipole ratio, or (3) local, with a large non-dipole component of the field associated with no dipole reversal (see Roberts, 2008, and references therein). Additionally, excursion signatures preserved in speleothems can be dated with unprecedented accuracy and precision, with the potential to improve chronological errors by up to an order of magnitude (Edwards et al., 2003; Dorale et al., 2004).

5.3. Potential for studies of regional climate variability

Speleothems are more than just attractive materials for paleomagnetic studies. Similar to other sedimentary deposits containing magnetic minerals, they may be used to characterize the evolution of local environmental parameters based on the concentration, composition and grain size of their magnetic mineral assemblages (e.g., Thompson and Oldfield, 1986; Evans and Heller, 2003). The number of publications in the field of environmental magnetism has grown exponentially in the past four decades, but speleothems have remained an untapped reservoir, primarily because of their low magnetic mineral concentration. With the instrument sensitivity and resolution achievable today, we envision speleothems having the potential to offer high quality data that can be compared to that from the most complete sedimentary magnetic records of lake and marine sediments, loess-paleosol sequences, modern soils, eolian, and glacial deposits.

Measurements of low-field magnetic susceptibility and various laboratory imparted magnetizations (e.g., ARM, IRM) allow the quantification of relative concentrations or absolute fluxes of magnetic components, thereby tracking climatic and environmental processes that control sediment-magnetic records (Lascu et al., 2010). Well dated environmental magnetic records from speleothems have the potential of yielding high resolution reconstructions of regional and local climatic, erosional, or pedogenic histories, and may also contain information about the local hydrogeological conditions and aquifer architecture. The advantage of obtaining such records from speleothems is that they can be directly compared to temperature and precipitation reconstructions based on isotopic and trace element compositions from the same specimens. Furthermore, environmental magnetic records from speleothems can be correlated with those from other archives for more robust regional paleoclimatic reconstructions. For example, one of the issues currently under debate concerns the history of the Asian monsoon. Variations in regional precipitation amounts reconstructed from soil magnetism-precipitation transfer functions (Maher et al., 2002; Maher and Hu, 2006) do not match those deduced from speleothem oxygen

isotope ratios (Wang et al., 2001; Yuan et al., 2004). Maher (2008) argues that speleothem records in China do not actually reflect precipitation amount, but changes in precipitation source and air mass trajectories, and that amount effects are reflected in the difference between the oxygen isotope records between sites, which appear to match the soil magnetism curves more closely. Measurements of magnetic properties of speleothems would offer a direct means of comparing the two archives and help bridge disparate interpretations of external climatic forcings.

6. Summary

Speleothem magnetism is a promising new tool for paleomagnetic and environmental magnetic studies. Speleothems, as geomagnetic recorders, hold key advantages over sediments, lava flows, and archeological artifacts, including instant lock-in of the magnetization, no post-depositional effects, and excellent age control. Their main limitations until now, namely low magnetic mineral concentrations and slow growth rates, can be readily overcome by using highly sensitive, high resolution magnetometers available today. The principal remanence carrier in speleothems is magnetite, with minor contributions from ferric oxy-hydroxides. The main remanence acquisition mechanism is depositional, through physical alignment of detrital magnetic grains in the water film draping the speleothem with the geomagnetic field lines. Detrital magnetic particles are deposited on speleothem surfaces either from receding flood waters, or directly from drip water percolating from the overlying soils. Chemical remanence, acquired *in situ* by particles growing through a critical volume, is only subordinate. Earlier workers have shown that geomagnetic features are successfully recorded by speleothems, and can be reproduced at a local and regional scale. Future studies that benefit from increasingly sensitive magnetometers, operating at high resolution, should be able to resolve short-term geomagnetic variability, and characterize events such as geomagnetic excursions at an unprecedented level of resolution. The environmental magnetism of speleothems is still an untapped reservoir, but holds the promise of bridging the gap between mineral-magnetic records from other sedimentary archives and established speleothem environmental proxies (e.g., oxygen isotopes).

References

Adams, J.W., Herries, A.I.R., Kuykendall, K.L., Conroy, G.C., 2007. Taphonomy of a South African cave: geological and hydrological influences on the GD1 fossil assemblage at Gondolin, a Plio-Pleistocene paleocave system in the Northwest Province, South Africa. Quaternary Science Reviews 26, 2526-2543.

Ben-Yosef, E., Tauxe, L., Levy, T.E., Shaar, R., Ron, H., Najjar, M., 2009. Geomagnetic intensity spike recorded in high resolution slag deposit in southern Jordan. Earth and Planetary Science Letters 287, 529-539.

Berger, L.R., Lacruz, R., de Ruiter, D.J., 2002. Revised age estimates of Australopithecus-bearing deposits at Sterkfontein, South Africa. American Journal of Physical Anthropology 119, 192-197.

Bleil, U., von Dobeneck, T., 2004. Late Quaternary terrigenous sedimentation in the western Equatorial Atlantic; South American versus African provenance discriminated by magnetic mineral analysis, in Wefer, G., Mulitza, S., Ratmeyer, V. (Eds.), The South Atlantic in the Late Quaternary; Reconstruction of Material Budgets and Current Systems. Springer-Verlag, Berlin, Federal Republic of Germany (DEU), Federal Republic of Germany (DEU), pp. 213-236.

Bloxham, J., Zatman, S., Dumberry, M., 2002. The origin of geomagnetic jerks. Nature 420, 65–68.

Bohnel, H., Molina-Garza, R., 2002. Secular variation in Mexico during the last 40,000 years. Physics of the Earth and Planetary Interiors 133, 99-109.

Bogue S.W., Glen, J.M.G., 2010. Very rapid geomagnetic field change recorded by the partial remagnetization of a lava flow. Geophysical Research Letters 37, doi:10.1029/2010GL044286.

Bosak, P., Hercman, H., Mihevc, A., Pruner, P., 2002. High-resolution magnetostratigraphy of speleothems from Snezna Jama, Kamnik-Savinja Alps, Slovenia. Acta Carsologica 31, 15-32.

Bosch, R.F., White, W.B., 2004. Lithofacies and transport of clastic sediments in karstic aquifers, in Sasowsky, I., Mylroie, J. (Eds.), Studies of Cave Sediments: Physical and Chemical Records of Paleoclimate. Springer, Dordrecht, Netherlands, pp. 1-12.

Brook, G.A., Ellwood, B.B., Railsback, L.B., Cowart, J.B., 2006. A 164 ka record of environmental change in the American Southwest from a Carlsbad Cavern speleothem. Palaeogeography Palaeoclimatology Palaeoecology 237, 483-507.

Bull, P.A., 1981. Some Fine-Grained Sedimentation Phenomena in Caves. Earth Surface Processes and Landforms 6, 11-22.

Burleson, D.J., Penn, R.L., 2006. Two-step growth of goethite from ferrihydrite. Langmuir 22, 402-409.

Dasgupta, S., 2008. High-resolution speleothem record of late Quaternary climate change from the Upper Midwest, USA. PhD Dissertation, University of Minnesota, Minneapolis, USA.

Dasgupta, S., Saar, M.O., Edwards, R.L., Shen, C., Cheng, H., Alexander, E.C., 2010. Three thousand years of extreme rainfall events recorded in stalagmites from Spring Valley Caverns, Minnesota. Earth and Planetary Science Letters 300, 46-54.

Dickson, J.A.D., 1993. Crystal growth diagrams as an aid to interpreting the fabrics of calcite aggregates. Journal of Sedimentary Petrology 63, 1-17.

Dirks, P.H.G.M., Kibii, J.M., Kuhn, B.F., Steininger, C., Churchill, S.E., Kramers, J.D., Pickering, R., Farber, D.L., Meriaux, A., Herries, A.I.R., King, G.C.P., Berger, L.R., 2010. Geological setting and age of Australopithecus sediba from Southern Africa. Science 328, 205-208.

Donadini, F., Korte, M., Constable, C., 2009. Geomagnetic field for 0–3 ka: 1. New data sets for global modeling. Geochemistry Geophysics Geosystems 10, doi:10.1029/2008GC002295.

Dorale, J.A., Edwards, R.L., Alexander, E.C., Shen, C., Richards, D.A., Cheng, H., 2004. Uranium-series dating of speleothems: current techniques, limits, & applications, in Sasowsky, I., Mylroie, J. (Eds.), Studies of Cave Sediments:

Physical and Chemical Records of Paleoclimate. Springer, Dordrecht, Netherlands, pp. 177-197.

Dumberry, M., 2008. Gravitational torque on the inner core and decadal polar motion. Geophysical Journal International 172, 903–920.

Dumberry, M., Bloxham, J., 2006. Azimuthal flows in the Earth's core and changes in length of day at millennial timescales. Geophysical Journal International 165, 32-46.

Dumberry, M., Finlay, C.C., 2007. Eastward and westward drift of the Earth's magnetic field for the last three millennia. Earth and Planetary Science Letters 254, 146–157.

Dunlop, D.J., 2002. Theory and application of the Day plot (M_{rs}/M_s versus H_{cr}/H_c): 1. Theoretical curves and tests using titanomagnetite data. Journal of Geophysical Research 107, doi:10.1029/2001JB000486.

Edwards, R.L., Gallup, C.D., Cheng, H., 2003. Uranium-series dating of marine and lacustrine carbonates, in Bourdon, B., Henderson, G.M., Lundstrom, C.C., Turner, S.P. (Eds.), Reviews in Mineralogy and Geochemistry: Uranium-Series Geochemistry. Mineralogical Society of America, Washington, DC, United States of America, pp. 363-405.

Egli, R., 2003. Analysis of the field dependence of remanent magnetization curves. Journal of Geophysical Research 108, doi:10.1029/2002JB002023.

Egli, R., 2004. Characterization of individual rock magnetic components by analysis of remanence curves: 1. Unmixing natural sediments. Studia Geophysica et Geodetica 48, 391-446.

Egli, R., Chen, A.P., Winklhofer, M., Kodama, K.P., Horng, C.-S., 2010. Detection of noninteracting single domain particles using first-order reversal curve diagrams. Geochemistry Geophysics Geosystems 11, doi:10.1029/2009GC002916.

Elmore, R.D., Engel, M.H., Crawford, L., Nick, K., Imbus, S., Sofer, Z., 1987. Evidence for a relationship between hydrocarbons and authigenic magnetite. Nature 325, 428-430.

Evans, M.E., Heller, F., 2003. Environmental magnetism: principles and applications of enviromagnetics. Academic Press, San Diego, USA.

Fairchild, I.J., Smith, C.L., Baker, A., Fuller, L., Spoetl, C., Mattey, D., McDermott, F., 2006. Modification and preservation of environmental signals in speleothems. Earth-Science Reviews 75, 105-153.

Fairchild, I.J., Frisia, S., Borsato, A., Tooth, A.F., 2007. Speleothems, in Nash, D.J., McLaren, S.J. (Eds.), Geochemical Sediments and Landscapes. Blackwell, Oxford, United Kingdom, pp. 200-245.

Finlay, C.C., Dumberry, M., Chulliat, A., Pais, M.A., 2010. Short timescale core dynamics: theory and observations. Space Science Reviews 155, 177-218.

Ford, D., Williams, P., 2007. Karst Hydrogeology and Geomorphology. John Wiley & Sons, Chichester, United Kingdom.

Frederichs, T., Bleil, U., Daeumler, K., von Dobeneck, T., Schmidt, A.M., 1999. The magnetic view on the marine paleoenvironment; parameters, techniques and potentials of rock magnetic studies as a key to paleoclimatic and paleoceanographic changes, in Fischer, G., Wefer, G. (Eds.), Use of Proxies in Paleoceanography; Examples from the South Atlantic. Springer, Berlin, Federal Republic of Germany (DEU), Federal Republic of Germany (DEU), pp. 575-599.

Gallet, Y., Genevey, A., Courtillot, V., 2003. On the possible occurrence of "archaeomagnetic jerks" in the geomagnetic field over the past three millennia. Earth and Planetary Science Letters 214, 237-242.

Gallet, Y., Hulot, G., Chulliat, A., Genevey, A., 2009. Geomagnetic field hemispheric asymmetry and archeomagnetic jerks. Earth and Planetary Science Letters 284, 179-186.

Gattacceca, J., Boustie, M., Weiss, B.P., Rochette, P., Lima, E.A., Fong, L.E., Baudenbacher, F.J., 2006. Investigating impact demagnetization through laser impacts and SQUID microscopy. Geology 34, 333-336.

Geiss, C.E., Zanner, C.W., Banerjee, S.K., Joanna, M., 2004. Signature of magnetic enhancement in a loessic soil in Nebraska, United States of America. Earth and Planetary Science Letters 228, 355-367.

Genevey, A., Gallet, Y., 2002. Intensity of the geomagnetic field in western Europe over the past 2000 years: new data from ancient French pottery. Journal of Geophysical Research 107, doi:10.1029/2001JB000701.

Gubbins, D., 2010. Terrestrial magnetism: Historical perspectives and future prospects. Space Science Reviews 155, 9–27.

Guyodo, Y., Mostrom, A., Penn, R.L., Banerjee, S.K., 2003. From nanodots to nanorods: Oriented aggregation and magnetic evolution of nanocrystalline goethite. Geophysical Research Letters 30, doi:10.1029/2003GL017021.

Guyodo, Y., LaPara, T.M., Anschutz, A.J., Penn, R.L., Banerjee, S.K., Geiss, C.E., Zanner, W., 2006. Rock magnetic, chemical and bacterial community analysis of a modern soil from Nebraska. Earth and Planetary Science Letters 251, 168-178.

Herries, A.I.R., Shaw, J., 2011. Palaeomagnetic analysis of the Sterkfontein palaeocave deposits: Implications for the age of the hominin fossils and stone tool industries. Journal of Human Evolution 60, 523-539.

Herries, A.I.R., Adams, J.W., Kuykendall, K.L., Shaw, J., 2006a. Speleology and magnetobiostratigraphic chronology of the GD2 locality of the Gondolin hominin-bearing paleocave deposits, North West Province, South Africa. Journal of Human Evolution 51, 617-631.

Herries, A.I.R., Reed, K.E., Kuykendall, K.L., Latham, A.G., 2006b. Speleology and magnetobiostratigraphic chronology of the Buffalo Cave fossil site, Makapansgat, South Africa. Quaternary Research 66, 233-245.

Heslop, D., Dekkers, M.J., Kruiver, P.P., van Oorschot, I.H.M., 2002. Analysis of isothermal remanent magnetization acquisition curves using the expectation-maximization algorithm. Geophysical Journal International 148, 58-64.

Huber, N., 1958. The environmental control of sedimentary iron minerals. Economic Geology 53, 123-140.

Hulot, G., Le Huy, M., Le Mouël, J.L., 1993. Geomagnetic jerks and flows in the Earth's core. Comptes Rendus de l'Academie de Sciences II 317, 333–341.

Hulot, G., Eymin, C., Langlais, B., Mandea, M., Olsen, N., 2002. Small-scale structure of the geodynamo inferred from Oersted and Magsat satellite data. Nature 416, 620-623.

Hulot, G., Finlay, C., Constable, C., Olsen, N., Mandea, M., 2010. The magnetic field of planet Earth. Space Science Reviews 152, 159-222.

Jackson, A., Jonkers, A.R.T., Walker, M.R., 2000. Four centuries of geomagnetic secular variation from historical records: Geomagnetic polarity reversals and long-term secular variation. Phil. Trans. R. Soc. Lond. A 358, 957-990.

Jackson, M., Bowles, J.A., Lascu, I., Solheid, P., 2010. Deconvolution of u channel magnetometer data: Experimental study of accuracy, resolution, and stability of different inversion methods. Geochemistry Geophysics Geosystems 11, doi:10.1029/2009GC002991.

Kendall, A.C., Broughton, P.L., 1978. Origin of fabrics in speleothems composed of columnar calcite crystals. Journal of Sedimentary Petrology 48, 519-538.

Korte, M., Constable, C., 2003. Continuous global geomagnetic field models for the past 3000 years. Physics of The Earth and Planetary Interiors 140, 73-89.

Korte, M., Constable, C.G., 2005. Continuous geomagnetic field models for the past 7 millennia: 2. CALS7K. Geochemistry, Geophysics, Geosystems 6, doi:10.1029/2004GC000801.

Korte, M., Constable, C., 2011. Improving geomagnetic field reconstructions for 0-3 ka. Physics of the Earth and Planetary Interiors, in press, doi:10.1016/j.pepi.2011.06.017.

Korte, M., Donadini, F., Constable, C., 2009. Geomagnetic field for 0–3 ka: 2. A new series of time-varying global models. Geochemistry Geophysics Geosystems 10, doi:10.1029/2008GC002297.

Kruiver, P.P., Dekkers, M.J., Heslop, D., 2001. Quantification of magnetic coercivity components by the analysis of acquisition curves of isothermal remanent magnetisation. Earth and Planetary Science Letters 189, 269-276.

Lachniet, M.S., 2009. Climatic and environmental controls on speleothem oxygen-isotope values. Quaternary Science Reviews 28, 412-432.

Lacruz, R.S., Brink, J.S., Hancox, P.J., Skinner, A.R., Herries, A., Schmid, P., Berger, L.R., 2002. Palaeontology and geological context of middle Pleistocene faunal assemblage from the Gladysvale Cave, South Africa. Palaeontologia Africana 38, 99-114.

Laj, C., Channell, J.E.T., 2007. Geomagnetic Excursions, in Kono, M. (Ed.), Treatise on Geophysics, Vol. 5 Geomagnetism. Elsevier, Amsterdam, Netherlands, pp. 373-416.

Lascu, I., Banerjee, S.K., Berquo, T.S., 2010. Quantifying the concentration of ferrimagnetic particles in sediments using rock magnetic methods. Geochemistry Geophysics Geosystems 11, doi:10.1029/2010GC003182.

Latham, A.G., Ford, D.C., 1993. The paleomagnetism and rock magnetism of cave and karst deposits, in Aissaoui, D. M., McNeill, D. F., Hurley, N. F. (Ed.), SEPM Special Publication 49: Applications of Paleomagnetism to Sedimentary Geology, pp. 149-155.

Latham, A.G., Schwarcz, H.P., Ford, D.C., Pearce, G.W., 1979. Paleomagnetism of Stalagmite Deposits. Nature 280, 383-385.

Latham, A.G., Schwarcz, H.P., Ford, D.C., Pearce, G.W., 1982. The paleomagnetism and U-Th dating of three Canadian speleothems: evidence for the westward drift, 5.4-2.1 ka BP. Canadian Journal of Earth Sciences 19, 1985-1995.

Latham, A.G., Schwarcz, H.P., Ford, D.C., 1986. The Paleomagnetism and U-Th Dating of Mexican Stalagmite, Das2. Earth and Planetary Science Letters 79, 195-207.

Latham, A.G., Schwarcz, H.P., Ford, D.C., 1987. Secular Variation of the Earth's Magnetic-Field from 18.5 to 15.0 ka BP, as Recorded in a Vancouver-Island Stalagmite. Canadian Journal of Earth Sciences 24, 1235-1241.

Latham, A.G., Ford, D.C., Schwarcz, H.P., Birchall, T., 1989. Secular Variation from Mexican Stalagmites - their Potential and Problems. Physics of the Earth and Planetary Interiors 56, 34-48.

Lauritzen, S., Lovlie, R., Moe, D., Ostbye, E., 1990. Paleoclimate deduced from a multidisciplinary study of a half-million-year-old stalagmite from Rana, Northern Norway. Quaternary Research 34, 306-316.

Lean, C.B., Latham, A.G., Shaw, J., 1995. Palaeosecular variation from a Vancouver Island stalagmite and comparison with contemporary North American records. Journal of Geomagnetism and Geoelectricity 47, 71-87.

Lees, J.A., 1997. Mineral magnetic properties of mixtures of environmental and synthetic materials; linear additivity and interaction effects. Geophysical Journal International 131, 335-346.

Liu, Q., Deng, C., Torrent, J., Zhu, R., 2007. Review of recent developments in mineral magnetism of the Chinese loess. Quaternary Science Reviews 26, 368-385.

Maher, B.A., 1998. Magnetic properties of modern soils and Quaternary loessic Paleosols: paleoclimatic implications. Palaeogeography, Palaeoclimatology, Palaeoecology 137, 25-54.

Maher, B.A., 2008. Holocene variability of the East Asian summer monsoon from Chinese cave records: a re-assessment. The Holocene 18, 861-866.

Maher, B.A., Hu, M., 2006. A high resolution record of Holocene rainfall variations from the western Chinese Loess Plateau: antiphase behaviour of the African/Indian and East Asian summer monsoons. The Holocene 16, 309–319.

Maher, B.A., Alekseev, A., Alekseeva, T., 2002. Variation of soil magnetism across the Russian steppe: Its significance for use of soil magnetism as a palaeorainfall proxy. Quaternary Science Reviews 21, 1571–1576.

Mandea, M., Olsen, N., 2009. Geomagnetic and archeomagnetic jerks: Where do we stand? EOS Transactions AGU 90.

Mandea, M., Holme, R., Pais, A., Pinheiro, K., Jackson, A., Verbanac, G., 2010. Geomagnetic jerks: Rapid core field variations and core dynamics. Space Science Reviews 155, 147-175.

Martin, K., 1990. Paleomagnetism of speleothems in Gardner Cave, Washington. National Speleological Society Bulletin 52, 87-94.

McDermott, F., 2004. Palaeo-climate reconstruction from stable isotope variations in speleothems: a review. Quaternary Science Reviews 23, 901-918.

Merrill, R.T., McFadden, P.L., 1994. Geomagnetic field stability: reversal events and excursions. Earth and Planetary Science Letters 121, 57-69.

Morinaga, H., Inokuchi, H., Yaskawa, K., 1986. Magnetization of a stalagmite in Akiyoshi Plateau as a record of the geomagnetic secular variation in West Japan. Journal of Geomagnetism and Geoelectricity 38, 27-44.

Morinaga, H., Inokuchi, H., Yaskawa, K., 1989. Palaeomagnetism of stalagmites (speleothems) in SW Japan. Geophysical Journal 96, 519-528.

Morinaga, H., Horie, I., Yaskawa, K., 1992. A geomagnetic reversal recorded in a stalagmite collected in western Japan. Journal of Geomagnetism and Geoelectricity 44, 661-675.

Nilsson, A., Snowball, I., Muscheler, R., Uvo, C.B., 2010. Holocene geocentric dipole tilt model constrained by sedimentary paleomagnetic data. Geochemistry Geophysics Geosystems 11, doi:10.1029/2010GC003118.

Oda, H., Usui, A., Miyagi, I., Joshima, M., Weiss, B.P., Shantz, C., Fong, L.E., McBride, K.K., Harder, R., Baudenbacher, F.J., 2011. Ultrafine-scale magnetostratigraphy of marine ferromanganese crust. Geology 39, 227-230.

Openshaw, S., Latham, A., Shaw, J., 1997. Speleothem palaeosecular variation records from China; their contribution to the coverage of Holocene palaeosecular variation data in East Asia; Paleosecular variation and intensity. Journal of Geomagnetism and Geoelectricity 49, 485-505.

Özdemir, Ö., Banerjee, S.K., 1982. A preliminary magnetic study of soil samples from West-central Minnesota. Earth and Planetary Science Letters 59, 393-403.

Partridge, T.C., Shaw, J., Heslop, D., Clarke, R.J., 1999. The new hominid skeleton from Sterkfontein, South Africa: age and preliminary assessment. Journal of Quaternary Science 14, 293-298.

Partridge, T.C., Latham, A.G., Heslop, D., 2000. Appendix on magnetostratigraphy of Makapansgat, Sterkfontein, Taung and Swartkrans, in Partridge, T.C., Maud,

R.R. (Eds.), The Cenozoic of Southern Africa. Oxford University Press, Oxford, UK, pp. 126-129.

Perkins, A.M., 1996. Observations under electron microscopy of magnetic minerals extracted from speleothems. Earth and Planetary Science Letters 139, 281-289.

Perkins, A.M., Maher, B.A., 1993. Rock magnetic and palaeomagnetic studies of British speleothems. Journal of Geomagnetism and Geoelectricity 45, 143-153.

Perrette, Y., Delannoy, J., Desmet, M., Lignier, V., Destombes, J., 2005. Speleothem organic matter content imaging: the use of a fluorescence index to characterise the maximum emission wavelength. Chemical Geology 214, 193-208.

Pruner, P., Hajna, N.Z., Mihevc, A., Bosak, P., Man, O., Schnabl, P., Venhodova, D., 2010. Magnetostratigraphy and fold tests from Raciska Pecina and Pecina v Borstu Caves (classical karst, Slovenia). Studia Geophysica et Geodaetica 54, 27-48.

Roberts, A.P., 2006. High-resolution magnetic analysis of sediment cores: strengths, limitations and strategies for maximizing the value of long core magnetic data. Physics of the Earth and Planetary Interiors 156, 162-178.

Roberts, A.P., 2008. Geomagnetic excursions: knowns and unknowns. Geophysical Research Letters 35, doi:10.1029/2008GL034719.

Roberts, A.P., Winklhofer, M., 2004. Why are geomagnetic excursions not always recorded in sediments? Constraints from post-depositional remanent magnetization lock-in modelling. Earth and Planetary Science Letters 227, 345-359.

Roberts, A.P., Pike, C.R., Verosub, K.L., 2000. First-order reversal curve diagrams; a new tool for characterizing the magnetic properties of natural samples. Journal of Geophysical Research 105, 28,461-28,475.

Roberts, A.P., Chang, L., Rowan, C.J., Horng, C.-S., Florindo, F., 2011. Magnetic properties of sedimentary greigite (Fe_3S_4): An update. Reviews of Geophysics 49, doi:10.1029/2010RG000336.

Robertson, D.J., France, D.E., 1994. Discrimination of remanence-carrying minerals in mixtures, using isothermal remanent magnetisation acquisition curves. Physics of the Earth and Planetary Interiors 82, 223-234.

Rusanov, V., Gilson, R.G., Lougear, A., Trautwein, A.X., 2000. Mossbauer, magnetic, X-ray fluorescence and transmission electron microscopy study of natural magnetic materials from speleothems: haematite and the Morin transition. Hyperfine Interactions 128, 353-373.

Shaar, R., Ron, H., Tauxe, L., Kessel, R., Agnon, A., Ben-Yosef, E., Feinberg, J.M., 2010. Testing the accuracy of absolute intensity estimates of the ancient geomagnetic field using copper slag material. Earth and Planetary Science Letters 290, 201-213.

Shaar, R., Ben-Yosef, E., Ron, H., Tauxe, L., Agnon, A., Kessel, R., 2011. Geomagnetic field intensity: How high can it get? How fast can it change? Constraints from Iron Age copper slag. Earth and Planetary Science Letters 301, 297-306.

Shopov, Y.Y., Ford, D.C., Schwarcz, H.P., 1994. Luminescent microbanding in speleothems: high-resolution chronology and paleoclimate. Geology 22, 407-410.

Singer, B.S., Guillou, H., Jicha, B.R., Laj, C., Kissel, C., Beard, B.L., Johnson, C.M., 2009. $^{40}Ar/^{39}Ar$, K–Ar and $^{230}Th–^{238}U$ dating of the Laschamp excursion: A radioisotopic tie-point for ice core and climate chronologies. Earth and Planetary Science Letters 286, 80-88.

Tarduno, J.A., 1995. Superparamagnetism and reduction diagenesis in pelagic sediments: enhancement or depletion? Geophysical Research Letters 22, 1337-1340.

Tauxe, L., Kent, D.V., 2004. A simplified statistical model for the geomagnetic field and the detection of shallow bias in paleomagnetic inclinations: was the ancient magnetic field dipolar?, in Channell, J.E.T., Kent, D.V., Lowrie, W., Meert, J.G. (Eds.), Timescales of the Paleomagnetic Field. American Geophysical Union, Washington DC, USA, pp. 101-115.

Thackeray, J.F., Kirschvink, J.L., Raub, T.D., 2002. Palaeomagnetic analyses of calcified deposits from the Plio-Pleistocene hominid site of Kromdraai, South Africa. South African Journal of Science 98, 537-540.

Thompson, R., Oldfield, F., 1986. Environmental Magnetism. Allen and Unwin, London, UK.

Verosub, K.L., 1977. Depositional and postdepositional processes in the magnetization of sediments. Reviews of Geophysics and Space Physics 15, 129-143.

Wagner, G.A., 1998. Age Determination of Young Rocks and Artifacts: Physical and Chemical Clocks in Quaternary Geology and Archaeology. Springer-Verlag, Berlin, Germany.

Wang, Y., Cheng, H., Edwards, R.L., An, Z.S., Wu, J.Y., Shen, C.C., Dorale, J.A., 2001. A high-resolution absolute-dated late Pleistocene monsoon record from Hulu Cave, China. Science 294, 2345-2348.

Wang, Y., Cheng, H., Edwards, R.L., He, Y., Kong, X., An, Z., Wu, J., Kelly, M.J., Dykoski, C.A., Li, X., 2005. The Holocene Asian monsoon: links to solar changes and North Atlantic climate. Science 308, 854-857.

Wang, Y., Cheng, H., Edwards, R.L., Kong, X., Shao, X., Chen, S., Wu, J., Jiang, X., Wang, X., An, Z., 2008. Millennial- and orbital-scale changes in the East Asian monsoon over the past 224,000years. Nature 451, 1090-1093.

Weeks, R., Laj, C., Endignoux, L., Fuller, M., Roberts, A., Manganne, R., Blanchard, E., Goree, W., 1993. Improvements in long-core measurement techniques: applications in palaeomagnetism and palaeoceanography. Geophysical Journal International 114, 651-662.

Weiss, B.P., Vali, H., Baudenbacher, F.J., Kirschvink, J.L., Stewart, S.T., Shuster, D.L., 2002. Records of an ancient Martian magnetic field in ALH84001. Earth and Planetary Science Letters 201, 449-463.

Weiss, B.P., Lima, E.A., Fong, L.E., Baudenbacher, F.J., 2007. Paleomagnetic analysis using SQUID microscopy. Journal of Geophysical Research 112, doi:10.1029/2007JB004940.

White, W.B., 1988. Geomorphology and Hydrology of Karst Terrains. Oxford University Press, Oxford, United Kingdom.

White, W.B., 2004. Paleoclimate records from speleothems in limestone caves, in Sasowsky, I.D., Mylroie, J. (Eds.), Studies of Cave Sediments: Physical and Chemical Records of Paleoclimate. Springer, Dordrecht, Netherlands.

Xie, Q., Chen, T., Xu, H., Chen, J., Ji, J., Lu, H., Wang, X., 2009. Quantification of the contribution of pedogenic magnetic minerals to magnetic susceptibility of loess and paleosols on Chinese Loess Plateau: Paleoclimatic implications. Journal of Geophysical Research 114, B09101.

Xie, S., Dearing, J.A., Bloemendal, J., 1999. A partial susceptibility approach to analysing the magnetic properties of environmental materials; a case study. Geophysical Journal International 138, 851-856.

Yuan, D., Cheng, H., Edwards, R.L., Dykoski, C., Kelly, M., Zhang, M., Qing, J., Lin, Y., Wang, Y., Wu, J., Dorale, J., An, Z., Cai, Y., 2004. Timing, duration and transition of the last interglacial Asian Monsoon. Science 304, 575–578.

Figures

Figure 1. Conceptual model of the processes affecting magnetism of speleothems. Magnetic enhancement in the topsoil occurs during wet periods, when magnetite is formed by inorganic precipitation, or possibly mediated by dissimilatory iron reducing bacteria. Addition of eolian dust to soils occurs during dry periods. Magnetic material is transported from the surface to the spelean environment by water percolating from the soil via cracks and fissures to the point sources for drip water from which speleothems form. Rivers transport larger detrital magnetic particles, which are deposited on speleothem surfaces during the quiescent stages of water retreat after a flooding episode. Insets show detailed structure of a periodically flooded stalagmite (A) at mm (B), sub-mm (C) and sub-μm (D) scales. Magnetic particles in flood layers are on the order of a few microns to tens of microns, with an upper grain size limit of ~100 μm controlled by the thickness of the water film coating the speleothem. The seasonal laminae are on the order of several tens of microns to a few hundred microns and can contain dissolved or particulate organic matter, which gives the calcite luminescent properties when exposed to ultraviolet light. Fine-grained magnetic particles transported by drip water or precipitated *in situ* are on the order of a few nanometers to a couple of hundred nanometers.

Figure 2. Confocal microscope image of the top of stalagmite SVC982 from Spring Valley Caverns, Minnesota. Detrital layers deposited during flood stages appear dark and irregular and are marked by peaks in Al concentration (superimposed curve). Organic-rich seasonal layers fluoresce in UV light (appear light colored) and correspond to peaks in P concentration. They are coupled with non-fluorescing organic-poor laminae with relative high concentrations of Sr. Data and image from Dasgupta (2008).

Figure 3. Comparison of stalagmite VCCL, Canada (Latham et al., 1982) with model CALS7K (Korte and Constable, 2005). a) Equal area projections of VGP wander paths reconstructed from the speleothem record (left) and CALS7K (right). Numbers corresponding to points on the curves represent ages (ka BP). b) Inclination

and declination values. The stalagmite record was plotted on the CALS7K time scale with errors bars from the age model of Latham et al. (1982).

Figure 4. Inclination and declination records from the five stalagmites (SC01, SC02, PT02, PT03, PT04) studied by Openshaw et al. (1997), compared to model CALS7K (Korte and Constable, 2005).

Figure 5. Magnetic components of specimens (diamonds) from four stalagmites (HL-06, YX-17, QT from China, and SVC982 from Minnesota) determined from deconvolution of ARM demagnetization (a), IRM demagnetization (b), and IRM acquisition (c) gradient curves using the software package MAG-MIX (Egli, 2003). ARM and IRM demagnetization experiments were conducted using one hundred logarithmically-spaced steps from a peak AF field of 170 mT. ARM and IRM were imparted using direct fields of 0.1 and 170 mT respectively. IRM acquisition experiments were performed using thirty logarithmically-spaced steps, between 1 and 1000 mT. HL-06 a,b,c and SVC982 a,b,c,d indicate samples with multiple specimens. Symbol size is proportional to the contribution of the component to the total magnetization of the sample. Black triangles and circles represent components defined by Egli (2004) from deconvolution of ARM and IRM demagnetization gradient curves: D-detrital magnetite transported by flowing water, EX-ultrafine extracellular magnetite, PD-pedogenic magnetite, ED-eolian dust, L-maghemite component of loess. Horizontal and vertical axes represent median demagnetization field (MDF) or median acquisition field (MAF), and dispersion parameter (DP) respectively.

Figure 6. Low temperature behavior of a TRM (circles) acquired by field cooling (FC) from 400 K to 300 K in a 0.3 T field, and of an IRM (diamonds) acquired at 300 K in a 0.3 T field after zero-field cooling (ZFC) from 400 K to 300 K, for speleothems SVC982 (a) and QT (b). The separation of the curves above ~120 K (Verwey transition, T_v) is diagnostic of magnetite. The difference (squares) between the TRM and IRM warming (closed symbols) and cooling (open symbols) curves respectively is a measure of the presence of goethite, which acquires remanence during the FC pretreatment and is demagnetized during the ZFC pretreatment. The increase (decrease) in goethite remanence with cooling (warming) by a factor of 2 is a

diagnostic feature and can be seen in SVC982, but not in QT. c) Room temperature IRM cooling and warming curves for synthetic magnetite, goethite, and a mixture of the two minerals. For illustration purposes the synthetic goethite was normalized to its 10 K remanence, whereas the magnetite and goethite-magnetite mixture were normalized to their initial 300 K remanence. d) Behavior of a 2.5 T IRM imparted at 10 K as a function of increasing temperature from 10 K to 300 K for SVC982 (triangles) and QT (inverted triangles). The samples were pretreated by cooling in zero field (ZFC, open symbols), and in a 2.5 T field (FC, closed symbols) from 300 K to 10 K. T_v is sharp for stoichiometric magnetite, and broader for partially oxidized magnetite. The FC curve has higher values than the ZFC curve indicating SD-type behavior. For SVC982, the separation of the FC and ZFC curves through T_v and continuing above 120 K is caused by the presence of goethite. e) Low temperature IRM FC-ZFC warming curves for synthetic magnetite and goethite (note the separate vertical axes).

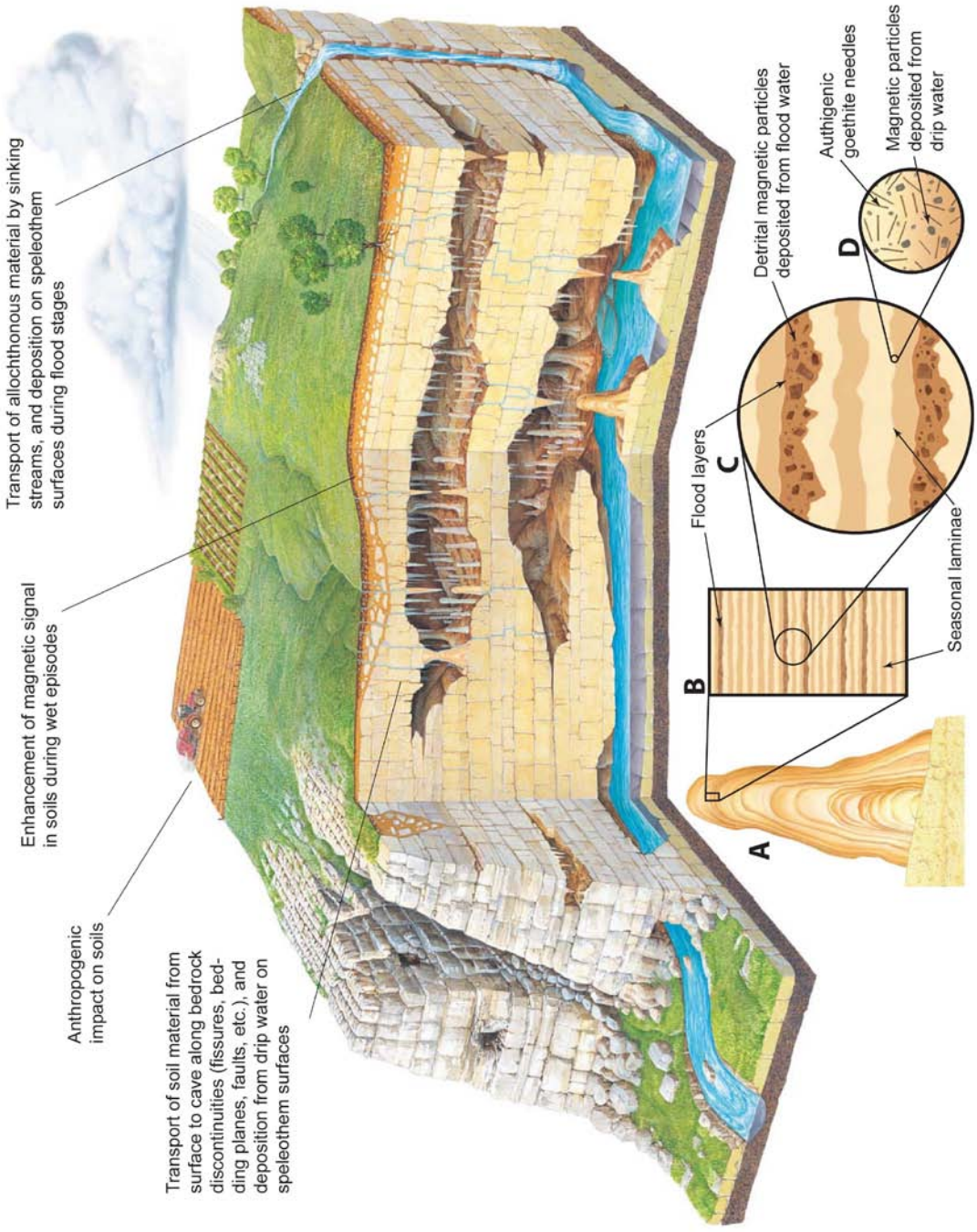

Figure 5.1 Conceptual model of the processes affecting magnetism of speleothems

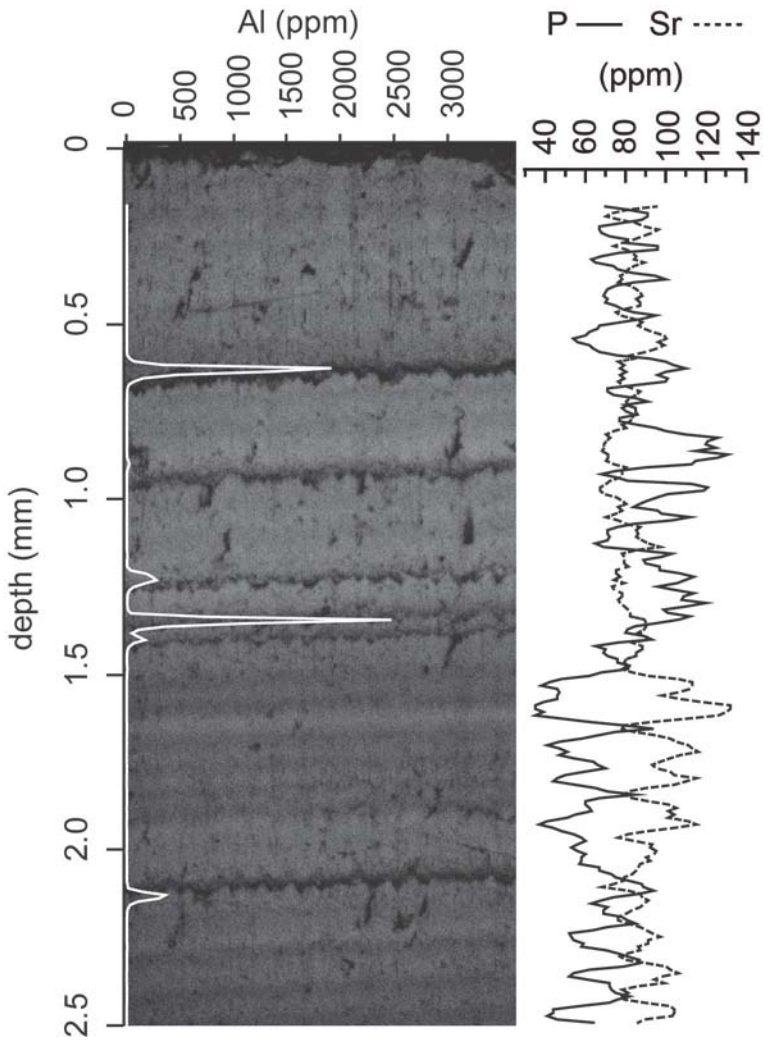

Figure 5.2 Flood layers and annual banding in stalagmite SVC982 from Spring Valley Caverns, Minnesota.

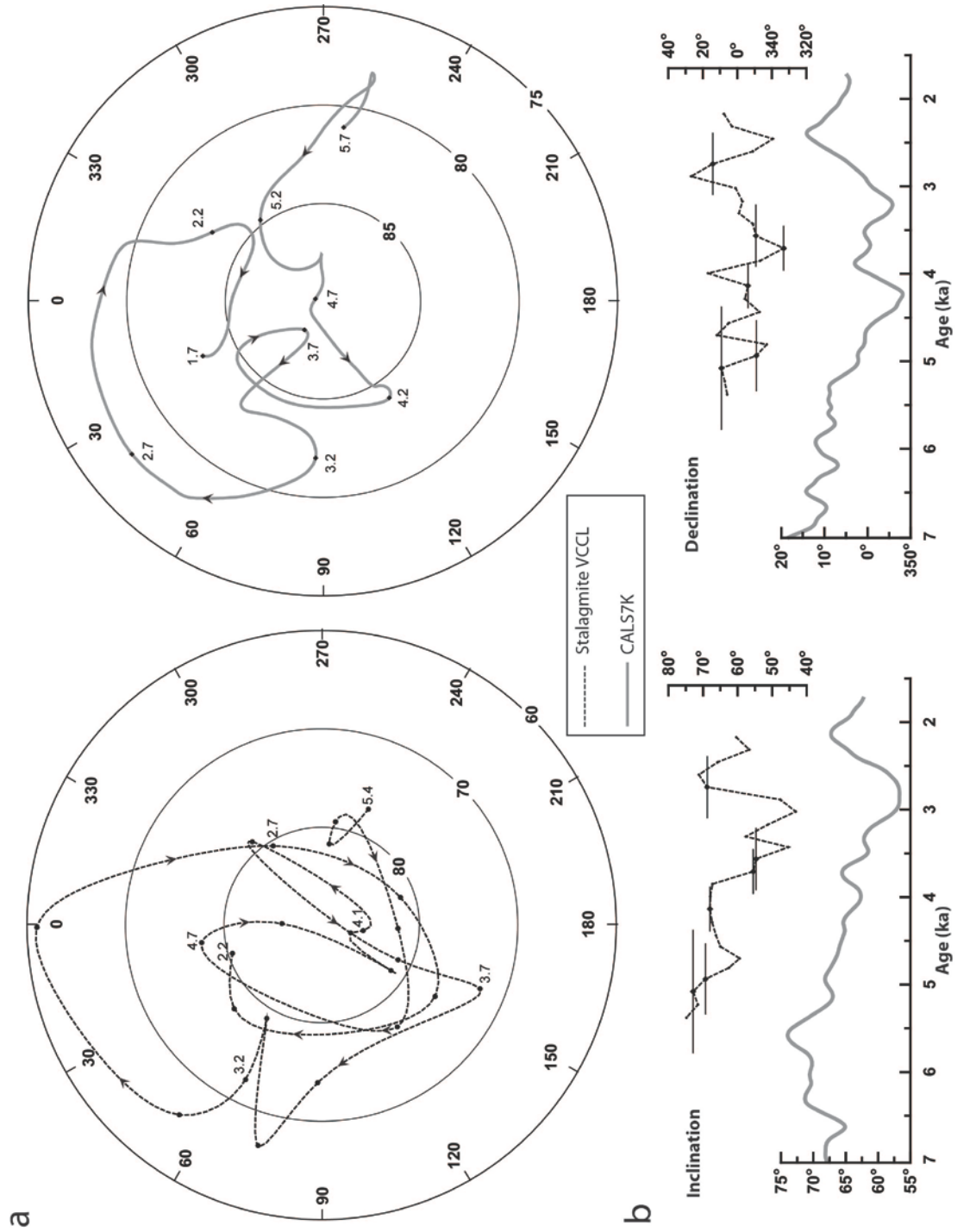

Figure 5.3 Comparison of polar wander, inclination, and declination from stalagmite VCCL, Canada with the CALS7K model curves for the region.

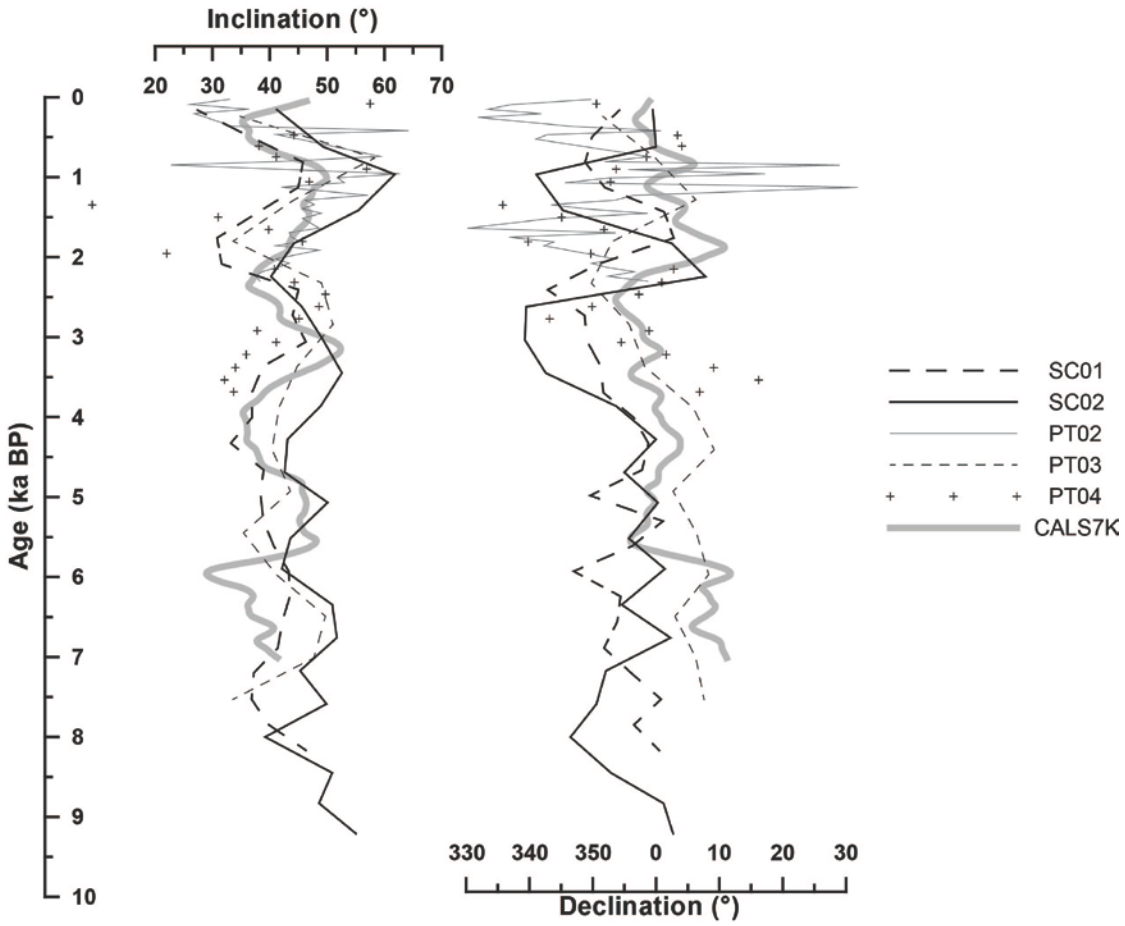

Figure 5.4 Inclination and declination records from the five Chinese stalagmites (SC01, SC02, PT02, PT03, PT04) compared to CALS7K model curves for the region.

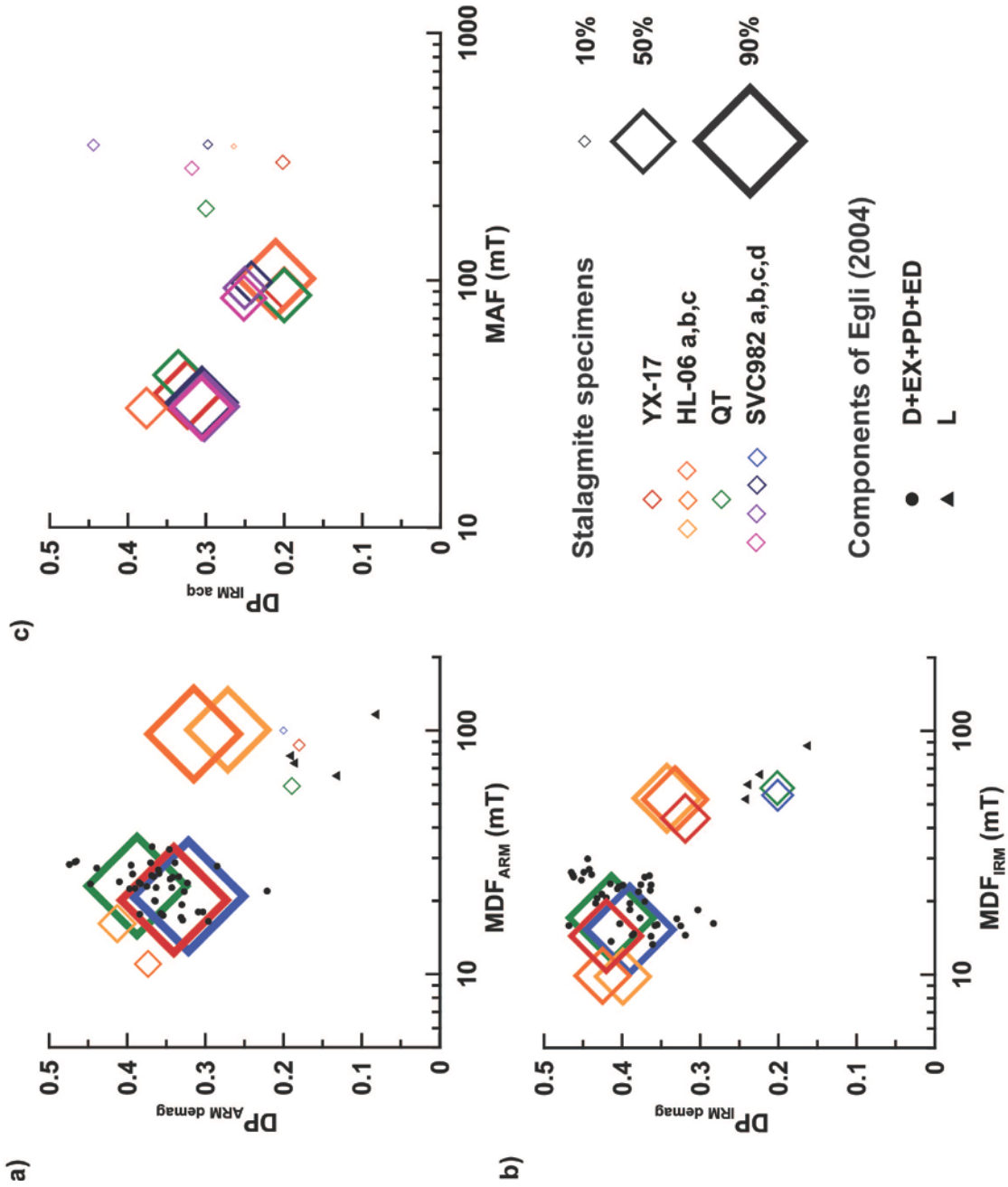

Figure 5.5 Magnetic components of stalagmite specimens.

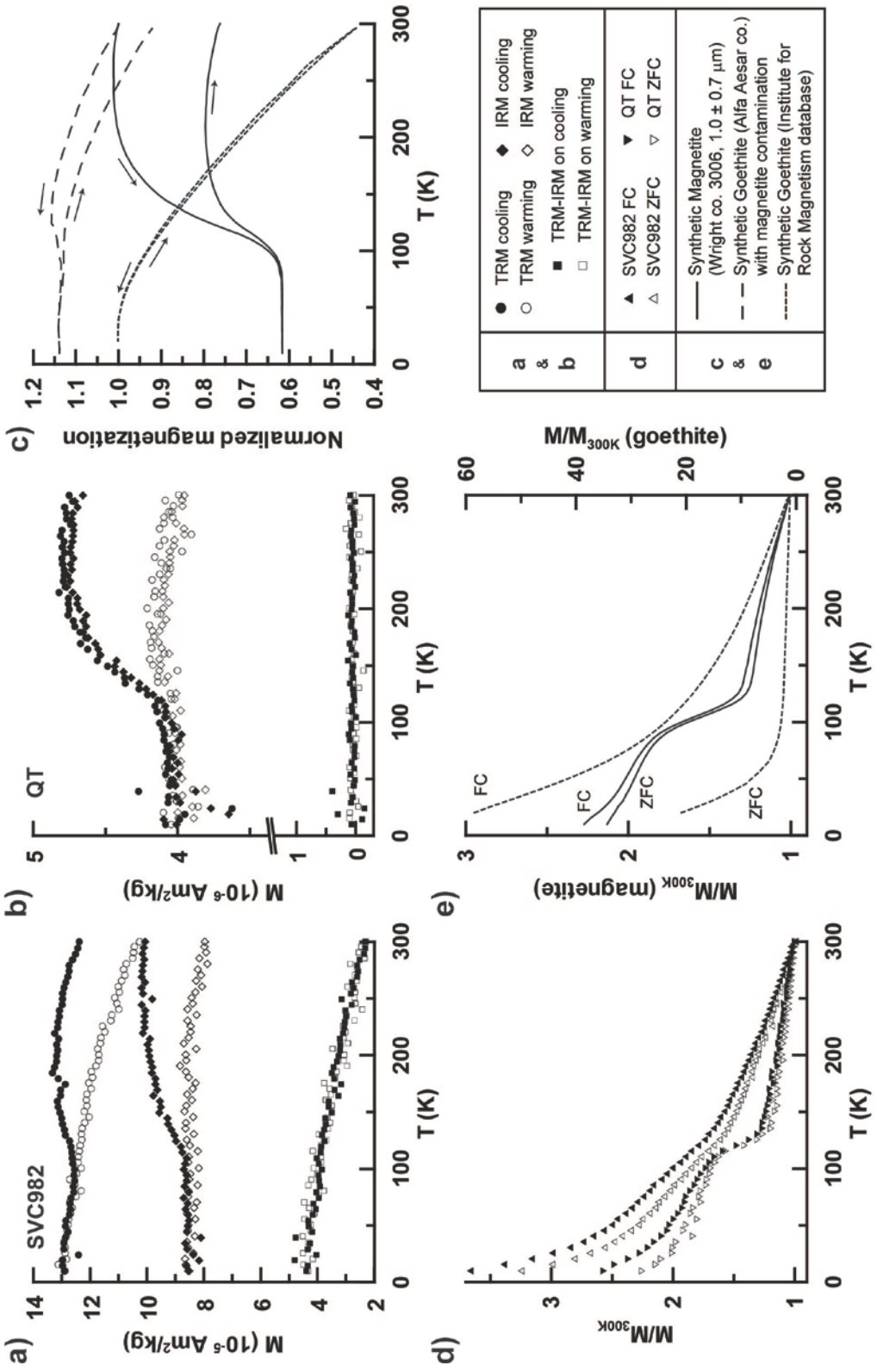

Figure 5.6 Low temperature properties of stalagmite specimens

Comprehensive bibliography

Adams, J.W., Herries, A.I.R., Kuykendall, K.L., Conroy, G.C., 2007. Taphonomy of a South African cave: geological and hydrological influences on the GD 1 fossil assemblage at Gondolin, a Plio-Pleistocene paleocave system in the Northwest Province, South Africa. Quaternary Science Reviews 26, 2526-2543.

Appleby, P.G., 2001. Chronostratigraphic techniques in recent sediments, in Last, W.M., Smol, J.P. (Eds.), Tracking Environmental Change using Lake Sediments, Vol. 1, Basin Analysis, Coring, and Chronological Techniques. Kluwer Academic Publishers, Dordrecht, Netherlands, pp. 171-204.

Benndorf, J., Proft, G., Recknagel, F., 1983. Calcite Precipitation as a Natural Control Mechanism of Eutrophication. Archiv Fur Hydrobiologie 98, 380-408.

Ben-Yosef, E., Tauxe, L., Levy, T.E., Shaar, R., Ron, H., Najjar, M., 2009. Geomagnetic intensity spike recorded in high resolution slag deposit in southern Jordan. Earth and Planetary Science Letters 287, 529-539.

Berger, L.R., Lacruz, R., de Ruiter, D.J., 2002. Revised age estimates of Australopithecus-bearing deposits at Sterkfontein, South Africa. American Journal of Physical Anthropology 119, 192-197.

Blaauw, M., Christen, J.A., 2011. Flexible Paleoclimate Age-Depth Models Using an Autoregressive Gamma Process. Bayesian Analysis 6, 457-474.

Blakemore, R., 1975. Magnetotactic bacteria. Science 190, 377.

Bleil, U., von Dobeneck, T., 2004. Late Quaternary terrigenous sedimentation in the western Equatorial Atlantic; South American versus African provenance discriminated by magnetic mineral analysis, in Wefer, G., Mulitza, S., Ratmeyer, V. (Eds.), The South Atlantic in the Late Quaternary; Reconstruction of Material Budgets and Current Systems. Springer-Verlag, Berlin, Germany, pp. 213-236.

Bohnel, H., Molina-Garza, R., 2002. Secular variation in Mexico during the last 40,000 years. Physics of the Earth and Planetary Interiors 133, 99-109.

Booth, R.K., Notaro, M., Jackson, S.T., Kutzbach, J.E., 2006. Widespread drought episodes in the western Great Lakes region during the past 2000 years: geographic extent and potential mechanisms. Earth and Planetary Science Letters 242, 415-427.

Bosak, P., Hercman, H., Mihevc, A., Pruner, P., 2002. High-resolution magnetostratigraphy of speleothems from Snezna Jama, Kamnik-Savinja Alps, Slovenia. Acta Carsologica 31, 15-32.

Bosch, R.F., White, W.B., 2004. Lithofacies and transport of clastic sediments in karstic aquifers, in Sasowsky, I., Mylroie, J. (Eds.), Studies of Cave Sediments: Physical and Chemical Records of Paleoclimate. Springer, Dordrecht, Netherlands, pp. 1-12.

Bradbury, J.P., Dean, W.E., 1993. Elk Lake, Minnesota: evidence for rapid climate change in the north-central United States. Geological Society of America Special Paper 276, 336 pp.

Bradbury, J.P., Dieterich-Rurup, K.V., 1993. Holocene diatom paleolimnology of Elk Lake, Minnesota, in Bradbury, J.P., Dean, W.E. (Eds.), Elk Lake, Minnesota: Evidence for Rapid Climate Change in the North-Central United States. Geological Society of America Special Paper 276, pp. 215-237.

Briggs, J.M., Knapp, A.K., 1995. Interannual variability in primary production in tallgrass prairie: climate, soil moisture, topographic position, and fire as determinants of aboveground biomass. American Journal of Botany 82, 1024-1030.

Brook, G.A., Ellwood, B.B., Railsback, L.B., Cowart, J.B., 2006. A 164 ka record of environmental change in the American Southwest from a Carlsbad Cavern speleothem. Palaeogeography, Palaeoclimatology, Palaeoecology 237, 483-507.

Bryson, R.A., Wendland, W.M., 1967. Tentative climatic patterns for some late glacial and post-glacial episodes in central North America. Life, land, and water: Proceedings of the 1966 conference on environmental studies of the Glacial Lake Agassiz region , 271-298.

Bull, P.A., 1981. Some Fine-Grained Sedimentation Phenomena in Caves. Earth Surface Processes and Landforms 6, 11-22.

Burleson, D.J., Penn, R.L., 2006. Two-step growth of goethite from ferrihydrite. Langmuir 22, 402-409.

Carter-Stiglitz, B., Moskowitz, B., Jackson, M., 2001. Unmixing magnetic assemblages and the magnetic behavior of bimodal mixtures. Journal of Geophysical Research 106, 26,397-26,411.

Chang, L., Roberts, A.P., Tang, Y., Rainford, B.D., Muxworthy, A.R., Chen, Q.W., 2008. Fundamental magnetic parameters from pure synthetic greigite (Fe_3S_4). Journal of Geophysical Research 113, B06104.

Clark, J.S., 1993. Fire, climate change, and forest processes during the past 2000 years, in Bradbury, J.P., Dean, W.E. (Eds.), Elk Lake, Minnesota: Evidence for Rapid Climate Change in the North-Central United States. Geological Society of America Special Paper 276, pp. 295-308.

Clark, J.S., 1990. Fire and climate change during the last 750 yr in northwestern Minnesota. Ecological Monographs 60, 133-159.

Clark, J.S., 1988. Effect of climate change on fire regimes in northwestern Minnesota. Nature 334, 233-235.

Cook, E.R., Woodhouse, C.A., Eakin, C.M., Meko, D.M., Stahle, D.W., 2004. Long-term aridity changes in the western United States. Science 306, 1015-1018.

Cook, E.R., Seager, R., Cane, M.A., Stahle, D.W., 2007. North American drought: reconstructions, causes, and consequences. Earth-Science Reviews 81, 93-134.

Cyr, H., 1998. Effects of wave disturbance and substrate slope on sediment characteristics in the littoral zone of small lakes. Canadian Journal of Fisheries and Aquatic Sciences 55, 967-976.

Dasgupta, S., Saar, M.O., Edwards, R.L., Shen, C., Cheng, H., Alexander, E.C., 2010. Three thousand years of extreme rainfall events recorded in stalagmites from Spring Valley Caverns, Minnesota. Earth and Planetary Science Letters 300, 46-54.

Davis, M.B., Ford, M.S., 1982. Sediment focusing in Mirror Lake, New Hampshire. Limnology and Oceanography 27, 137-150.

Dean, W.E., Gorham, E., 1976. Major chemical and mineral components of profundal surface sediments in Minnesota lakes. Limnology and Oceanography 21, 259-284.

Dean, W.E., 2002. A 1500-year record of climatic and environmental change in Elk Lake, Clearwater County, Minnesota: II, Geochemistry, mineralogy, and stable isotopes. Journal of Paleolimnology 27, 301-319.

Dean, W.E., 1997. Rates, timing, and cyclicity of Holocene eolian activity in north-central United States: evidence from varved lake sediments. Geology 25, 331-334.

Dean, W.E.,Jr, 1974. Determination of carbonate and organic matter in calcareous sediments and sedimentary rocks by loss on ignition: comparison with other methods. Journal of Sedimentary Petrology 44, 242-248.

Dean, W.E., Gorham, E., Swaine, D.J., 1993. Geochemistry of surface sediments of Minnesota lakes, in Bradbury, J.P., Dean, W.E. (Eds.), Elk Lake, Minnesota: Evidence for Rapid Climate Change in the North-Central United States. Geological Society of America Special Paper 276, pp. 115-133.

Dearing, J.A., 1999. Holocene environmental change from magnetic proxies in lake sediments, in Maher, B.A., Thompson, R. (Eds.), Quaternary Climates, Environments and Magnetism. Cambridge University Press, Cambridge, United Kingdom (GBR), United Kingdom (GBR), pp. 231-278.

Dearing, J.A., 1999. Magnetic susceptibility, in Walden, J., Oldfield, F., Smith, J.P. (Eds.), Environmental Magnetism: A Practical Guide. Quaternary Research Association, London, pp. 35-53.

Dearing, J.A., 1997. Sedimentary indicators of lake-level changes in the humid temperate zone: a critical review. Journal of Paleolimnology 18, 1-14.

Dearing, J.A., Boyle, J.F., Appleby, P.G., Mackay, A.W., Flower, R.J., 1998. Magnetic properties of recent sediments in Lake Baikal, Siberia; Lake Baikal paleolimnology. Journal of Paleolimnology 20, 163-173.

Dekkers, M.J., 1989. Magnetic Properties of Natural Goethite-II. TRM Behaviour During Thermal and Alternating Field Demagnetization and Low-Temperature Treatment. Geophysical Journal International 97, 341-355.

Demory, F., Oberhaensli, H., Nowaczyk, N.R., Gottschalk, M., Wirth, R., Naumann, R., 2005. Detrital input and early diagenesis in sediments from Lake Baikal revealed by rock magnetism; Progress towards reconstructing past climate in central Eurasia, with special emphasis on Lake Baikal. Global Planet. Change 46, 145-166.

Dickson, J.A.D., 1993. Crystal growth diagrams as an aid to interpreting the fabrics of calcite aggregates. Journal of Sedimentary Petrology 63, 1-17.

Digerfeldt, G., 1986. Studies on past lake-level fluctuations, in Berglund, B.E. (Ed.), Handbook of Holocene Palaeoecology and Palaeohydrology. John Wiley & Sons, Chichester, United Kingdom, pp. 127-144.

Dirks, P.H.G.M., Kibii, J.M., Kuhn, B.F., Steininger, C., Churchill, S.E., Kramers, J.D., Pickering, R., Farber, D.L., Meriaux, A., Herries, A.I.R., King, G.C.P., Berger, L.R., 2010. Geological setting and age of Australopithecus sediba from Southern Africa. Science 328, 205-208.

Dorale, J.A., Edwards, R.L., Alexander, E.C., Shen, C., Richards, D.A., Cheng, H., 2004. Uranium-series dating of speleothems: current techniques, limits, & applications, in Sasowsky, I., Mylroie, J. (Eds.), Studies of Cave Sediments: Physical and Chemical Records of Paleoclimate. Springer, Dordrecht, Netherlands, pp. 177-197.

Dunlop, D.J., 2002. Theory and application of the Day plot (M_{rs}/M_s versus H_{cr}/H_c): 1. Theoretical curves and tests using titanomagnetite data. Journal of Geophysical Research 107, doi:10.1029/2001JB000486.

Dunlop, D.J., Carter-Stiglitz, B., 2006. Day plots of mixtures of superparamagnetic, single-domain, pseudosingle-domain, and multidomain magnetites; Rock magnetism; fundamentals and frontiers. Journal of Geophysical Research 111.

Dunlop, D.J., Özdemir, Ö., 1997. Rock Magnetism: Fundamentals and Frontiers. Cambridge University Press, Cambridge, United Kingdom.

Eakins, J.D., Morrison, R.T., 1978. New Procedure for Determination of Pb-210 in Lake and Marine Sediments. International Journal of Applied Radiation and Isotopes 29, 531-536.

Edwards, R.L., Gallup, C.D., Cheng, H., 2003. Uranium-series dating of marine and lacustrine carbonates, in Bourdon, B., Henderson, G.M., Lundstrom, C.C., Turner, S.P. (Eds.), Reviews in Mineralogy and Geochemistry: Uranium-Series Geochemistry. Mineralogical Society of America, Washington, DC, United States of America, pp. 363-405.

Egli, R., Chen, A.P., Winklhofer, M., Kodama, K.P., Horng, C.S., 2010. Detection of noninteracting single domain particles using first-order reversal curve diagrams. Geochemistry, Geophysics, Geosystems 11, doi: 10.1029/2009GC002916.

Egli, R., 2004. Characterization of individual rock magnetic components by analysis of remanence curves: 1. Unmixing natural sediments. Studia Geophysica et Geodetica 48, 391-446.

Egli, R., 2003. Analysis of the field dependence of remanent magnetization curves. Journal of Geophysical Research 108, 10.1029/2002JB002023.

Egli, R., Lowrie, W., 2002. Anhysteretic remanent magnetization of fine magnetic particles. Journal of Geophysical Research 107, doi: 10.1029/2001JB000671.

Egli, R., 2006. Theoretical aspects of dipolar interactions and their appearance in first-order reversal curves of thermally activated single-domain particles. Journal of Geophysical Research 111, 10.1029/2006JB004567.

Egli, R., 2006. Theoretical considerations on the anhysteretic remanent magnetization of interacting particles with uniaxial anisotropy. Journal of Geophysical Research 111, doi: 10.1029/2006JB004577.

Ellwood, B.B., Balsam, W.L., Roberts, H.H., 2006. Gulf of Mexico sediment sources and sediment transport trends from magnetic susceptibility measurements of surface samples. Marine Geology 230, 237-248.

Elmore, R.D., Engel, M.H., Crawford, L., Nick, K., Imbus, S., Sofer, Z., 1987. Evidence for a relationship between hydrocarbons and authigenic magnetite. Nature 325, 428-430.

Evans, M.E., Heller, F., 2003. Environmental Magnetism: Principles and Applications of Enviromagnetics. Academic Press, San Diego United States.

Fairchild, I.J., Frisia, S., Borsato, A., Tooth, A.F., 2007. Speleothems, in Nash, D.J., McLaren, S.J. (Eds.), Geochemical Sediments and Landscapes. Blackwell, Oxford, United Kingdom, pp. 200-245.

Fairchild, I.J., Smith, C.L., Baker, A., Fuller, L., Spoetl, C., Mattey, D., McDermott, F., 2006. Modification and preservation of environmental signals in speleothems. Earth-Science Reviews 75, 105-153.

Ford, D., Williams, P., 2007. Karst Hydrogeology and Geomorphology. John Wiley & Sons, Chichester, United Kingdom.

Frank, U., Nowaczyk, N.R., 2008. Mineral magnetic properties of artificial samples systematically mixed from haematite and magnetite. Geophysical Journal International 175, 449-461.

Frederichs, T., Bleil, U., Daeumler, K., von Dobeneck, T., Schmidt, A.M., 1999. The magnetic view on the marine paleoenvironment; parameters, techniques and potentials of rock magnetic studies as a key to paleoclimatic and paleoceanographic changes, in Fischer, G., Wefer, G. (Eds.), Use of Proxies in Paleoceanography; Examples from the South Atlantic. Springer, Berlin, Germany, pp. 575-599.

Funk, J.A., von Dobeneck, T., Wagner, T., Kasten, S., 2004. Late Quaternary sedimentation and early diagenesis in the Equatorial Atlantic Ocean; patterns, trends and processes deduced from rock magnetic and geochemical records, in Wefer, G., Mulitza, S., Ratmeyer, V. (Eds.), The South Atlantic in the Late Quaternary; Reconstruction of Material Budgets and Current Systems. Springer-Verlag, Berlin, Germany, pp. 461-497.

Gallet, Y., Genevey, A., Courtillot, V., 2003. On the possible occurrence of "archaeomagnetic jerks" in the geomagnetic field over the past three millennia. Earth and Planetary Science Letters 214, 237-242.

Gallet, Y., Hulot, G., Chulliat, A., Genevey, A., 2009. Geomagnetic field hemispheric asymmetry and archeomagnetic jerks. Earth and Planetary Science Letters 284, 179-186.

Garcin, Y., Williamson, D., Taieb, M., Vincens, A., Mathe, P., Majule, A., 2006. Centennial to millennial changes in maar-lake deposition during the last 45,000 years in tropical Southern Africa. Palaeogeography, Palaeoclimatology, Palaeoecology 239, 334-354.

Gattacceca, J., Boustie, M., Weiss, B.P., Rochette, P., Lima, E.A., Fong, L.E., Baudenbacher, F.J., 2006. Investigating impact demagnetization through laser impacts and SQUID microscopy. Geology 34, 333-336.

Geiss, C.E., Banerjee, S.K., 1999. Comparison of two interglacial records from the midwestern U.S.A; Rock magnetism, palaeomagnetism and environmental magnetism. Physics and Chemistry of the Earth.Part A: Solid Earth and Geodesy 24, 793-798.

Geiss, C.E., Zanner, C.W., Banerjee, S.K., Joanna, M., 2004. Signature of magnetic enhancement in a loessic soil in Nebraska, United States of America. Earth and Planetary Science Letters 228, 355-367.

Geiss, C.E., Banerjee, S.K., 1997. A multi-parameter rock magnetic record of the last glacial-interglacial paleoclimate from south-central Illinois, USA. Earth Planet. Sci. Lett. 152, 203-216.

Geiss, C.E., Banerjee, S.K., Camill, P., Umbanhowar, C.E., 2004. Sediment-magnetic signature of land-use and drought as recorded in lake sediment from south-central Minnesota, USA. Quaternary Research 62, 117-125.

Geiss, C.E., Egli, R., Zanner, C.W., 2008. Direct estimates of pedogenic magnetite as a tool to reconstruct past climates from buried soils. Journal of Geophysical Research 113, B11102.

Geiss, C.E., Umbanhowar, C.E., Camill, P., Banerjee, S.K., 2003. Sediment magnetic properties reveal Holocene climate change along the Minnesota prairie-forest ecotone; Lake basins as archives of continental tectonics and paleoclimate. J. Paleolimnol. 30, 151-166.

Geiss, C.E., Zanner, C.W., 2006. How abundant is pedogenic magnetite? Abundance and grain size estimates for loessic soils based on rock magnetic analyses; Rock magnetism; fundamentals and frontiers. Journal of Geophysical Research 111.

Gibbs-Eggar, Z., Jude, B., Dominik, J., Loizeau, J., Oldfield, F., 1999. Possible evidence for dissimilatory bacterial magnetite dominating the magnetic properties of Recent lake sediments. Earth Planet. Sci. Lett. 168, 1-6.

Grimm, E.C., 1983. Chronology and Dynamics of Vegetation Change in the Prairie-Woodland Region of Southern Minnesota, USA. New Phytologist 93, 311-350.

Grimm, E.C., 1981. An ecological and paleoecological study of the vegetation in the Big Woods region of Minnesota. PhD Dissertation, University of Minnesota, Minneapolis, USA.

Gu, B., Chapman, A.D., Schelske, C.L., 2006. Factors controlling seasonal variations in stable isotope composition of particulate organic matter in a soft water eutrophic lake. Limnology and Oceanography 51, 2837-2848.

Guyodo, Y., Mostrom, A., Penn, R.L., Banerjee, S.K., 2003. From Nanodots to Nanorods: Oriented aggregation and magnetic evolution of nanocrystalline goethite. Geophysical Research Letters 30, 10.1029/2003GL017021.

Guyodo, Y., LaPara, T.M., Anschutz, A.J., Penn, R.L., Banerjee, S.K., Geiss, C.E., Zanner, W., 2006. Rock magnetic, chemical and bacterial community analysis of a modern soil from Nebraska. Earth and Planetary Science Letters 251, 168-178.

Hakanson, L., 1977. The influence of wind, fetch, and water depth on the distribution of sediments in Lake Vanern, Sweden. Canadian Journal of Earth Sciences 14, 397-412.

Haltia-Hovi, E., Nowaczyk, N., Saarinen, T., Plessen, B., 2010. Magnetic properties and environmental changes recorded in Lake Lehmilampi (Finland) during the Holocene. Journal of Paleolimnology 43, 1-13.

Hanzlik, M., Petersen, N., Keller, R., Schmidbauer, E., 1996. Electron microscopy and 57Fe Moessbauer spectra of 10-nm particles, intermediate in composition between Fe_3O_4 and γ-Fe_2O_3, produced by bacteria. Geophysical Research Letters 23, 479-482.

Hanzlik, M., Winklhofer, M., Petersen, N., 1996. Spatial arrangement of chains of magnetosomes in magnetotactic bacteria. Earth and Planetary Science Letters 145, 125-134.

Hatfield, R.G., Maher, B.A., 2009. Fingerprinting upland sediment sources; particle size-specific magnetic linkages between soils, lake sediments and suspended sediments. Earth Surface Processes and Landforms 34, 1359-1373.

Heiri, O., Lotter, A.F., Lemcke, G., 2001. Loss on ignition as a method for estimating organic and carbonate content in sediments; reproducibility and comparability of results. Journal of Paleolimnology 25, 101-110.

Herries, A.I.R., Adams, J.W., Kuykendall, K.L., Shaw, J., 2006. Speleology and magnetobiostratigraphic chronology of the GD2 locality of the Gondolin hominin-bearing paleocave deposits, North West Province, South Africa. Journal of Human Evolution 51, 617-631.

Herries, A.I.R., Reed, K.E., Kuykendall, K.L., Latham, A.G., 2006. Speleology and magnetobiostratigraphic chronology of the Buffalo Cave fossil site, Makapansgat, South Africa. Quaternary Research 66, 233-245.

Herries, A.I.R., Shaw, J., 2011. Palaeomagnetic analysis of the Sterkfontein palaeocave deposits: Implications for the age of the hominin fossils and stone tool industries. Journal of Human Evolution 60, 523-539.

Heslop, D., Dekkers, M.J., Kruiver, P.P., van Oorschot, I.H.M., 2002. Analysis of isothermal remanent magnetization acquisition curves using the expectation-maximization algorithm. Geophysical Journal International 148, 58-64.

Hollander, D.J., Smith, M.A., 2001. Microbially mediated carbon cycling as a control on the d13C of sedimentary carbon in eutrophic Lake Mendota (USA): New models for interpreting isotopic excursions in the sedimentary record. Geochimica et Cosmochimica Acta 65, 4321-4337.

Huber, N., 1958. The environmental control of sedimentary iron minerals. Economic Geology 53, 123-140.

Hunt, C.P., Moskowitz, B.M., Banerjee, S.K., 1995. Magnetic properties of rocks and minerals, in Ahrens, T.J. (Ed.), Rock Physics and Phase Relations: A Handbook of Physical Constants. American Geophysical Union, Washington DC, pp. 189-204.

Hunt, C.P., Banerjee, S.K., Han, J., Solheid, P.A., Oches, E., Sun, W., Liu, T., 1995. Rock-magnetic proxies of climate change in the loess-Palaeosol sequences of the western Loess Plateau of China. Geophysical Journal International 123, 232-244.

Hutchinson, G.E., 1957. A Treatise on Limnology, Volume 1. Geography, Physics and Chemistry. Wiley, New York, New York, United States of America.

Jackson, A., Jonkers, A.R.T., Walker, M.R., 2000. Four centuries of geomagnetic secular variation from historical records: Geomagnetic polarity reversals and long-term secular variation. Phil. Trans. R. Soc. Lond. A 358, 957-990.

Jackson, M., Bowles, J.A., Lascu, I., Solheid, P., 2010. Deconvolution of u channel magnetometer data: Experimental study of accuracy, resolution, and stability of different inversion methods. Geochemistry Geophysics Geosystems 11, doi:10.1029/2009GC002991.

Jacobson, G.L., 1979. Paleoecology of White Pine (Pinus strobus) in Minnesota. Journal of Ecology 67, 697-726.

Jones, B., 2010. Microbes in caves: agents of calcite corrosion and precipitation, in Pedley, H.M., Rogerson, M. (Eds.), Tufas and Speleothems: Unravelling the Microbial and Physical Controls. Geological Society of London, London, Special Publication 336, pp. 7-30.

Kendall, A.C., Broughton, P.L., 1978. Origin of fabrics in speleothems composed of columnar calcite crystals. Journal of Sedimentary Petrology 48, 519-538.

Kilham, P., Kilham, S.S., Hecky, R.E., 1986. Hypothesized Resource Relationships among African Planktonic Diatoms. Limnology and Oceanography 31, 1169-1181.

Kim, B., Kodama, K.P., Moeller, R.E., 2005. Bacterial magnetite produced in water column dominates lake sediment mineral magnetism: Lake Ely, USA. Geophys. J. Int. 163, 26-37.

Kopp, R.E., Nash, C.Z., Kobayashi, A., Weiss, B.P., Bazylinski, D.A., Kirschvink, J.L., 2006. Ferromagnetic resonance spectroscopy for assessment of magnetic anisotropy and magnetostatic interactions: a case study of mutant magnetotactic bacteria. Journal of Geophysical Research 111.

Korte, M., Constable, C.G., 2005. Continuous geomagnetic field models for the past 7 millennia: 2. CALS7K. Geochemistry, Geophysics, Geosystems 6, doi:10.1029/2004GC000801.

Korte, M., Constable, C., 2011. Improving geomagnetic field reconstructions for 0-3 ka. Physics of the Earth and Planetary Interiors, doi:10.1016/j.pepi.2011.06.017.

Koschel, R., Benndorf, J., Proft, G., Recknagel, F., 1983. Calcite precipitation as a natural control mechanism of eutrophication. Archive fur Hydrobiologie 98, 380-408.

Kruiver, P.P., Dekkers, M.J., Heslop, D., 2001. Quantification of magnetic coercivity components by the analysis of acquisition curves of isothermal remanent magnetisation. Earth and Planetary Science Letters 189, 269-276.

Lachniet, M.S., 2009. Climatic and environmental controls on speleothem oxygen-isotope values. Quaternary Science Reviews 28, 412-432.

Lacruz, R.S., Brink, J.S., Hancox, P.J., Skinner, A.R., Herries, A., Schmid, P., Berger, L.R., 2002. Palaeontology and geological context of middle Pleistocene faunal assemblage from the Gladysvale Cave, South Africa. Palaeontologia Africana 38, 99-114.

Laj, C., Channell, J.E.T., 2007. Geomagnetic Excursions, in Kono, M. (Ed.), Treatise on Geophysics, Vol. 5 Geomagnetism. Elsevier, Amsterdam, pp. 373-416.

Lascu, I., Banerjee, S.K., Berquo, T.S., 2010. Quantifying the concentration of ferrimagnetic particles in sediments using rock magnetic methods. Geochemistry, Geophysics, Geosystems 11, doi: 10.1029/2010GC003182.

Latham, A.G., Ford, D.C., 1993. The paleomagnetism and rock magnetism of cave and karst deposits, in Aissaoui, D. M., McNeill, D. F., Hurley, N. F. (Ed.), SEPM Special Publication 49: Applications of Paleomagnetism to Sedimentary Geology, pp. 149-155.

Latham, A.G., Schwarcz, H.P., Ford, D.C., Pearce, G.W., 1982. The paleomagnetism and U-Th dating of three Canadian speleothems: evidence for the westward drift, 5.4-2.1 ka BP. Canadian Journal of Earth Sciences 19, 1985-1995.

Latham, A.G., Ford, D.C., Schwarcz, H.P., Birchall, T., 1989. Secular Variation from Mexican Stalagmites - their Potential and Problems. Physics of the Earth and Planetary Interiors 56, 34-48.

Latham, A.G., Schwarcz, H.P., Ford, D.C., 1987. Secular Variation of the Earths Magnetic-Field from 18.5 to 15.0 ka BP, as Recorded in a Vancouver-Island Stalagmite. Canadian Journal of Earth Sciences 24, 1235-1241.

Latham, A.G., Schwarcz, H.P., Ford, D.C., 1986. The Paleomagnetism and U-Th Dating of Mexican Stalagmite, Das2. Earth and Planetary Science Letters 79, 195-207.

Latham, A.G., Schwarcz, H.P., Ford, D.C., Pearce, G.W., 1979. Paleomagnetism of Stalagmite Deposits. Nature 280, 383-385.

Lau Lam, Y., Engel, P., 1999. Inception of sediment transport on steep slopes. Journal of Hydraulic Engineering 125, 544-547.

Lauritzen, S., Lovlie, R., Moe, D., Ostbye, E., 1990. Paleoclimate deduced from a multidisciplinary study of a half-million-year-old stalagmite from Rana, Northern Norway. Quaternary Research 34, 306-316.

Lean, C.B., Latham, A.G., Shaw, J., 1995. Palaeosecular variation from a Vancouver Island stalagmite and comparison with contemporary North American records. Journal of Geomagnetism and Geoelectricity 47, 71-87.

Lees, J.A., 1997. Mineral magnetic properties of mixtures of environmental and synthetic materials; linear additivity and interaction effects. Geophysical Journal International 131, 335-346.

Li, Y., Yu, Z., Kodama, K.P., Moeller, R.E., 2006. A 14,000-year environmental change history revealed by mineral magnetic data from White Lake, New Jersey, USA. Earth and Planetary Science Letters 246, 27-40.

Liu, J., Chen, Z., Chen, M., Yan, W., Xiang, R., Tang, X., 2010. Magnetic susceptibility variations and provenance of surface sediments in the South China Sea. Sedimentary Geology 230, 77-85.

Liu, Q., Deng, C., Torrent, J., Zhu, R., 2007. Review of recent developments in mineral magnetism of the Chinese loess. Quaternary Science Reviews 26, 368-385.

Maher, B.A., 2008. Holocene variability of the East Asian summer monsoon from Chinese cave records: a re-assessment. The Holocene 18, 861-866.

Maher, B.A., 1998. Magnetic properties of modern soils and Quaternary loessic Paleosols: paleoclimatic implications. Palaeogeography, Palaeoclimatology, Palaeoecology 137, 25-54.

Martin, K., 1990. Paleomagnetism of speleothems in Gardner Cave, Washington. National Speleological Society Bulletin 52, 87-94.

McDermott, F., 2004. Palaeo-climate reconstruction from stable isotope variations in speleothems: a review. Quaternary Science Reviews 23, 901-918.

Merrill, R.T., McFadden, P.L., 1994. Geomagnetic field stability: reversal events and excursions. Earth and Planetary Science Letters 121, 57-69.

Moeller, R.E., Wetzel, R.G., 1988. Littoral vs. profundal components of sediment accumulation: contrasting roles as phosphorous sinks. Verh. Internat. Verein. Limnol. 23, 386-393.

Morinaga, H., Horie, I., Yaskawa, K., 1992. A geomagnetic reversal recorded in a stalagmite collected in western Japan. Journal of Geomagnetism and Geoelectricity 44, 661-675.

Morinaga, H., Inokuchi, H., Yaskawa, K., 1989. Palaeomagnetism of stalagmites (speleothems) in SW Japan. Geophysical Journal 96, 519-528.

Morinaga, H., Inokuchi, H., Yaskawa, K., 1986. Magnetization of a stalagmite in Akiyoshi Plateau as a record of the geomagnetic secular variation in West Japan. Journal of Geomagnetism and Geoelectricity 38, 27-44.

Moskowitz, B.M., Bazylinski, D.A., Egli, R., Frankel, R.B., Edwards, K.J., 2008. Magnetic properties of marine magnetotactic bacteria in a seasonally stratified coastal pond (Salt Pond, MA, USA). Geophysical Journal International 174, 75-92.

Moskowitz, B.M., Frankel, R.B., Bazylinski, D.A., 1993. Rock magnetic criteria for the detection of biogenic magnetite. Earth and Planetary Science Letters 120, 283-300.

Muxworthy, A.R., Dunlop, D.J., Özdemir, Ö., 2003. Low-temperature cycling of isothermal and anhysteretic remanence; microcoercivity and magnetic memory. Earth and Planetary Science Letters 205, 173-184.

Myrbo, A., Shapley, M.D., 2006. Seasonal water-column dynamics of dissolved inorganic carbon stable isotopic compositions ($\delta^{13}C_{DIC}$) in small hardwater lakes in Minnesota and Montana. Geochimica et Cosmochimica Acta 70, 2699-2714.

Neel, L., 1949. Theorie du trainage magnetique des ferromagnetiques en grains fins avec applications aux terres cuites. Ann. Geophys. 5, 99-136.

Nilsson, A., Snowball, I., Muscheler, R., Uvo, C.B., 2010. Holocene geocentric dipole tilt model constrained by sedimentary paleomagnetic data. Geochemistry Geophysics Geosystems 11, doi:10.1029/2010GC003118.

Nowaczyk, N.R., 2001. Logging of magnetic susceptibility, in Last, W.M., Smol, J.P. (Eds.), Tracking Environmental Change using Lake Sediments; Volume 1,

Basin Analysis, Coring, and Chronological Techniques. Kluwer Academic Publishers, Dordrecht, Netherlands, pp. 155-170.

Nuhfer, E.B., Anderson, R.Y., Bradbury, J.P., Dean, W.E., 1993. Modern sedimentation in Elk Lake, Clearwater County, Minnesota, in Bradbury, J.P., Dean, W.E. (Eds.), Elk Lake, Minnesota: Evidence for Rapid Climate Change in the North-Central United States. Geological Society of America Special Paper 276, pp. 75-96.

Oda, H., Usui, A., Miyagi, I., Joshima, M., Weiss, B.P., Shantz, C., Fong, L.E., McBride, K.K., Harder, R., Baudenbacher, F.J., 2011. Ultrafine-scale magnetostratigraphy of marine ferromanganese crust. Geology 39, 227-230.

Oldfield, F., Wake, R., Boyle, J., Jones, R., Nolan, S., Gibbs, Z., Appleby, P., Fisher, E., Wolff, G., 2003. The late-Holocene history of Gormire Lake (NE England) and its catchment: a multiproxy reconstruction of past human impact. The Holocene 13, 677-690.

Openshaw, S., Latham, A., Shaw, J., 1997. Speleothem palaeosecular variation records from China; their contribution to the coverage of Holocene palaeosecular variation data in East Asia; Paleosecular variation and intensity. Journal of Geomagnetism and Geoelectricity 49, 485-505.

Ortega, B., Caballero, M., Lozano, S., Vilaclara, G., Rodriguez, A., 2006. Rock magnetic and geochemical proxies for iron mineral diagenesis in a tropical lake: Lago Verde, Los Tuxtlas, east-central Mexico. Earth and Planetary Science Letters 250, 444-458.

Ortega, B., Caballero, M., Lozano, S., Vilaclara, G., Rodriguez, A., 2006. Rock magnetic and geochemical proxies for iron mineral diagenesis in a tropical lake; Lago Verde, Los Tuxtlas, east-central Mexico. Earth Planet. Sci. Lett. 250, 444-458.

Özdemir, Ö., Banerjee, S.K., 1982. A preliminary magnetic study of soil samples from West-central Minnesota. Earth and Planetary Science Letters 59, 393-403.

Özdemir, Ö., Dunlop, D.J., 2010. Hallmarks of maghemitization in low-temperature remanence cycling of partially oxidized magnetite nanoparticles. J. Geophys. Res. 115, B02101.

Özdemir, Ö., Dunlop, D.J., Moskowitz, B.M., 1993. The effect of oxidation on the Verwey transition in magnetite. Geophys. Res. Lett. 20, 1671-1674.

Paasche, O., Lovlie, R., Dahl, S.O., Bakke, J., Nesje, A., 2004. Bacterial magnetite in lake sediments: late glacial to Holocene climate and sedimentary changes in Northern Norway. Earth and Planetary Science Letters 223, 319-333.

Palmer, W.C., 1965. Meteorological Drought. Weather Bureau Research Paper No. 45, U.S. Dept. of Commerce, Washington D.C.

Partridge, T.C., Latham, A.G., Heslop, D., 2000. Appendix on magnetostratigraphy of Makapansgat, Sterkfontein, Taung and Swartkrans, in Partridge, T.C., Maud, R.R. (Eds.), The Cenozoic of Southern Africa. Oxford University Press, Oxford, United Kingdom, pp. 126-129.

Partridge, T.C., Shaw, J., Heslop, D., Clarke, R.J., 1999. The new hominid skeleton from Sterkfontein, South Africa: age and preliminary assessment. Journal of Quaternary Science 14, 293-298.

Peck, J.A., King, J.W., 1996. Magnetofossils in the sediment of Lake Baikal, Siberia. Earth Planet. Sci. Lett. 140, 159-172.

Perkins, A.M., Maher, B.A., 1993. Rock magnetic and palaeomagnetic studies of British speleothems. Journal of Geomagnetism and Geoelectricity 45, 143-153.

Perkins, A.M., 1996. Observations under electron microscopy of magnetic minerals extracted from speleothems. Earth and Planetary Science Letters 139, 281-289.

Perrette, Y., Delannoy, J., Desmet, M., Lignier, V., Destombes, J., 2005. Speleothem organic matter content imaging: the use of a fluorescence index to characterise the maximum emission wavelength. Chemical Geology 214, 193-208.

Pruner, P., Hajna, N.Z., Mihevc, A., Bosak, P., Man, O., Schnabl, P., Venhodova, D., 2010. Magnetostratigraphy and fold tests from Raciska Pecina and Pecina v Borstu Caves (classical karst, Slovenia). Studia Geophysica et Geodaetica 54, 27-48.

Readman, P.W., O'Reilly, W., 1972. Magnetic Properties of Oxidized (Cation-Deficient) Titanomagnetites (Fe, Ti)$_3O_4$. Journal of Geomagnetism and Geoelectricity 24, 69-90.

Readman, P.W., O'Reilly, W., 1971. Oxidation Processes in Titanomagnetites. Z. Geophys. 37, 329-338.

Reimer, P.J., Baillie, M.G.L., Bard, E., Bayliss, A., Beck, J.W., Blackwell, P.G., Ramsey, C.B., Buck, C.E., Burr, G.S., Edwards, R.L., Friedrich, M., Grootes, P.M., Guilderson, T.P., Hajdas, I., Heaton, T.J., Hogg, A.G., Hughen, K.A., Kaiser, K.F., Kromer, B., McCormac, F.G., Manning, S.W., Reimer, R.W., Richards, D.A., Southon, J.R., Talamo, S., Turney, C.S.M., van der Plicht, J., Weyhenmeye, C.E., 2009. Intcal09 and Marine09 Radiocarbon Age Calibration Curves, 0-50,000 Years Cal BP. Radiocarbon 51, 1111-1150.

Reynolds, R.L., Rosenbaum, J.G., Rapp, J., Kerwin, M.W., Bradbury, P.J., Colman, S., Adam, D., 2004. Record of Late Pleistocene Glaciation and Deglaciation in the Southern Cascade Range. I. Petrological Evidence from Lacustrine Sediment in Upper Klamath Lake, Southern Oregon. J. Paleolimnol. 31, 217-233.

Roberts, A.P., Chang, L., Rowan, C.J., Horng, C.S., Florindo, F., 2011. Magnetic properties of sedimentary greigite (Fe_3S_4): An update. Reviews of Geophysics 49, doi:10.1029/2010RG000336.

Roberts, A.P., 2008. Geomagnetic excursions: knowns and unknowns. Geophysical Research Letters 35, doi:10.1029/2008GL034719.

Roberts, A.P., 2006. High-resolution magnetic analysis of sediment cores: strengths, limitations and strategies for maximizing the value of long core magnetic data. Physics of the Earth and Planetary Interiors 156, 162-178.

Roberts, A.P., Pike, C.R., Verosub, K.L., 2000. First-order reversal curve diagrams; a new tool for characterizing the magnetic properties of natural samples. Journal of Geophysical Research 105, 28,461-28,475.

Roberts, A.P., Winklhofer, M., 2004. Why are geomagnetic excursions not always recorded in sediments? Constraints from post-depositional remanent

magnetization lock-in modelling. Earth and Planetary Science Letters 227, 345-359.

Robertson, D.J., France, D.E., 1994. Discrimination of remanence-carrying minerals in mixtures, using isothermal remanent magnetisation acquisition curves. Phys. Earth Planet. Inter. 82, 223-234.

Rosenbaum, J.G., Reynolds, R.L., 2004. Record of Late Pleistocene Glaciation and Deglaciation in the Southern Cascade Range. II. Flux of Glacial Flour in a Sediment Core from Upper Klamath Lake, Oregon. J. Paleolimnol. 31, 235-252.

Rosenbaum, J.G., Reynolds, R.L., 2004. Basis for Paleoenvironmental Interpretation of Magnetic Properties of Sediment from Upper Klamath Lake (Oregon): Effects of Weathering and Mineralogical Sorting. J. Paleolimnol. 31, 253-265.

Rosenbaum, J.G., Reynolds, R.L., Adam, D.P., Drexler, J., Sarna-Wojcicki, A.M., Whitney, G.C., 1996. Record of middle Pleistocene climate change from Buck Lake, Cascade Range, southern Oregon; evidence from sediment magnetism, trace-element geochemistry, and pollen. Geological Society of America Bulletin 108, 1328-1341.

Rusanov, V., Gilson, R.G., Lougear, A., Trautwein, A.X., 2000. Mossbauer, magnetic, X-ray fluorescence and transmission electron microscopy study of natural magnetic materials from speleothems: haematite and the Morin transition. Hyperfine Interactions 128, 353-373.

Shaar, R., Ben-Yosef, E., Ron, H., Tauxe, L., Agnon, A., Kessel, R., 2011. Geomagnetic field intensity: How high can it get? How fast can it change? Constraints from Iron Age copper slag. Earth and Planetary Science Letters 301, 297-306.

Shaar, R., Ron, H., Tauxe, L., Kessel, R., Agnon, A., Ben-Yosef, E., Feinberg, J.M., 2010. Testing the accuracy of absolute intensity estimates of the ancient geomagnetic field using copper slag material. Earth and Planetary Science Letters 290, 201-213.

Shopov, Y.Y., Ford, D.C., Schwarcz, H.P., 1994. Luminescent microbanding in speleothems: high-resolution chronology and paleoclimate. Geology 22, 407-410.

Shuman, B., 2003. Controls on loss-on-ignition variation in cores from two shallow lakes in the northeastern United States. Journal of Paleolimnology 30, 371-385.

Shuman, B., Henderson, A.K., Plank, C., Stefanova, I., Ziegler, S.S., 2009. Woodland-to-forest transition during prolonged drought in Minnesota after ca. AD 1300. Ecology 90, 2792-2807.

Singer, B.S., Guillou, H., Jicha, B.R., Laj, C., Kissel, C., Beard, B.L., Johnson, C.M., 2009. 40Ar/39Ar, K–Ar and 230Th–238U dating of the Laschamp excursion: A radioisotopic tie-point for ice core and climate chronologies. Earth and Planetary Science Letters 286, 80-88.

Smyth, C., Hay, A.E., 2002. Wave friction factors in nearshore sands. Journal of Physical Oceanography 32, 3490-3498.

Snowball, I.F., 1994. Bacterial magnetite and the magnetic properties of sediments in a Swedish lake. Earth Planet. Sci. Lett. 126, 129-142.

Snowball, I., Sandgren, P., Petterson, G., 1999. The mineral magnetic properties of an annually laminated Holocene lake-sediment sequence in northern Sweden. Holocene 9, 353-362.

Snowball, I., Zillen, L., Sandgren, P., 2002. Bacterial magnetite in Swedish varved lake-sediments; a potential bio-marker of environmental change; The value of annually laminated lake sediments in palaeoenvironment reconstruction; dedicated to Bjorn E. Berglund. Quaternary International 88, 13-19.

St. Jacques, J., Cumming, B.F., Smol, J.P., 2008. A 900-year pollen-inferred temperature and effective moisture record from varved Lake Mina, west-central Minnesota, USA. Quaternary Science Reviews 27, 781-796.

Stoner, E.C., Wohlfarth, E.P., 1948. A Mechanism of Magnetic Hysteresis in Heterogeneous Alloys. Phil. Trans. R. Soc. Lond. A 240, 599-642.

Swain, E.B., 1984. The paucity of blue-green algae in meromictic Brownie Lake; iron limitation or heavy metal toxicity? Ph.D. thesis, University of Minnesota, Twin Cities, MN, USA.

Tarduno, J.A., 1995. Superparamagnetism and reduction diagenesis in pelagic sediments; enhancement or depletion? Geophys. Res. Lett. 22, 1337-1340.

Tauxe, L., Kent, D.V., 2004. A simplified statistical model for the geomagnetic field and the detection of shallow bias in paleomagnetic inclinations: was the ancient magnetic field dipolar?, in Channell, J.E.T., Kent, D.V., Lowrie, W., Meert, J.G. (Eds.), Timescales of the Paleomagnetic Field. American Geophysical Union, Washington DC, United States, pp. 101-115.

Teranes, J.L., Bernasconi, S.M., 2005. Factors controlling d13C values of sedimentary carbon in hypertrophic Baldeggersee, Switzerland, and implications for interpreting isotope excursions in lake sedimentary records. Limnology and Oceanography 50, 914-922.

Thackeray, J.F., Kirschvink, J.L., Raub, T.D., 2002. Palaeomagnetic analyses of calcified deposits from the Plio-Pleistocene hominid site of Kromdraai, South Africa. South African Journal of Science 98, 537-540.

Thompson, R., 1986. Modelling magnetization data using SIMPLEX: Mineral magnetic studies. Phys. Earth Planet. Inter. 42, 113-127.

Tian, J., Nelson, D.M., Hu, F.S., 2006. Possible linkages of late-Holocene drought in the North American midcontinent to Pacific Decadal Oscillation and solar activity. Geophysical Research Letters 33, doi: 10.1029/2006GL028169.

Tracey, B., Lee, N., Card, V., 1996. Sediment indicators of meromixis: comparison of laminations, diatoms, and sediment chemistry in Brownie Lake, Minneapolis, USA. Journal of Paleolimnology 15, 129-132.

Trenberth, K.E., Branstator, G.W., Arkin, P.A., 1988. Origins of the 1988 North-American Drought. Science 242, 1640-1645.

Umbanhowar, C.E., 2004. Interaction of fire, climate and vegetation change at a large landscape scale in the Big Woods of Minnesota, USA. The Holocene 14, 661-676.

van der Post, K.D., Oldfield, F., Haworth, E.Y., Crooks, P.R.J., Appleby, P.G., 1997. A record of accelerated erosion in the Recent sediments of Blelham Tarn in the English Lake District. J. Paleolimnol. 18, 103-120.

van Donk, E., van de Bund, W.J., 2002. Impact of submerged macrophytes including charophytes on phyto- and zooplankton communities: allelopathy versus other mechanisms. Aquatic Botany 72, 261-274.

van Donk, E., van de Bund, W.J., 2002. Impact of submerged macrophytes including charophytes on phyto- and zooplankton communities: allelopathy versus other mechanisms. Aquatic Botany 72, 261-274.

Verosub, K.L., 1977. Depositional and postdepositional processes in the magnetization of sediments. Reviews of Geophysics and Space Physics 15, 129-143.

von Dobeneck, T., 1998. The concept of partial susceptibilities. Geol. Carpath. 49, 228-229.

Wagner, G.A., 1998. Age Determination of Young Rocks and Artifacts: Physical and Chemical Clocks in Quaternary Geology and Archaeology. Springer-Verlag, Berlin, Germany.

Wang, Y., Cheng, H., Edwards, R.L., He, Y., Kong, X., An, Z., Wu, J., Kelly, M.J., Dykoski, C.A., Li, X., 2005. The Holocene Asian monsoon: links to solar changes and North Atlantic climate. Science 308, 854-857.

Wang, Y.J., Cheng, H., Edwards, R.L., An, Z.S., Wu, J.Y., Shen, C.C., Dorale, J.A., 2001. A high-resolution absolute-dated late Pleistocene monsoon record from Hulu Cave, China. Science 294, 2345-2348.

Wang, Y., Cheng, H., Edwards, R.L., Kong, X., Shao, X., Chen, S., Wu, J., Jiang, X., Wang, X., An, Z., 2008. Millennial- and orbital-scale changes in the East Asian monsoon over the past 224,000years. Nature 451, 1090-1093.

Weeks, R., Laj, C., Endignoux, L., Fuller, M., Roberts, A., Manganne, R., Blanchard, E., Goree, W., 1993. Improvements in long-core measurement techniques: applications in palaeomagnetism and palaeoceanography. Geophysical Journal International 114, 651-662.

Weiss, B.P., Lima, E.A., Fong, L.E., Baudenbacher, F.J., 2007. Paleomagnetic analysis using SQUID microscopy. Journal of Geophysical Research 112, doi:10.1029/2007JB004940.

Weiss, B.P., Vali, H., Baudenbacher, F.J., Kirschvink, J.L., Stewart, S.T., Shuster, D.L., 2002. Records of an ancient Martian magnetic field in ALH84001. Earth and Planetary Science Letters 201, 449-463.

Wetzel, R.G., 2001. Limnology: Lake and River Ecosystems, 3rd ed. Academic Press, San Diego, California, United States of America.

Wetzel, R.G., Likens, G.E., 1991. Limnological Analyses. Springer-Verlag, New York, New York, United States of America.

White, W.B., 2004. Paleoclimate records from speleothems in limestone caves, in Sasowsky, I.D., Mylroie, J. (Eds.), Studies of Cave Sediments: Physical and Chemical Records of Paleoclimate. Springer, Dordrecht, Netherlands.

White, W.B., 1998. Geomorphology and Hydrology of Karst Terrains. Oxford University Press, Oxford, United Kingdom.

Whitlock, C., Bartlein, P.J., Watts, W.A., 1993. Vegetation history of Elk Lake, in Bradbury, J.P., Dean, W.E. (Eds.), Elk Lake, Minnesota: Evidence for Rapid Climate Change in the North-Central United States. Geological Society of America Special Paper 276, pp. 251-274.

Wilhite, D.A., 2007. Drought, in Stoltman, J.P., Lidstone, J., Dechano, L.M. (Eds.), International Perspectives on Natural Disasters: Occurrence, Mitigation, and Consequences. Springer, Netherlands, pp. 147-162.

Williamson, D., Jackson, M.J., Banerjee, S.K., Marvin, J., Merdaci, O., Thouveny, N., Decobert, M., Gibert-Massault, E., Massault, M., Mazaudier, D., Taieb, M., 1999. Magnetic signatures of hydrological changes in a tropical Maar-Lake (Lake Massoko, Tanzania): preliminary results. Physics and Chemistry of the Earth 24, 799-803.

Wohlfarth, B., Veres, D., Ampel, L., Lacourse, T., Blaauw, M., Preusser, F., Andrieu-Ponel, V., Keravis, D., Lallier-Verges, E., Bjorck, S., Davies, S.M., de Beaulieu, J., Risberg, J., Hormes, A., Kasper, H.U., Possnert, G., Reille, M.,

Thouveny, N., Zander, A., 2008. Rapid ecosystem response to abrupt climate changes during the last glacial period in Western Europe, 40-16 ka. Geology 36, 407-410.

Woodhouse, C.A., Overpeck, J.T., 1998. 2000 years of drought variability in the central United States. Bulletin of the American Meteorological Society 79, 2693-2714.

Worm, H., 1998. On the superparamagnetic-stable single domain transition for magnetite, and frequency dependence of susceptibility. Geophysical Journal International 133, 201-206.

Xie, Q., Chen, T., Xu, H., Chen, J., Ji, J., Lu, H., Wang, X., 2009. Quantification of the contribution of pedogenic magnetic minerals to magnetic susceptibility of loess and paleosols on Chinese Loess Plateau: Paleoclimatic implications. J. Geophys. Res. 114, B09101.

Xie, S., Dearing, J.A., Bloemendal, J., 1999. A partial susceptibility approach to analysing the magnetic properties of environmental materials; a case study. Geophysical Journal International 138, 851-856.

Yamazaki, T., 2008. Magnetostatic interactions in deep-sea sediments inferred from first-order reversal curve diagrams; implications for relative paleointensity normalization. Geochem. Geophys. Geosyst. 9, Q02005.

Yamazaki, T., Kawahata, H., 1998. Organic carbon flux controls the morphology of magnetofossils in marine sediments. Geology 26, 1064-1066.

Yu, Y., Dunlop, D.J., Ozdemir, O., 2002. Partial anhysteretic remanent magnetization in magnetic; 1, Additivity. Journal of Geophysical Research 107.

Zillen, L., Snowball, I., 2009. Complexity of the 8 ka climate event in Sweden recorded by varved lake sediments. Boreas 38, 493-503.

Appendix

Figures

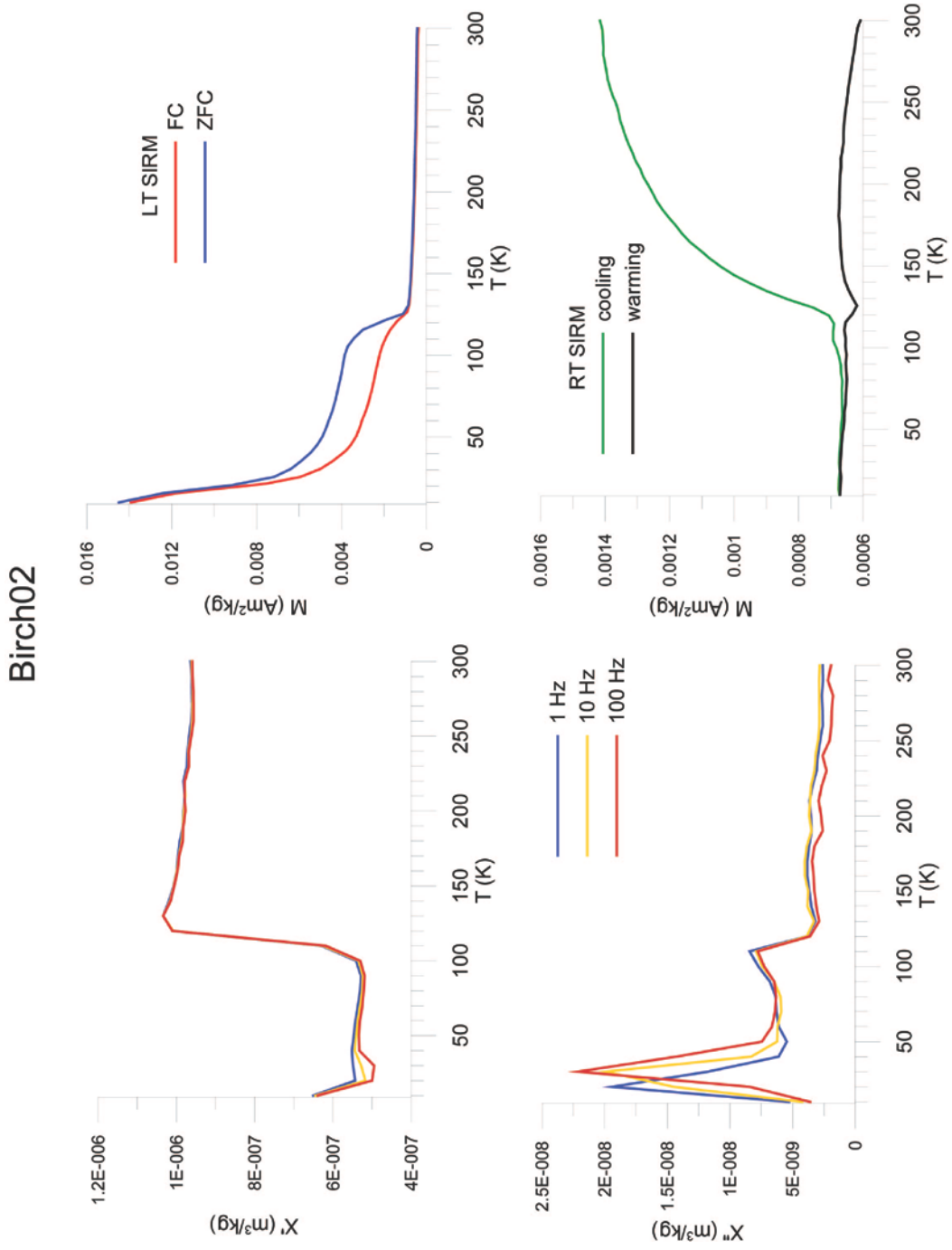

Figure A.1 Low temperature magnetic properties of a shoreline sample from Birch

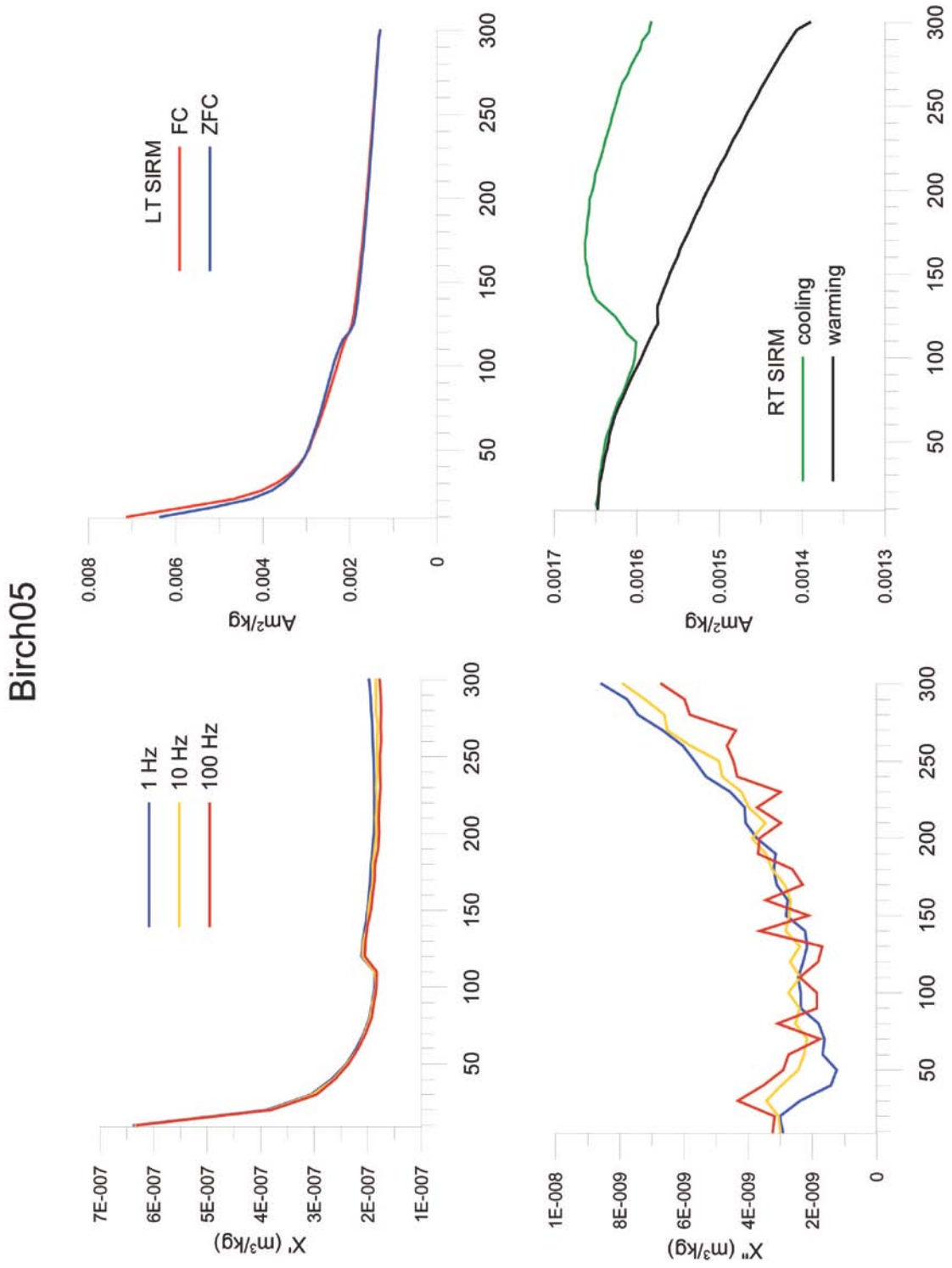

Figure A.2 Low temperature magnetic properties of a littoriprofundal sample from Birch

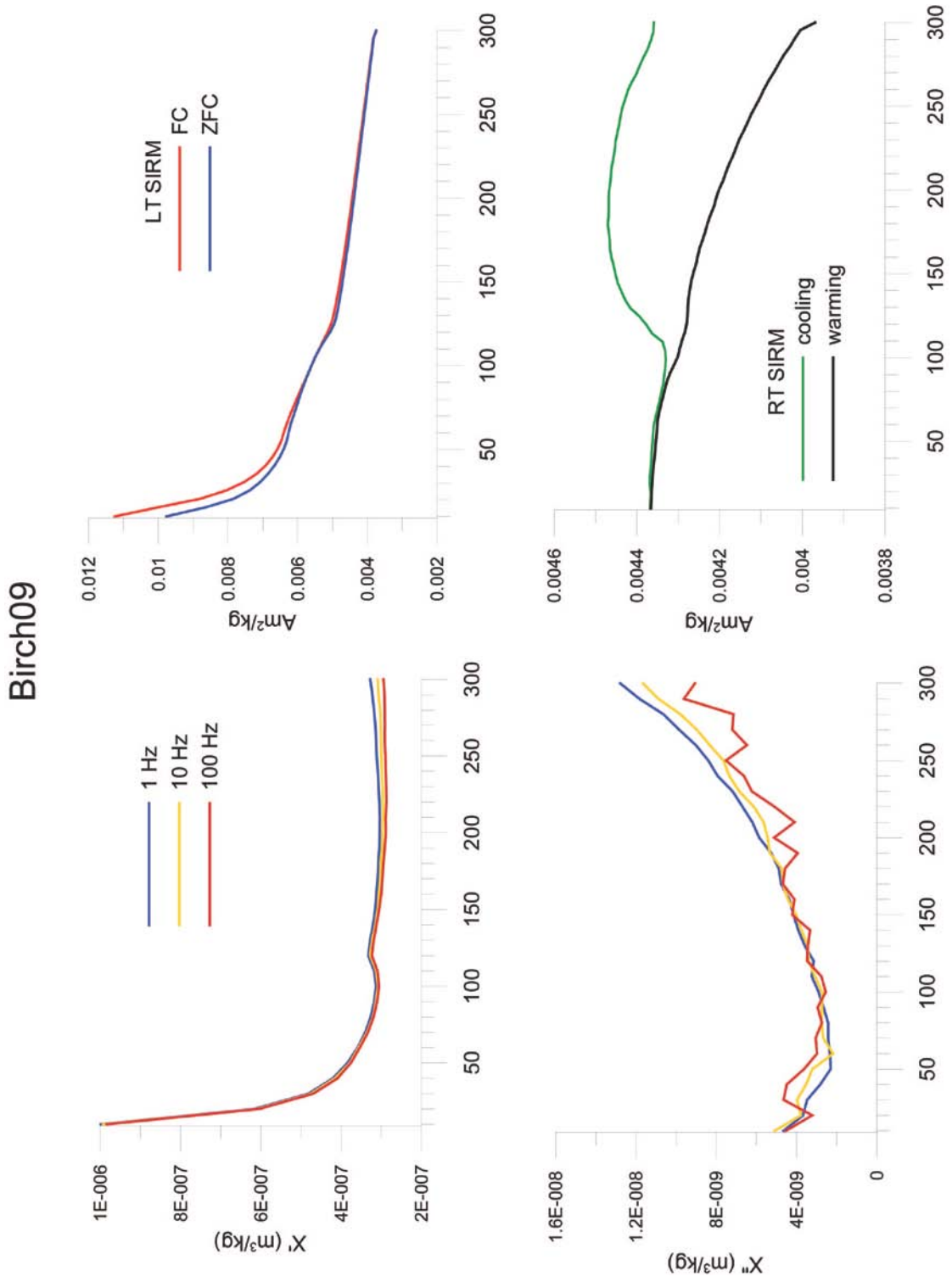

Figure A.3 Low temperature magnetic properties of a profundal sample from Birch

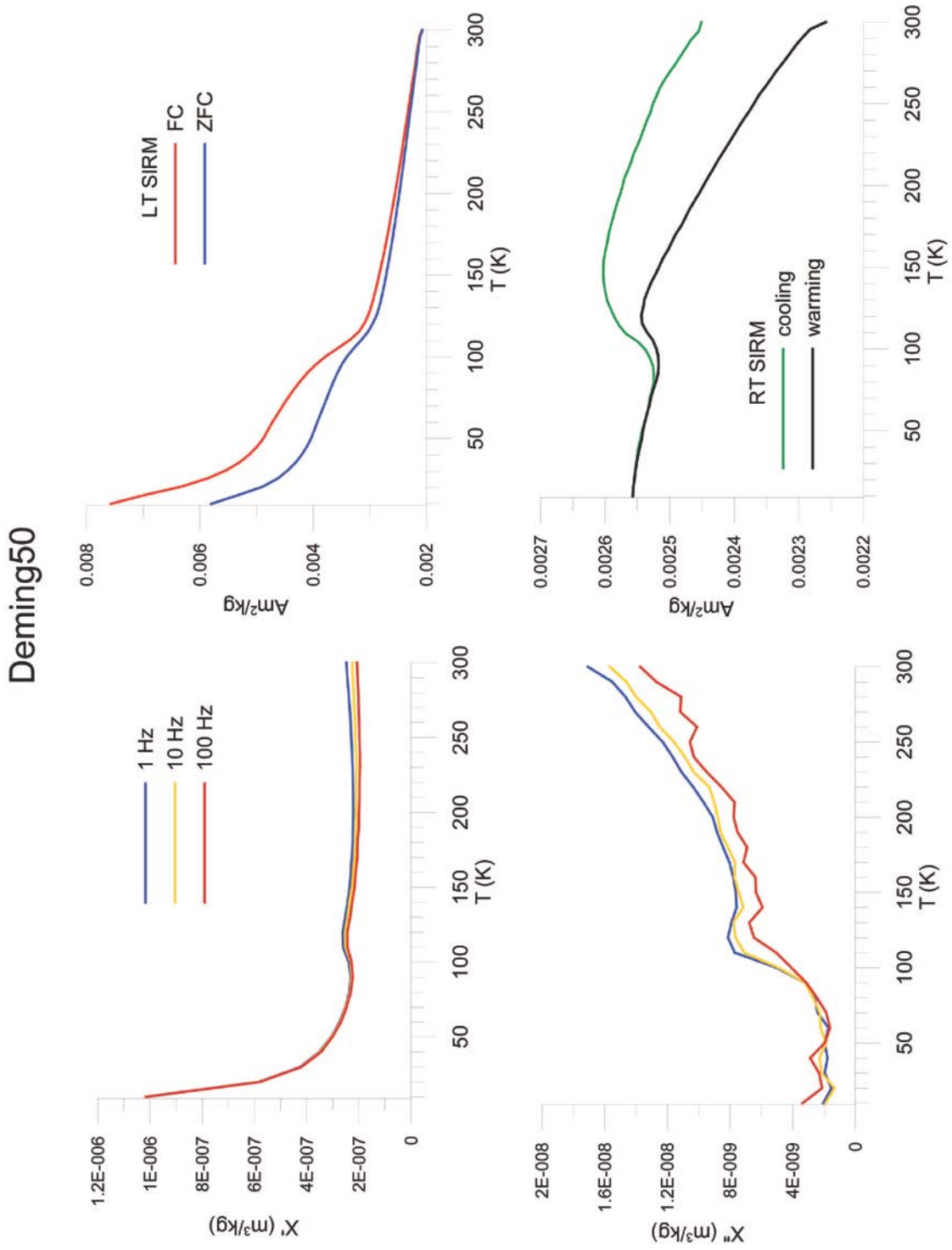

Figure A.4 Low temperature magnetic properties of a profundal sample from Deming

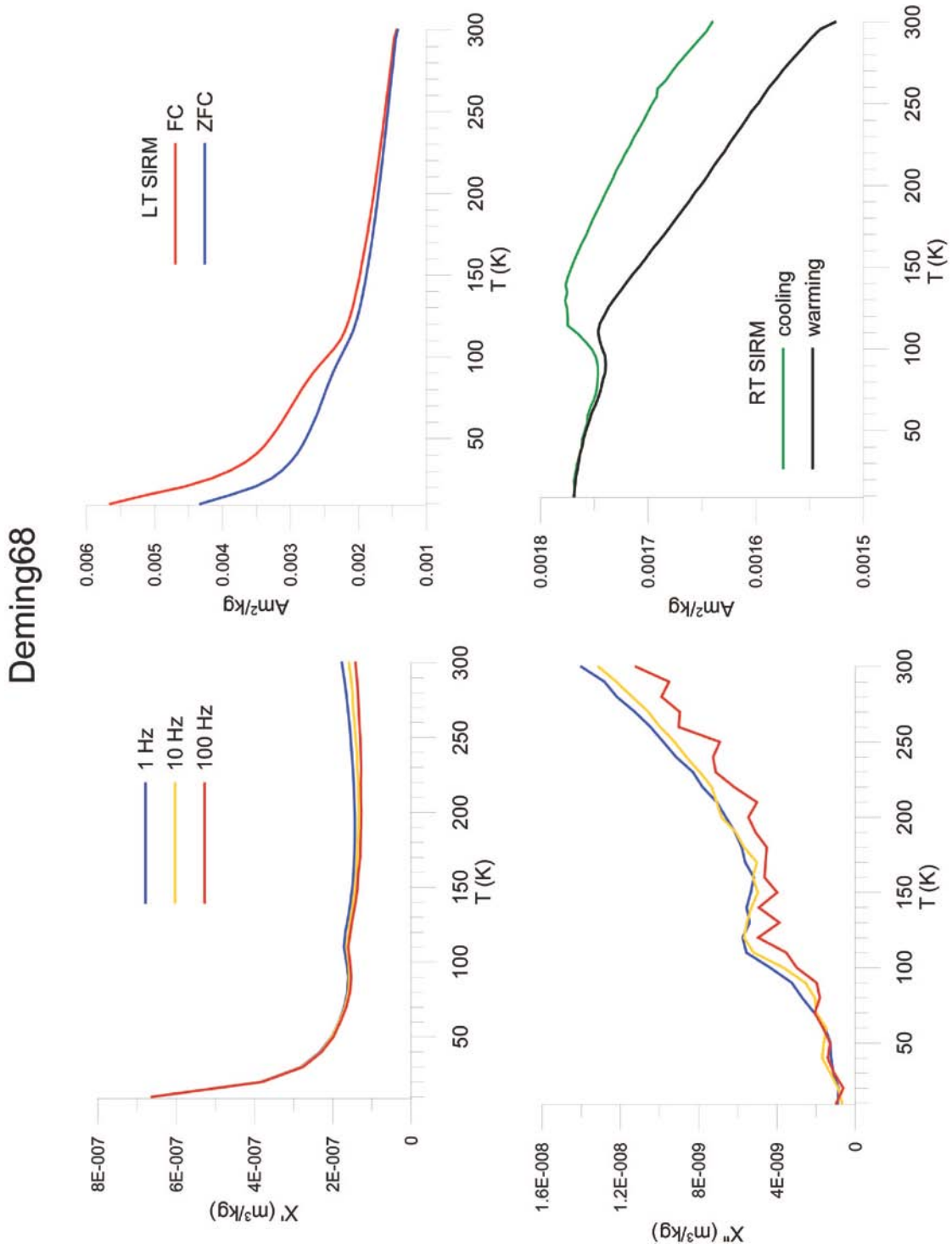

Figure A.5 Low temperature magnetic properties of a littoriprofundal sample from Deming

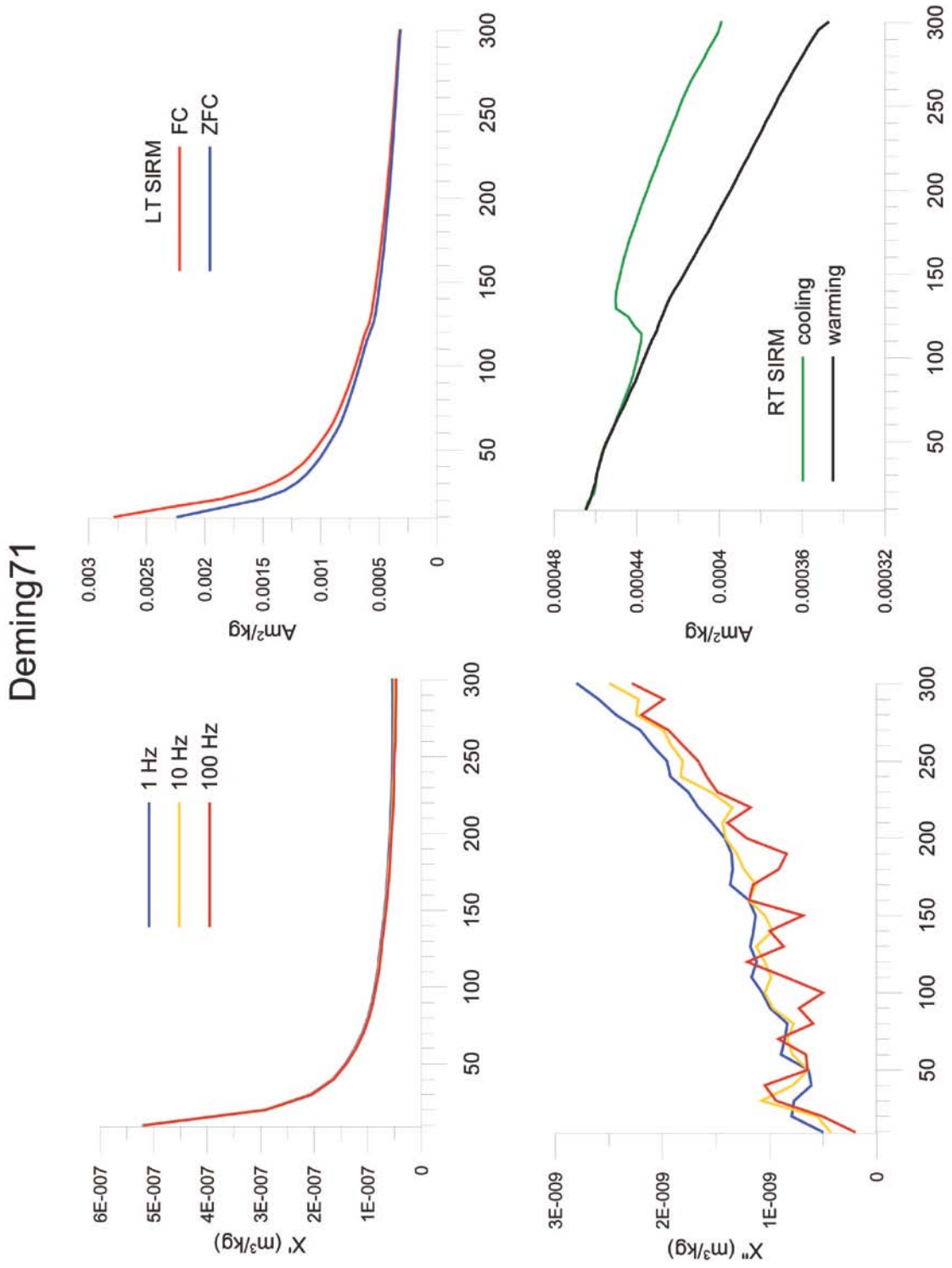

Figure A.6 Low temperature magnetic properties of a shallow littoral sample from Deming

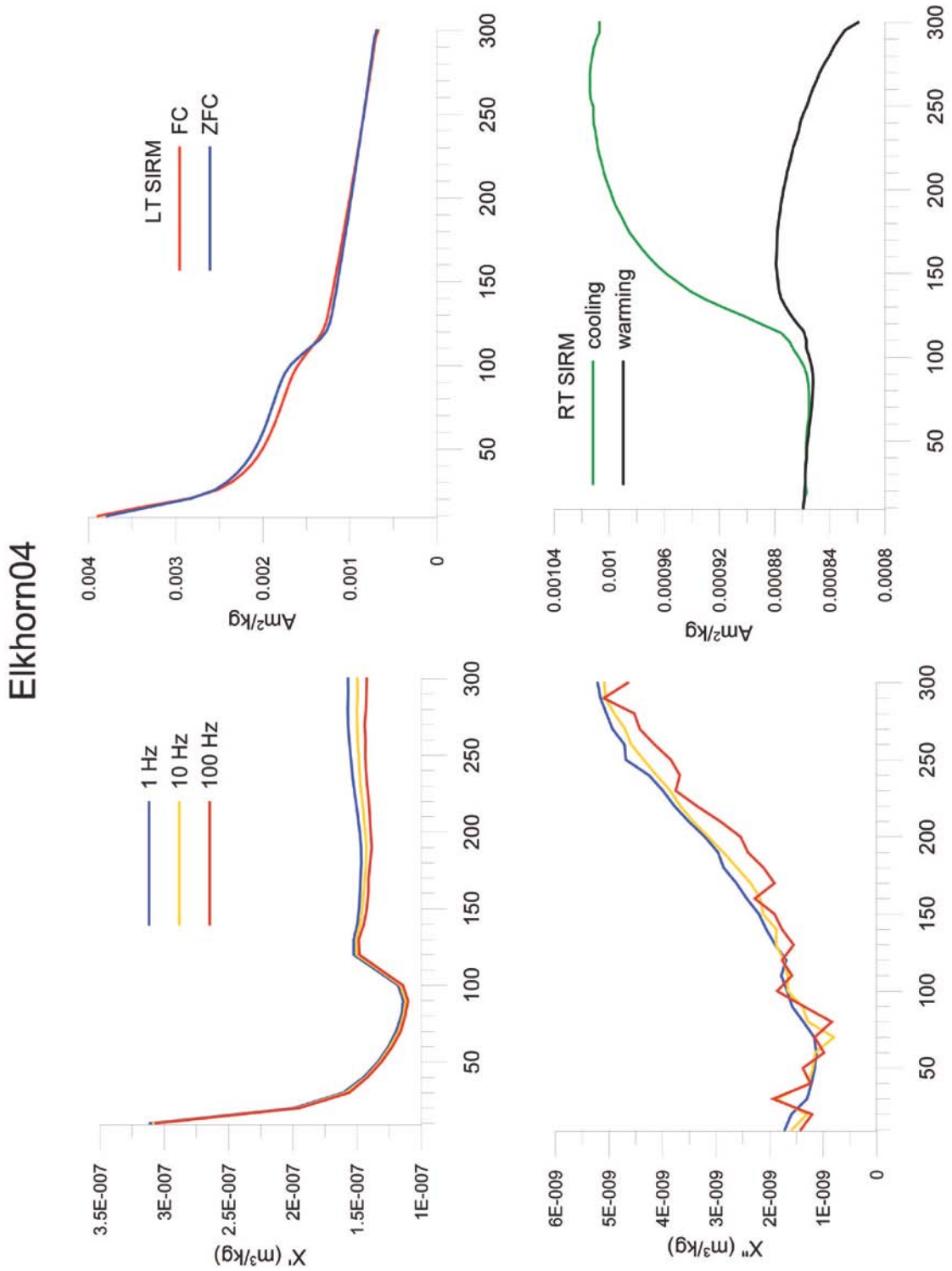

Figure A.7 Low temperature magnetic properties of a shallow-littoral sample from Elkhorn

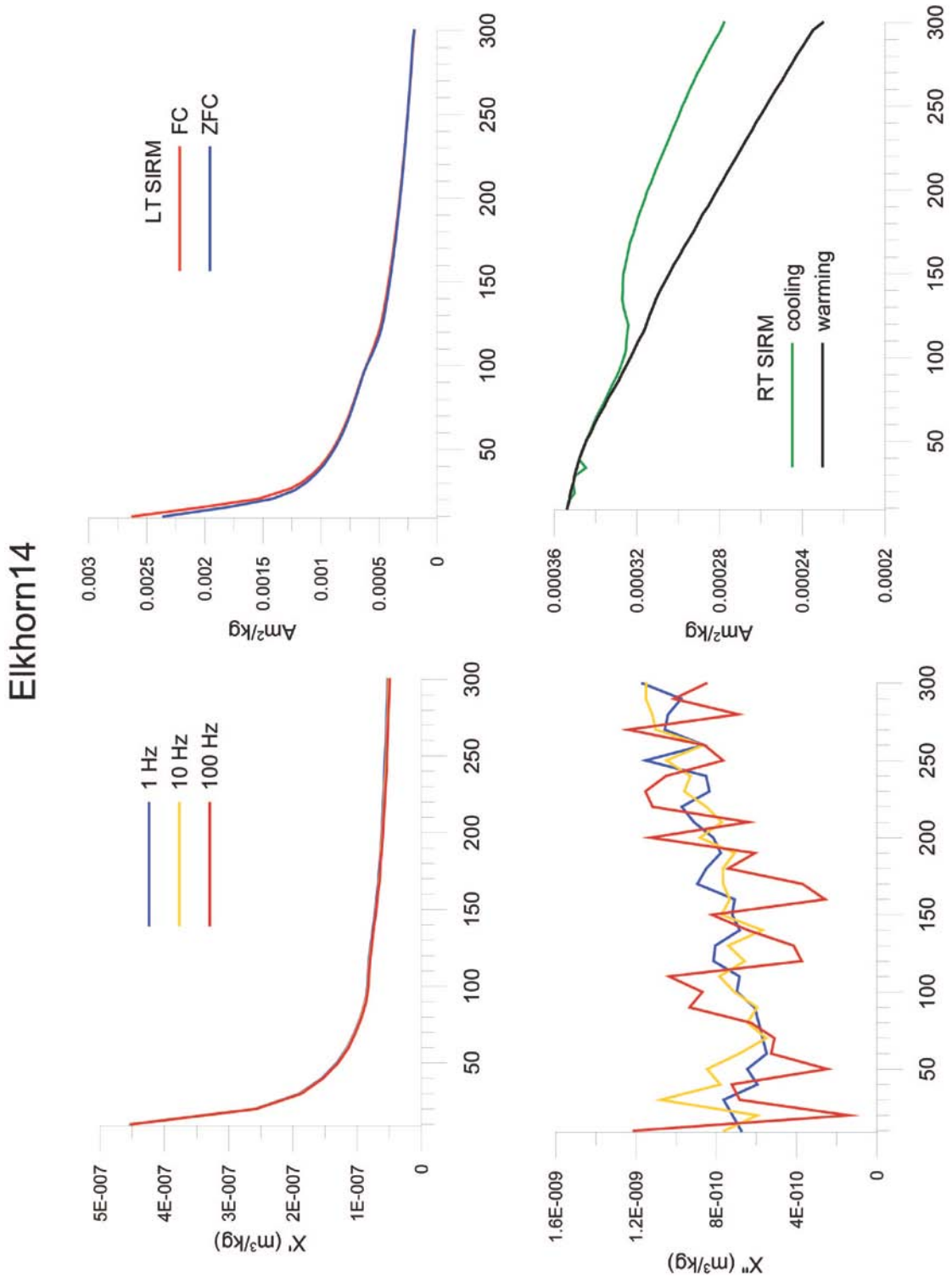

Figure A.8 Low temperature magnetic properties of a profundal sample from Elkhorn

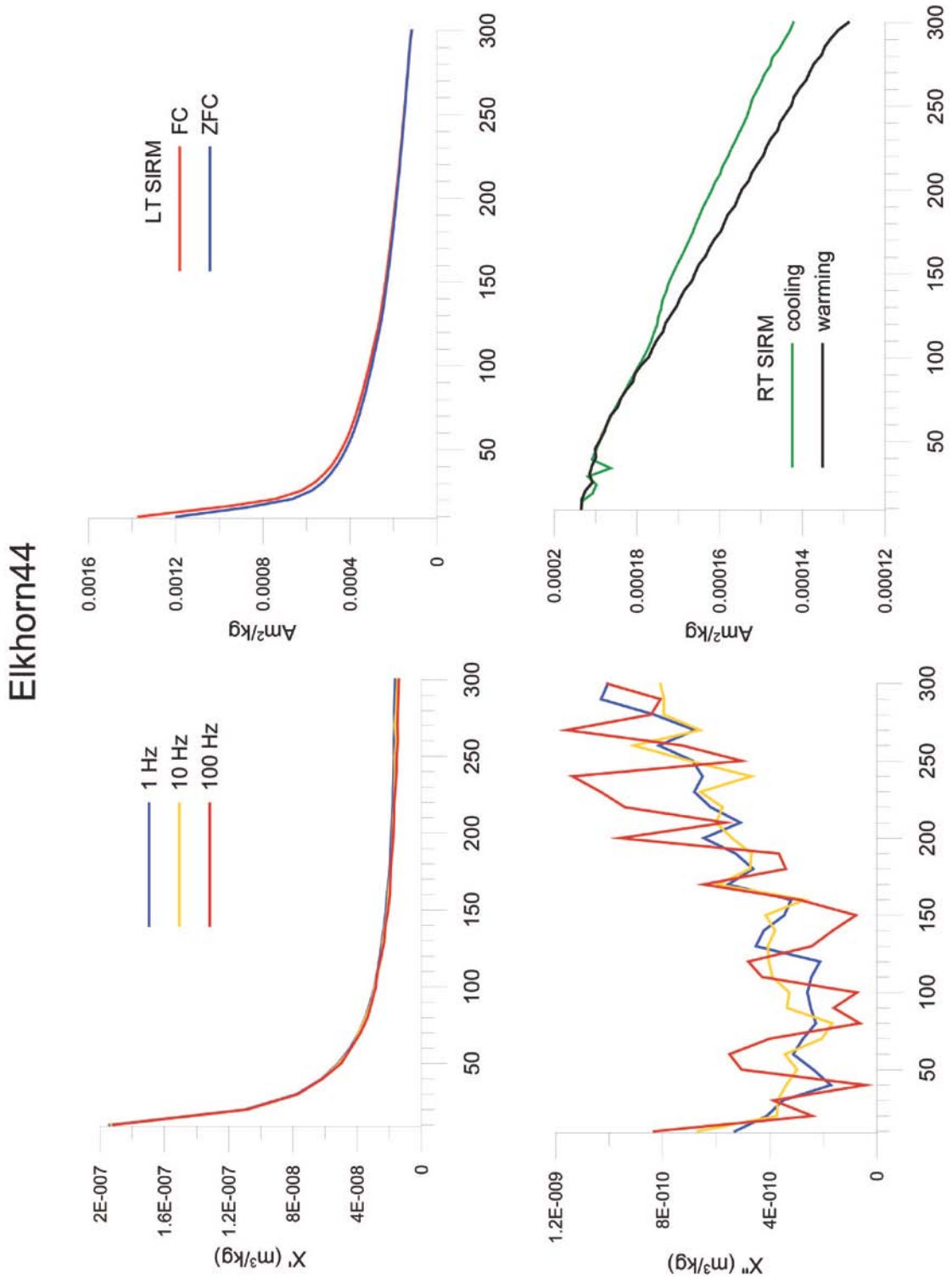

Figure A.9 Low temperature magnetic properties of a littoriprofundal sample from Elkhorn

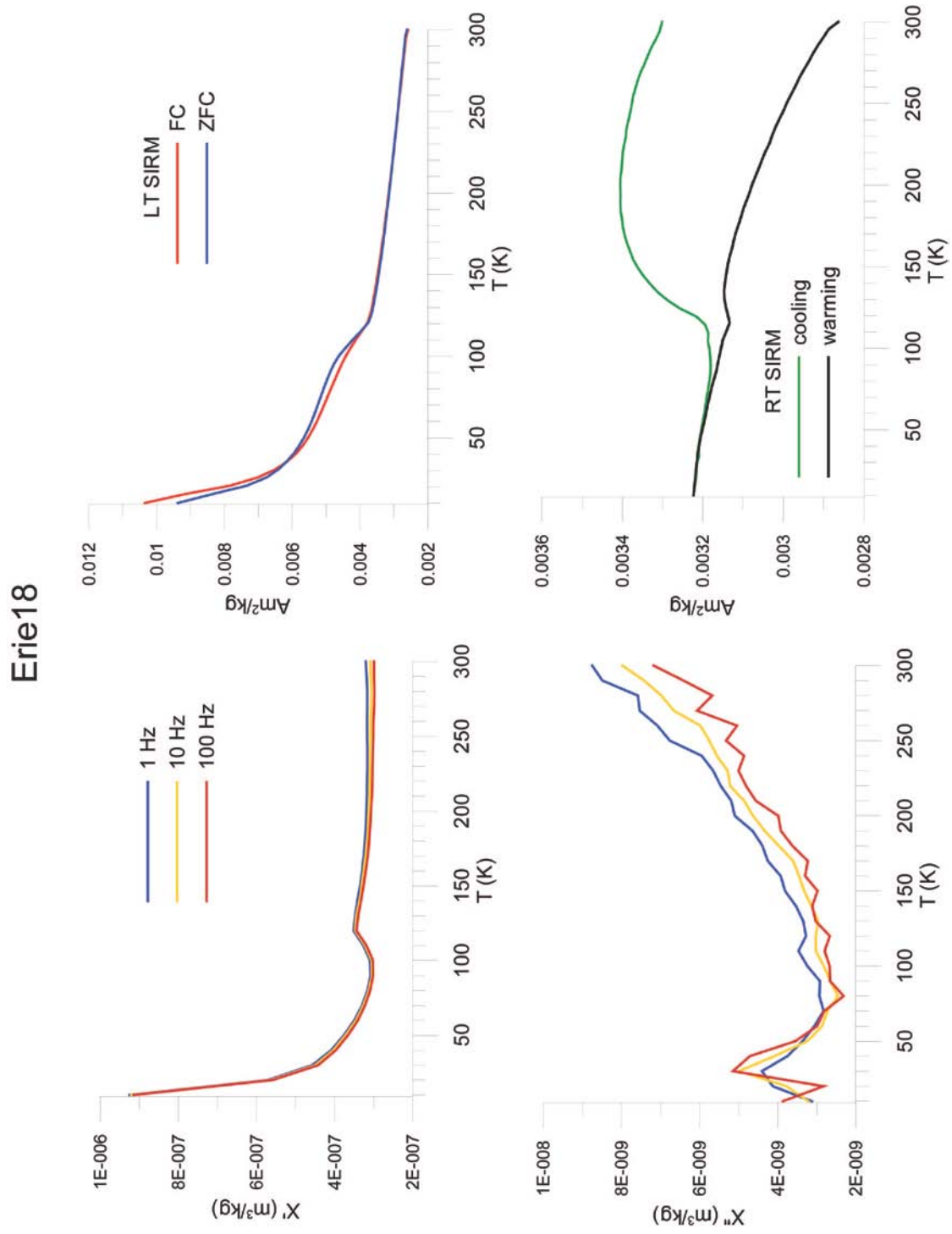

Figure A.10 Low temperature magnetic properties of a littoriprofundal sample from Erie

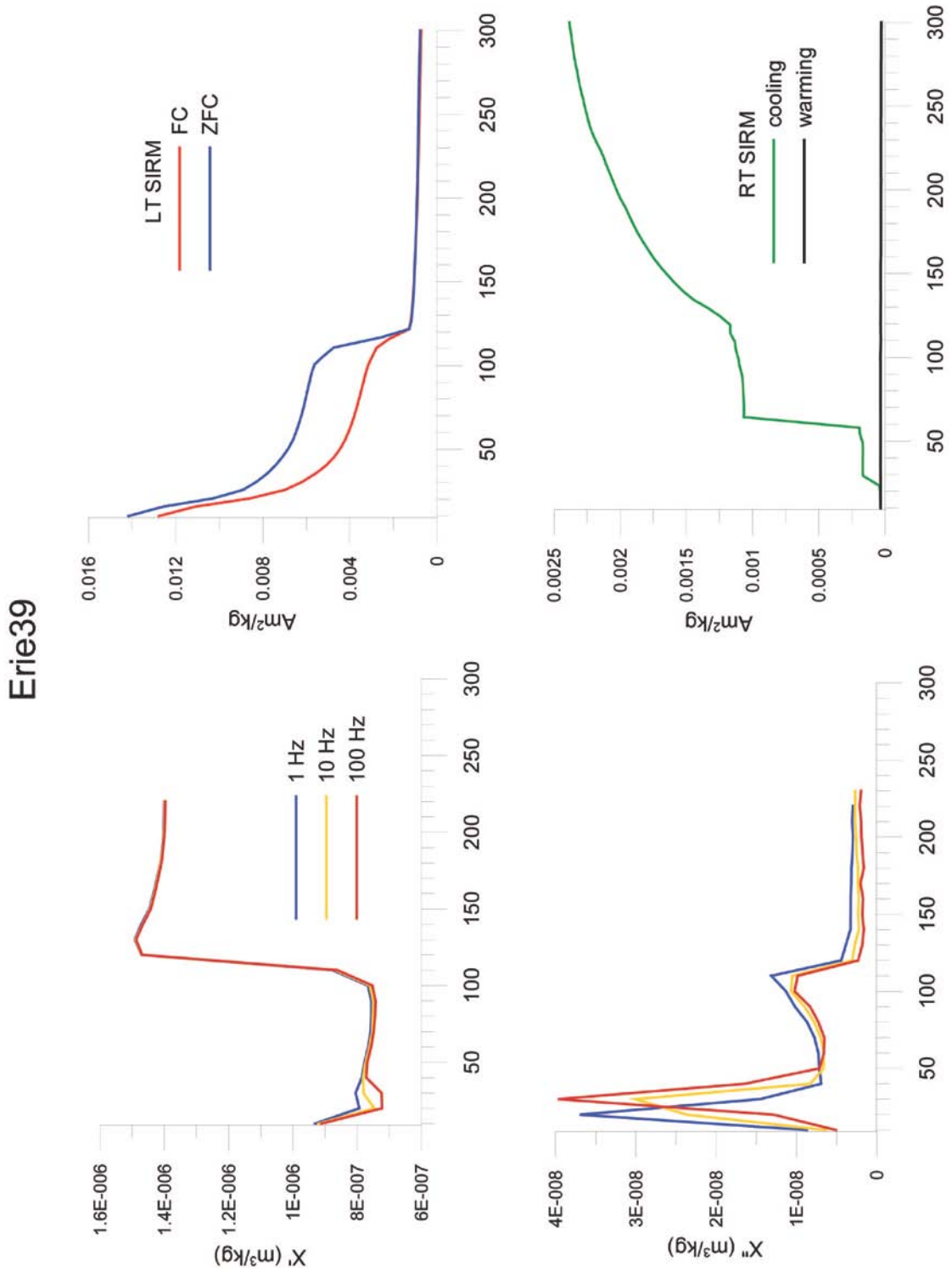

Figure A.11 Low temperature magnetic properties of a shoreline sample from Erie

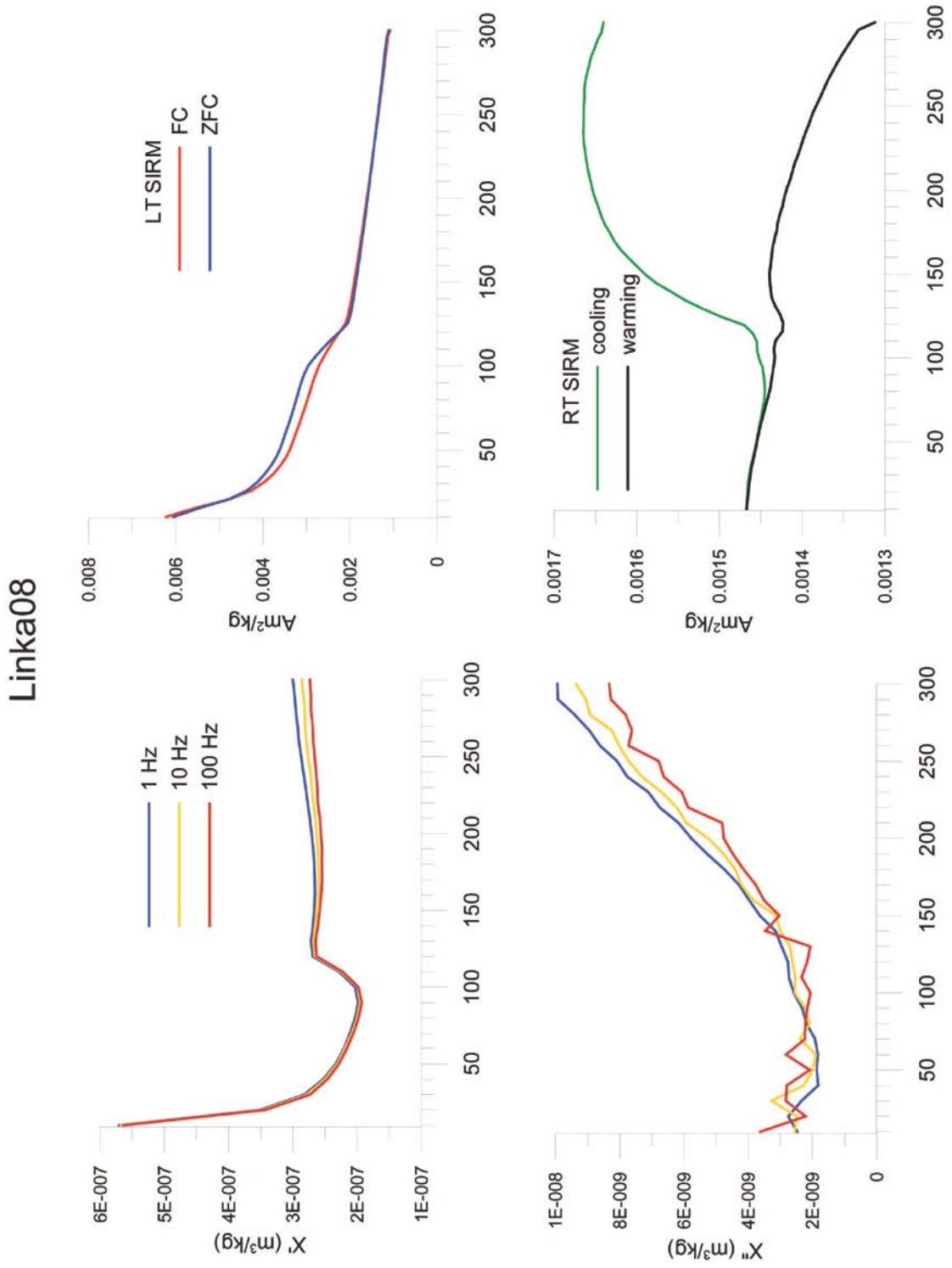

Figure A.12 Low temperature magnetic properties of a littoriprofundal sample from Linka

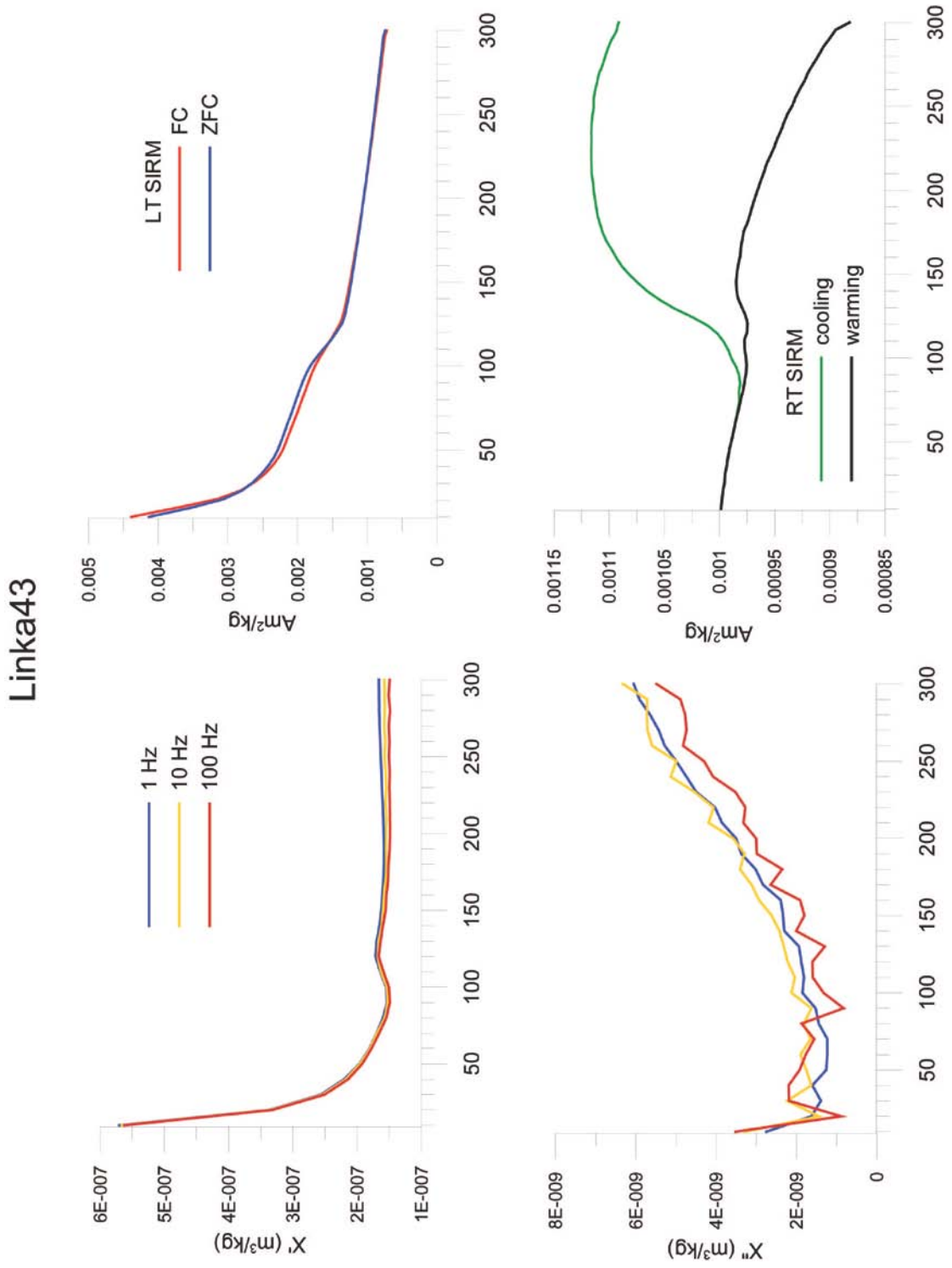

Figure A.13 Low temperature magnetic properties of a profundal sample from Linka

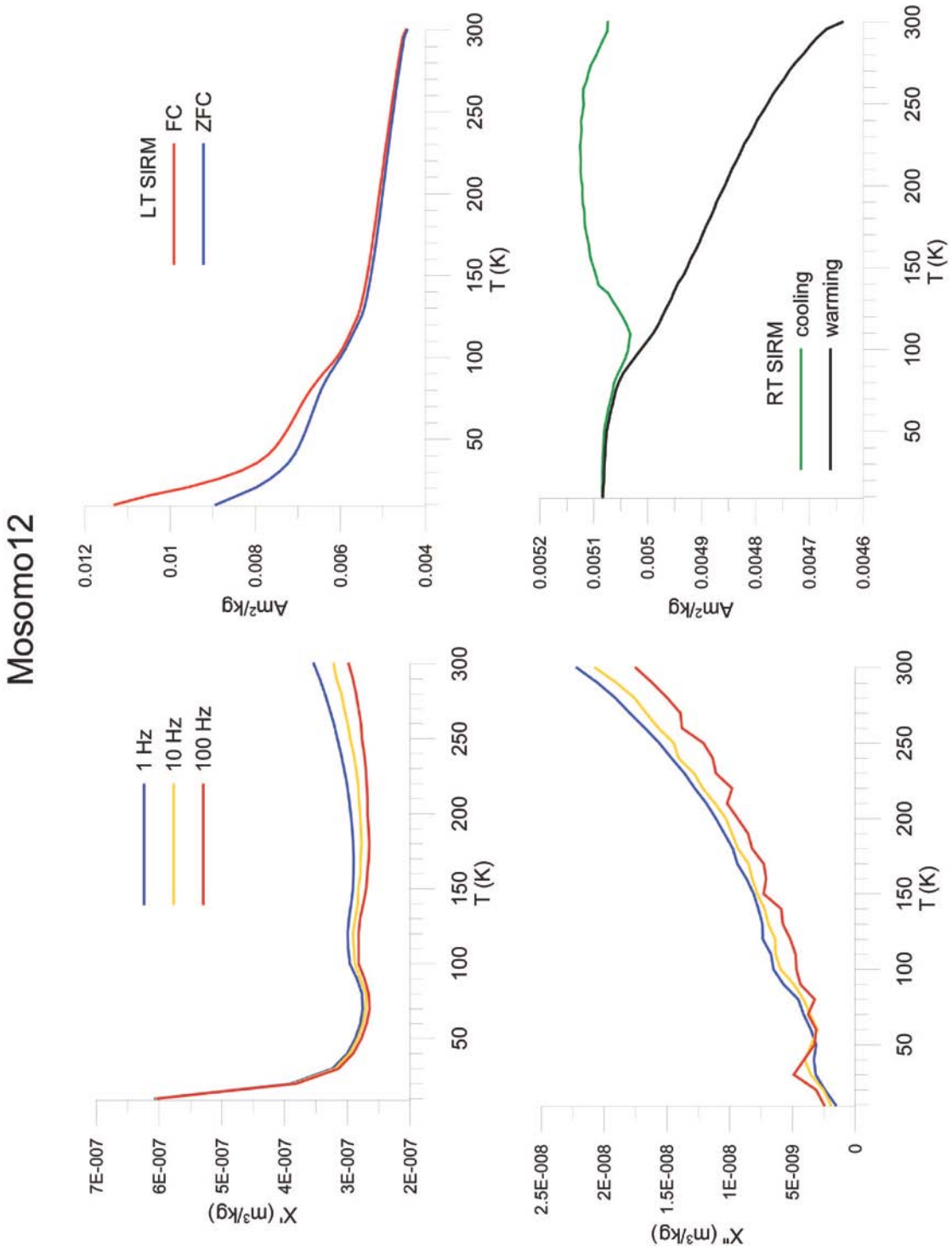

Figure A.14 Low temperature magnetic properties of a profundal sample from Mosomo

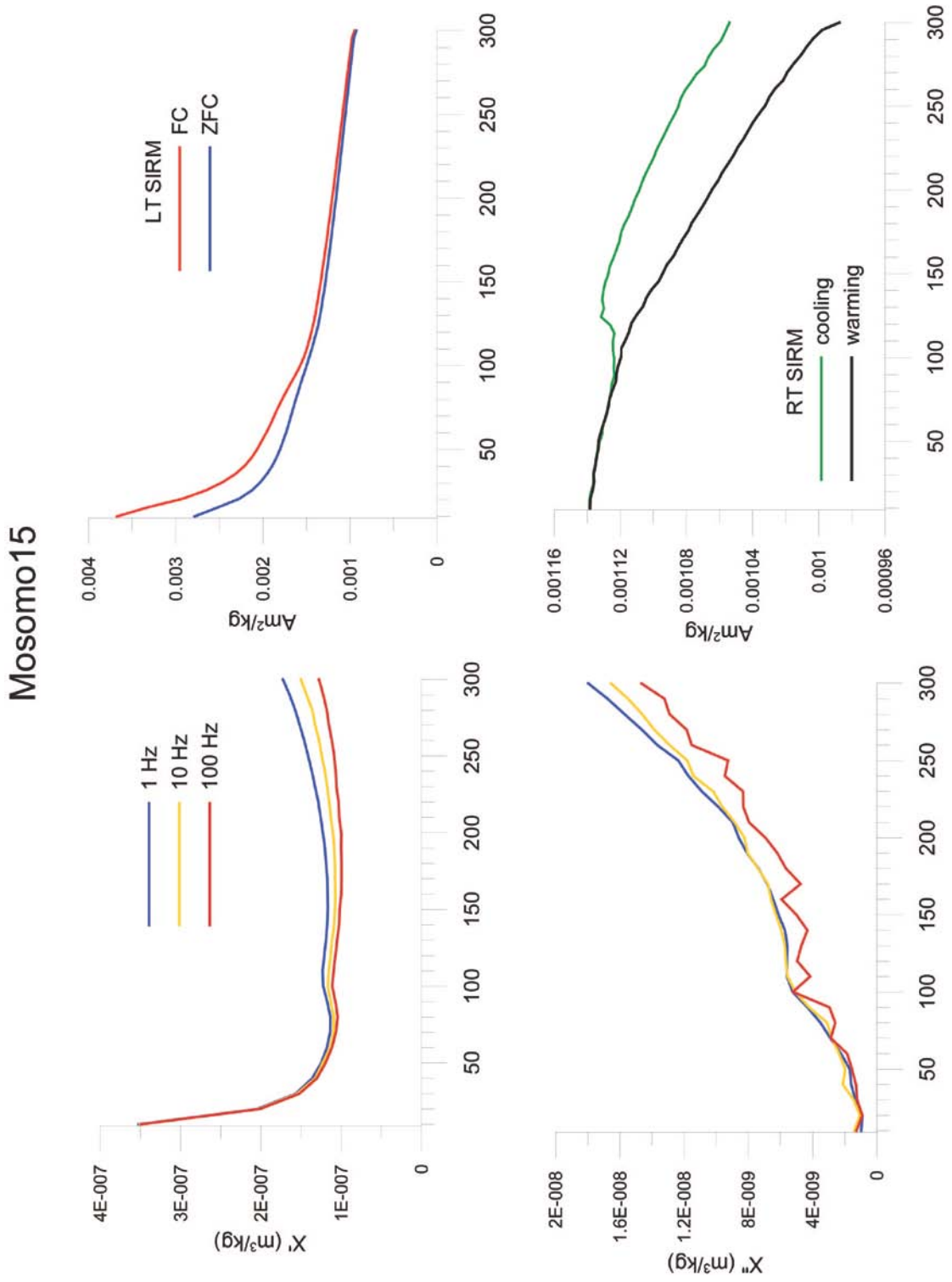

Figure A.15 Low temperature magnetic properties of a littoriprofundal sample from Mosomo

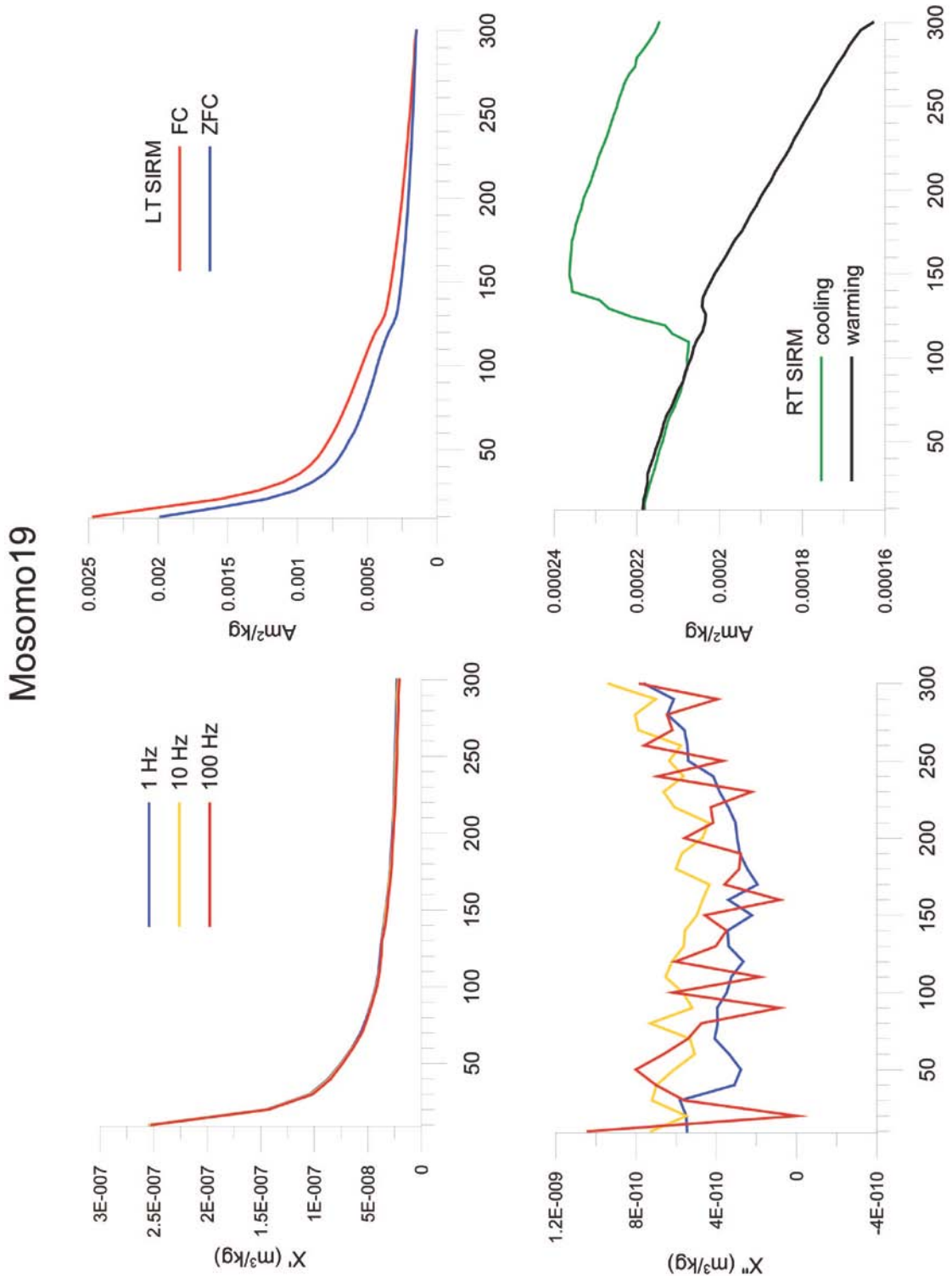

Figure A.16 Low temperature magnetic properties of a shallow littoral sample from Mosomo

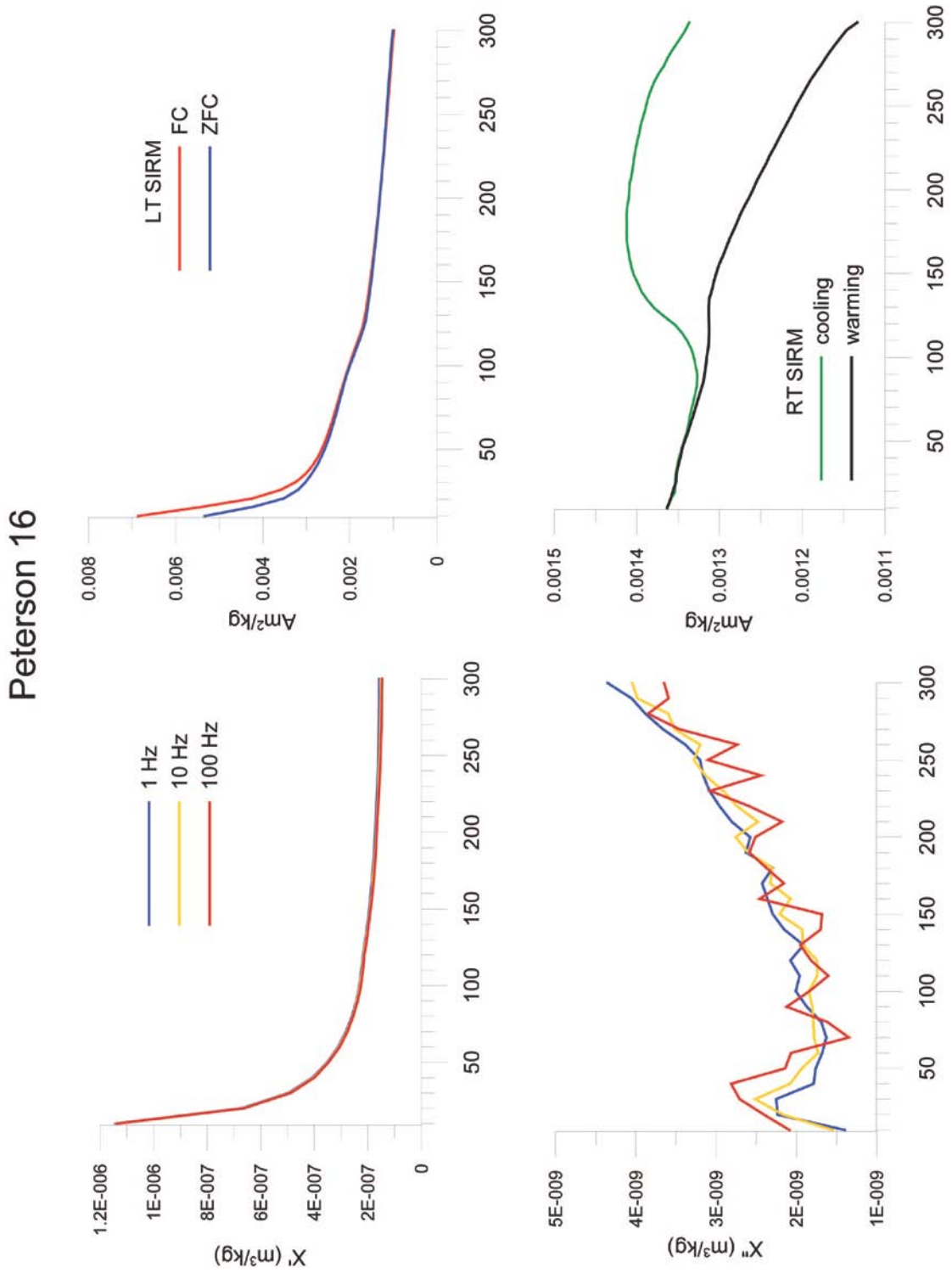

Figure A.17 Low temperature magnetic properties of a profundal sample from Peterson

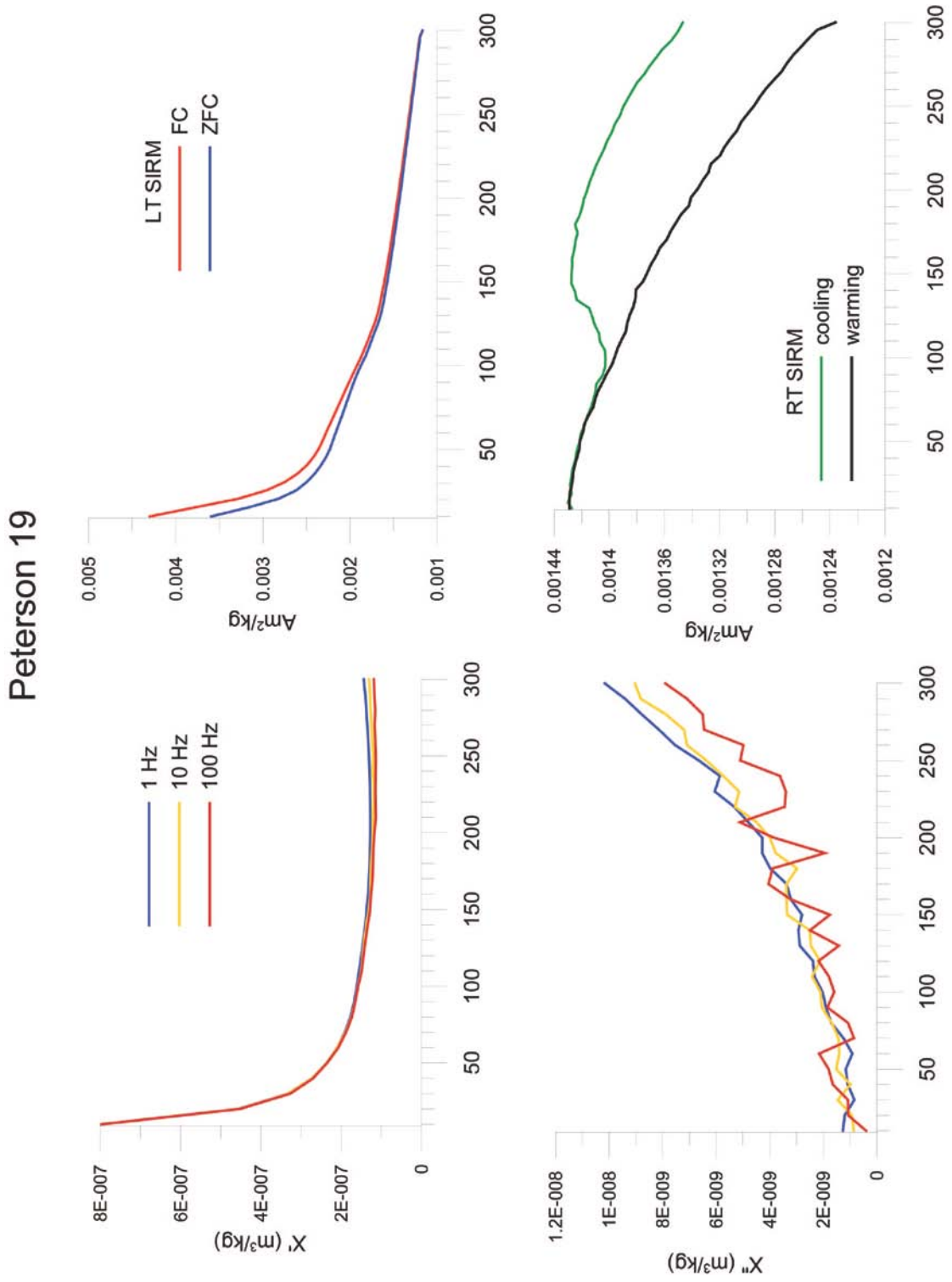

Figure A.18 Low temperature magnetic properties of a littoral sample from Peterson

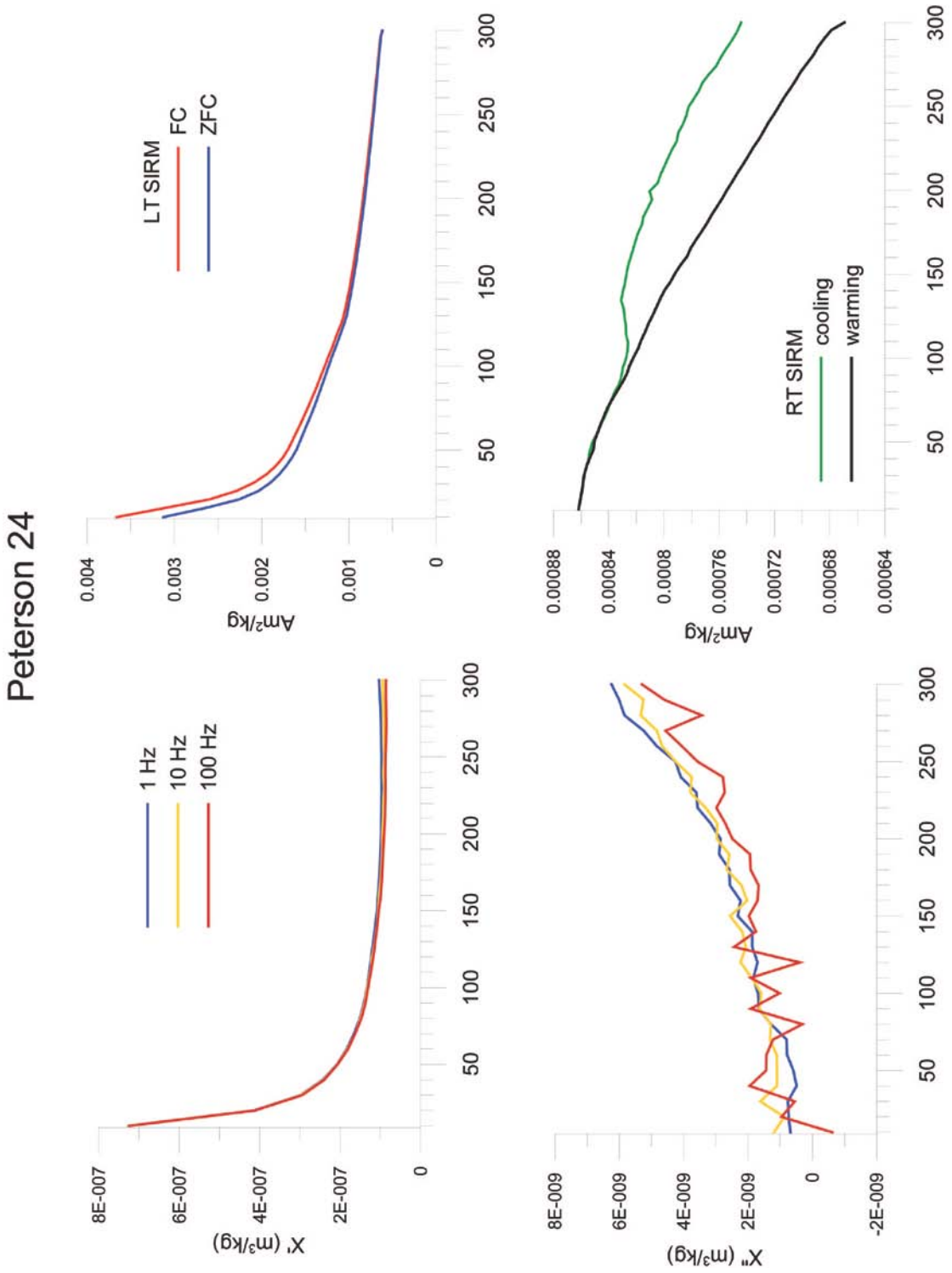

Figure A.19 Low temperature magnetic properties of a littoral sample from Peterson

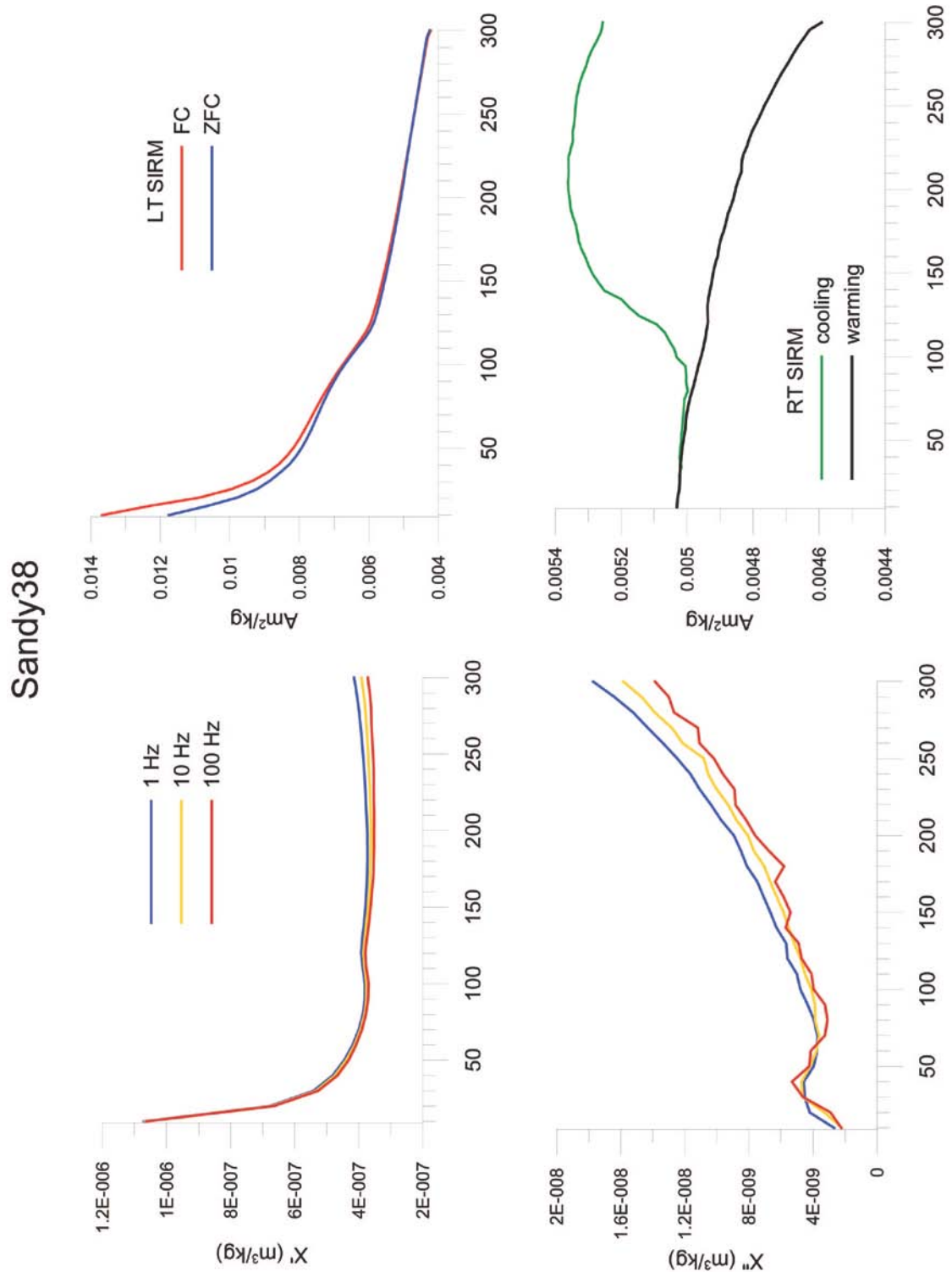

Figure A.20 Low temperature magnetic properties of a profundal sample from Sandy

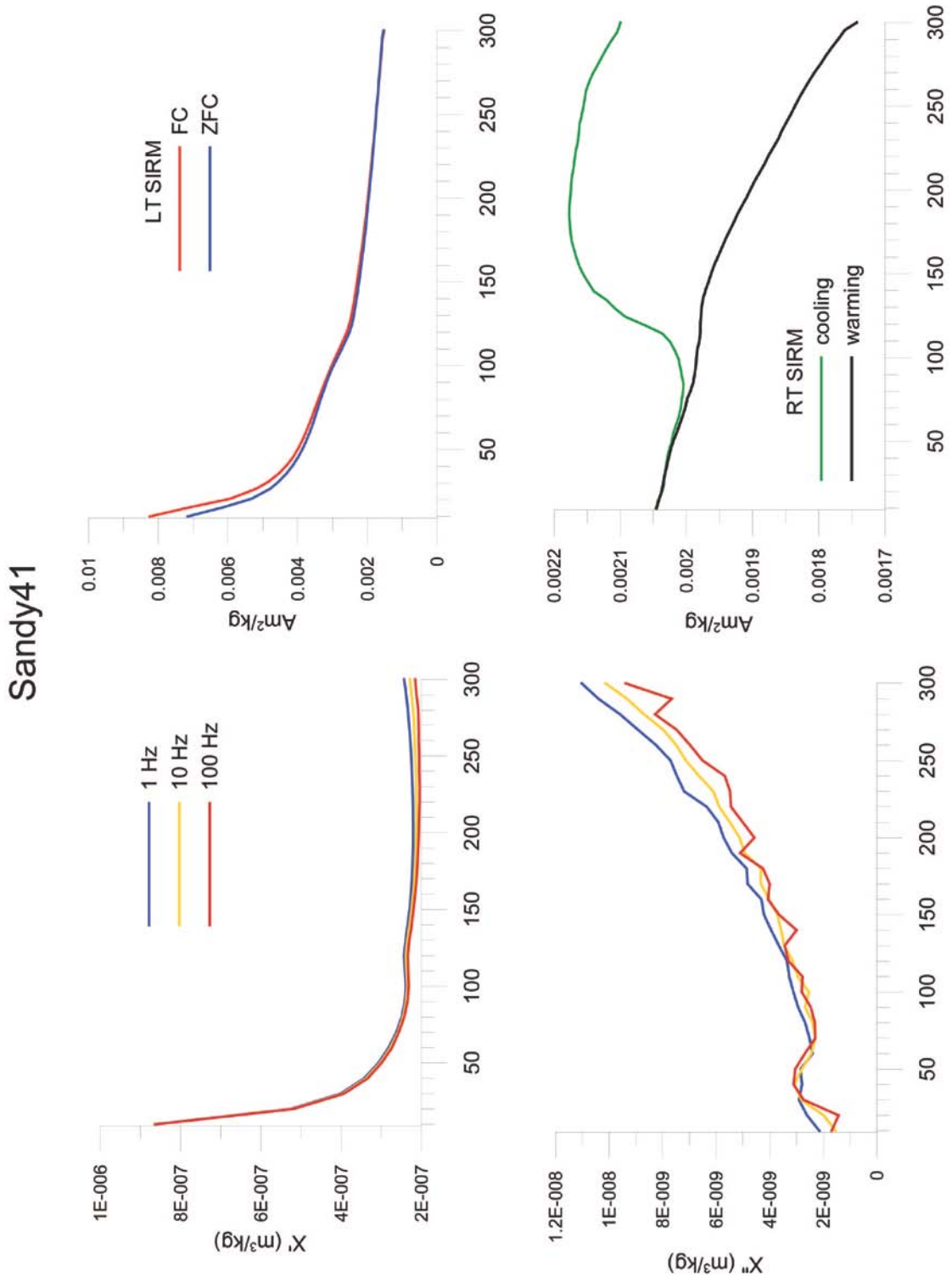

Figure A.21 Low temperature magnetic properties of a profundal sample from Sandy

Tables

Table A.1 Brownie Lake magnetic parameters

Year	χ (m^3/kg)	χ_{ARM} (m^3/kg)	M_{rs} (Am^2/kg)	M_s (Am^2/kg)	χ_{hf} (m^3/kg)	χ_f (m^3/kg)	χ_{ARM}/M_{rs} (10^{-3} m/A)	M_{rs}/M_s	M_{rs}/χ_f (kA/m)	χ_f/M_s (μm/A)
2007	1.2E-06	1.3E-05	0.02212	0.125	5.87E-08	1E-06	0.61	0.18	19.83	8.92
2003	1.1E-06	1.1E-05	0.02018	0.117	6.29E-08	1E-06	0.55	0.17	18.86	9.15
2000	1.1E-06	1.4E-05	0.02094	0.116	2.94E-08	1E-06	0.67	0.18	18.89	9.56
1998	1.1E-06	9.7E-06	0.01897	0.113	8.07E-08	1E-06	0.51	0.17	18.41	9.11
1994	1.1E-06	8.7E-06	0.01655	0.104	8.90E-08	1E-06	0.52	0.16	17.15	9.25
1991	1.1E-06	8.7E-06	0.01741	0.105	9.49E-08	1E-06	0.50	0.17	17.53	9.44
1989	7.9E-07	7.5E-06	0.01317	0.076	7.35E-08	7E-07	0.57	0.17	18.41	9.45
1985	8.1E-07	6.7E-06	0.01283	0.079	8.57E-08	7E-07	0.52	0.16	17.82	9.14
1983	9.2E-07	7E-06	0.01435	0.090	5.93E-08	9E-07	0.49	0.16	16.70	9.57
1979	8.9E-07	8.4E-06	0.01502	0.094	4.92E-08	8E-07	0.56	0.16	17.80	8.97
1977	1.2E-06	8.6E-06	0.02082	0.133	5.62E-08	1E-06	0.41	0.16	17.77	8.78
1973	1.1E-06	8.7E-06	0.01939	0.121	6.58E-08	1E-06	0.45	0.16	18.34	8.72
1969	1E-06	7.7E-06	0.01758	0.106	6.69E-08	9E-07	0.44	0.17	18.64	8.88
1967	1.2E-06	6.9E-06	0.02023	0.135	7.66E-08	1E-06	0.34	0.15	17.94	8.37
1963	1.7E-06	1.1E-05	0.03142	0.163	6.53E-08	2E-06	0.36	0.19	18.72	10.28
1959	1.1E-06	7.7E-06	0.0201	0.124	7.88E-08	1E-06	0.38	0.16	19.59	8.28
1956	9.6E-07	6.9E-06	0.01793	0.104	9.04E-08	9E-07	0.38	0.17	20.64	8.34
1953	1.1E-06	8E-06	0.02217	0.133	6.86E-08	1E-06	0.36	0.17	21.17	7.86
1950	9.6E-07	7.5E-06	0.01818	0.108	8.57E-08	9E-07	0.41	0.17	20.81	8.08
1946	7.3E-07	6.6E-06	0.01249	0.076	7.78E-08	7E-07	0.53	0.16	19.12	8.56
1943	7.7E-07	6.4E-06	0.01386	0.082	8.19E-08	7E-07	0.46	0.17	20.19	8.35
1939	8E-07	5.7E-06	0.01431	0.088	8.39E-08	7E-07	0.40	0.16	19.90	8.18
1937	4.8E-07	5.2E-06	0.00897	0.050	5.53E-08	4E-07	0.58	0.18	20.95	8.56
1935	6.1E-07	5.7E-06	0.01136	0.066	8.58E-08	5E-07	0.50	0.17	21.74	7.96
1932	4.3E-07	5.6E-06	0.00785	0.039	7.99E-08	4E-07	0.72	0.20	22.33	8.91
1928	5.4E-07	6.4E-06	0.01003	0.053	7.40E-08	5E-07	0.63	0.19	21.36	8.88
1927	5.3E-07	6.6E-06	0.00999	0.058	6.86E-08	5E-07	0.66	0.17	21.54	8.06
1923	5.6E-07	4.9E-06	0.00939	0.059	7.57E-08	5E-07	0.52	0.16	19.35	8.21
1920	8.7E-07	6.7E-06	0.01415	0.098	7.36E-08	8E-07	0.48	0.14	17.68	8.18
1912	1.3E-06	3.2E-06	0.01599	0.180	4.77E-08	1E-06	0.20	0.09	12.74	6.97
1905	3.9E-07	3.6E-06	0.00737	0.043	-5.54E-10	4E-07	0.49	0.17	18.66	9.10
1895	7.7E-07	5.5E-06	0.01449	0.088	6.07E-08	7E-07	0.38	0.16	20.38	8.08
1881	5.1E-07	1.9E-06	0.00888	0.058	3.45E-08	5E-07	0.21	0.15	18.83	8.14
1877	4.6E-07	2E-06	0.00735	0.052	2.39E-08	4E-07	0.27	0.14	16.73	8.50
1867	1.6E-06	6.6E-06	0.02305	0.173	5.41E-08	2E-06	0.29	0.13	15.18	8.80
1829	6.9E-07	1.2E-05	0.01234	0.072	1.04E-09	7E-07	0.96	0.17	18.02	9.55
1807	4E-07	1.2E-05	0.00678	0.026	1.15E-08	4E-07	1.75	0.26	17.45	14.68
1784	3.9E-07	1.3E-05	0.00679	0.026	-9.46E-09	4E-07	1.87	0.26	16.85	15.42
1765	4.5E-07	1.4E-05	0.00844	0.032	3.77E-09	4E-07	1.61	0.26	18.79	13.90
1735	6.8E-07	1.8E-05	0.01151	0.040	1.52E-07	5E-07	1.53	0.29	21.91	13.09
1715	7.8E-07	2.3E-05	0.01605	0.056	1.61E-07	6E-07	1.41	0.28	25.74	11.06
1685	8.7E-07	3.2E-05	0.02483	0.070	9.31E-08	8E-07	1.30	0.35	31.84	11.14
1665	7E-07	2.6E-05	0.02001	0.062	4.78E-08	7E-07	1.30	0.32	30.71	10.53
1645	9.4E-07	3.1E-05	0.02276	0.078	1.39E-07	8E-07	1.36	0.29	28.42	10.30
1624	8.8E-07	3.1E-05	0.02284	0.072	1.20E-07	8E-07	1.35	0.32	30.20	10.52

1605	7.7E-07	2.7E-05	0.01826	0.067	7.32E-08	7E-07	1.46	0.27	26.31	10.43
1585	6.8E-07	2E-05	0.01367	0.054	1.22E-07	6E-07	1.50	0.25	24.54	10.38
1575	5.5E-07	2E-05	0.01226	0.044	5.77E-08	5E-07	1.64	0.28	24.92	11.10
1555	6.6E-07	2.3E-05	0.01675	0.058	8.51E-08	6E-07	1.38	0.29	28.95	10.00
1535	7.3E-07	2.9E-05	0.01805	0.060	3.32E-08	7E-07	1.63	0.30	26.09	11.50
1515	5.8E-07	2.3E-05	0.01386	0.046	2.80E-08	6E-07	1.65	0.30	25.02	12.10
1495	5.9E-07	2.1E-05	0.0129	0.044	6.17E-08	5E-07	1.61	0.29	24.58	11.90
1475	8.5E-07	2.9E-05	0.01726	0.056	1.23E-07	7E-07	1.67	0.31	23.84	12.91
1445	8.2E-07	3.2E-05	0.01673	0.056	1.01E-07	7E-07	1.92	0.30	23.36	12.69
1425	8.9E-07	3.2E-05	0.01731	0.055	2.17E-07	7E-07	1.84	0.31	25.54	12.25
1405	9.6E-07	3.5E-05	0.01921	0.060	2.34E-07	7E-07	1.83	0.32	26.35	12.18
1385	1E-06	4E-05	0.01995	0.063	2.70E-07	8E-07	1.98	0.32	25.69	12.28
1375	7.7E-07	3E-05	0.0156	0.050	1.19E-07	7E-07	1.95	0.31	23.81	13.06
1365	7.8E-07	3E-05	0.01837	0.053	1.24E-07	7E-07	1.66	0.35	27.85	12.46
1355	9.5E-07	3.2E-05	0.02257	0.069	1.81E-07	8E-07	1.43	0.33	29.19	11.25
1345	8.2E-07	3E-05	0.0211	0.064	9.56E-08	7E-07	1.40	0.33	29.10	11.38
1335	7.9E-07	2.7E-05	0.01734	0.054	1.56E-07	6E-07	1.54	0.32	27.49	11.69
1325	5.9E-07	2.1E-05	0.01123	0.036	1.13E-07	5E-07	1.87	0.32	23.38	13.48
1305	8.2E-07	3.5E-05	0.01923	0.059	5.91E-08	8E-07	1.80	0.33	25.37	12.95
1295	7.8E-07	3E-05	0.0164	0.050	1.32E-07	6E-07	1.81	0.33	25.34	12.87
1285	1E-06	3.9E-05	0.02137	0.071	2.30E-07	8E-07	1.83	0.30	26.72	11.28
1275	1E-06	4.2E-05	0.02285	0.073	1.96E-07	9E-07	1.86	0.31	26.86	11.68
1265	1.2E-06	5.1E-05	0.02627	0.087	2.46E-07	9E-07	1.95	0.30	27.71	10.90
1255	1.2E-06	5.5E-05	0.02617	0.087	2.55E-07	1E-06	2.08	0.30	26.60	11.30
1245	1.2E-06	5.2E-05	0.02673	0.090	2.42E-07	1E-06	1.93	0.30	27.81	10.70
1235	1.2E-06	5E-05	0.02678	0.091	2.59E-07	9E-07	1.86	0.30	28.24	10.45
1225	1.3E-06	5.3E-05	0.02868	0.099	2.82E-07	1E-06	1.84	0.29	28.46	10.16
1215	1.4E-06	6E-05	0.0304	0.099	2.88E-07	1E-06	1.97	0.31	27.71	11.05
1205	1.5E-06	5.6E-05	0.03128	0.104	3.32E-07	1E-06	1.78	0.30	27.33	11.00
1195	1.4E-06	5.8E-05	0.03077	0.098	3.44E-07	1E-06	1.90	0.31	28.51	11.03
1185	1.4E-06	5.8E-05	0.03073	0.096	3.64E-07	1E-06	1.89	0.32	29.50	10.89
1175	1.4E-06	5.5E-05	0.02939	0.093	3.59E-07	1E-06	1.87	0.31	28.45	11.07
1165	1.4E-06	5.5E-05	0.03205	0.100	3.42E-07	1E-06	1.72	0.32	30.03	10.68
1155	1.4E-06	5.3E-05	0.03365	0.103	3.23E-07	1E-06	1.57	0.33	30.97	10.52
1145	1.2E-06	3.6E-05	0.02527	0.085	2.14E-07	1E-06	1.42	0.30	26.60	11.23
1135	1.3E-06	5.1E-05	0.02971	0.092	2.96E-07	1E-06	1.71	0.32	29.13	11.03
1125	1.3E-06	5.3E-05	0.02917	0.091	3.07E-07	1E-06	1.82	0.32	29.24	10.98
1115	1.3E-06	5.3E-05	0.02886	0.090	3.28E-07	1E-06	1.83	0.32	28.74	11.12
1105	1.3E-06	5.3E-05	0.0292	0.091	3.37E-07	1E-06	1.82	0.32	29.27	10.99
1095	1.3E-06	5.1E-05	0.02805	0.087	3.54E-07	1E-06	1.81	0.32	29.52	10.88
1085	1.3E-06	4.4E-05	0.02582	0.084	3.43E-07	9E-07	1.70	0.31	27.73	11.06
1075	1.3E-06	5E-05	0.02606	0.080	3.68E-07	9E-07	1.90	0.32	29.49	11.00

Table A.2 Brownie Lake model components

Year	g_{UNISD}	g_{ISD}	g_{MD}	f_{SP}	c_{ferri} (mg/g)	ϕ_{ferri} (mg/cm^2/yr)	ϕ_{UNISD} (mg/cm^2/yr)	ϕ_{ISD} (mg/cm^2/yr)	ϕ_{MD} (mg/cm^2/yr)	ϕ_{SP} (mg/cm^2/yr)
2007	0.05	0.29	0.66	0.07	1.420	0.115	0.005	0.031	0.071	0.008
2003	0.04	0.29	0.67	0.08	1.330	0.199	0.008	0.052	0.123	0.016
2000	0.06	0.29	0.65	0.09	1.318	0.198	0.011	0.052	0.118	0.018
1998	0.04	0.28	0.68	0.08	1.285	0.200	0.007	0.051	0.126	0.015
1994	0.04	0.25	0.71	0.08	1.185	0.240	0.008	0.056	0.157	0.019
1991	0.04	0.27	0.69	0.08	1.196	0.299	0.010	0.075	0.189	0.025
1989	0.05	0.29	0.67	0.09	0.860	0.276	0.012	0.072	0.169	0.024
1985	0.04	0.26	0.70	0.08	0.895	0.291	0.010	0.071	0.187	0.022
1983	0.03	0.26	0.70	0.09	1.020	0.282	0.009	0.067	0.181	0.025
1979	0.04	0.25	0.71	0.07	1.069	0.291	0.011	0.068	0.191	0.021
1977	0.03	0.26	0.71	0.07	1.516	0.257	0.007	0.062	0.171	0.017
1973	0.03	0.27	0.70	0.07	1.378	0.259	0.008	0.064	0.170	0.017
1969	0.03	0.28	0.69	0.07	1.207	0.241	0.007	0.063	0.154	0.017
1967	0.02	0.25	0.73	0.06	1.531	0.299	0.006	0.072	0.205	0.017
1963	0.03	0.36	0.61	0.11	1.855	0.228	0.006	0.073	0.124	0.025
1959	0.03	0.28	0.69	0.05	1.409	0.254	0.006	0.067	0.167	0.014
1956	0.03	0.31	0.67	0.06	1.184	0.259	0.007	0.074	0.163	0.015
1953	0.02	0.29	0.68	0.04	1.515	0.266	0.006	0.074	0.173	0.012
1950	0.03	0.29	0.68	0.05	1.228	0.291	0.008	0.081	0.188	0.015
1946	0.04	0.27	0.69	0.06	0.867	0.222	0.008	0.056	0.145	0.014
1943	0.03	0.29	0.68	0.06	0.934	0.196	0.006	0.053	0.125	0.011
1939	0.03	0.28	0.69	0.05	1.000	0.189	0.005	0.050	0.124	0.010
1937	0.05	0.30	0.65	0.06	0.568	0.147	0.007	0.041	0.090	0.009
1935	0.04	0.29	0.67	0.05	0.746	0.142	0.005	0.040	0.090	0.007
1932	0.07	0.33	0.60	0.08	0.448	0.119	0.008	0.036	0.067	0.009
1928	0.06	0.32	0.63	0.07	0.601	0.129	0.007	0.038	0.075	0.010
1927	0.06	0.27	0.67	0.05	0.654	0.115	0.006	0.030	0.073	0.006
1923	0.04	0.26	0.71	0.05	0.672	0.127	0.005	0.031	0.085	0.007
1920	0.03	0.22	0.74	0.05	1.111	0.207	0.006	0.044	0.147	0.010
1912	0.00	0.10	0.89	0.01	2.048	0.236	0.001	0.024	0.209	0.002
1905	0.04	0.29	0.68	0.08	0.494	0.059	0.002	0.016	0.037	0.005
1895	0.03	0.29	0.69	0.05	1.000	0.056	0.001	0.015	0.037	0.003
1881	0.01	0.28	0.72	0.05	0.658	0.046	0.000	0.012	0.031	0.002
1877	0.01	0.24	0.75	0.06	0.588	0.039	0.000	0.009	0.028	0.002
1867	0.01	0.22	0.77	0.06	1.960	0.020	0.000	0.004	0.014	0.001
1829	0.09	0.23	0.68	0.09	0.814	0.011	0.001	0.002	0.007	0.001
1807	0.25	0.26	0.49	0.18	0.339	0.007	0.001	0.002	0.003	0.001
1784	0.27	0.25	0.48	0.20	0.335	0.007	0.001	0.001	0.003	0.001
1765	0.23	0.30	0.47	0.17	0.414	0.009	0.002	0.002	0.003	0.001
1735	0.24	0.36	0.40	0.15	0.514	0.008	0.002	0.002	0.003	0.001
1715	0.22	0.38	0.40	0.11	0.722	0.013	0.003	0.005	0.005	0.001
1685	0.25	0.54	0.22	0.12	0.897	0.016	0.004	0.008	0.003	0.002
1665	0.23	0.48	0.30	0.10	0.793	0.015	0.003	0.006	0.004	0.001
1645	0.22	0.40	0.38	0.09	0.996	0.018	0.004	0.007	0.006	0.002
1624	0.23	0.45	0.31	0.10	0.922	0.018	0.004	0.007	0.005	0.002
1605	0.22	0.35	0.43	0.09	0.853	0.017	0.003	0.005	0.006	0.002
1585	0.21	0.31	0.48	0.09	0.688	0.013	0.003	0.004	0.006	0.001

1575	0.25	0.32	0.43	0.11	0.568	0.013	0.003	0.004	0.005	0.001
1555	0.22	0.40	0.39	0.09	0.742	0.013	0.003	0.005	0.005	0.001
1535	0.27	0.36	0.37	0.12	0.771	0.012	0.003	0.004	0.004	0.001
1515	0.27	0.36	0.37	0.13	0.587	0.010	0.002	0.003	0.003	0.001
1495	0.26	0.35	0.39	0.13	0.566	0.010	0.002	0.003	0.004	0.001
1475	0.28	0.36	0.36	0.15	0.719	0.010	0.002	0.003	0.003	0.002
1445	0.32	0.29	0.39	0.15	0.724	0.009	0.002	0.002	0.003	0.001
1425	0.32	0.33	0.35	0.14	0.709	0.007	0.002	0.002	0.002	0.001
1405	0.33	0.35	0.33	0.14	0.768	0.010	0.003	0.003	0.003	0.001
1385	0.35	0.30	0.35	0.14	0.811	0.011	0.003	0.003	0.003	0.001
1375	0.34	0.30	0.36	0.16	0.643	0.009	0.002	0.002	0.003	0.001
1365	0.32	0.43	0.25	0.15	0.679	0.009	0.002	0.003	0.002	0.001
1355	0.25	0.45	0.29	0.12	0.881	0.012	0.003	0.005	0.003	0.001
1345	0.25	0.47	0.28	0.12	0.817	0.012	0.003	0.005	0.003	0.001
1335	0.27	0.42	0.31	0.13	0.692	0.010	0.002	0.004	0.003	0.001
1325	0.33	0.33	0.35	0.16	0.457	0.007	0.002	0.002	0.002	0.001
1305	0.33	0.37	0.31	0.15	0.751	0.009	0.002	0.003	0.002	0.001
1295	0.33	0.36	0.31	0.15	0.645	0.008	0.002	0.002	0.002	0.001
1285	0.31	0.32	0.38	0.11	0.909	0.010	0.003	0.003	0.003	0.001
1275	0.32	0.33	0.35	0.12	0.934	0.011	0.003	0.003	0.004	0.001
1265	0.33	0.29	0.38	0.11	1.115	0.014	0.004	0.004	0.005	0.001
1255	0.35	0.26	0.39	0.11	1.116	0.016	0.005	0.004	0.005	0.002
1245	0.32	0.29	0.39	0.10	1.151	0.017	0.005	0.004	0.006	0.002
1235	0.30	0.30	0.39	0.10	1.163	0.016	0.005	0.004	0.006	0.002
1225	0.29	0.30	0.41	0.09	1.271	0.018	0.005	0.005	0.007	0.002
1215	0.34	0.29	0.37	0.11	1.273	0.019	0.006	0.005	0.006	0.002
1205	0.30	0.33	0.38	0.11	1.335	0.019	0.005	0.005	0.006	0.002
1195	0.33	0.32	0.35	0.11	1.255	0.019	0.006	0.005	0.006	0.002
1185	0.34	0.33	0.33	0.11	1.226	0.019	0.006	0.006	0.006	0.002
1175	0.33	0.33	0.35	0.11	1.197	0.019	0.006	0.006	0.006	0.002
1165	0.30	0.37	0.32	0.10	1.281	0.018	0.005	0.006	0.005	0.002
1155	0.28	0.42	0.30	0.10	1.324	0.019	0.005	0.007	0.005	0.002
1145	0.23	0.40	0.37	0.11	1.085	0.018	0.004	0.006	0.006	0.002
1135	0.30	0.37	0.32	0.11	1.185	0.015	0.004	0.005	0.004	0.002
1125	0.32	0.35	0.33	0.11	1.165	0.015	0.004	0.005	0.004	0.002
1115	0.32	0.34	0.33	0.11	1.158	0.017	0.005	0.005	0.005	0.002
1105	0.32	0.35	0.33	0.11	1.164	0.017	0.005	0.005	0.005	0.002
1095	0.32	0.35	0.33	0.11	1.120	0.018	0.005	0.005	0.005	0.002
1085	0.29	0.35	0.36	0.11	1.080	0.016	0.004	0.005	0.005	0.002
1075	0.34	0.33	0.32	0.11	1.030	0.014	0.004	0.004	0.004	0.002

Table A.3 Deming Lake freeze core sedimentary parameters

Year CE	Organic flux ($g/cm^2/yr$)	Mineral flux ($g/cm^2/yr$)	$\delta^{13}C$ (‰)	TC (%)	$\chi_{ARM}/IRM_{0.2T}$ (mm/A)
2005	0.006	0.016	-31.5	12.6	2.04
2002	0.010	0.041	-28.6	9.6	1.78
1999	0.009	0.039	-28.5	9.7	1.84
1998	0.007	0.028	-28.5	9.8	1.90
1995	0.006	0.016	-28.6	14.0	1.90
1993	0.007	0.013	-29.1	17.6	1.89
1991	0.007	0.011	-28.6	19.0	1.92
1989	0.007	0.012	-28.6	18.6	1.95
1987	0.006	0.011	-28.6	17.8	1.88
1985	0.007	0.010	-28.9	21.0	1.80
1983	0.007	0.011	-28.6	20.1	1.67
1981	0.008	0.010	-29.0	21.1	1.66
1979	0.007	0.010	-28.3	20.7	1.64
1976	0.005	0.007	-28.8	20.0	1.62
1972	0.004	0.005	-28.8	22.3	1.51
1968	0.004	0.010	-29.2	14.5	1.34
1964	0.007	0.010	-29.3	21.0	1.50
1960	0.010	0.014	-28.6	20.5	1.64
1957	0.015	0.023	-27.9	20.0	1.69
1953	0.005	0.008	-28.1	18.6	1.65
1950	0.005	0.009	-27.4	17.4	1.63
1947	0.005	0.009	-27.2	18.6	1.61
1944	0.006	0.011	-28.4	17.5	1.79
1941	0.006	0.011	-27.7	16.9	1.72
1939	0.006	0.010	-27.5	19.2	1.86
1936	0.005	0.008	-28.3	20.2	1.98
1933	0.005	0.006	-29.3	22.7	1.96
1930	0.006	0.007	-29.3	22.2	1.95
1927	0.006	0.009	-29.4	18.6	1.78
1925	0.006	0.008	-29.3	21.5	1.59
1922	0.006	0.008	NA	20.8	1.75
1919	0.005	0.006	NA	NA	1.91
1916	0.005	0.004	NA	26.5	2.01
1913	0.004	0.005	-30.0	22.7	2.04
1910	0.005	0.005	-29.8	23.4	1.99
1907	0.004	0.004	-29.8	25.9	1.95
1903	0.004	0.003	-29.7	27.2	2.10
1899	0.004	0.003	-29.9	29.3	2.11
1894	0.004	0.003	-29.7	28.2	2.18
1890	0.004	0.003	-30.1	28.9	2.25
1885	0.003	0.002	-30.4	29.8	2.23
1881	0.004	0.002	-30.8	31.8	2.22
1876	0.004	0.002	-30.3	32.0	2.16
1872	0.004	0.002	-30.5	31.7	2.08
1867	0.004	0.002	-31.4	33.0	2.07
1863	0.004	0.002	-32.0	33.5	2.12
1858	0.003	0.001	-31.0	34.3	2.08
1854	0.003	0.002	-30.6	33.5	2.03
1850	0.004	0.002	-30.5	34.2	2.16

1845	0.003	0.001	-30.4	34.5	2.11
1841	0.003	0.002	-30.2	32.3	2.02
1836	0.003	0.001	-30.9	32.9	1.93
1829	0.002	0.001	-31.4	32.2	2.01
1823	0.003	0.001	-31.6	31.9	2.04
1817	0.004	0.002	-30.0	32.1	2.11
1814	0.002	0.001	-30.2	34.2	2.19
1804	0.003	0.001	-30.6	33.8	2.23
1797	0.002	0.001	-31.8	34.3	2.20
1789	0.002	0.001	-31.9	32.9	2.12
1782	0.002	0.001	-32.2	33.7	2.05
1774	0.002	0.001	-32.1	34.9	2.12
1766	0.002	0.001	-32.3	33.9	2.13
1759	0.003	0.001	-32.3	35.1	2.28
1751	0.003	0.001	-32.4	35.0	2.17
1744	0.003	0.001	-31.5	32.7	2.18
1736	0.002	0.001	-31.7	33.2	2.19
1729	0.003	0.001	-31.8	33.7	2.06
1721	0.003	0.002	-30.7	32.8	2.12
1713	0.004	0.002	-31.2	34.0	2.19
1706	0.003	0.001	-31.2	33.9	2.28
1698	0.002	0.001	-31.3	30.4	1.94
1691	0.004	0.003	-30.2	29.4	2.12
1683	0.002	0.002	-29.9	25.0	1.97
1676	0.003	0.003	-30.2	26.1	1.92
1668	0.002	0.002	-30.1	25.1	1.88
1660	0.003	0.003	-30.3	25.2	1.92
1653	0.003	0.003	-29.4	25.1	1.91
1645	0.003	0.003	-30.2	25.4	1.93
1638	0.002	0.003	-30.9	23.7	1.93
1630	0.002	0.002	-31.2	24.8	1.84
1623	0.003	0.002	-31.1	25.4	1.85
1615	0.003	0.003	-31.1	24.7	1.85
1607	0.002	0.002	-30.4	25.4	1.92
1600	0.003	0.002	-30.2	26.8	1.91
1592	0.002	0.003	-31.1	22.3	1.85
1585	0.002	0.003	-31.3	22.7	1.89
1577	0.003	0.003	-31.7	24.0	1.86
1570	0.003	0.003	-31.9	24.8	1.85
1562	0.003	0.003	-31.6	22.9	1.90
1555	0.003	0.003	-31.1	23.7	1.88
1547	0.003	0.003	-30.4	25.7	1.87
1539	0.002	0.002	-28.9	25.7	1.93
1532	0.002	0.002	-28.8	26.8	1.69
1524	0.002	0.002	-29.3	27.3	1.97
1517	0.002	0.002	-29.3	26.0	1.80
1509	0.002	0.002	-29.4	25.0	1.91
1502	0.003	0.003	-29.3	24.6	1.91
1494	0.003	0.003	-29.2	23.1	1.91
1486	0.002	0.003	-29.1	23.3	1.91
1479	0.002	0.002	-29.7	24.7	1.94
1471	0.002	0.003	-30.8	23.5	1.90
1464	0.003	0.003	-30.8	24.0	1.88
1456	0.003	0.003	-31.5	23.1	1.77
1449	0.003	0.003	-30.7	23.9	1.80

1441	0.003	0.003	-30.1	23.9	1.80
1433	0.002	0.002	-29.1	24.6	1.88
1426	0.002	0.002	-29.1	24.8	1.79
1418	0.002	0.002	-28.8	24.3	1.87
1411	0.002	0.002	-28.8	25.3	1.74
1403	0.002	0.003	-28.3	22.9	1.85
1396	0.002	0.003	-30.0	21.8	1.77
1388	0.003	0.004	-30.2	21.3	1.79
1380	0.002	0.003	-27.8	21.5	1.76
1373	0.002	0.003	-27.8	23.8	1.67
1365	0.002	0.002	-28.8	24.3	1.71
1358	0.002	0.003	-28.8	23.8	1.68
1350	0.002	0.002	-28.8	24.4	1.82
1343	0.002	0.002	-28.6	25.8	1.81
1335	0.002	0.003	-28.6	19.8	1.57
1328	0.003	0.002	-28.9	26.0	1.79
1320	0.002	0.002	-27.8	24.9	1.95
1312	0.002	0.002	-27.8	26.1	1.96
1305	0.002	0.003	-27.9	23.8	1.97
1297	0.002	0.002	-28.5	25.5	1.88
1290	0.002	0.002	-28.8	26.6	1.94
1282	0.002	0.002	-29.0	25.5	1.95
1275	0.002	0.002	-29.1	24.4	1.95
1267	0.002	0.002	-29.0	24.2	2.14
1259	0.002	0.003	-29.1	23.3	1.94
1252	0.002	0.003	-29.6	23.6	1.84
1244	0.002	0.003	-29.8	23.5	1.70
1237	0.002	0.003	-29.4	22.2	1.59
1229	0.003	0.004	-29.9	20.4	1.45
1222	0.003	0.005	-30.3	17.6	1.47
1214	0.003	0.005	-31.0	17.9	1.51
1206	0.003	0.005	-30.7	17.9	1.64
1199	0.003	0.004	-29.8	18.7	1.39
1191	0.002	0.003	-29.5	20.6	1.51
1184	0.003	0.006	-31.7	17.7	1.34
1173	0.008	0.012	-30.0	18.6	1.41
1161	0.003	0.005	-29.5	19.8	1.71
1150	0.003	0.007	-30.7	14.1	1.50
1136	0.003	0.053	-28.5	1.8	0.60
1124	0.004	0.009	-31.8	19.2	1.32
1111	0.004	0.004	-30.7	23.1	1.55
1098	0.004	0.005	-30.4	21.7	1.22
1086	0.004	0.004	-29.5	26.3	1.49
1075	0.004	0.003	-31.2	27.2	1.66
1063	0.004	0.003	-30.9	27.9	1.78
1051	0.004	0.006	-32.4	22.6	1.43
1041	0.010	0.006	-31.7	19.3	1.58
1031	0.007	0.004	-30.4	19.0	1.47
1020	0.004	0.003	-29.3	29.4	1.79
1010	0.004	0.002	-30.5	31.7	1.98

Table A.4 Deming Lake piston core ferrimagnetic fractions and fluxes

Year CE	ϕ_{ferri} (mg/cm^2/ year)	ϕ_{UNISD} (mg/cm^2/ year)	ϕ_{ISD} (mg/cm^2/ year)	ϕ_{MD} (mg/cm^2/ year)	ϕ_{SP} (mg/cm^2/ year)	g_{UNISD}	g_{ISD}	g_{MD}	f_{SP}
2005	0.006790	0.002139	0.002307	0.002249	0.000095	0.32	0.34	0.33	0.01
2002	0.002777	0.000834	0.000903	0.000944	0.000096	0.30	0.33	0.34	0.03
1993	0.002660	0.000834	0.000865	0.000865	0.000097	0.31	0.32	0.33	0.04
1987	0.004080	0.000995	0.001096	0.001862	0.000127	0.24	0.27	0.46	0.03
1982	0.004263	0.000795	0.000758	0.002597	0.000113	0.19	0.18	0.61	0.03
1976	0.004679	0.000575	0.000988	0.002998	0.000118	0.12	0.21	0.64	0.03
1964	0.003933	0.000359	0.000896	0.002618	0.000061	0.09	0.23	0.67	0.02
1953	0.003197	0.000445	0.000829	0.001847	0.000075	0.14	0.26	0.58	0.02
1946	0.005557	0.000615	0.001239	0.003586	0.000117	0.11	0.22	0.65	0.02
1939	0.004748	0.000578	0.001200	0.002865	0.000104	0.12	0.25	0.60	0.02
1933	0.003438	0.000730	0.000962	0.001631	0.000115	0.21	0.28	0.47	0.03
1922	0.001654	0.000292	0.000499	0.000799	0.000064	0.18	0.30	0.48	0.04
1911	0.001186	0.000276	0.000348	0.000500	0.000063	0.23	0.29	0.42	0.05
1898	0.001040	0.000268	0.000230	0.000476	0.000066	0.26	0.22	0.46	0.06
1885	0.001065	0.000322	0.000359	0.000316	0.000068	0.30	0.34	0.30	0.06
1872	0.000649	0.000220	0.000228	0.000147	0.000054	0.34	0.35	0.23	0.08
1858	0.000518	0.000188	0.000192	0.000091	0.000047	0.36	0.37	0.18	0.09
1845	0.000374	0.000135	0.000062	0.000138	0.000038	0.36	0.17	0.37	0.10
1831	0.000320	0.000126	0.000055	0.000103	0.000036	0.39	0.17	0.32	0.11
1818	0.000404	0.000150	0.000101	0.000112	0.000041	0.37	0.25	0.28	0.10
1804	0.000225	0.000093	0.000045	0.000052	0.000034	0.42	0.20	0.23	0.15
1781	0.000232	0.000071	0.000072	0.000066	0.000023	0.30	0.31	0.28	0.10
1758	0.000208	0.000077	0.000055	0.000052	0.000024	0.37	0.27	0.25	0.12
1734	0.000272	0.000096	0.000093	0.000057	0.000025	0.35	0.34	0.21	0.09
1711	0.000257	0.000081	0.000101	0.000050	0.000025	0.31	0.39	0.19	0.10
1691	0.000324	0.000082	0.000101	0.000114	0.000027	0.25	0.31	0.35	0.08
1665	0.000360	0.000081	0.000156	0.000097	0.000025	0.23	0.43	0.27	0.07
1642	0.000487	0.000101	0.000236	0.000126	0.000025	0.21	0.48	0.26	0.05
1620	0.000567	0.000122	0.000265	0.000153	0.000028	0.22	0.47	0.27	0.05
1596	0.000816	0.000112	0.000258	0.000422	0.000024	0.14	0.32	0.52	0.03
1576	0.000586	0.000105	0.000304	0.000150	0.000027	0.18	0.52	0.26	0.05
1554	0.000768	0.000094	0.000522	0.000128	0.000025	0.12	0.68	0.17	0.03
1533	0.000274	0.000062	0.000139	0.000053	0.000021	0.22	0.51	0.19	0.08
1510	0.000161	0.000040	0.000057	0.000047	0.000017	0.25	0.36	0.29	0.11
1487	0.000321	0.000057	0.000124	0.000121	0.000019	0.18	0.39	0.38	0.06
1464	0.000278	0.000047	0.000103	0.000108	0.000020	0.17	0.37	0.39	0.07
1442	0.000487	0.000072	0.000243	0.000153	0.000019	0.15	0.50	0.31	0.04
1418	0.000369	0.000055	0.000191	0.000106	0.000016	0.15	0.52	0.29	0.04
1395	0.000498	0.000059	0.000245	0.000176	0.000018	0.12	0.49	0.35	0.04
1372	0.000473	0.000066	0.000196	0.000193	0.000018	0.14	0.41	0.41	0.04
1349	0.000432	0.000049	0.000139	0.000228	0.000016	0.11	0.32	0.53	0.04
1327	0.000379	0.000073	0.000148	0.000139	0.000020	0.19	0.39	0.37	0.05
1304	0.000370	0.000067	0.000138	0.000146	0.000019	0.18	0.37	0.40	0.05
1280	0.000267	0.000045	0.000081	0.000124	0.000018	0.17	0.30	0.46	0.07
1260	0.000398	0.000065	0.000132	0.000183	0.000019	0.16	0.33	0.46	0.05
1238	0.000911	0.000078	0.000251	0.000561	0.000022	0.09	0.28	0.62	0.02
1215	0.001078	0.000080	0.000280	0.000695	0.000023	0.07	0.26	0.64	0.02
1191	0.000834	0.000080	0.000215	0.000520	0.000020	0.10	0.26	0.62	0.02

1169	0.000635	0.000075	0.000192	0.000348	0.000020	0.12	0.30	0.55	0.03
1145	0.008550	0.000126	0.001177	0.007218	0.000030	0.01	0.14	0.84	0.00
1131	0.001894	0.000083	0.000281	0.001509	0.000021	0.04	0.15	0.80	0.01
1107	0.000647	0.000040	0.000305	0.000287	0.000015	0.06	0.47	0.44	0.02
1086	0.000708	0.000071	0.000263	0.000356	0.000018	0.10	0.37	0.50	0.03
1064	0.000448	0.000076	0.000182	0.000170	0.000021	0.17	0.41	0.38	0.05
1038	0.000819	0.000100	0.000295	0.000400	0.000024	0.12	0.36	0.49	0.03
1015	0.000892	0.000076	0.000202	0.000593	0.000021	0.09	0.23	0.66	0.02

Table A.5 Birch Lake transect data

Dist. from SE shore (m)	Depth (m)	Org (%)	Carb. (%)	Inorg. (%)	χ (10^{-7} m^3/kg)	$IRM_{0.2T}$ (10^{-3} Am^2/kg)	ARM (10^{-3} Am^2/kg)	χ_{ARM}/IRM (mm/A)	Clay (%)	Silt (%)	Sand (%)
0	0.7	2	4	94	4.7	0.9	0.0	0.6	1	4	95
20	1.3	2	5	93	2.5	0.8	0.1	0.8	0	0	100
36	1.9	22	13	64	3.5	1.5	0.2	1.7	14	49	37
56	2.9	29	10	62	3.1	1.9	0.3	2.3	17	54	29
94	3.9	40	8	52	3.0	2.7	0.5	2.3	22	61	17
114	4.7	42	6	52	3.6	4.2	0.8	2.4	29	71	0
132	6.3	40	6	54	3.5	3.9	0.7	2.4	23	59	17
185	6.9	37	6	56	3.9	5.5	1.1	2.5	22	66	12
340	6.0	37	7	56	3.6	4.6	0.9	2.5	27	64	8
369	4.8	36	7	57	3.4	4.4	0.9	2.4	26	65	9
390	4.0	37	7	55	4.4	5.5	1.1	2.4	23	64	13
468	3.0	41	11	48	4.4	4.6	0.9	2.4	26	66	8
538	1.7	35	18	47	2.2	1.7	0.3	2.0	23	72	5
629	1.2	51	7	42	1.9	1.5	0.3	2.2	30	66	4
716	1.0	46	5	49					28	65	7
Dist. from W shore (m)											
15	0.9	13	11	76	2.4	1.3	0.1	1.0	20	60	20
47	1.6	35	34	31	1.8	1.7	0.3	2.2	36	63	1
77	2.0	30	36	33	1.9	2.0	0.4	2.2	25	68	7
122	3.2	43	7	50	3.3	3.3	0.7	2.5	25	64	11
140	4.1	37	6	57	4.0	6.0	1.2	2.5	24	63	14
194	4.9	36	7	57	3.7	4.7	0.9	2.4	26	66	9
226	5.9	35	7	58	3.7	4.8	0.9	2.4	22	61	18
245	6.7	38	6	56	3.4	4.4	0.9	2.5	25	64	11
321	7.8	35	7	58	4.2	5.4	1.1	2.6	28	67	5
368	8.2	37	6	57	4.8	6.7	1.4	2.6	30	65	6
513	7.0	42	6	53	3.1	3.8	0.7	2.4	32	62	6
521	6.3	42	5	52	4.5	4.3	0.8	2.4	28	67	5
535	5.0	53	4	43	2.5	2.7	0.5	2.5	23	60	17
556	3.8	53	4	43	3.2	2.4	0.5	2.6	19	49	33
570	3.0	30	12	57	3.5	2.1	0.3	2.0	14	42	44
589	1.7	5	7	88	7.3	1.4	0.1	0.8	3	8	90
604	0.9	2	4	94	10.8	1.8	0.1	0.5	3	4	93

Table A.6 Deming Lake transect data

Dist. from NW shore (m)	Depth (m)	Org (%)	Carb. (%)	Inorg. (%)	χ (10^{-7} m^3/kg)	$IRM_{0.2T}$ (10^{-3} Am^2/kg)	ARM (10^{-3} Am^2/kg)	χ_{ARM}/IRM (mm/A)	Clay (%)	Silt (%)	Sand (%)
0	0.5	16	1	83	0.8	0.4	0.1	2.5	17	44	38
20	1.0	13	1	86	0.7	0.6	0.1	2.2	8	29	63
31	2.0	29	2	69	1.8	1.2	0.2	2.6	16	69	15
50	3.3	14	2	84	2.6	1.3	0.2	1.9	12	65	23
72	4.0	16	2	81	3.6	2.4	0.3	1.5	15	69	16
82	5.0	22	2	76	1.9	1.4	0.2	2.1	19	65	15
93	6.0	43	3	54	2.1	1.5	0.3	2.1	22	67	11
106	7.0	22	4	73	1.8	1.2	0.2	1.7	17	63	20
112	8.0	25	5	70	2.2	1.8	0.2	1.6	33	63	4
116	9.0	20	6	74	1.4	0.9	0.1	1.7	24	69	7
120	10.0	23	7	70	1.7	1.3	0.2	1.7	26	67	7
132	11.0	25	5	70	5.5	4.1	0.4	1.1	20	69	11
136	12.0	19	5	76	1.4	1.2	0.2	1.9	19	58	24
151	13.0	35	7	58	1.7	1.2	0.2	1.9	32	66	3
154	14.0	42	7	51	2.0	1.5	0.2	2.0	33	66	1
158	15.0	40	7	53	2.5	1.8	0.3	1.9	31	67	2
164	16.0	40	7	53	2.2	1.6	0.2	1.7	32	67	2
193	17.0	28	6	66	2.7	2.4	0.3	1.6	22	71	7
204	16.0	32	7	62	2.0	1.4	0.2	1.9	21	72	7
208	15.0	18	5	76	1.2	0.8	0.1	1.8	24	73	3
213	14.2	29	7	64	2.0	1.6	0.2	1.9	28	69	3
216	12.8	28	7	65	1.4	1.0	0.2	2.1	29	68	2
220	12.0	22	6	72	1.7	1.4	0.2	1.8	24	73	3
222	10.8	43	8	49	3.4	2.6	0.4	1.8	29	69	2
226	10.2	43	8	48	2.2	1.5	0.2	1.7	29	69	2
230	9.0	11	4	86	0.5	0.5	0.1	1.7	23	72	5
235	7.5	43	7	50	2.1	1.6	0.3	2.0	28	69	3
242	7.0	11	5	84	0.3	0.2	0.0	2.6	28	71	1
247	6.1	35	6	59	1.7	1.4	0.2	2.2	23	74	3
252	5.0	41	7	52	1.7	1.2	0.3	2.6	27	71	1
267	3.8	43	5	52	2.2	1.8	0.4	2.8	24	74	2
273	3.3	34	22	44	1.9	1.4	0.3	2.8	25	75	0
280	2.0	24	3	73	1.5	1.0	0.2	2.5	16	70	14
290	1.0	3	1	96	0.6	0.4	0.1	1.7	2	9	89
299	0.5	2	1	97	0.5	0.2	0.0	2.3	4	11	85
303	0.2	5	1	94	3.4	0.9	0.1	1.0	2	9	89

Table A.6 –continued

Dist. from NE shore (m)	Depth (m)	Org (%)	Carb. (%)	Inorg. (%)	χ (10^{-7} m^3/kg)	$IRM_{0.2T}$ (10^{-3} Am^2/kg)	ARM (10^{-3} Am^2/kg)	χ_{ARM}/IRM (mm/A)	Clay (%)	Silt (%)	Sand (%)
0	0.3	10	1	90	0.7	0.4	0.1	2.2	13	41	46
6	1.0	2	1	97	0.6	0.3	0.1	2.4	9	32	59
9	2.0	39	3	58	1.9	1.5	0.3	2.9	18	70	13
23	3.0	41	3	56	2.1	1.5	0.3	3.0	21	74	5
34	4.0	36	4	60	1.7	1.3	0.3	2.5	25	72	3
39	4.8	37	4	59	1.9	1.3	0.2	2.3	25	71	4
47	6.0	43	4	53	1.8	1.5	0.3	2.2	27	71	2
51	7.0	28	4	68	2.0	1.3	0.2	1.8	24	73	3
56	8.0	39	5	56	2.5	2.1	0.3	2.0	27	71	2
58	8.9	41	5	54	2.6	2.1	0.3	2.1	26	73	1
64	10.0	27	5	68	2.3	1.6	0.2	1.7	29	69	2
73	11.0	28	5	67	2.6	1.8	0.2	1.7	27	71	2
77	12.0	41	6	52	3.7	3.9	0.6	2.0	31	66	2
80	13.0	40	6	54	3.8	3.9	0.6	2.0	31	66	3
84	14.0	28	5	67	2.3	1.9	0.3	1.9	28	69	3
87	15.0	34	6	60	3.8	3.4	0.5	1.9	31	66	2
91	16.0	39	6	55	3.1	3.0	0.5	2.0	29	67	5
105	16.8	28	6	66	3.3	3.0	0.4	1.8	22	72	6
110	16.0	34	7	58	3.7	3.6	0.6	1.9	30	68	3
115	15.0	28	6	65	3.1	2.7	0.4	1.8	26	71	3
117	13.8	33	6	61	3.1	2.8	0.4	1.9	29	71	0
125	13.0	32	5	63	2.9	2.1	0.3	1.7	25	72	3
128	12.0	21	5	74	2.5	2.0	0.3	1.6	25	72	3
130	11.0	32	6	62	3.0	2.4	0.4	1.8	27	70	3
137	10.0	43	6	51	3.0	2.6	0.4	2.1	32	67	2
139	9.0	46	6	48	2.6	1.9	0.3	2.2	31	67	2
144	7.8	26	5	69	2.3	1.9	0.3	1.8	30	69	2
148	6.9	30	5	65	2.8	2.2	0.3	1.7	30	69	2
154	6.0	43	5	51	2.2	1.7	0.3	2.4	29	69	2
165	5.2	46	5	49	3.7	3.3	0.5	2.1	29	69	2
180	4.1	48	5	48	2.3	1.9	0.4	2.8	29	68	3
198	3.0	56	4	40	2.6	2.0	0.5	3.1	30	69	2
229	2.0	53	4	43	2.5	2.1	0.5	3.1	27	71	2
256	1.0	16	1	82	0.7	0.5	0.1	2.5	9	39	53
262	0.3	6	1	94	0.7	0.3	0.1	2.5	7	29	64

Table A.7 Elkhorn Lake transect data

Dist. from SW shore (m)	Depth (m)	Org (%)	Carb. (%)	Inorg. (%)	χ (10^{-7} m^3/kg)	$IRM_{0.2T}$ (10^{-3} Am^2/kg)	ARM (10^{-3} Am^2/kg)	χ_{ARM}/IRM (mm/A)	Clay (%)	Silt (%)	Sand (%)
0	0.2	1			1.7	0.7	0.0	0.6	12	20	68
14	1.0	13	55	32	2.2	1.4	0.1	0.8	10	48	42
49	1.8	11	73	16	0.4	0.3	0.0	1.2	16	65	19
68	2.8	13	66	21	0.5	0.3	0.0	1.1	15	55	30
78	3.9	16	58	26	0.6	0.2	0.0	1.2	9	72	18
83	4.9	9	76	15	0.4	0.2	0.0	1.2	14	63	23
97	6.2	15	58	27	1.1	0.6	0.0	1.0	13	59	28
108	6.9	16	53	31	1.0	0.6	0.0	0.9	18	70	12
131	8.0	16	45	39	0.9	0.4	0.0	0.9	21	71	8
148	8.9	16	42	41	1.3	0.4	0.0	0.9	20	65	15
159	10.0	16	40	44	1.0	0.3	0.0	0.8	22	68	10
192	11.0	16	39	45	1.1	0.4	0.0	0.8	24	71	5
382	10.0	16	41	44	1.0	0.4	0.0	0.9	23	73	5
441	9.3	19	43	38	1.4	0.5	0.0	0.9	24	71	5
511	8.0	17	43	40	1.0	0.3	0.0	1.0	19	62	19
554	7.2	18	45	37	1.1	0.4	0.0	1.0	22	72	6
595	6.0	17	53	31	1.1	0.4	0.0	1.0			
599	5.3	16	57	27	0.7	0.3	0.0	1.0	12	58	30
614	3.9	14	68	18	0.9	0.4	0.0	1.3	13	81	6
629	3.1	18	61	22	0.6	0.2	0.0	1.4			
646	2.2	11	74	15	0.4	0.1	0.0	1.3	14	78	8
661	1.0	7	83	10	0.6	0.2	0.0	1.2	19	75	6
696	0.3	1	14	85	0.0	0.0	0.0	1.5	0	2	98
Dist. from NW shore (m)											
0	0.3	1	24	75	7.7	2.4	0.1	0.6	19	32	50
6	1.1	2	22	77	6.7	3.8	0.1	0.3	14	18	68
16	2.0	6	35	59	2.7	2.1	0.1	0.5	6	20	73
21	3.0	13	56	30	0.7	0.4	0.0	1.0	15	64	21
34	4.2	12	61	27	0.4	0.3	0.0	1.1	11	59	30
41	5.2	13	62	25	1.3	0.7	0.1	0.9	7	36	58
52	6.0	14	57	30	1.0	0.6	0.0	1.0	9	59	32
71	7.1	19	45	35	1.1	0.8	0.1	1.1	17	75	8
96	8.1	17	43	39	0.9	0.5	0.0	1.0	17	76	7
107	9.0	17	43	40	1.0	0.6	0.0	1.0	16	75	9
118	10.0	16	41	43	0.6	0.4	0.0	0.9	22	73	5
365	9.8	15	44	41	0.8	0.5	0.0	0.9	23	69	8
384	8.9	15	48	38	1.0	0.6	0.1	1.0	21	73	6
399	7.9	14	50	36	0.8	0.6	0.0	1.0	23	68	9
413	6.9	14	54	32	0.7	0.5	0.0	1.0	21	64	15
419	6.1	9	70	21	0.7	0.6	0.0	1.0	13	49	39
428	5.0	8	77	15	0.3	0.2	0.0	1.2	20	64	16
432	4.2	8	74	18	0.3	0.1	0.0	1.2	17	63	20
438	3.0	7	73	19	0.3	0.1	0.0	1.2	13	50	37
447	2.1	10	74	16	0.5	0.4	0.0	1.0	17	61	22

468	1.0	1	16	83	0.1	0.1	0.0	1.0	3	11	86
479	0.4	1	33	67	0.6	0.4	0.0	0.9			
58	8.9	41	5	54	2.6	2.1	0.3	2.1	26	73	1
64	10.0	27	5	68	2.3	1.6	0.2	1.7	29	69	2
73	11.0	28	5	67	2.6	1.8	0.2	1.7	27	71	2
77	12.0	41	6	52	3.7	3.9	0.6	2.0	31	66	2
80	13.0	40	6	54	3.8	3.9	0.6	2.0	31	66	3
84	14.0	28	5	67	2.3	1.9	0.3	1.9	28	69	3
87	15.0	34	6	60	3.8	3.4	0.5	1.9	31	66	2
91	16.0	39	6	55	3.1	3.0	0.5	2.0	29	67	5
105	16.8	28	6	66	3.3	3.0	0.4	1.8	22	72	6
110	16.0	34	7	58	3.7	3.6	0.6	1.9	30	68	3
115	15.0	28	6	65	3.1	2.7	0.4	1.8	26	71	3
117	13.8	33	6	61	3.1	2.8	0.4	1.9	29	71	0
125	13.0	32	5	63	2.9	2.1	0.3	1.7	25	72	3
128	12.0	21	5	74	2.5	2.0	0.3	1.6	25	72	3
130	11.0	32	6	62	3.0	2.4	0.4	1.8	27	70	3
137	10.0	43	6	51	3.0	2.6	0.4	2.1	32	67	2
139	9.0	46	6	48	2.6	1.9	0.3	2.2	31	67	2
144	7.8	26	5	69	2.3	1.9	0.3	1.8	30	69	2
148	6.9	30	5	65	2.8	2.2	0.3	1.7	30	69	2
154	6.0	43	5	51	2.2	1.7	0.3	2.4	29	69	2
165	5.2	46	5	49	3.7	3.3	0.5	2.1	29	69	2
180	4.1	48	5	48	2.3	1.9	0.4	2.8	29	68	3
198	3.0	56	4	40	2.6	2.0	0.5	3.1	30	69	2
229	2.0	53	4	43	2.5	2.1	0.5	3.1	27	71	2
256	1.0	16	1	82	0.7	0.5	0.1	2.5	9	39	53
262	0.3	6	1	94	0.7	0.3	0.1	2.5	7	29	64

Table A.8 Erie Lake transect data

Dist. from NW shore (m)	Depth (m)	Org (%)	Carb. (%)	Inorg. (%)	χ (10^{-7} m^3/kg)	$IRM_{0.2T}$ (10^{-3} Am^2/kg)	ARM (10^{-3} Am^2/kg)	χ_{ARM}/IRM (mm/A)	Clay (%)	Silt (%)	Sand (%)
0	0.4	0	2	97	3.6	2.1	0.1	0.3	3	5	92
1	1.0	1	5	94	8.3	1.4	0.1	0.5	1	3	96
19	2.0	1	3	97	6.1	1.3	0.1	0.5	2	6	92
41	3.1	2	10	88	3.1	1.0	0.1	1.1			
57	3.7	18	21	62	4.9	2.9	0.4	1.8			
86	5.1	19	18	64	4.1	4.1	0.8	2.3	13	66	21
117	6.0	20	19	61	4.0	4.5	0.8	2.2			
146	6.9	20	16	64	5.0	5.8	1.0	2.2			
321	8.1	24	12	63	4.5	5.6	1.0	2.3	25	69	5
509	9.4	23	14	62	4.6	5.9	1.0	2.2	29	70	1
652	8.3	26	13	61	3.8	4.9	0.9	2.4	27	70	3
779	7.1	19	16	65	1.2	1.3	0.3	2.5	18	64	19
819	6.1	1	58	41	9.0	2.0	0.1	0.5			
1081	4.9	20	17	63	4.6	4.9	0.9	2.3			
1290	6.1	20	23	57	3.1	3.2	0.5	1.9	17	67	16
1312	5.0	23	20	57	5.1	3.6	0.6	2.1			
1327	3.8	4	7	88	2.7	1.0	0.1	1.1	3	11	86
1339	3.0	1	4	95	2.7	0.9	0.1	0.9			
1359	1.9	1	3	97	3.1	0.9	0.1	0.7			
1379	1.0	1	3	96	2.6	0.9	0.1	0.8	1	4	95
1384	0.5	1	6	93	2.3	0.7	0.0	0.7	38	58	4
Dist. from SW shore (m)											
0	0.1	1	20	79	34.1	3.5	0.1	0.3	39	53	8
7	1.0	1	14	85	9.2	1.2	0.1	0.5	9	22	69
19	1.8	1	3	97	6.8	1.0	0.1	0.7	2	5	93
25	3.0	1	2	97	3.8	0.9	0.1	0.7	1	3	95
35	4.1	7	17	75	3.2	1.2	0.1	1.1			
46	4.8	11	22	67	4.6	2.5	0.3	1.5			
64	6.1	20	20	59	3.3	3.4	0.6	2.2	22	63	15
99	7.1	23	18	59	5.6	6.6	1.2	2.2	27	68	6
127	7.7	27	15	58	6.0	7.1	1.3	2.4	26	67	7
243	7.0	2	19	80	7.0	2.1	0.1	0.6	10	19	71
359	6.1	1	23	77	18.4	6.0	0.2	0.4			
456	4.8	1	19	80	5.8	4.4	0.1	0.2	12	15	73
486	6.0	20	15	65	5.3	5.6	0.9	2.0	26	68	6
528	7.0	21	16	64	6.9	7.6	1.2	1.9	25	70	5
566	8.0	20	17	63	4.5	4.8	0.6	1.5	28	69	3
604	6.9	18	18	63	3.2	3.0	0.4	1.7	26	70	4
624	6.0	18	20	61	2.9	2.7	0.4	1.7	25	69	6
655	5.0	18	22	60	3.6	3.4	0.5	1.9	19	74	7
672	4.0	18	29	54	3.0	1.8	0.3	1.8	10	48	42
702	3.1	17	26	57	3.0	1.4	0.2	1.5	17	61	23
715	1.9	6	19	75	3.8	1.3	0.1	0.8			
726	1.0	1	5	95	5.2	1.2	0.1	0.5	1	4	95
736	0.3	1	9	90	22.1	2.7	0.1	0.3	9	20	71

Table A.9 Linka Lake transect data

Dist. from NE shore (m)	Depth (m)	Org (%)	Carb. (%)	Inorg. (%)	χ (10^{-7} m^3/kg)	$IRM_{0.2T}$ (10^{-3} Am^2/kg)	ARM (10^{-3} Am^2/kg)	χ_{ARM}/IRM (mm/A)	Clay (%)	Silt (%)	Sand (%)
0	0.1	1	7	92	5.8	1.2	0.0	0.0	0	0	100
13	1.0	1	6	93	4.2	1.1	0.1	0.0	2	3	95
68	2.0	10	48	43	1.4	1.1	0.1	0.1	14	60	26
80	3.1	9	58	33	0.9	0.4	0.0	0.1	12	44	44
83	4.1	10	56	34	0.5	0.2	0.0	0.1	12	58	29
96	5.2	10	49	41	1.1	0.4	0.0	0.1	10	54	36
99	6.1	4	60	35	2.9	1.3	0.1	0.1	5	19	76
118	7.2	12	39	49	3.9	2.4	0.2	0.1	9	52	39
157	8.2	13	51	36	5.7	4.7	0.5	1.3	11	65	25
188	9.2	15	49	36	7.0	5.8	0.6	1.2	14	69	18
215	10.2	14	52	34	3.9	3.1	0.3	1.2	11	62	27
243	11.0	15	44	41	5.0	3.9	0.3	1.1	16	71	13
282	11.9	15	40	44	4.3	3.4	0.3	1.0	14	69	17
323	12.8	15	43	42	4.3	3.3	0.3	1.1	16	72	12
448	12.9	15	40	45	4.2	2.7	0.2	1.0			
589	12.0	15	43	42	2.9	2.1	0.2	1.1	16	66	18
789	10.9	14	42	44	5.7	3.6	0.3	1.0	11	56	33
811	10.0	12	44	44	5.4	2.5	0.2	1.0	6	31	64
835	8.9	3	14	83	3.8	1.0	0.1	0.8	1	3	95
840	8.0	2	11	87	2.5	1.0	0.1	0.8	0	0	100
843	7.0	1	11	88	1.7	0.6	0.0	1.0	0	1	99
849	6.1	1	17	82	0.9	0.4	0.0	1.3	0	0	100
854	5.0	1	15	84	1.6	0.5	0.0	1.1			
860	4.0	1	9	90	0.6	0.3	0.0	1.4			
863	3.0	1	7	91	0.5	0.3	0.0	1.5			
881	1.9	2	10	87	2.6	1.0	0.1	0.9			
902	1.2	1	3	97	0.9	0.4	0.0	1.2			
Dist. from NW shore (m)											
0	0.1	1	26	74	21.6	2.2	0.1	0.3	5	9	87
23	1.0	1	7	92	1.1	0.3	0.0	1.3	1	3	96
118	2.0	3	35	62	1.5	0.8	0.1	1.2	15	46	39
130	2.8	4	25	71	1.8	1.0	0.1	1.3	2	10	87
145	4.2	2	61	37	19.6	11.4	0.3	0.3	10	21	69
150	4.8	1	34	65					32	45	23
159	5.8	1	36	63	3.8	2.2	0.1	0.4	10	20	71
162	7.1	2	36	63					16	32	52
169	8.0	1	19	80	3.6	1.3	0.1	0.8	5	13	82
191	9.0	12	49	39	3.9	2.4	0.2	1.2	4	34	62
217	10.0	15	51	34	4.3	3.3	0.3	1.2	15	73	12
239	10.9	15	46	39	2.5	1.9	0.2	1.2	12	66	21
257	11.8	15	46	39	4.7	3.6	0.3	1.2	15	70	15
279	13.1	15	39	46	4.3	3.3	0.3	1.1	16	71	13
372	12.9	15	40	45	4.2	2.7	0.2	1.0			
574	12.1	14	39	47	3.9	3.8	0.3	1.1	14	65	21
616	11.0	16	43	42	3.3	2.4	0.2	1.0	15	75	10

660	10.0	15	51	34	4.8	4.4	0.5	1.4	16	76	8
700	9.0	12	46	42	6.2	5.2	0.5	1.1	13	73	14
728	8.2	5	23	72	3.0	2.2	0.2	1.4	7	54	38
737	7.1	1	16	83	1.1	0.6	0.1	1.6	4	20	77
753	6.0	4	46	50	0.6	0.4	0.1	1.6	0	0	100
764	4.9	4	37	58	2.9	1.8	0.2	1.4	0	3	97
768	3.9	2	42	56	0.5	0.5	0.0	1.0	7	33	60
776	2.9	4	23	73	1.1	0.9	0.0	0.7	26	52	22
819	1.8	8	63	29	2.8	2.8	0.3	1.3	10	59	32
856	1.0	2	12	86	1.9	1.6	0.1	0.5	5	12	84
868	0.1	1	5	94	42.1	7.4	0.1	0.2	1	4	95

Table A.10 Mosomo Lake transect data

Dist. from NW shore (m)	Depth (m)	Org (%)	Carb. (%)	Inorg. (%)	χ (10^{-7} m^3/kg)	$IRM_{0.2T}$ (10^{-3} Am^2/kg)	ARM (10^{-3} Am^2/kg)	χ_{ARM}/IRM (mm/A)	Clay (%)	Silt (%)	Sand (%)
0	0.2	6	0	94	0.3	0.2	0.0	2.3	0	3	97
14	0.5	27	1	72	0.6	0.6	0.1	2.9	4	16	80
89	0.7	69	3	28	2.3	2.0	0.4	2.8			
133	1.5	73	3	24	2.2	1.8	0.5	3.1	14	86	0
143	2.4	69	4	27	2.7	2.5	0.5	2.7	18	82	0
153	3.0	69	3	28	3.0	2.6	0.6	2.7	16	84	0
181	3.8	72	4	25	2.4	1.9	0.4	2.7	14	85	1
260	5.0	68	4	28	2.5	2.1	0.4	2.7	15	83	2
272	6.1	69	4	27	2.8	2.5	0.5	2.5	16	83	1
286	7.2	67	4	29	3.2	3.1	0.6	2.5	15	84	1
339	8.2	69	4	28	3.4	3.8	0.7	2.4			
357	9.5	63	5	32	4.5	7.2	1.2	2.1			
422	5.0	68	4	28	2.2	1.7	0.4	2.8			
434	4.2	71	3	26	2.2	1.7	0.4	2.7	20	79	1
466	3.3	72	3	25	2.3	1.7	0.4	3.1	12	84	4
492	2.3	70	4	26	2.3	1.6	0.4	3.1	24	74	2
529	1.0	70	2	27	2.1	1.6	0.4	3.3	19	75	6
561	0.5	64	3	33	3.5	3.3	0.8	3.2	16	61	23
594	0.2	4	0	96	0.3	0.3	0.1	2.3	0	2	98
Dist. from E shore (m)											
0	0.2	10	1	89	0.8	0.5	0.1	1.8	3	13	84
4	0.5	5	1	94	0.4	0.3	0.0	2.1	4	14	82
11	1.0	7	1	92	0.4	0.4	0.1	2.2	5	15	80
25	2.0	40	1	59	1.6	1.2	0.3	2.7	17	59	24
36	3.2	63	2	35	2.4	2.3	0.4	2.0	20	69	11
47	4.2	65	3	32	2.3	2.3	0.4	2.5	16	81	3
53	5.0	68	2	30	1.9	1.5	0.3	2.2	15	81	4
63	6.0	65	4	32	3.3	3.6	0.5	1.7	27	72	1
83	7.0	64	4	32	4.0	5.1	0.8	2.1	27	73	1
100	6.0	63	4	33	3.6	4.5	0.8	2.1	27	72	1
111	5.0	67	3	30	3.3	3.4	0.6	2.3	19	79	3
133	4.0	67	3	30	3.1	1.7	0.3	2.4	25	74	1
158	5.0	68	3	30	2.4	1.8	0.3	2.3	20	77	4
171	6.0	66	4	30	2.9	2.5	0.5	2.3	25	72	3
188	8.0	65	4	31	3.2	3.2	0.6	2.2	19	78	3
209	8.0	62	4	33	3.4	3.8	0.6	2.1	27	71	2
216	7.0	64	4	32	3.8	4.1	0.7	2.0	26	73	1
221	6.0	68	3	29	2.9	2.4	0.5	2.5	25	73	2
230	5.0	68	3	28	2.6	2.2	0.4	2.4	20	76	4
240	3.9	66	3	31	2.8	2.1	0.4	2.6	22	72	5
247	3.0	68	3	29	3.0	2.0	0.4	2.8	22	71	8
257	2.1	61	3	37	3.0	2.6	0.7	3.3	20	61	20
287	1.0	26	1	73	1.1	0.9	0.2	2.6	5	22	73
307	0.5	48	2	50	1.1	0.9	0.2	2.4	9	34	57
316	0.1	16	1	83	0.2	0.2	0.0	2.6	2	7	92

Table A.11 Peterson Lake transect data

Dist. from W shore (m)	Depth (m)	Org (%)	Carb. (%)	Inorg. (%)	χ (10^{-7} m^3/kg)	$IRM_{0.2T}$ (10^{-3} Am^2/kg)	ARM (10^{-3} Am^2/kg)	χ_{ARM}/IRM (mm/A)	Clay (%)	Silt (%)	Sand (%)
0	1.0	51	5	44	1.0	0.6	0.1	1.5	51	49	0
211	1.8	54	4	42	1.7	1.8	0.4	2.5	42	58	0
376	2.8	42	3	55	3.0	2.2	0.3	1.9	41	58	1
518	4.0	35	6	59	2.1	1.5	0.1	1.3	39	61	1
656	5.2	36	7	57	2.5	1.7	0.2	1.3	40	59	1
789	6.1	31	7	63	2.8	2.3	0.2	1.2	41	57	2
847	4.8	33	6	61	2.0	1.7	0.2	1.4	42	57	1
894	4.1	41	6	53	1.7	1.3	0.2	1.6	33	62	5
935	3.0	45	5	50	2.2	1.5	0.2	2.0	33	61	5
967	2.0	42	5	53	2.9	2.0	0.3	2.1	36	62	2
990	0.9	3	1	97	1.0	1.1	0.0	0.4	5	22	72
Dist. from NE shore (m)											
0	0.9	12	2	85	0.8	0.4	0.0	1.1	17	56	26
231	2.4	29	4	67	1.9	1.5	0.2	1.8	26	61	13
464	3.1	35	7	58	2.2	1.9	0.3	1.9			
695	4.2	33	6	61	1.9	1.1	0.1	1.3			
921	5.1	31	7	62	4.5	2.1	0.2	1.3	41	58	1
1081	5.8	25	7	69	2.9	2.5	0.3	1.5	42	56	1
1143	5.2	34	7	59	3.6	3.0	0.4	1.5			
1206	4.3	38	7	56	1.9	1.4	0.2	1.5	38	61	2
1258	3.2	43	7	50	3.2	2.3	0.3	1.7	37	60	3
1309	2.0	43	5	52	1.9	1.7	0.3	2.4	35	61	4
1349	0.2	2	1	97	0.7	0.3	0.0	1.0	7	24	69

Table A.12 Sandy Lake transect data

Dist. from NW shore (m)	Depth (m)	Org (%)	Carb. (%)	Inorg. (%)	χ (10^{-7} m^3/kg)	$IRM_{0.2T}$ (10^{-3} Am^2/kg)	ARM (10^{-3} Am^2/kg)	χ_{ARM}/IRM (mm/A)	Clay (%)	Silt (%)	Sand (%)
8	1.0	0	0	99	1.9	1.7	0.1	0.4	1	4	94
34	1.8	2	1	97	1.8	2.0	0.2	1.1			
53	2.8	54	5	41	4.4	5.2	1.0	2.5			
55	3.9	53	5	42	15.9	19.2	3.5	2.2	27	70	3
77	5.0	40	5	55	13.6	19.1	3.2	2.1	26	71	3
97	6.3	43	5	52	14.6	20.4	3.5	2.1			
104	6.8	40	5	55	18.8	23.7	3.7	1.9	27	70	3
137	8.0	45	5	50	7.9	6.8	1.0	1.8			
162	9.1	45	5	50	6.0	5.3	0.8	1.9			
196	9.8	47	5	48	8.1	8.2	1.3	1.9			
275	11.3	45	5	50	10.0	13.4	2.0	1.9			
300	9.8	48	5	48	4.5	4.4	0.7	1.9			
309	8.8	41	5	54	5.0	4.7	0.7	1.9	26	71	3
326	8.2	38	5	57	5.8	4.9	0.7	1.9	25	68	7
350	7.3	38	5	57	13.6	13.4	1.8	1.7			
385	6.1	44	6	51	11.2	11.6	1.9	2.1			
402	5.0	13	2	85	5.4	5.2	0.2	0.6	15	42	43
413	4.0	62	6	32	6.4	7.4	1.4	2.3			
435	2.8	37	4	59	3.9	4.3	0.7	2.1	31	68	1
556	1.9	3	1	96	2.5	2.0	0.1	0.9	5	24	71
575	1.1	1	1	98	2.9	2.5	0.1	0.4	6	21	72
577	0.6	2	1	97	1.6	1.5	0.0	0.4			
Dist. from NE shore (m)											
0	0.5	2	0	97	0.7	0.7	0.0	0.6	4	15	81
10	0.9	9	1	90	1.0	1.0	0.1	1.3	5	21	73
67	2.0	48	3	49	1.6	1.5	0.3	2.5	24	73	3
151	2.4	50	4	46	2.9	2.8	0.5	2.2	26	70	4
252	2.9	25	2	73	3.2	3.9	0.3	1.0	15	42	43
267	3.9	1	1	98	5.1	4.2	0.1	0.2	8	27	65
282	5.2	4	3	94	4.9	4.7	0.2	0.4	5	12	83
284	5.9	23	2	76					18	51	31
302	6.9	40	4	56	5.3	5.3	0.8	1.8	28	69	2
326	8.1	42	4	55	3.0	2.4	0.4	1.9	28	70	1
347	9.4	39	4	57	4.1	3.8	0.4	1.3	26	70	4
361	11.1	46	5	49	5.6	5.2	0.6	1.5	24	75	1
365	10.1	46	5	49	4.8	3.8	0.5	1.7	27	72	1
375	11.8	43	6	51	15.4	23.8	3.3	1.8	27	72	1
430	10.9	47	5	48					27	72	1
441	9.9	47	7	47	5.9	5.5	0.8	1.8	29	71	0
446	8.9	49	6	45	3.7	3.2	0.5	1.8	26	73	1
453	8.0	39	6	55							
477	6.9	38	5	57					27	70	3
482	6.4	4	1	94	5.5	5.2	0.2	0.4	12	31	57
487	5.3	1	1	98	9.0	7.9	0.2	0.3	5	13	82

500	3.8	1	9	89					22	51	26
509	2.9	46	5	49	2.4	2.7	0.5	2.2	27	71	3
607	2.1	17	3	80	4.3	3.1	0.3	1.4	13	54	33
620	1.0	2	0	98	1.2	1.2	0.1	0.7	5	26	69
625	0.5	1	0	98	1.7	1.8	0.0	0.3			

Table A.13 Hysteresis ratios and component fractions for analyzed surface sediments

Lake	Water depth (m)	Distance from shore (m)	Shore	M_{rs}/M_s	H_{cr}/H_c	g_{UNISD}	g_{ISD}	g_{MD}
Birch	0.9	604	**E**	0.0	3.3	0.00	0.01	0.98
Birch	1.7	589		0.0	9.3	0.01	0.03	0.96
Birch	3.8	556		0.1	2.6	0.14	0.09	0.78
Birch	5.0	535		0.2	3.0	0.18	0.13	0.69
Birch	8.2	368		0.2	2.4	0.22	0.16	0.62
Birch	7.8	321		0.2	2.6	0.22	0.17	0.62
Birch	4.1	140		0.2	2.4	0.21	0.17	0.61
Birch	3.2	122		0.2	2.7	0.19	0.15	0.66
Birch	2.0	77		0.2	2.5	0.17	0.19	0.64
Birch	1.6	47		0.2	3.0	0.18	0.18	0.64
Birch	0.9	15	**W**	0.1	4.0	0.04	0.16	0.80
Birch	1.3	20	**SE**	0.0	7.8	0.01	0.05	0.94
Birch	1.9	36		0.0	6.4	0.03	0.04	0.93
Birch	2.9	56		0.1	3.7	0.09	0.07	0.84
Birch	4.7	114		0.2	2.6	0.18	0.15	0.68
Birch	6.9	185		0.2	2.5	0.21	0.16	0.63
Birch	4.0	390		0.2	2.5	0.18	0.16	0.66
Birch	3.0	468	**NW**	0.1	2.8	0.16	0.14	0.70
Deming	0.8	232	**SE**	0.1	5.5	0.08	0.13	0.80
Deming	1.8	229		0.2	0.0	0.23	0.18	0.59
Deming	3.0	218		0.2	2.8	0.29	0.18	0.52
Deming	7.0	195		0.2	3.7	0.30	0.23	0.47
Deming	10.8	180		0.2	3.0	0.16	0.27	0.57
Deming	17.0	156		0.2	3.3	0.11	0.23	0.66
Deming	11.0	112		0.1	3.6	0.06	0.24	0.70
Deming	3.8	59		0.1	4.2	0.06	0.12	0.82
Deming	1.5	21	**NW**	0.2	2.8	0.27	0.21	0.52
Deming	0.3	0	**NE**	0.1	3.0	0.11	0.12	0.77
Deming	3.0	23		0.3	1.9	0.37	0.19	0.44
Deming	12.0	77		0.2	2.6	0.22	0.30	0.48
Deming	16.8	105		0.2	2.5	0.15	0.24	0.61
Deming	9.0	139		0.3	2.2	0.29	0.33	0.38
Deming	4.1	180		0.3	2.4	0.33	0.20	0.47
Deming	0.6	256	**SW**	0.2	1.7	0.21	0.17	0.62
Elkhorn	1.0	14	**SW**	0.1	5.1	0.03	0.14	0.84
Elkhorn	1.8	49		0.2	3.3	0.08	0.29	0.63
Elkhorn	3.9	78		0.1	2.8	0.07	0.22	0.71
Elkhorn	6.2	97		0.1	3.8	0.05	0.19	0.76
Elkhorn	11.0	192		0.1	6.1	0.03	0.17	0.80
Elkhorn	6.0	595		0.1	3.1	0.05	0.20	0.75
Elkhorn	3.9	614		0.1	3.2	0.09	0.24	0.68
Elkhorn	3.1	629		0.3	2.5	0.16	0.41	0.43
Elkhorn	1.0	661	**NE**	0.2	2.5	0.09	0.32	0.59
Elkhorn	1.1	6	**NW**	0.0	5.2	0.00	0.08	0.92
Elkhorn	4.2	34		0.2	2.9	0.09	0.31	0.61
Elkhorn	10.0	118		0.1	3.6	0.04	0.22	0.74
Elkhorn	5.0	428	**SE**	0.2	5.4	0.10	0.34	0.56
Erie	1.9	1359	**SE**	0.0	3.2	0.01	0.02	0.97
Erie	6.1	1290		0.1	3.4	0.08	0.11	0.81
Erie	6.1	819		0.0	9.3	0.00	0.02	0.97

Erie	9.4	509		0.2	2.4	0.17	0.19	0.64
Erie	5.1	86		0.1	2.8	0.14	0.13	0.73
Erie	0.4	0	**NW**	0.0	6.2	0.00	0.05	0.95
Erie	1.0	726	**NE**	0.0	9.6	0.01	0.03	0.96
Erie	1.9	715		0.0	7.9	0.01	0.05	0.94
Erie	3.1	702		0.1	4.9	0.04	0.07	0.89
Erie	4.0	672		0.1	4.4	0.06	0.09	0.85
Erie	6.9	604		0.1	2.7	0.10	0.18	0.72
Erie	6.0	486		0.1	2.9	0.11	0.15	0.74
Erie	6.1	359		0.0	11.0	0.00	0.01	0.99
Erie	7.7	127		0.2	2.5	0.18	0.17	0.65
Erie	7.1	99		0.2	2.6	0.16	0.17	0.67
Erie	4.1	35		0.0	8.0	0.02	0.05	0.93
Erie	1.8	19		0.0	17.3	0.00	0.00	0.99
Erie	0.1	0	**SW**	0.0	0.0	0.00	0.00	1.00
Linka	0.1	0	**NW**	0.0	8.9	0.00	0.01	0.99
Linka	2.0	68		0.2	2.5	0.11	0.24	0.65
Linka	7.2	118		0.1	4.6	0.03	0.10	0.87
Linka	12.0	589		0.1	3.5	0.05	0.16	0.79
Linka	8.9	835		0.0	6.9	0.01	0.04	0.95
Linka	3.0	863	**SE**	0.0	12.6	0.02	0.03	0.94
Linka	0.1	868	**SW**	0.0	5.8	0.00	0.04	0.96
Linka	1.8	819		0.1	2.9	0.08	0.24	0.68
Linka	2.9	776		0.2	2.7	0.04	0.36	0.60
Linka	6.0	753		0.1	3.3	0.10	0.21	0.69
Linka	9.0	700		0.1	3.2	0.05	0.18	0.77
Linka	12.1	574		0.1	2.8	0.06	0.22	0.72
Linka	12.9	372		0.1	2.8	0.04	0.16	0.80
Linka	13.1	279		0.1	3.5	0.05	0.18	0.77
Linka	10.0	217		0.1	3.2	0.06	0.17	0.77
Linka	4.2	145		0.1	7.0	0.00	0.12	0.88
Linka	2.0	118		0.1	4.2	0.04	0.12	0.84
Linka	2.8	130		0.1	5.2	0.04	0.11	0.85
Linka	0.1	0	**NE**	0.0	0.0	0.00	0.01	0.99
Mosomo	0.2	0	**NW**	0.2	2.5	0.26	0.26	0.48
Mosomo	1.5	133		0.3	2.2	0.41	0.17	0.42
Mosomo	2.4	144		0.2	2.4	0.29	0.18	0.53
Mosomo	5.0	264		0.2	2.7	0.23	0.16	0.60
Mosomo	9.5	383		0.3	1.8	0.26	0.31	0.43
Mosomo	3.3	501		0.3	1.9	0.38	0.16	0.47
Mosomo	0.5	607		0.3	2.2	0.44	0.17	0.39
Mosomo	0.2	647	**SE**	0.1	1.6	0.15	0.14	0.71
Peterson	0.9	990	**E**	0.1	3.7	0.02	0.30	0.68
Peterson	6.1	789		0.1	2.9	0.08	0.25	0.67
Peterson	1.8	211		0.3	2.2	0.29	0.26	0.45
Peterson	3.0	935	**W**	0.2	2.3	0.21	0.29	0.51
Sandy	0.9	10	**NE**	0.2	3.5	0.10	0.28	0.62
Sandy	2.0	67		0.2	2.6	0.27	0.23	0.49
Sandy	2.9	252		0.1	3.0	0.06	0.26	0.69
Sandy	3.9	267		0.1	3.6	0.00	0.18	0.82
Sandy	6.9	302		0.2	3.0	0.13	0.21	0.65
Sandy	11.8	375		0.2	2.2	0.16	0.28	0.56
Sandy	1.0	620		0.1	3.4	0.04	0.28	0.68
Sandy	2.9	509		0.2	2.7	0.19	0.21	0.59
Sandy	5.3	487	**SW**	0.1	3.8	0.00	0.14	0.85

Sandy	1.1	575	**SE**	0.1	0.9	0.01	0.14	0.85
Sandy	2.8	435		0.2	2.7	0.17	0.20	0.63
Sandy	5.0	402		0.1	3.9	0.02	0.15	0.83
Sandy	11.3	275		0.2	2.2	0.17	0.26	0.58
Sandy	8.0	137		0.1	2.6	0.12	0.18	0.70
Sandy	2.8	53		0.2	2.5	0.24	0.20	0.56
Sandy	1.0	8	**NW**	0.1	5.0	0.01	0.13	0.87